THIN FILM BEARINGS WITH PHASE CHANGE OF LUBRICANT

NASSER SAADAT

Doctor of Philosophy

THE UNIVERSITY OF ASTON IN BIRMINGHAM

July 1991

The University of Aston in Birmingham

THIN FILM BEARINGS WITH PHASE CHANGE OF LUBRICANT

Thesis submitted for the degree of Doctor of Philosophy

by Nasser Saadat

July 1991

Summary

The possible evaporation of lubricant in fluid film bearings has been investigated theoretically and by experiment using a radial flow hydrostatic bearing supplied with liquid refrigerant R114. Good correlation between measured and theoretical values was obtained using a bespoke computational fluid dynamic model in which the flow was assumed to be laminar and adiabatic. The effects of viscous dissipation and vapour generation within the fluid film are fully accounted for by applying a fourth order Runge-Kutta routine to satisfy the radial and filmwise transverse constraints of momentum, energy and mass conservation. The results indicate that the radial velocity profile remains parabolic while the flow remains in the liquid phase and that the radial rate of enthalpy generation is then constant across the film at a given radius. The results also show that evaporation will commence at a radial location determined by geometry and flow conditions and in fluid layers adjacent to the solid boundaries. Evaporation is shown to progress in the radial direction and the load carrying capacity of such a bearing is reduced significantly.

Expressions for the viscosity of the liquid/vapour mixture found in the literature survey have not been tested against experimental data. A new formulation is proposed in which the suitable choice of a characteristic constant yields a close representation to any of these expressions. Operating constraints imposed by the design of the experimental apparatus limited the extent of the surface over which evaporation could be obtained, and prevented clear identification of the most suitable relationship for the viscosity of the liquid/vapour mixture.

The theoretical model was extended to examine the development of two phase flow in a rotating shaft face seal of uniform thickness. Previous theoretical analyses have been based on the assumption that the radial velocity profile of the flow is always parabolic, and that the tangential component of velocity varies linearly from the value at the rotating surface, to zero at the stationary surface. The computational fluid dynamic analysis shows that viscous shear and dissipation in the fluid adjacent to the rotating surface leads to developing evaporation with a consequent reduction in tangential shear forces. The tangential velocity profile is predicted to decay rapidly through the film, exhibiting a profile entirely different to that assumed by previous investigators. Progressive evaporation takes place close to the moving wall and does not occur completely at a single radial location, as has been claimed in earlier work.

Key words: Bearings, lubricant evaporation, refrigerant compressors, sliding vane machines.

DEDICATION

To the Almighty from whom the truly faithful acquire their will and hope when there is none.

To my mother, Sekineh

for her love and dedication to provide her son with a good education.

To my late father, Hossein who had so much hope in me,

I write this for all to see,

the sorrow in me that'll never be free

of being too late to do my duty

to make my father as happy as can be.

Father, forgive me

ACKNOWLEDGEMENTS

I would like to thank my supervisor, Mr. W.L. Flint not only for his invaluable guidance but also for giving me moral support throughout the course of the research programme.

Thanks are also due to the Department of Mechanical & Electrical Engineering at the University of Aston in Birmingham for providing financial support and the use of Computing and Laboratory facilities.

The assistance and expertise of Drs B. Martin, R. Summers, F. Carter, workshop and laboratory staff at the Department of Mechanical & Electrical Engineering is acknowledged.

Lastly thanks are due to my family, in particular my brother Reza without whom the opportunity of undertaking this work would have never existed.

Table of Contents

List of Figures

List of Tables

Publication

In the course of the research a paper entitled "Phase Change in Face Seals" based on some of the work described in this thesis has been written which is to be presented at the Second Biennial European Joint Conference on Engineering Systems Design and Analysis, July 4-7, 1994, London, England organised by ASME.

CHAPTER ONE

INTRODUCTION

1.1 Introduction

The sliding vane gas compressor uses oil injection to lubricate the moving components and provide cooling to reduce the work of compression. A suggestion that this type of compressor might be employed in a vapour compression refrigeration plant using the liquid phase of the refrigerant for lubrication and cooling was accompanied with the concern that such a lubricant could evaporate within a bearing or face seal. The aim of the present work was to provide guidance concerning the effect of lubricant evaporation on the performance of thin film bearings and seals in a liquid injected sliding vane compressor.

The bearing surfaces which are of importance in the sliding vane compressor are:

1. Vane tips sliding on the inner wall of the stator.
2. Vane and rotor end faces sliding on the stator end covers.
3. Vanes sliding in and out within the slots in the rotor.

In each of these situations there is considerable geometric complexity that adds to the difficulty of establishing a suitable mathematical model of the tribological and thermodynamic phenomena which occur in the presence of phase change of lubricant.

An extensive survey of the literature relating to phase change of bearing lubricants revealed no direct correlation between measured effects and predicted values. The discharge of vapour from rotating face seals retaining liquid within rotary machines has been observed, and a significant number of theoretical papers have been published which indicate that the phenomenon will arise in appropriate circumstances.

The need for direct correlation between predicted and measured values prompted an examination of the most manageable type of experimental equipment which would

provide suitable data. It was first considered that high velocity flow through a capillary would provide the requisite amount of dissipation to obtain phase change, but it was impossible to ensure that the pressure distribution along the capillary could be measured accurately due to the fact that sensing connections would upset the local flow.

To minimize the theoretical and experimental difficulties the performance characteristics of an axially symmetrical hydrostatic thrust bearing was examined. The construction materials of the experimental bearing and the conditions of the test were designed to be such that heat transfer to or from the surroundings would be entirely negligible. The choice of a suitable refrigerant would allow the geometric scale of a physical model to be such that the anticipated phenomena could be measured accurately and might be visualized. The adequacy of the corresponding theoretical model could then be established by comparison with measured data and the findings applied to the conditions that prevail in sliding vane compressors employing liquid refrigerant as a lubricant.

1.2 Background

In a vapour compression refrigerator or heat pump, the high pressure vapour is delivered to the condenser, and leaves as a subcooled liquid which passes on to the throttle and evaporator. The present investigation considers the possible consequences of using some part of this high pressure liquid refrigerant for supply as a lubricant to the bearings, end faces of the rotor and to the vane tips of a sliding vane compressor. In particular, it examines the possibility that viscous dissipation of energy within the lubricant film would raise its temperature to a point at which phase change would occur causing some part of the liquid to evaporate. The rotor end face is identified as the location where phase change is most likely to take place. Appendix 1 provides a review of the investigation for the other bearing surfaces in a sliding vane compressor.

The liquid injected sliding vane machine has been developed over many years as a highly effective gas compressor using oil as the lubricant/coolant. The general arrangement of the sliding vane compressor is shown in Figure 1.1, where the rotor is mounted eccentrically within a stator that is fitted with appropriate inlet and delivery ports, while the vanes move radially in the rotor slots as the rotor turns. The lubricant/coolant oil is injected in the cells between adjacent vanes and is separated from the compressed gas after delivery. The pressure in the delivery plenum is used to recirculate the separated oil and re-inject it directly into the cells during an early part of the compression process. In such compressors, the reduction of compression work by cooling is a common practice that is achieved with great effectiveness. About 90% of the work input energy is removed as heat by direct contact between the gas and coolant during compression.

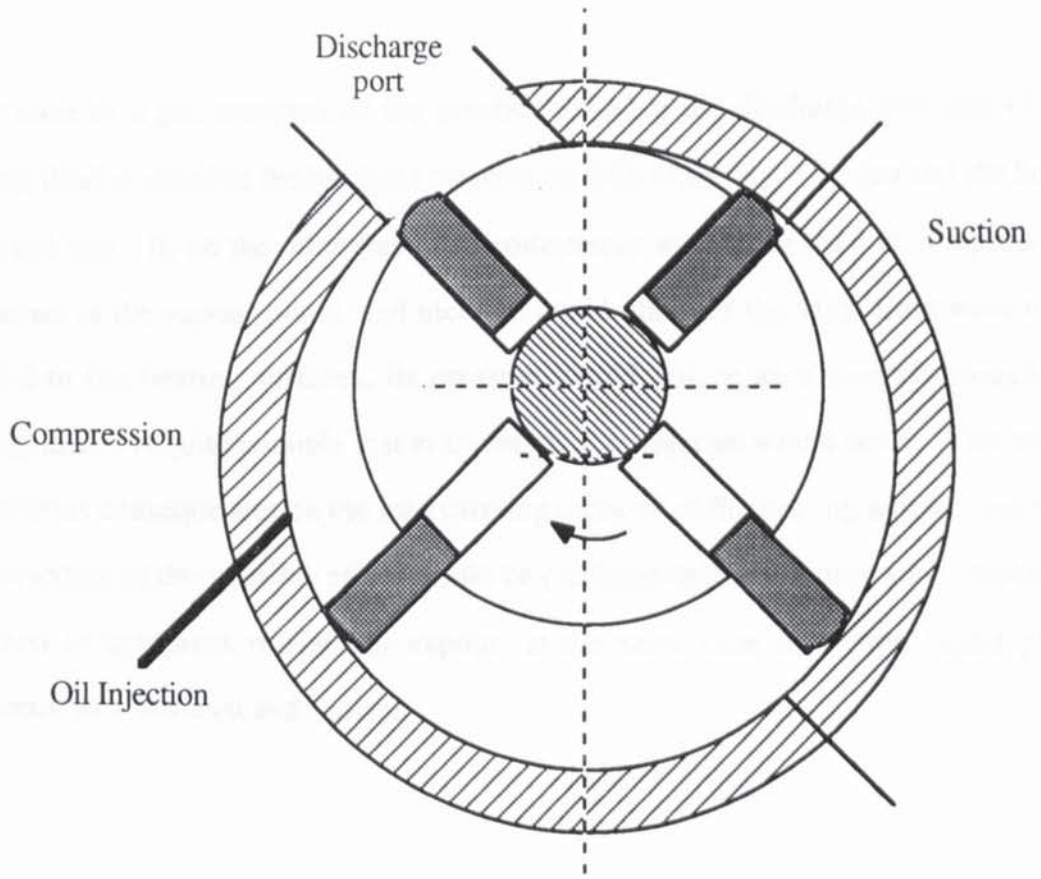

Figure 1.1
Basic Compressor Operation

It can be shown theoretically that substantial improvements in the COP of a refrigerator or heat pump can be achieved through the use of cooled compression. However, the lubricating performance of standard oils is greatly reduced when in contact with refrigerant fluid, due to absorption of liquid refrigerant, while the thermodynamic performance of the refrigerant fluid is degraded by the presence of oil. The oil is also carried over in the refrigerant vapour and remains on heat transfer surfaces in the condenser and the evaporator, thus reducing the effectiveness of these components.

To avoid these undesirable effects, the possibility was envisaged of using liquid phase refrigerant to act as both coolant and lubricant in the sliding vane compressor. The lubricating properties of chlorinated hydrocarbon refrigerant fluids are recognized to be significantly poorer than those of standard oils, but allowance can be made for this in the design of bearing surfaces.

In the case of a gas compressor the practice of using the discharge pressure of the working fluid to circulate the lubricant presents no difficulties, since the gas and the liquid oil do not mix. If, on the other hand, the compressor were to be used to compress the refrigerant in the vapour phase, and then the liquid phase of the same fluid were to be injected to the bearing surfaces, its pressure would reduce as it passed through the bearing, then it is quite possible that evaporation of refrigerant would occur. This would have serious consequences on the load carrying capacity of the bearing and it is essential that the extent of this possible effect should be predicted before a sliding vane machine is designed to compress refrigerant vapour, at the same time using the liquid phase refrigerant as a lubricant and coolant.

CHAPTER TWO

LITERATURE SURVEY

2.1 Introduction

This chapter outlines the work carried out by researchers whose findings are considered to be relevant to the present work. The chapter has been divided into four parts, each devoted to a particular topic.

The first part, section 2.2 gives a general introduction to lubrication. Here, a brief reference is made to fluid film lubrication with particular attention to the theory of hydrodynamic lubrication pioneered by Osborne Reynolds in 1886. An historical perspective is presented to show the early developments of lubrication theory. In this section letter h has been used to denote the film thickness since in lubrication theory this has always been the practice. However in Chapter 3, h will be used to denote the enthalpy and letter z to denote lubricating film thickness.

The second part, section 2.3 covers works in the field of two phase lubrication and the effect of air/vapour bubbles on the pressure distribution and the load carrying capacity of bearings. Since the study of two-phase lubrication involves not only the generation of vapour, but also the variation in viscosity and density of the mixture, this section discusses the relevant findings of other researchers. Thermodynamic analysis of bubbly oil is also discussed. This analysis is commonly used in lubrication systems where the heat conduction within the lubricating film, as well as the heat conduction between the lubricant and the surrounding parts, is considered.

Part three, section 2.4 discusses the effect of refrigerant dissolution in lubricating oil, with particular attention to refrigeration compressors. In the last part, section 2.5 the potential of refrigerant for use as either gaseous or liquid lubricant or anti-wear additive is discussed.

The method of analysis developed for the present investigation is detailed in Chapter 3.

2.2 Lubrication

The process of lubrication is to separate any two solid surfaces sliding past each other with a film of some substance which can be sheared without causing any damage to the surfaces.

In order to ensure that no direct contact can occur between the two surfaces, it is essential that the lubricating film be of sufficient thickness. Most journal and thrust bearings employ this type of lubrication mechanism, known as full fluid film or hydrodynamic lubrication[1]. The lubricant is normally a mineral oil, water, gas, or when unusual conditions of temperature or speed prevail a synthetic liquid is used. For example, during the industrial revolution full hydrodynamic lubrication was used when shaft rotational speeds rose beyond those of the windmill and cart axle.

There are several types of fluid film bearing in use nowadays. Probably the simplest form is the Tilting Pad, shown in Figure 2.2.1. Pad AB is stationary, with an entry gap h_1 that is larger than the exit gap h_2. The opposing surface moves in the direction indicated, with a velocity U and the lubricant in contact with each solid surface moves with the velocity of that surface. The velocity distribution across the film between the moving and stationary surfaces is generated by viscous forces. If the flow in the gap is assumed to be laminar, then the viscous forces must also generate a rise in pressure to promote the acceleration of fluid streaming through the gradually reducing gap. The combination of viscous and pressure forces within the film results in an increase in the resistance to externally applied forces, thus enhancing the load carrying capacity of the film. It must be noted that due the consideration of continuity in the flow regime, the lubricant is customarily assumed to be an incompressible fluid.

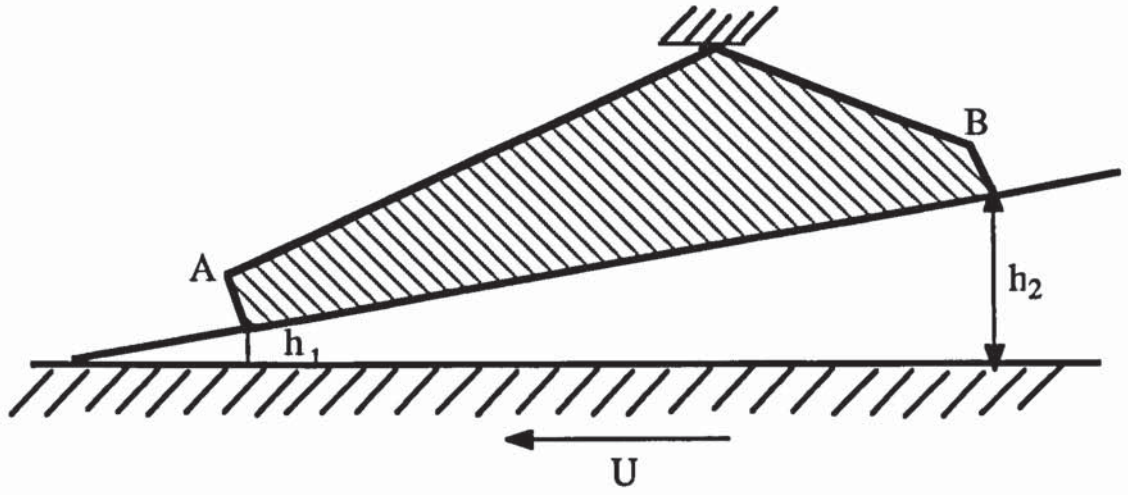

Figure 2.2.1
Geometry of a tilting pad

Another example of a fluid film bearing is the journal bearing; this type has the longest history of scientific study of any class of bearing[1]. The journal bearing system consists essentially of a circular shaft rotating inside a circular bush, as shown in Figure 2.2.2. In operation, the viscous forces generated in the fluid between the rotating shaft and the stationary bearing liner lift the shaft to a position in which its axis is eccentric to the bearing shell. The initial bearing clearance is a fundamental parameter of bearing design which, together with the viscosity of the lubricant, the diameter and the rotational speed of the shaft and the load, determine the eccentricity which will arise in normal operation. The minimum film thickness, its location and the amount of flow through the bearing are important factors[2] in ensuring that sufficient lubricant can flow through to the bearing, to provide adequate cooling and removal of the heat energy generated by viscous effects and dissipated in the bearing.

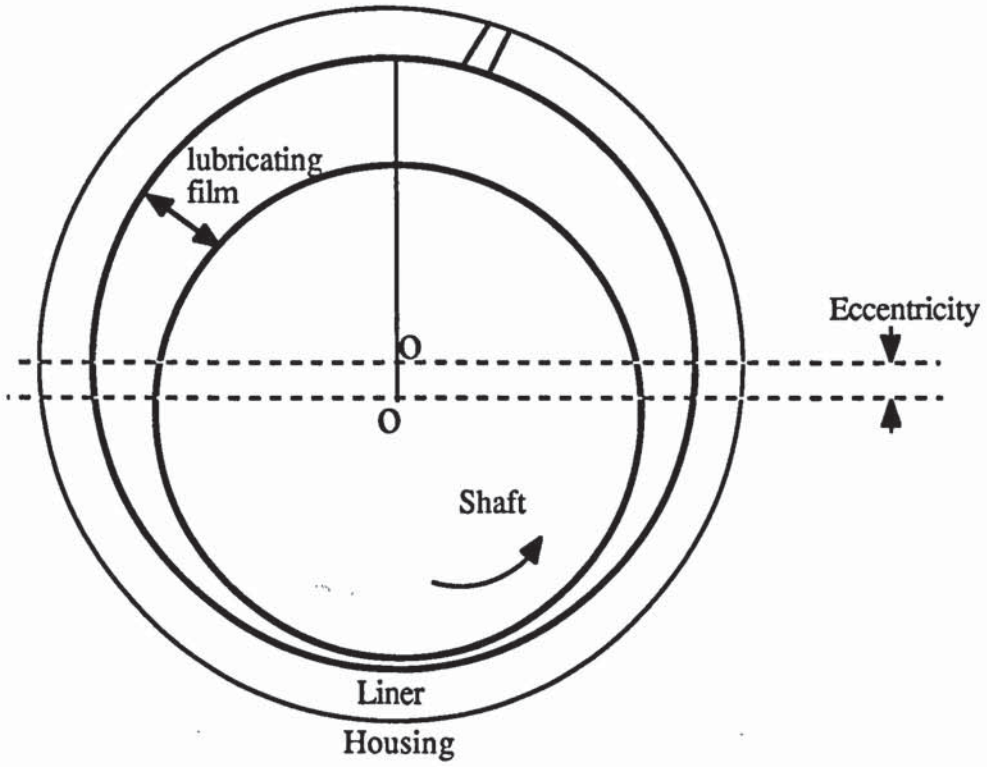

Figure 2.2.2
Eccentric Journal Bearing

The primary function of a lubricant is to minimize friction and prevent wear. A lubricant achieves this purpose by forming an easily sheared layer between the moving and stationary surfaces of a bearing. Ideally, this layer of lubricant will completely prevent the surfaces from touching each other. However, this will not always be the case. For example, in a journal bearing when the shaft is at rest, the lubricant exists only as a discontinuous film and some metal to metal contact occurs at the bottom of the shaft. When the shaft begins to turn, there can be no layer of liquid lubricant to separate the surfaces. This is characterized by high frictional resistance and is known as boundary lubrication[3].

Stribeck[4] conducted a series of experiments on such bearings, in which both the load and the speed were varied, and determined the condition which gave rise to the different regimes of "boundary lubrication" and "full fluid-film lubrication". Figure 2.2.3 shows the Stribeck curve illustrating different modes of lubrication depending on the speed (N), load (w) and viscosity (η) which in turn influence the coefficient of friction (μ).

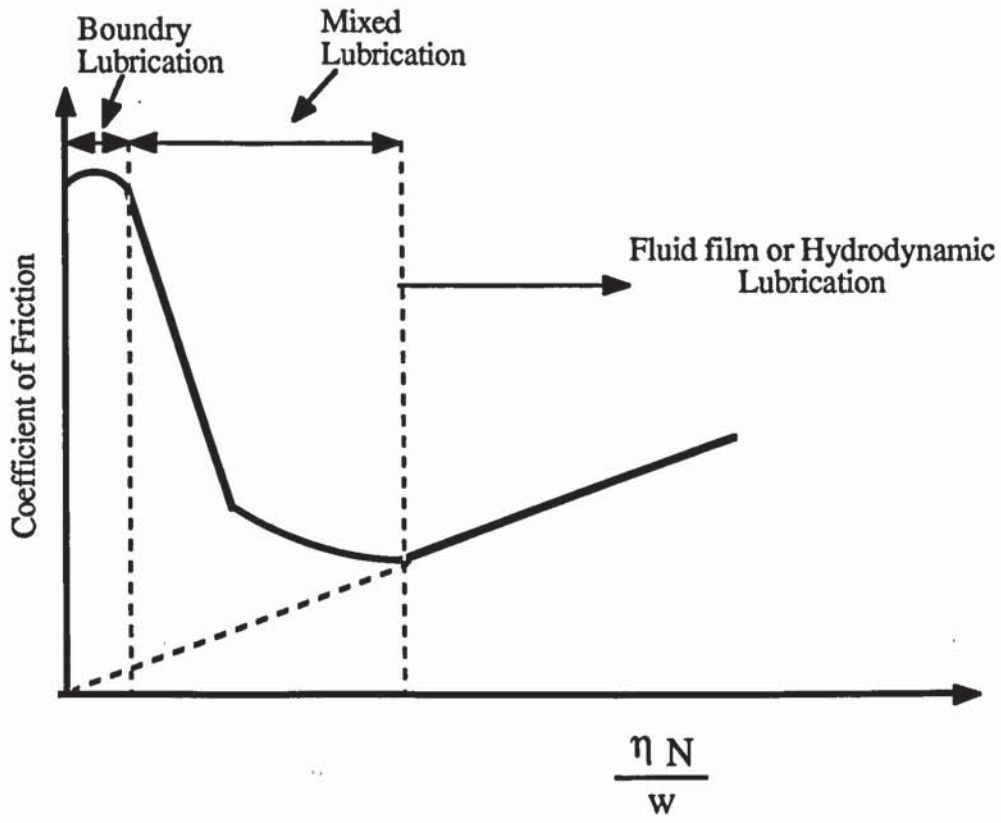

Figure 2.2.3
Stribeck Curve showing different modes of lubrication

The two types of bearing mentioned above are self acting or hydrodynamic. In these types, the film thickness decreases as the applied load increases and/or the sliding speed or the fluid-entraining capability decreases. This characteristic can therefore limit the maximum load and the minimum speed of the bearing. To remedy this an alternative is used in which the lubricant is pressurized before it enters the bearing and therefore it maintains a space between the opposing solid surfaces even in the absence of relative motion. Figure 2.2.4 illustrates a schematic diagram of a hydrostatic bearing where the lubricant is supplied via a pump. The pressure generated lifts the "load" and maintains a film between the surfaces.

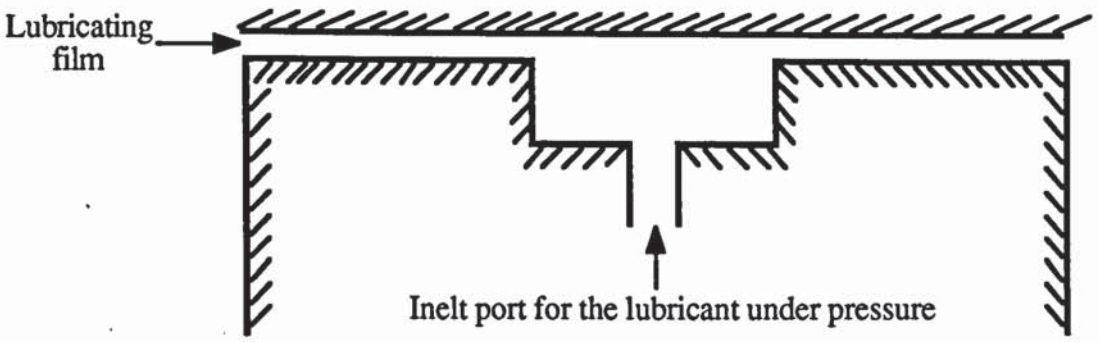

Figure 2.2.4

Geometry of a Circular-Step Hydrostatic Bearing

Although it has been implied until now that liquid lubricants are always employed, it is entirely feasible to use compressible fluids as lubricants and indeed, when equipment requires to be lubricated in extreme environments, e.g. extreme heat or irradiation, then it is common to use gas bearings. A gas cooled nuclear reactor is an example where conventional liquid lubricant would deteriorate due to irradiation, and hence designer's use gaseous carbon dioxide as both a coolant and a lubricant for the shafts of the gas circulating fans.

2.2.1 Hydrodynamic Lubrication Theory

The theory of fluid film lubrication dates back as far as 1687, when Sir Issac Newton (1642-1727) examined the circular motion of fluids. As quoted by Dowson[5], Newton was in fact seeking an explanation of the motion of bodies in the heavens and his work can be seen as a link between general studies of the motion of bodies in a resisting medium and his mathematical statement of the system of the world. His studies showed that a fluid obeying his hypothesis would form a vortex around a rotating sphere with a periodic time proportional to the square of the distance from the centre of the motion. He suggested that the shear stress between the adjacent fluid layers could be directly related to

the change of velocity across the layer leading to a relationship of the form given by equation (2.2.1).

$$\tau = \eta \frac{\partial u}{\partial y} \qquad (2.2.1)$$

where

τ = Shear stress

η = Viscosity

$\frac{\partial u}{\partial y}$ = Velocity gradient

Fluids which obey the hypothesis are known as Newtonian fluids and fluid film lubrication theory has been built upon this foundation. However, it was not until 150 years later that Navier (1785-1836) introduced the coefficient of viscosity into the equations of fluid motion.

The hydrodynamic equation for flow in the fluid film of a bearing was first deduced by Osborne Reynolds [2] and published through the Royal Society in 1886.

The assumptions made in deriving the hydrodynamic equation are briefly listed as follows.

1 The fluid flow is laminar.

2 The film thickness is small compared with its length and breadth.

3 The fluid inertia forces are small compared to the viscous forces.

4 Body forces, e.g gravity, are negligible.

5 There is no slip between the fluid and the surface of the bearing.

6 The lubricant is Newtonian i.e $\tau = \eta\, \partial u/\partial y$

By considering pressure and shear forces acting on faces of an element of a fluid, as shown in Figure 2.2.1.1, and applying the above assumptions, Reynolds first derived

expressions for the velocities in x and z directions, and by integrating those expressions from 0 to h (the film thickness), obtained equations for flow parameters.

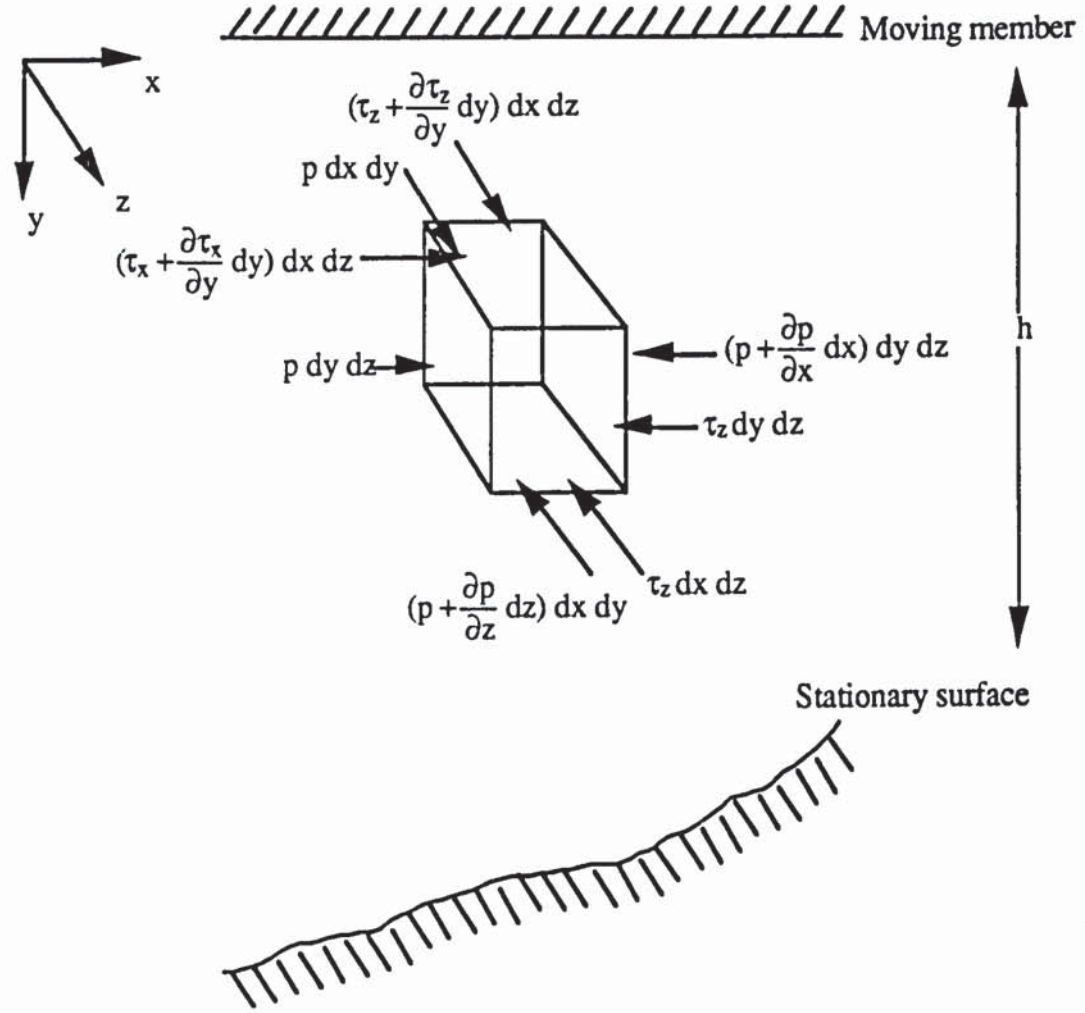

Figure 2.2.1.1

Stressed element in fluid film

Finally by applying the principle of conservation of momentum, Reynolds deduced equation (2.2.2).

$$\frac{\partial}{\partial x}\left(\frac{\rho h^3}{\eta}\frac{\partial p}{\partial x}\right) + \frac{\partial}{\partial z}\left(\frac{\rho h^3}{\eta}\frac{\partial p}{\partial z}\right) = 6U\frac{\partial}{\partial x}(\rho h) + 6\rho h\frac{\partial U}{\partial x} + 12\frac{\partial}{\partial t}(\rho h) \qquad (2.2.2)$$

The terms on the right of the equation are referred to as

1) $6\,U\frac{\partial}{\partial x}(\rho h)$ Wedging term

2) $6\,\rho\,h\frac{\partial U}{\partial x}$ Stretching term

3) $12\frac{\partial}{\partial t}(\rho h)$ Squeeze-film term

The stretching term can usually be neglected, as can the squeeze film term, when a steady-state bearing condition is considered. Thus, for oil and other incompressible lubricants the Reynolds' equation becomes, for isoviscous operation

$$\frac{\partial}{\partial x}(h^3 \frac{\partial p}{\partial x}) + \frac{\partial}{\partial z}(h^3 \frac{\partial p}{\partial z}) = 6\eta U h \frac{\partial h}{\partial x} \qquad (2.2.3)$$

The pressure gradients are therefore related to the viscosity of the lubricant, the relative velocity of the solid boundaries and the rate of change of the gap between these surfaces.

In the case of steady flow in an axially symmetric hydrostatic bearing the equation reduces to an identical form in which the pressure gradient is related to volume flow rate rather than the relative velocity, as demonstrated in Chapter 3.

2.2.1.1 Effect of Lubricant Inertia in Reynolds' Equation

One of the assumptions made by Reynolds is that the fluid inertia forces are small compared to the viscous forces. In some lubrication systems, where the flow is laminar, and in systems where a conventional lubricant is employed, this assumption is valid. However, the validity of this assumption for cases of non-laminar flow in bearings due to either a high-speed operation or the use of non-conventional lubricants such as water, liquid refrigerant or liquid metals, is questionable.

The importance of inertia forces in the equation of motion was probably first considered in 1946 when Fog[6] investigated the fluid film lubrication of parallel surfaces. In his experiments, the operating conditions for various types of thrust bearings were different from those commonly practiced. The speed of rotating members of the bearing, for instance, was considerably higher in terms of angular velocity, than had been common for shafts subjected to high thrust loads. The author's work showed that centrifugal forces

could be important in producing positive pressure in such operating conditions. The importance of consideration of inertia forces became more evident when Shaw and Strang[7], developed a new hydrodynamic bearing called the Hydrosphere. In this bearing, it seemed evident that the load capacity was increased by pressure recovery due to deceleration in the increasing flow cross-section rather than any additional pressure generated by centripetal acceleration of the fluid. They showed that the bearing represented in Figure 2.2.1.1.1 was capable of hydrodynamically supporting loads of great magnitude.

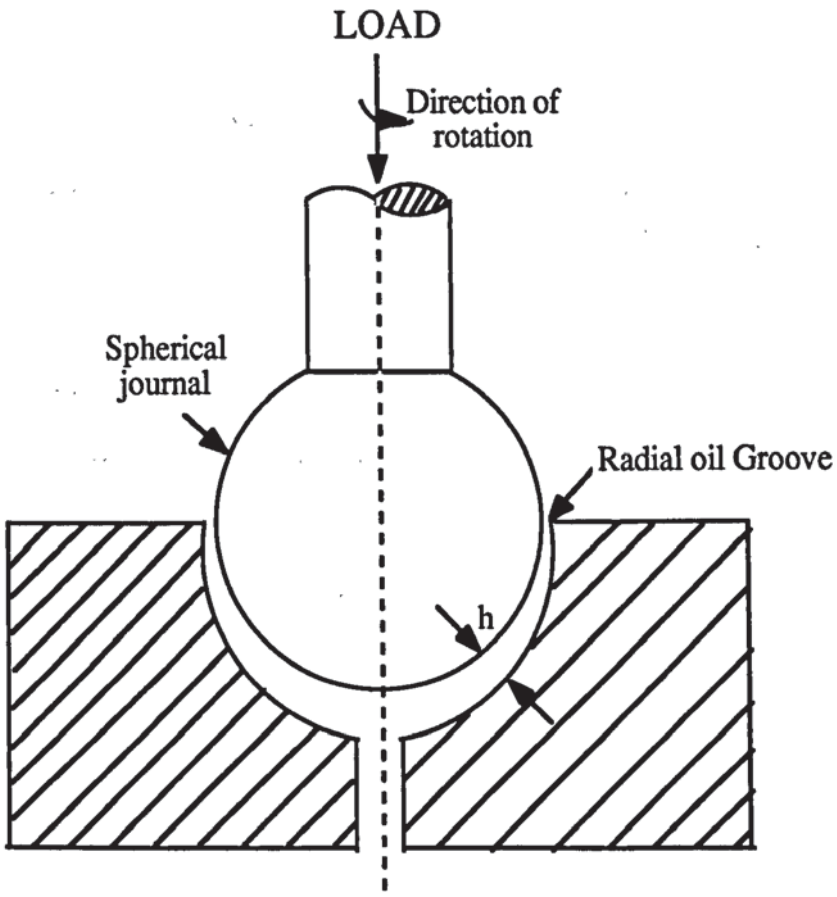

Figure 2.2.1.1.1
The Hydrosphere showing the shape of lubricating film

This bearing consisted of a spherical ball seating in a hemispherical or semi-hemispherical seat, with the seat having the same or greater radius than the ball, which may be grooved or plain. It was evident that despite the absence of the usual wedge-shaped oil film in the direction of motion of the moving bearing surfaces, the bearing produced positive pressure. As stated by the authors, this was achieved, by the presence of a wedge normal to the direction of motion. This wedge would exist as long as there was flow within the

bearing in the normal direction. When applying Reynolds' differential equation to the bearing, the authors discovered that there seemed no evidence that this wedge normal to the direction of motion would be capable of producing a positive pressure. By studying this work conclusions can be made that Reynolds' assumption that he might neglect the inertia forces in developing an expression for the pressure distribution equation would not apply to such bearings. This was argued by Blok and Cameron[8] in the following year after Shaw and Strang had presented their work. Blok and Cameron put forward an elaborate analysis to prove that the centrifugal forces which act on oil are small compared with the corresponding pressure and viscous forces.

Amongst others who commented on the theoretical analysis carried out by Shaw and Strang were Dowson and Taylor[9], who confirmed Strang's analysis. Despite their earlier confirmation Dowson and Taylor[10] in a later paper argued that the inertia effect could not account for the performance of the Hydrosphere bearing. Other factors such as thermal effects on the lubricant, and differential expansion of the bearing solids needed to be considered to account for the performance of such bearings. By analysing the thermal effect, they concluded that the probable explanation of the performance of these bearings would be "the hot land between the cool bearing surfaces distorting to give a true physical wedge, and hence the hydrodynamic action". In further consideration of the thermal effect, the authors considered the variation of viscosity with temperature due to the high speed of the hydrosphere. Their analysis indicated that an increase in the temperature caused a decrease in the viscosity of the lubricant and this resulted in a decrease in the load carrying capacity of the bearing. Nevertheless, Blok[8] commented that the effect of inertia in producing positive pressure in thrust bearings can "be evident and play an important secondary or triggering role".

The effect of inertia may be similar to the effect of viscosity in other problems in fluid mechanics. The drag on an aerofoil is one such example. It is debatable that viscous forces are completely negligible since aerofoils operate at high values of Reynolds' number, which means that viscous forces are small compared with inertia forces.

However, viscosity plays an important secondary role in the relatively thin layer of fluid immediately adjacent to the aerofoil, that is, within the boundary layer. In this example the viscosity alters the point of separation of the fluid from the aerofoil surface which results in large changes in pressure drag. Thus in aerofoil theory, viscosity introduces a negligible viscous drag, but it provides the mechanism for triggering large changes in pressure drag. Therefore in hydrodynamic lubrication problems with a low value of Reynolds' number the inertia forces may be negligible relative to viscous forces, but this fact should not exclude the possibility that these small forces can instigate significant effects.

The effect of inertia on the performance of gas lubricated thrust bearings has also been considered over the years. Gupta and Kapur[11] carried out an investigation which included the consideration of the effect of both radial and rotational inertia while assuming the gas to be supersonic at the entry to such bearings. They concluded that there was a reduction in the load carrying capacity of the bearing. The reduction of this load carrying capacity, they state, could be lessened by increasing the speed of the rotor.

Hasegawa and Izuchi[12], however, when investigating the performance of the same bearing under the same conditions concluded that the load carrying capacity of the bearing increased due to the compressibility of the gas. Although the findings of these authors differ, it should be noted that the important factor to be remembered is that the effect of inertia forces in lubrication system cannot be ignored where a non-conventional lubricant is used

In 1970 Constantinescu[13] presented a paper in which he investigated the influence of inertia forces in turbulent and laminar self-acting films. The author developed an analytical method for an infinitely long bearing, applicable to both laminar and turbulent films for both incompressible and compressible flow assumptions. By considering the conservation of streamwise momentum across the gap and assuming the velocity profile to have a parabolic form, he derived an expression for the pressure distribution allowing

for inertia effects. The author concluded that the magnitude of inertia forces in the case of incompressible flow is controlled by a modified Reynolds' number, that the effect of inertia may be significant for high Reynolds' number and particularly for geometries where there is an abrupt change of film thickness e.g. step bearing. The author provided no experimental results but stated that the solutions obtained showed a good agreement with experimental data by Smalley *et al.*[14].

In the present work there is no abrupt change of film thickness to justify the inclusion of inertia effects in the analysis. Nonetheless the lubricant considered has a very low viscosity compared with the conventional lubricating oil for which the inertia forces are negligible by comparison with viscous forces and it is judged that inertia effects should be included.

Constantinescu and Galetuse[15] later developed the original analysis by Constantinescu to improve the accuracy of evaluation of inertia effects in laminar and turbulent films. Using the momentum integral equations in the same form as in the earlier work[13], the authors presented an analysis from which they concluded that the influence of inertia forces would be to convert the static pressure into dynamic pressure only partially, when the flow is accelerated, as opposed to the previous findings that a total conversion would take place. The expression deduced for the pressure distribution contained three correction factors for the inertia effects whereas the previous expression[13] contained only one. A comparison between some measurements and the solutions obtained from theory was presented. However, the authors did not state when or under what conditions the inertia effects could be neglected.

Constantinescu *et al.*[16] extended the previous analyses to compare the effect of inertia forces in lubrication theory for both laminar and turbulent flows. A number of cases were considered, namely, air flow past a semi-circular protuberance to represent an asperity, i.e. point of metal to metal contact, within the flow field, air flow in a partial arc journal bearing and a journal bearing operating in a vortex flow regime. The authors modified the

motion and energy equations together with the velocity profile in order to consider each individual case, and included proper consideration of conditions for film rupture, cavitation or separation. They presented a number of graphs and tables comparing experimental and calculated pressure distribution for the various situations which show a reasonably good correlation. As the authors themselves suggest, it should be noted that a proper comparison between experimental results and prediction using their theory can be achieved only by giving full consideration to factors in the experimental data. These include establishing the true extent of lubrication region, imposition of proper boundary conditions, consideration of type of flow, entrance conditions, cavitation, separation or conditions for film rupture.

Kennedy *et al.*[17] presented a second paper on the subject of inertia effects in thin film lubrication, expanding their earlier investigation[15]. The authors determined the effect of inertia in lubricating flow past protuberances shaped either like circular disks with parallel surfaces or like spherical segments. By introducing a numerical solution, the authors attempted to improve their previous analytical solution to overcome the need for peculiar features of the flow such as inlet conditions, boundary conditions etc, when attempting to use the method for comparison with a physical situation. By considering the equations of motion and continuity together with an assumption of parabolic velocity distribution, which was not affected by the inertia forces, the authors developed expressions for the pressure and flow distribution both with and without the inclusion of inertia effects.

The equations were solved numerically using finite element methods and results were compared for the cases with and without inertia. Kennedy *et al.* concluded that convective inertia would significantly affect the pressure distribution, even at moderate Reynolds' numbers. They also concluded that the effect was more significant with disk shaped protuberance than with spherical ones, and in general inertia effects cause a pressure drop in the region of the asperity, and an increase of smaller magnitude, outside the asperity boundary. The authors did not present any direct comparison between their predictions and experimental results. However, they did compare the predictions with

those previously obtained by other analytical methods, which had shown a reasonably good correlation with direct measurement.

The effect of fluid inertia forces on the dynamic behaviour of journal bearings in a 'superlaminar' flow regime was investigated by Hashimto *et al.* [18]. Assuming a "short bearing", in the case of the length-to-diameter ratio of 0.5 and by using a velocity averaging method, the authors solved the momentum and continuity equations analytically with inclusion of the inertia term for flow regimes with Reynolds' numbers of Re=2750, 4580 and 5500. They concluded that the inertia effects on the dynamic behaviour of oil film journal bearings were even more pronounced than the effects of turbulence, and that under certain operating conditions they contributed to enhancing the stability of rotor-bearing systems. The authors did not present any comparison between their predictions and experimental measurements.

The effect of lubricant inertia in an externally pressurised thrust bearing with an viscoelastic lubricant was investigated by Roy and Biswel[19]. They concluded that with a given flow rate the load carrying capacity of the bearing reduced due to the inertia forces, while the elasticity of the lubricant made this parameter increase.

In 1955, Brand[20] published a valuable paper in which he showed that the consideration of inertia forces in some laminar oil film flow in lubrication systems may explain certain high speed phenomena not adequately accounted for by the usual Reynolds' analysis. By equating the inertia term and that of viscosity in the equation of motion developed by Navier, Brand defined a modified Reynolds' number. If, in any laminar flow system, this number was unity then the inertia term becomes of the same order as the viscous term in that lubrication system. For a thrust bearing if the Reynolds' number $\rho\omega h/\eta$ is of the same order as R/h (where ρ,ω,h,R,η are the density, rotational speed, film thickness, the radius of the runner and viscosity respectively), then the inertia forces will be the same order as the viscous term. In the case of a journal bearing $\rho\omega c/\eta$ should be the same

order as R/c (where c is the radial clearance), for the inertia force to be the same order as the viscous term.

Since the launch of nuclear reactors for the generation of electrical power in recent years, there has been a steady increase in the use of unconventional lubricants such as liquid metal which have a low kinematic viscosity. These changes have resulted in bearings being operated at a large Reynolds' number and consequently there may be turbulent flow within the film. The effect of inertia and thermal distortion of bearings in such applications has therefore become more evident. A number of researches have investigated these effects in detail. Macken and Saibel[21] listed investigators who had examined the inertia effects in bearings operating under turbulent conditions. Searching through the reported work, they conclude that due to the nature of turbulence in bearings, complicated by the formation of vortices, more thorough analysis is necessary in order to to understand the nature of such phenomena. Since the turbulent flow in bearings is different to that inside pipes, these authors also recommend that for understanding this effect more measurements of the mean and fluctuating components in such systems are required.

In more recent work Chowdhury and Ahmadi[22] investigated the operation of thrust bearings in turbulent inertial regimes. As previously found by Sinha Roy[19], these authors conclude that a rise in the temperature of the lubricant due to the high speed, reduces the viscosity of the lubricant which in turn decreases the load carrying capacity of the bearing. The effect of inertia on the performance of the bearing is reported to be very significant and justifies further investigation. The authors presented no direct comparison between measured and predicted results.

In the present work the effect of inertia has been included in the analysis, since the lubricant used is of a low kinematic viscosity when compared with a conventional lubricating oil, but the analysis used has retained the assumption of laminar flow.

Despite the limitation of the assumption made by Reynolds, his equation for the pressure distribution of bearings has been widely used for many types of bearings and applications including the sliding vane compressor. Platts[23], in a paper presented at the 1972 compressor conference at Purdue University, states that before 1960 this type of compressor was used to supply workshop air at moderate pressures of about 6 to 8 bar. Therefore the vanes could be made of Phenolic resin laminates using various bases such as asbestos cloth to give a strong, light weight with non-scoring properties. However, by 1967 the vane tip speed and loads were increasing to produce higher air pressures and as a result, vanes had to be made from aluminium-silicon alloy to give a good resistance to wear and corrosion. Aluminium-silicon alloys have a low thermal coefficient of expansion. Platts deduced the pressure distribution in the oil film at the interface of the vane tip and the stator by solving Reynolds' equation of the following form.

$$\frac{\partial p}{\partial x} = 6\eta\ U\left(\frac{1}{h^2} - \frac{k}{h^3}\right) \qquad (2.2.3)$$

where η is the absolute viscosity of the fluid, h is the film thickness and k is a constant related to the geometry of the bearing.

A more detailed discussion of Platts' analysis is given in Appendix 1.

2.3 Two-Phase lubrication

The importance of investigating two-phase lubrication systems was recognized when the use of unconventional lubricants in bearing systems became more widespread. These unconventional lubricants undergo a phase change due to either a high operating temperature or a high shaft speed, resulting in the formation of bubbles which can alter the bearing performance. The subject has been studied by several researchers over many

years to determine the effect of phase change of the lubricant on the characteristics of bearings operating under these conditions.

A theoretical analysis of parallel surfaces lubricated by bubbly oil was carried out by Tonder[24]. In order to simplify the analysis the author considered an infinitely wide hydrodynamic bearing and as a result the variation of pressure along the width of the bearing was ignored. The author also neglected the effect of the viscosity changes in the lubricant due to the presence of bubbles and considered only the variation of the density of the lubricant due to the bubbles. By introducing the isentropic relation given by equation (2.3.1) for the density of the lubricant and substituting it into the Reynolds equation for a parallel surface hydrodynamic bearing, Tonder developed an expression for the pressure distribution along the surfaces of the bearing lubricated by bubbly oil.

$$\rho_d = \rho_r \frac{1}{1+\beta p_k^{-1/\gamma}} \qquad (2.3.1)$$

where ρ_d is the density of the mixture, p_k is the bearing pressure, γ is the exponent in the pressure-density relationship and β is the volume ratio of gas to pure lubricant at atmospheric pressure.

From this analysis, Tonder concluded that :

1) The presence of gas bubbles would not generate positive pressures and thereby load carrying ability, but would modify and inflate the pressure produced by other means such as the decrease of the density due to the increase in the temperature, thereby causing a pressure build up.
2) In the case of the externally pressurised bearing, for a given geometry, the entrapped bubbles in the lubricant would increase the load carrying capacity of the bearing.
3) The lubricant volume flow rate would increase while the mass flow was reduced.

The findings of Tonder were not supported by any physical investigation. His first conclusion listed above was, in particular, based on the assumption that the bearing had an infinite width. However, as stated by the author this assumption was made to simplify the mathematical analysis and its validity although not proved, could be justified mathematically.

Tonder[25] also investigated the effects of gas bubbles in oil on the lubrication of parallel surfaces. His physical model included a small leading chamfer which was capable of producing load capacities comparable with those of Mitchell bearings having a similar temperature distribution. Taking into account that bubbles can cause a pressure build up, as concluded in his earlier work, Tonder neglected the effect of surface roughness/waviness and temperature changes within the film. He then applied a simplified approach to the problem of oil temperature, by assuming that the temperature increases from the leading edge towards the outlet region caused the density to decrease. By solving the Reynolds' equation and considering that the density and viscosity of the lubricant are functions of temperature but are unaffected by the presence of gas bubbles, Tonder predicted the pressure distribution for the bearing. His graphs of pressure distribution show that the peak pressure for the bearing is larger in the case of non-bubbly oil than with bubbles present. They also show that the presence of bubbles resulted in an increase in the load capacity of the bearing.

In a later paper Tonder[26] considered the effect of gas bubbles on the behaviour of an isothermal Mitchell bearing. His approach to the problem was similar to his previous work[24] and the predictions show that the non-dimensional load capacity of the Mitchell bearing is almost unchanged by the presence of gas bubbles.

Although in Tonder's analysis the model is further simplified by neglecting any possible temperature distribution, the conclusion is very important in that it suggests caution should be exercised in connection with straight Mitchell bearings if the presence of bubbles in the lubricant is suspected. The pressure distribution curves presented in

Tonder's paper are included here in Figure 2.3.1. Note that the parameter k is defined by the author as $(H_{max} - H_{min})/H_{min}$.

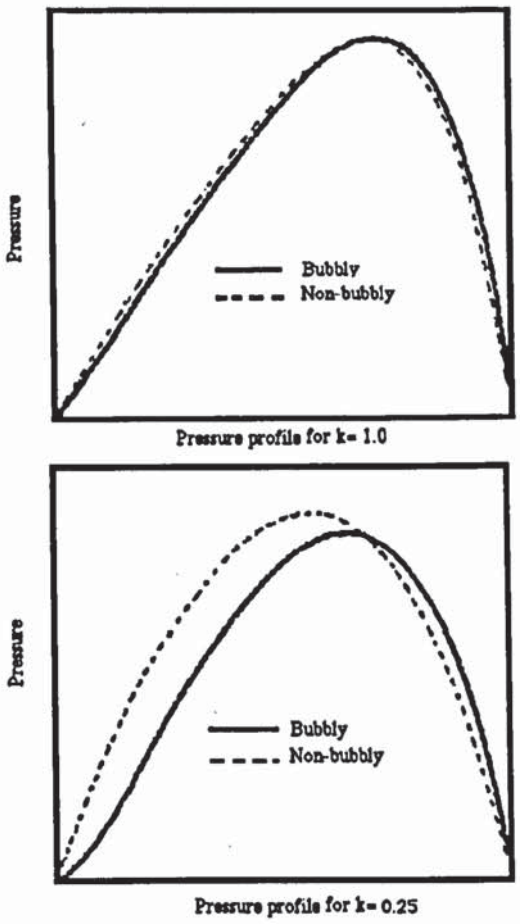

Figure 2.3.1
Pressure profile given by Tonder

F.K. Orcutt [27] investigated a steam lubricated thrust bearing. Since under most practical conditions, condensation can be expected to occur in a such bearing, this will become a problem of two-phase flow. His physical model consisted of a plane circular surface thrust bearing with a single, centrally loaded inlet nozzle. To study the significance of condensation, Orcutt cooled the stationary lower bearing plate in a controlled fashion, while the upper rotor which was made of glass, a low conductive material cemented to the end of a spindle was maintained at a fixed temperature so that an adiabatic upper boundary would be provided for the lubricant film.

From his investigation, Orcutt concluded that there was a sharply defined load carrying limitation for the steam lubricated bearing, which, when exceeded, resulted in a sudden

collapse of the bearing and surface contact after condensation. By comparing the pressure distribution measured in the steam lubricated experimental bearing with the theoretical pressures for the same conditions, but assuming a single-phase lubricant having the properties of dry steam, he also concluded that the experimental pressures and, therefore, that the load carrying capacity are lower.

It is unfortunate that although Orcutt's findings provided valuable practical information, no correlation was produced between theory and practice. There also seemed to be some defect with the test apparatus which tended to produce unexpected results for the performance of vapour lubricated thrust bearings. For example the glass rotor plate used in his apparatus would be liable to distort due to the temperature gradient, which resulted in non-uniform bearing clearances. This is probably why there is a large discrepancy between the theoretical pressure distribution of a single-phase lubricated bearing and that which Orcutt observed from his experimental apparatus.

Zuber and Dougherty[28] derived a system of equations which described a two-phase Reynolds' film flow with a phase change of lubricant. They solved the equations of continuity, motion and state for the mixture, the equation of thermal equilibrium for the vapour and the constitutive equation of condensation or of evaporation simultaneously. Using these equations they showed that the process of condensation and/or evaporation could be accounted for by a dimensionless phase change number, which appeared respectively as a vapour sink or a vapour source in the governing equations. The authors also showed that this sink or source could become the dominant term in determining the state and dynamic characteristics of a vapour-lubricated bearing. When the phase change number is zero, their equation reduces to the saturated Reynolds' equation for gas lubrication film flows. The authors did not make any experimental investigations to show if their analysis would agree with any physical situation, but anticipated that the equations which they had derived would be used in two-phase, vapour-liquid lubrication systems to modify Reynolds' equation from the form used in gas and liquid lubrication systems. No paper has been found which adapts these analyses.

During another investigation F.K.Orcutt[29] observed for the first time that film boiling can also occur in mechanical end face seals. In a mechanical seal the aim is to keep the separation between solid surfaces to a minimum so that any leakage can be minimised. But it is also desired to reduce wear and also maintain separation of the faces by using a lubricating film. It is these requirements of the face seal which must be met in spite of changing operating conditions and in the presence of machinary vibrations that could lead to an extremely high shear rate within the lubricating film, resulting in film boiling. Based on his experimental observation, Orcutt concluded that the mechanics of lubrication and leakage control in face seals are characterized by two large-scale regions which he describes as "the first is an annular region in the film adjacent to the seal cavity which is occupied almost entirely by liquid with a second annular region extending from the atmospheric edge of the interface to a semi-stable boundary with the liquid-filled region. This region is occupied by a mixture of liquid and vapour with vapour as the matrix phase." Orcutt did not present any analysis by which this problem could be studied but his observations led to a number of investigations into the mechanics of lubrication of face seals by various researchers who treated the problem by assuming that the lubricating film was not simply a liquid-filled interfacial film but a multi phase film.

In a recent publication by Nau[30] a comprehensive survey of research in mechanical seals has been carried out. The author examined the extent of knowledge of, how and why mechanical seals perform so well at times but are occasionally so unpredictable. One of the problems discussed was the performance of seals when used in environments where volatile liquids were close to their boiling point. It was stated by the author that in such circumstances bursts of leaking vapour escape discontinuously, with accompanying friction fluctuations on a time scale of the order of one second which introduces noise pollution. Although Nau presents some useful but brief information on how these problems can be overcome he provides no detailed analysis of the phenomenon or the basic causes. However, the author has listed a number of researchers who have investigated the phase change in face seals since it was first observed by Orcutt [29].

Hughes *et al.* [31] were, perhaps, foremost amongst those who developed Orcutt's ideas of the concentric two-part film, namely liquid and vapour. The authors confirmed Orcutt's finding in that under appropriate conditions, boiling or flashing may occur in the seal with a consequent drastic reduction in leakage rate. This can take place when the liquid being sealed is near to saturation conditions: a phase change from liquid to vapour may take place because of the simultaneous rise in the temperature due to viscous dissipation and the pressure drop through the seal. In their report, the authors analysed the phase change, taking into account the heat transfer in the seal plate. They concluded that for a seal of given film thickness and pressure differential, the mass flow rate is less for a gas than a liquid, even though the volumetric leakage rate of gas is greater than for a liquid. This is primarily the result of the density ratio of liquid/gas being much greater than the viscosity ratio. The model described by Hughes *et al.* is based on the assumption that boiling takes place at a discrete interface and also that water vapour close to its boiling point may be treated as an ideal gas. The authors took no account of the effect of vapour formation on density and viscosity and limit their consideration to the effect of leakage through the seal as the result of vapourisation. Their assumption that phase change is instantaneous and complete at a discrete radius in the seal, and the neglect of the effect of vapour on density and viscosity during phase change introduces errors which limit the value of their analysis. The instantaneous phase change can only take place at supercritical pressures e.g. greater than 221 bar and 370 $^{\circ}$C for water.

Hughes and Chao[32] developed an earlier investigation[31] which considered the phase change in liquid face seals taking into account both isothermal and adiabatic solutions, with particular attention to the leakage rate and the stability. Their isothermal and adiabatic models for a low Reynolds' number included consideration of numerical integration of the descriptive equation for a real fluid, including in the computer program the properties of steam and water to represent the working fluid. The authors concluded that for a low leakage rate the isothermal model can be used to describe the seal performance whereas for high leakage rate the adiabatic model can be regarded as more reliable. In claiming this, the authors provided no experimental evidence nor did they

make any comparison with any other work which might have been carried out previously. The adiabatic model which they describe takes no account of lubricant property changes across the lubricating gap. In addition, for the viscosity of the mixture they employed a linear relationship based on vapour quality without any comment on whether the use of other relationships might have had any influence on the results.

Turbulent two phase flow in shaft face seals was later investigated by Beatty and Hughes[33]. These authors presented an analysis for the calculation of leakage rate and opening force for aligned face seals operating in two phase flow regimes. Their analysis included integration of the continuity equation across the lubricating film and the use of a simple equation for the film- averaged radial velocity, while assuming that heat transfer between the fluid film and the seal could be neglected on account of the high radial velocity. Again the assumption of ideal gas behaviour was employed for the all-vapour flow zone. From their analysis, the authors concluded that the leakage rate could be reduced when vapour is produced by the combined effects of viscous dissipation and pressure drop. By subcooling the incoming fluid partially, they stated that the effect of dissipation and pressure drop on the leakage would be reduced. Again the authors provided no experimental results to verify their theoretical findings, and in their mathematical model they ignored the variation of properties of lubricant across the gap, an assumption which may introduce serious errors, as discussed in relation to reference[32].

The research considered most relevant to the present investigation was carried out by Yasuna and Hughes[34]. This model takes account of varying temperature, continuous boiling and thermal effects in the fluid, and predicts the resultant effect on seal stability and leakage rate. From their analysis the authors concluded that for most seals operating under laminar flow conditions and for large film thicknesses, the convective heat transfer within the fluid film effects are important and often dominate dissipation effects; thus the isothermal discrete boiling model may be inadequate to describe fully the seal behaviour. As for leakage, they concluded that when convection becomes important a higher leakage can be expected. The authors did not take account of the variation in thermodynamic

properties of the lubricant across the film thickness, nor did they provide any experimental results for verification of the mathematical model. In addition, the thermodynamic properties of the lubricant were determined from the equivalent saturation properties at the same temperature which was acceptable for water but may not be suitable for other fluids where the densities and viscosities are sensitive to pressure variation.

While the fundamental equations of motion and heat transfer used by the investigators obviously apply to the conditions of the present investigation, the manner in which the authors have used average values of velocity to determine viscous dissipation does not represent dissipation correctly within the fluid film. Also their use of average fluid properties based on a local mean film temperature to determine the pressure distribution compounds the error.

2.3.1 Viscosity and Density Variation in Lubrication Systems

In any two phase lubrication system there are two parameters which need particular consideration. These are the viscosity and density of the fluid. The effect of variable viscosity and density of the lubricant has been investigated by a number of groups.

Under most normal bearing operations viscosity changes are not due to the development of a two-phase mixture, but an increase in the temperature of the lubricant. For instance, Rajalingham and Prodhu[35] presented a paper in which they investigated the influence of temperature on journal bearing characteristics with a particular reference to the variation of viscosity. Their investigation lead to the understanding that the early theoretical predictions of the characteristics of these bearings had deviated from those obtained in practice due to the neglect of the effect of the temperature on the viscosity of the lubricant. By taking into account these variations, the authors concluded that for a given load and speed the decrease of viscosity caused by viscous dissipation increased the peak pressure and the volume flow rate but decreased the friction. The authors state that when considering the dependence of the viscosity on the temperature, their predicted results agreed more clearly with the measured values, than when assuming an isoviscous solution.

Jain *et al.*[36] also investigated the effect of viscosity variation in determining the performance of journal bearings. Their work was concerned with the effect of pressure on viscosity for both laminar and turbulent regimes in these bearings. In high pressure contacts such as those of journal bearings, the viscosity of the lubricant was high compared to that at ambient pressure. They concluded that both in laminar and turbulent flow conditions, the load capacity increases with an increase in the sensitivity of the lubricant viscosity to the pressure. The authors did not state any experimental results to confirm the validity of their findings.

Variation of viscosity in lubrication systems has not only been considered in two-phase cases, but also in problems where the viscosity variation with temperature are of exponential form. Tipei and Beguevrce[37] investigated the thermodynamic problem for an exponential lubricating film shape. The authors introduced an energy equation to be solved simultaneously with Reynolds' equation, by using a relationship between viscosity and film thickness. The viscosity was exponentially related to the film thickness as

$$M = \left(\frac{H}{H_1}\right)^q \qquad (2.3.2)$$

where $M = \frac{\eta}{\eta_1}$ = dimensionless viscosity

$H = \frac{h}{h_2}$ = dimensionless film thickness

$H_1 = \frac{h_1}{h_2}$ = Max dimensionless film

q = exponent characterizing viscosity variation with film thickness

From this assumption, the authors developed more simplified forms of the Reynolds and energy equation, each of which could be solved analytically. By solving these simple formulae, the characteristics of bearings operating with convergent lubricating films was predicted. However, the theoretical predictions were not compared with results obtained in practice.

Shukla *et al.*[38] considered the effect of viscosity variation in lubrication of rough surfaces. As in the case of viscosity variation along the film thickness for smooth and curved surfaces with converging films[37], Shukla *et al.* assumed a power relation between viscosity and film thickness. They concluded that in the case of a hydrostatic bearing with longitudinal radial roughness exhibiting a viscosity variation across the film, the load carrying capacity increased with a rise in viscosity across the film. The authors' theoretical results were not confirmed with any form of physical model and their validity remains uncertain.

In the case of bearings with rough surfaces, the power relation used for the viscosity of the lubricant is given as equation (2.3.3)

$$\eta = \eta_0 \left(\frac{H}{h_1}\right)^n \qquad (2.3.3)$$

where

η = The variable viscosity

η_0 = The minimum viscosity

H = Total film thickness

n = A variable between 0 and 1 depending upon the operating conditions of the bearing

h_1 = nominal part of the film thickness

It can be seen clearly, $H/h_1 <= 1$ and H decreases as x increases, the viscosity decreases along the film and it is highest when n=0 and lowest when n=1.

The effect of variable viscosity on the stability of plain journal bearings and floating-ring journal bearing operating with an incompressible single phase lubricant was first investigated by Nikolajsen[39]. Most previous theoretical analyses of the subject had treated the lubricating film as isothermal, an assumption which can be shown to be particularly invalid when the lubricant is compressible, where it results in a rise of temperature through the bearing film due to the film friction and a pressure/temperature relation of the isentropic form

$$\frac{p}{\frac{\gamma}{T^{\gamma-1}}} = \text{constant} \qquad (2.3.4)$$

Nikolajsen concluded that while the incorporation of a variable viscosity of the bearing film into the analysis complicates both the analytical and the numerical equation, its effect on the results was not very significant. In the case of the plain journal bearing, when treating the viscosity as a variable property, he finds that the minimum film thickness and the friction power loss do not deviate from the values obtained when assuming the viscosity to be constant. In the case of the floating-ring journal bearing a reduction of the friction power loss was noticed when the variable viscosity was taken into consideration. However, Nikolajsen's investigation was purely theoretical and did not have any practical results to verify his findings.

D. Dowson and J. D. Hudson[40,41] studied the thermo-hydrodynamic analysis of the infinite slider-bearing using a single phase lubricant. Although a thermo-hydrodynamic analysis normally considers the basic Reynolds' and energy equations, here the authors have attempted to introduce more realistic boundary conditions by considering the equation of heat conduction to the stationary and moving surfaces. A modified form of Reynolds' equation has been introduced, which allows for property variations along and across the lubricating film. In order to show the separate and combined effects of density and viscosity changes for constant and equal surface temperatures, they have presented computer solutions for the equations. They concluded that the change in lubricant density has a small effect upon the operating characteristics of a plane-inclined slider-bearing, but viscosity changes impose a serious reduction on the load carrying capacity. They also concluded that, for equal inlet conditions, the stationary surface achieved the higher temperature while the comparatively cool moving surface carried away the greater heat. Figure 2.3.1.1 shows the dimensionless pressure distribution curves obtained by Dowson and Hudson for both the stationary surface where the oil temperature is constant and the moving surface where it is changing linearly.

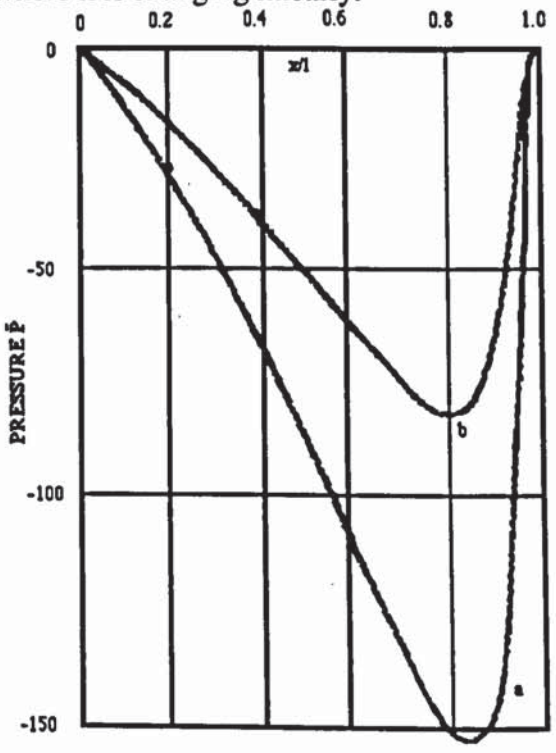

Figure 2.3.1.1
Pressure distribution curve presented by Dowson and Hudson
a) Constant oil temperature
b) Linear oil temperature

Figure 2.3.1.1 shows the dramatic change in pressure distribution brought about by a full thermo-hydrodynamic lubrication analysis. This change is due to the fact that the moving surface of the bearing receives a relatively small temperature rise compared with the corresponding rise on the stationary surface, with a corresponding effect on the distribution of fluid viscosity across the film.

Hahn and Kettleborough[42] presented a paper in which they predict the pressure and temperature distribution in an infinite slider bearing considering the effect of the thermal expansion of the lubricant and the thermal distortion of the bearing but neglecting the internal heat transfer in the lubricating film. This they achieved by solving the momentum, energy and continuity equations simultaneously for any given shape of the distorted profile. By taking into account the heat transfer to the bearing surfaces, they also presented a numerical procedure for obtaining the pressure and temperature distribution in the lubricant. These authors employed an exponential variation of viscosity and density with temperature. They concluded that the effect of variation of viscosity in the energy equation must not be neglected when the performance of these bearings is to be investigated, but did not have any practical results to support their theory.

Ezzat and Rohde[43] studied the thermohydrodynamic performance of the finite slider bearing. The equations of fluid film momentum, and energy were coupled to the heat conduction equations for solid surfaces of the bearing and were solved numerically. The effect of convective heat transfer in the lubricating film was neglected. By comparing their results to the isothermal theory, the authors concluded that the latter could overestimate or underestimate the bearing load carrying capacity and friction force, depending on the magnitude of the velocity of the moving surface. Although the authors did not compare their theoretical results with any experimental measurements, they did confirm the findings of Hahn and Kettleborough[42].

Huebner[44] considered a three-dimensional thermohydrodynamic analysis of sector thrust bearings. The author examined the steady-state behaviour of a bearing and presented a

numerical solution of the governing equations for the incompressible laminar flow of a Newtonian lubricant. The method of solution permits the use of a general film profile with viscosity taken to be a function of the three-dimensional temperature distribution in the film. Three dimensional heat transfer between the lubricant and the bearing surfaces was included in the analysis. In addition, the author has compared the thermohydrodynamic solutions with simplified solutions, including the isothermal and adiabatic cases. The research work conducted by Huebner in this paper is very similar to work of Ezzats[43], Hahn and Kettelborough[42] except that Huebner describes the application in more general terms.

Comparison of the thermohydrodynamic and the adiabatic solutions showed that the predicted bearing load, friction, and lubricant flow was more accurate when considered thermohydrodynamically, although significantly more computing time was required to solve the problem. A graph of non-dimensional pressure against the non-dimensional circumferential co-ordinates given by these authors is reproduced as Figure 2.3.1.2.

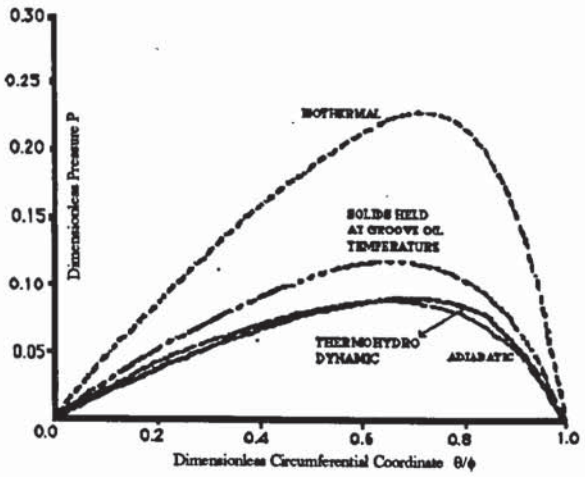

Figure 2.3.1.2
Pressure distribution for different solutions given by Huebner

The graph shows the isothermal solution compared to a solution of the fluid film equation with prescribed thermal boundaries. Both solutions are then compared with the thermohydrodynamic solution. It can be seen that, for a given set of operating

conditions, the former solutions overestimate the load carrying capacity. The authors did not include any experimental results for comparison with their theoretical findings.

The method which most closely relates to the problem of phase change within a bearing is the Bubbly oil-Thermohydrodynamic Analysis. In this analysis the heat convection within the lubricating film as well as the heat conduction between the lubricant and the surrounding bearing parts are included.

Abdel-Latif *et al.* [45] have used the thermohydrodynamic analysis of a thrust-bearing with circular pads running on bubbly oil, and have considered the steady-state behaviour of the rigid circular pads. They employed an iterative numerical scheme to solve the governing equations, viz. Reynolds' equation, the energy equation of the oil film, and the heat conduction equation for the pad. The system of equations was put into finite difference form and solved numerically. These authors assume that the viscosity of the lubricant (oil) varies in three dimensions and that the oil properties change due to the presence of bubbles. For calculating the viscosity distribution, they solve the energy equation of the lubricant using the three dimensional velocity components, which come from the solution of Reynolds' equation. In order to define the boundary conditions of the oil film Abdel-Latiff *et al.* included an additional equation for heat conduction between the oil film, moving and stationary parts of the bearing.

The Abdel-Latif *et al.* analysis is among the most advanced yet for the thermohydrodynamic analysis of bearings based on the assumption of constant density for the lubricant without reference to the possibility of phase change of lubricant.

In 1985, Feng and Hahn[46] published a paper in which they presented density and viscosity models for two-phase homogeneous hydrodynamic damper fluids. The authors state that the previous theoretical cavitation models adapted in analyzing dynamically loaded hydrodynamic bearings did not yield results consistent with experimental observations. Once bubbles are formed, they do not redissolve completely when the fluid

pressure has increased. They therefore suggest that the lubricant should be modelled as a homogeneous two-phase gas-liquid mixture, and the density and viscosity of such a homogeneous mixture should each be represented as, functions of the pressure and the known mole fractions of the noncondensable inert gas and liquid at supply entry.

In determining the density of the homogeneous mixture, they assumed that the effect of the dissolved gas molecules on the density of the liquid may be ignored and that the perfect gas law and Henry's law are still valid in the pressure range of interest. They also assumed that the mole fraction of the noncondensable gas to the liquid at the supply entry was known.

Feng and Hahn give two different expressions for the density of the mixture and quote four expressions for the viscosity which are as follows

$$\eta_m = \eta_f \qquad \text{(Owens)} \qquad (2.3.5)$$

$$\eta_m = \frac{1}{\frac{X}{\eta_g} + \frac{1-X}{\eta_f}} \qquad \text{(Isbin)} \qquad (2.3.6)$$

$$\eta_m = X\,\eta_g + (1-X)\,\eta_f \qquad \text{(Cicchitti)} \qquad (2.3.7)$$

$$\eta_m = X\,\eta_g \frac{\rho_m}{\rho_g} + (1-X)\,\eta_f \frac{\rho_m}{\rho_f} \qquad \text{(Duckler)} \qquad (2.3.8)$$

where η_m, η_g, η_f are the viscosities of the mixture, vapour and liquid phase of the lubricant respectively.

ρ_m,ρ_g,ρ_f are the densities of the mixture, vapour and liquid phase of the lubricant.

X is the mass fraction of vapour generated.

Feng and Hahn stated that the agreement between correlations for the theoretical predictions of equations (2.3.7-8) and experimental results was not very good. For an air-water flow, Gill *et al.*[47] compared correlations (2.3.5-6) with measurements and concluded that Owens' correlation usually overestimates, whereas Isbin's underestimates the pressure drop in two phase flow. This means that the equivalent viscosity of the

mixture in such a system is less than that evaluated by Owens and greater than that by Isbin. Although it should be recommended that the air and water mixture is not two phases of the same substance and may produce very different results from a single substance two phase mixture.

In order to see how the above correlations differed, graphs were plotted of the proportion of vapour against the relative viscosity of refrigerant Arcton R114. Figure 2.3.1.3 shows that a comparison of each expression proposed for a mixture which as shown by Feng and Hahn.

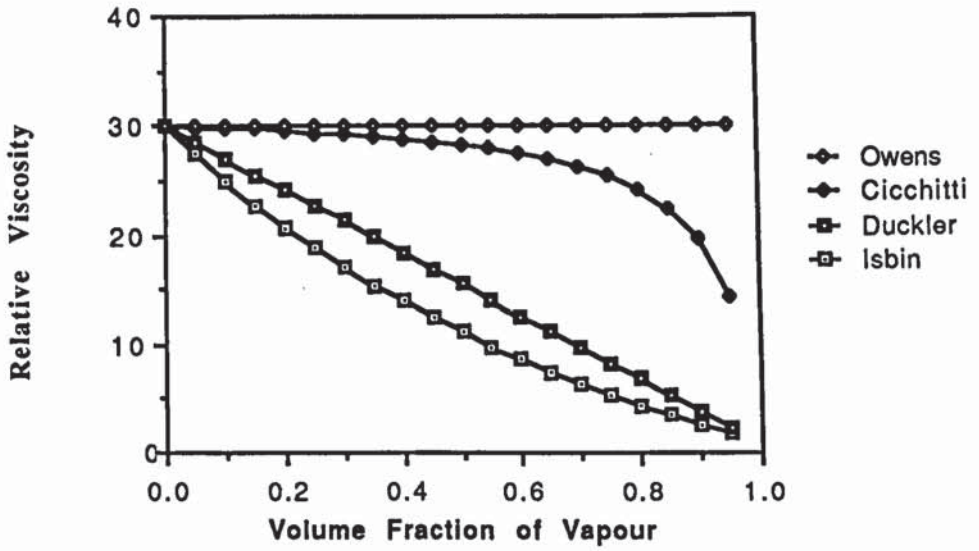

Figure 2.3.1.3
Comparison of expressions for viscosity of mixture listed by Feng and Hahn

It is evident from Figure 2.3.1.3 that Cicchitti predicts that the viscosity of a mixture is not altered by the presence of a small proportion of vapour, but it decreases as the vapour proportion increases. Duckler assumes a linear variation with the volume formation of vapour with mixture, while Isbin attributes an even greater effect to the presence of vapour.

2.4 Refrigerant Dissolving in Lubricating Oils

As mentioned in Chapter 1, refrigerant dissolved in oil can affect the lubrication properties of the oil used in compressors of refrigeration systems. This problem was recognized and studied as far back as 1938, when Ruttledge[48] published a paper in which he presented an analysis for the viscosity of oil diluted with refrigerants.

Beerbower *et al.*[49] published a paper in 1961 which produced valuable data for oils in contact with gases such as carbon dioxide, helium, argon, hydrogen and nitrogen. They examined many aspects of the problem from:

(i) Entrainment of gases in oil

(ii) Solubility of gases in lubricating oil

(iii) Stability of oils in contact with gases

(iv) Effect of dissolved gas on oil viscosity

(v) Lubricating quality of gas-saturated oils

Their one finding of relevance to the present work is that dissolved helium, halogen and nitrogen did not cause any appreciable loss of viscosity, while dissolved carbon dioxide reduced the oil viscosity and thereby causing a reduction in the load carrying capacity of bearings. This is in contrary to Tonder's[26] conclusion that the non-dimensional load capacity of the bearing was unaffected by the presence of gas bubbles. Beerbower's work was purely experimental and the authors did not present any expression for the viscosity of lubricating oils containing dissolved gases.

The dissolving of oil in liquid refrigerant, however, affects the thermodynamic properties of the working fluid[50]. The vapour pressures of the refrigerant-oil solutions at a given temperature are always less than the vapour pressure of pure refrigerant at that temperature. The presence of dissolved oil in an evaporator would therefore lead to a lower suction pressure and higher evaporator temperature than expected from pure

refrigerant tables. This would mean that in the design of a refrigeration system the selection of the compressor should be done with appropriate care.

The tribological performance of bearings is affected by refrigerant dissolved in oil. H. Kobayshi and N.Murata[51] carried out an investigation to find the cause of this. In a hermetically sealed compressor, they tested seven different bearings, each with a different length to diameter ratio and some with grooves for removing any entrained gases. The bearings were supplied with 20% and 0% of refrigerant to oil mixture and by producing the pressure distribution for each bearing, the authors obtained the following results.

In their type 1 bearing (see Figure 2.4.1) with a L/D of 2 and no groove, the pressure profile with 20% refrigerant in oil had a narrower width and a higher peak than that with 0% refrigerant. The 20% refrigerant in oil showed the typical pressure profile of starved lubrication. In type 2 bearing, which had a groove for oil supply, the same phenomenon as type 1 appeared except that the degree of starvation was somewhat less. In type 3 bearing which contained a groove not connected to the oil supply hole and open to the bearing side, the pressure profile with both 0% and 20% refrigerant were almost identical. This indicated that the groove removed the refrigerant gas accumulating in the cavitation region of the bearing clearance. The pressure profile for the type 4 bearing which had grooves for both oil supply and gas removal indicated that both grooves functioned well in removing the entrained gas and thereby preventing oil starvation. In type 5 bearing which had only one groove, whose lower edge was connected to the oil hole and upper edge open to the bearing sides, the pressure profile showed results very similar to that of type 4, indicating that the specially designed groove combined the functions of the oil supply and the gas removal groove. The effect of L/D was determined by using type 6 bearing (L/D=1) and type 7 (L/D=1/2). The pressure distribution of 20% refrigerant showed some degree of starvation but not as remarkable as type 1. Apparently, the smaller the fraction of L/D, the more refrigerant gas tend to flow towards the bearing sides.

The conclusion reached by Kobayshi and Murata was that the fundamental problem associated with refrigerant dissolving in oil used in compressors was that the refrigerant gas which evaporates and accumulates in the bearing clearance disturbs the oil supply distribution within the bearing. This problem can be overcome by designing a gas removal groove in the bearing.

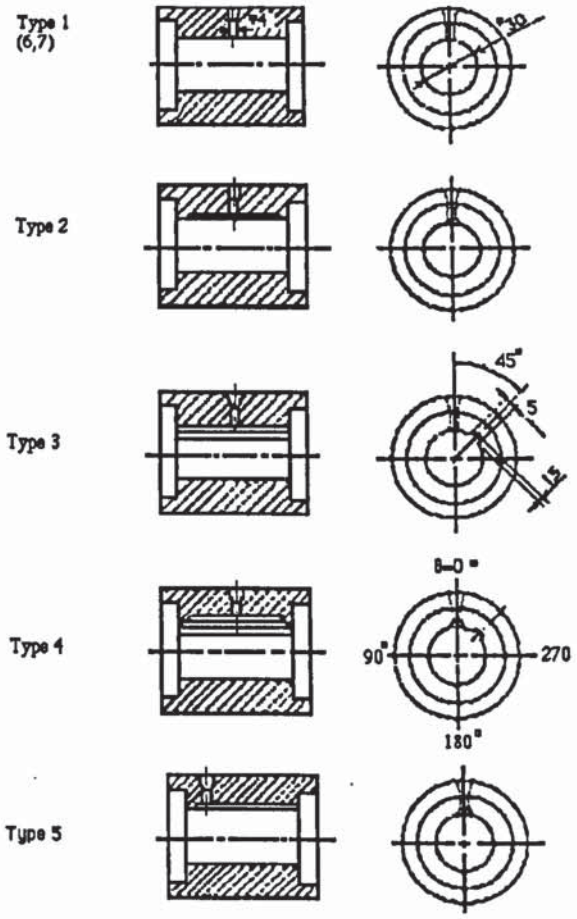

Figure 2.4.1
7 types of bearing used by Murata *et al.*

2.5 Liquid refrigerant used for lubrication

Halocarbon refrigerants have long been thought of as suitable lubricants to eliminate or reduce boundary lubrication. In 1956, S. Murry *et al.* [52] carried out an investigation to use difluorodichloromethane as an effective gaseous lubricant for steel bearing surfaces employed in turbine engines in particular. They used a kinetic-friction apparatus having a hemispherical specimen sliding on a rotating disk which was operated in an atmosphere of difluorodichlorometahne. They measured the friction force at a specified velocity and load for several types of steel materials each with a different hardness. The authors concluded that lubrication by these gases was dependent on a chemical reaction to form surface films and therefore it should be expected that for a given gas, lubrication effectiveness would vary with different metal combinations.

Amongst others who studied the potential of refrigerants for use as lubricants were Sanvordenker *et al.* [53] who reported that both R12 and R22 atmospheres had beneficial effects on an oils' boundary lubrication characteristic when compared to tests in air. They showed this by carrying out a series of tests to evaluate bearing materials, surface treatment and lubricants with a particular interest in fluorocarbon refrigerants. It must be noted that there are several bearings or rubbing surfaces in a refrigerant compressor, each of which may, use different materials and operate under different conditions. Therefore the conditions under which tests were carried out by Sanvordenker must be considered carefully before any conclusion can be drawn as to their importance relative to the lubrication of the sliding vane compressor. This is particularly true following the earlier warning by Murray *et al.*[52] that lubrication by halocarbon refrigerant is believed to be dependent on chemical reaction between the refrigerant and the surface to be lubricated.

Amongst other researchers who have investigated the effect of different fluorocarbon refrigerants as special lubricant for use in extreme conditions are Kools *et al.*[54]. In their report they concluded that chlorine- and fluorine- substituted methane and ethane

compounds can be regarded and employed not only as compounds used as refrigerants, but also, as gaseous lubricants or anti-wear additives. The work confirms the findings by Murry *at al*[52]. Both groups concluded that under boundary lubricated conditions the gaseous refrigerant dissolved in oil/lubricant can have tribochemical effectiveness. The refrigerant dissolving into the lubricant is transported to the point of contact between the friction bodies and forms reaction layers. In this event the refrigerant has the function of an anti-wear additive. The dissolution of the refrigerant into the lubricant does, however cause a reduction in the viscosity of the lubricant, and this would lead to a drop in the load carrying capacity of the bearing when supplied with lubricant-refrigerant mixture as opposed to being supplied with the lubricant only

2.6 Summary

The majority of practical and theoretical investigation of bearing and face seal performance related to a single phase of the lubricant. Only Hughes *et al.*[31] appears to have given detailed consideration on the generation of a liquid/vapour mixture within the lubricant film, due to viscous dissipation, yet the use of assumed velocity profile and the averaging of fluid properties across the film thickness must leave considerable doubt as to the adequacy of the predictions. It must also be recommended that these were not compared with measured experimental evidence.

The principal properties governing the effects resulting from vapour generation are viscosity and density. A range of viscosity relations have been proposed for liquid/vapour mixtures, but the only experimentally evident found relates to viscosity of bubbly oil, a mixture of two phases of two substances.

CHAPTER THREE

THEORY

3.1 Introduction

A theoretical approach is described in this chapter which considers the energy and momentum transfer between the fluid and its surroundings, together with mass conservation and the thermodynamic equation of state. This chapter also includes the development of a numerical method for predicting pressure, enthalpy, temperature, velocity, density and viscosity distribution for the rotor end face of a sliding vane compressor and a radially symmetrical hydrostatic bearing, taking full account of possible phase change developing within the lubricant film.

As stated in Chapter 2, Osborn Reynolds developed the first sophisticated analysis of thin film fluid flow, adapting the more general form of the momentum equations of Navier to the case of a single phase fluid flowing isothermally and essentially two-dimensionally, allowing for possible variation in film thickness. The treatment of situations in which there are significant changes in fluid density and viscosity requires that the energy equation and fluid property equations are also included in the analysis.

The intention to obtain experimental evidence of the pressure distribution in a hydrostatic thrust bearing with purely radial flow was outlined in Chapter 1. Details of the experimental bearing, ancillary equipment and test instrumentation are presented in Chapter 4. Since it is intended that predictions will be extended to investigate the possible development of two phase flow in the fluid film between the rotor end face and the stator of a sliding vane compressor, the full three dimensional equations are required. The fluid which offered the best opportunity for the experimental investigation of two phase flow was found to be the refrigerant R114, with a saturation pressure of 1.6 bar at atmospheric temperature, enabling evaporation conditions to be established at fluid temperatures which allow the neglect of heat transfer to the solid surfaces bounding the fluid film.

If the fluid film can be treated as a continuum then the momentum changes are characterised by the Navier-Stokes equations. These require to be expressed in a form

which allows for viscosity and density gradients. The analysis is based on laminar flow assumptions. The greatest dissipation of energy within the fluid film occurs close to the solid boundaries, in the layers of fluid subjected to the greatest shear effects. Unless the energy dissipated is conducted within the fluid or convected to the solid boundaries, the local temperature of the fluid will rise and the density and viscosity will change accordingly. When the local value of enthalpy exceeds that of saturated liquid at the local pressure, then evaporation takes place and the fluid properties become those of a mixture of liquid and vapour. The most general equations available to determine the property relations of the vapour phase are the Beattie-Bridgeman equations, which express the pressure in the manner of a polynomial form of Van der Vaals' equation using experimentally determined coefficients. The thermodynamic properties of the vapour phase, specifically the enthalpy, are found from general thermodynamic equations.

The following notation is used to outline the necessary momentum, energy and property equations:-

a, b, c	=Constants used for expressing velocity profile, defined where used
A	=Cross-sectional area
c_p	=Specific heat capacity at constant pressure(J/kgK)
h	=Specific Enthalpy (J/kg)
k	=Thermal conductivity (W/mK)
$\dot{m}$	=mass flow rate (kg/s)
r	=Radial co-ordinate
T	=Absolute temperature (K)
T_{crit}	=Critical temperature. For R114, T_{crit}=418.86 (K)
T_R	=Reduced temperature i.e. T/T_{crit}
u	=Radial lubricant velocity (m/s)
v	=Normal lubricant velocity (m/s)
w	=Circumferential lubricant velocity (m/s)
$\dot{V}$	=Volume flow rate (m^3/s)
x	=Mass fraction of vapour
y	=Normal co-ordinate
z	=Elementary layer thickness (m)
Z	=Total film thickness (m)
ρ	=Density (kg/m^3)

η =Dynamic Viscosity (Ns/m^2)

θ =Circumferential angular co-ordinate

Suffices

f ≡ fluid

g ≡ gas

m ≡ mixture

w ≡ at the wall

3.2 Momentum Equations

The Navier-Stokes equations describe the relationship between fluid pressure and momentum in shear flows. In cylindrical polar co-ordinates (r,θ,y), appropriate to the present investigation and allowing for viscosity and density gradients the equations take the following form as suggested by Byron Bird *et al.*[55]:

In the radial direction

$$\rho \frac{du}{dt} = -\frac{\partial p}{\partial r} - \left(\frac{1}{r}\frac{\partial}{\partial r}(r\tau_{rr}) + \frac{1}{r}\frac{\partial \tau_{r\theta}}{\partial \theta} - \frac{\tau_{\theta\theta}}{r} + \frac{\partial \tau_{ry}}{\partial y}\right) \qquad (3.2.1)$$

In the circumferential direction

$$\rho \frac{dw}{dt} = -\frac{1}{r}\frac{\partial p}{\partial \theta} - \left(\frac{1}{r^2}\frac{\partial}{\partial r}(r^2\tau_{r\theta}) + \frac{1}{r}\frac{\partial \tau_{\theta\theta}}{\partial \theta} + \frac{\partial \tau_{\theta y}}{\partial y}\right) \qquad (3.2.2)$$

In the axial direction

$$\rho \frac{dv}{dt} = -\frac{1}{r}\frac{\partial p}{\partial y} - \left(\frac{1}{r}\frac{\partial}{\partial r}(r\tau_{ry}) + \frac{1}{r}\frac{\partial \tau_{\theta y}}{\partial \theta} + \frac{\partial \tau_{yy}}{\partial y}\right) \qquad (3.2.3)$$

where

$$\frac{du}{dt} = \frac{\partial u}{\partial t} + u\frac{\partial u}{\partial r} + \frac{w\partial u}{r\partial\theta} + v\frac{\partial u}{\partial y} - \frac{w^2}{r}$$

$$\frac{dw}{dt} = \frac{\partial w}{\partial t} + u\frac{\partial w}{\partial r} + \frac{w\partial w}{r\partial\theta} + v\frac{\partial w}{\partial y} + \frac{uw}{r}$$

$$\frac{dv}{dt} = \frac{\partial v}{\partial t} + u\frac{\partial v}{\partial r} + \frac{w\partial v}{r\partial\theta} + v\frac{\partial v}{\partial y}$$

$$\tau_{rr} = -\eta\left[2\frac{\partial u}{\partial r} - \frac{2}{3}(\nabla.v)\right]$$

$$\tau_{r\theta} = \tau_{\theta r} = -\eta\left[r\frac{\partial}{\partial r}\left(\frac{w}{r}\right) + \frac{1}{r}\frac{\partial u}{\partial\theta}\right]$$

$$\tau_{\theta\theta} = -\eta\left[2\left(\frac{1}{r}\frac{\partial w}{\partial\theta} + \frac{u}{r}\right) - \frac{2}{3}(\nabla.v)\right]$$

$$\tau_{yr} = \tau_{ry} = -\eta\left[\frac{\partial v}{\partial r} + \frac{\partial u}{\partial y}\right]$$

$$\tau_{\theta y} = \tau_{y\theta} = -\eta\left[\frac{\partial w}{\partial y} + \frac{1}{r}\frac{\partial v}{\partial\theta}\right]$$

$$\tau_{yr} = \tau_{ry} = -\eta\left[\frac{\partial v}{\partial r} + \frac{\partial u}{\partial y}\right]$$

$$(\nabla.v) = \frac{1}{r}\frac{\partial}{\partial r}(ru) + \frac{1}{r}\frac{\partial w}{\partial\theta} + \frac{\partial v}{\partial y}$$

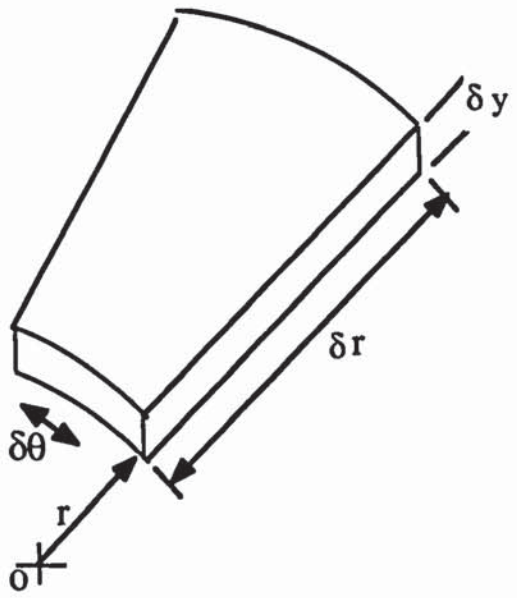

Figure 3.2.1
Details of a fluid element

The following assumptions are made in the present analysis:-

(1) Radially symmetrical adiabatic laminar flow with constant film thickness.

(2) Lubricating film subdivided into layers; layer thickness allowed to vary.

(3) Fluid, R114, behaves as a Newtonian fluid at all times.

(4) Property variations and phase change are fully accounted for.

(5) Heat transfer between the solid surface and the fluid is neglected. The heat transfer by conduction within the fluid film is accounted for.

(6) Negligible transverse velocities within the film.

It follows from the above assumptions, and the steady state conditions, that the Navier-Stokes equations reduce to:

$$\frac{\partial u}{\partial r}\left(\rho u - \frac{4}{3}\frac{\partial \eta}{\partial r} - \frac{4}{3}\frac{\eta}{r}\right) = \frac{\rho w^2}{r} - \frac{\partial p}{\partial r} - \frac{2u}{3r}\frac{\partial \eta}{\partial r} + \frac{\partial \eta}{\partial y}\frac{\partial u}{\partial y} + \eta\left[-\frac{4u}{3r^2} + \frac{4}{3}\frac{\partial^2 u}{\partial r^2} + \frac{\partial^2 u}{\partial y^2}\right] \qquad (3.2.4)$$

$$\frac{\partial w}{\partial r}\left(\rho u - \frac{\partial \eta}{\partial r} - \frac{\eta}{r}\right) = \frac{-\rho u w}{r} - \frac{w}{r}\frac{\partial \eta}{\partial r} + \frac{\partial \eta}{\partial y}\frac{\partial w}{\partial y} + \eta\left[\frac{\partial^2 w}{\partial r^2} + \frac{\partial^2 w}{\partial y^2} - \frac{w}{r^2}\right] \qquad (3.2.5)$$

The prediction of the local pressure gradient in the fluid film is complicated by the constraints of momentum, mass and energy conservation. The problem is greatly simplified if the nature of the directional components of velocity gradient can be assumed, as has been done by previous researchers. Hughes *et al.* [35,36] assumed a parabolic profile for the radial component of velocity within the film of a face seal and also for the axial velocity component in a shaft seal at all stations in the flow direction; this determines the velocity gradient explicitly. They then assumed that the tangential velocity component varies linearly between zero on the stationary surface and the local value on the moving surface. These two assumptions and a further assumption that the thermodynamic properties of the fluid do not vary across the thickness of the fluid film, but only in the flow direction, enabled the total dissipation of energy within the film to be evaluated. An average value of fluid temperature was then determined using the energy equation, from which any phase change could be determined.

It is inappropriate to evaluate the pressure gradient and property changes in relation to the average effect which the gross dissipation of energy has upon fluid properties. The generation of vapour bubbles locally within the film greatly reduces the viscosity and density and, in turn determines changes in the component velocity profiles of the film. If no assumptions are made concerning these profiles then it is necessary to iterate among the governing equations until the correct value of pressure gradient is found to satisfy the equations for momentum, mass and energy conservation, taking full account of local property variation within the film, and the constraint of a known film thickness.

Under suitable conditions, the film thickness and corresponding Reynolds number of the flow are such that laminar conditions should prevail. It is therefore possible to consider the film to be comprised of a number of unmixing shear layers whose individual thicknesses may vary in the direction of flow, but the sum of whose thicknesses must equal the local film thickness. For a seal with parallel faces the rate of change of layer thickness in the flow direction may be assumed to be negligible so that there is no transverse pressure gradient within the film. These assumptions and the tangential velocity of the moving surface, together with a prescribed distribution for the flow component of velocity only at the inlet to the bearing/seal enable a Runge-Kutta routine to be employed to determine the local pressure gradient in the flow direction.

3.3 The Energy Equation

In the steady fluid flow situation investigated, the energy equation relates the changes in fluid enthalpy and kinetic energy, to the effects of viscous dissipation and heat transfer within the fluid and possible heat transfer to the surroundings. The conditions of the experimental investigation were such that heat transfer to the surroundings was negligible and only conduction due to the transverse temperature gradients within the film needed to be considered in the theoretical approach.

3.3.1 Viscous Dissipation

The rate of viscous dissipation of energy due to shearing and strain in the fluid per unit volume of fluid is given by the equation[55]:

$$\Phi = 2\eta\{(\frac{\partial u}{\partial r})^2+[\frac{1}{r}(\frac{\partial w}{\partial \theta}+u)]^2+(\frac{\partial v}{\partial y})^2\}+\eta\{(\frac{\partial w}{\partial y}+\frac{1}{r}\frac{\partial v}{\partial \theta})^2+(\frac{\partial v}{\partial r}+\frac{\partial u}{\partial y})^2+[(\frac{1}{r}\frac{\partial u}{\partial \theta}+r\frac{\partial}{\partial r}(\frac{w}{r})]^2\} \quad (3.3.1)$$

The rate of dissipation per unit mass flow is given by:

$$\frac{\Phi}{\rho\sqrt{u^2+w^2}} \quad (3.3.2)$$

3.3.2 Conduction Heat Transfer

The rate of heat conduction across the film is determined by the Fourier equation as:

$$k A \frac{\partial T}{\partial y}, \text{ where } A = 2\pi r \delta r \quad (3.3.3)$$

Thus the complete energy equation becomes:

$$\frac{\partial h}{\partial r} = \frac{\Phi}{\rho\sqrt{u^2+w^2}} - u\frac{\partial u}{\partial r} - w\frac{\partial w}{\partial r} + k\frac{1}{\rho u z}\frac{\partial T}{\partial y} \quad (3.3.4)$$

3.4 Continuity Equation

In the present analysis it is assumed that the film thickness is subdivided into elementary layers and that the thickness of each layer varies in the direction of flow. The sum of all

layer thicknesses must be equal to the local film thickness, and the sum of all changes in thicknesses over a radial step must be zero.

The continuity equation for flow within an elementary laminar layer film may be written as

$$\frac{\partial z}{\partial r} = -z \left\{ \frac{1}{r} + \frac{1}{\rho}\frac{\partial \rho}{\partial r} + \frac{1}{u}\frac{\partial u}{\partial r} \right\} \qquad (3.4.1)$$

3.5 Thermodynamic and Transport Properties of the Fluid

The property equations are quoted with reference to the fluid chosen for use in the experimental investigation, i.e. R114, but the form of the equations is typical for any fluid.

3.5.1 Liquid Phase

3.5.1.1 Density

While the fluid remains in the liquid phase, its density is not significantly affected by pressure, except over extreme ranges. For the refrigerant R114 density is given by

$$\rho_f = 1 + C1(1-T_R) + C2(1-T_R)^{1/2} + C3(1-T_R)^{1/3} + C4(1-T_R)^2 \qquad (3.5.1)$$

where constants C1-C4 are deduced from the experimental determination of fluid properties. The values used are those quoted by Imperial Chemical Industries for their Arcton 114 refrigerant.

Equation (3.5.1) can be differentiated to give the density distribution as

$$\frac{\partial \rho_f}{\partial r} = -\frac{\partial T_R}{\partial r}\left[C1 + \frac{C2}{2}(1-T_R)^{-1/2} + \frac{C3}{3}(1-T_R)^{-2/3} + 2C4(1-T_R) \right] \qquad (3.5.2)$$

3.5.1.2 Viscosity and Thermal Conductivity

Again, as in the case of density, viscosity changes in the liquid phase are not significantly affected by fluid pressure. In the present situation the viscosity may be related to the temperature of the fluid. For the refrigerant R114 the ASHRAE Guide and Data Book[50] recommends the use of the relations:

$$\eta = 1454000\, T^{-3.8784} \qquad (3.5.3)$$

$$k = 0.057 \text{ W/mK}$$

3.5.1.3 Enthalpy

The enthalpy of the liquid is a function of temperature only, due to the incompressible nature, and has the approximate value of the enthalpy of liquid saturated at the given temperature, even if the actual state is that of a subcooled liquid. The enthalpy of saturated liquid is calculated using the Calusius-Clapeyron, as given in section 3.5.3.1. Calculation of enthalpies of saturated vapour and of the two phase region will be discussed in the following paragraphs.

3.5.1.4 Temperature

In single phase flow the enthalpy is directly related to the rate of change of temperature. If the specific heat capacity is assumed to remain constant then before evaporation takes place, the changes in temperature can be expressed as

$$\frac{\partial T}{\partial r} = \frac{1}{c_{pf}} \frac{\partial h}{\partial r} \qquad (3.5.5)$$

where c_{pf} is specific heat capacity of saturated liquid at constant pressure.

3.5.2 The Vapour Phase

3.5.2.1 Enthalpy

The pressure, specific volume and temperature of the vapour phase are related by the Beattie-Bridgeman equation, in which it is customary to employ 'reduced' values of these properties. The reduced values are obtained as the quotient of the true value divided by the property value at the upper triple point, the state of pressure and temperature at which the specific volume of saturated liquid and saturated vapour are equal. The appropriate values for the refrigerant R114 are as follows:

p_{crit}	=32.62508 bar
T_{crit}	=418.861 K
v_{crit}	=0.001718831 m^3/kg
subscript crit	≡ critical

In order to calculate the enthalpy of vapour it is necessary to know the saturation temperature of the fluid for any given pressure. Imperial Chemical Industries (ICI) relate the vapour pressure of R114 to temperature by equation (3.5.6).

$$\log_e p = \sum_{i=1}^{6} A_i y^{i+1} \qquad (3.5.6)$$

where A_i are given constants and $y = (\frac{1}{T} - 1)^{1/2}$

An iterative process allows this relationship to be inverted to find T (the saturation temperature, as a function of pressure), for use in the prediction of the fluid pressure gradient. To find T, the first constant is set as A(1)= -7.5 and the given pressure used as follows

$$\{(\frac{1}{T} - 1)^{1/2}\} = \frac{\log_e p}{-7.5} = -7.5 \quad \text{Or} \quad T = \frac{1}{A_1 + 1} \qquad (3.5.7)$$

The remaining terms in equation (3.5.6) are then included in the iterative process to give the accurate value of saturation temperature.

As quoted by Muneer & Scott [56], the difference in internal energy between two closely adjoining states is given by

$$de = C_v dT + p\,v + [\,T(\frac{\partial p}{\partial T})_v - p\,]\,dv \qquad (3.5.8)$$

But specific enthalpy is defined in terms of the specific energy, e, pressure, p, and specific volume, v as

$$h = e + pv \qquad (3.5.9)$$

Then using equation (3.5.8), the enthalpy can be written as

$$H = \int_{T_0}^{T} C_{v_\infty} dT + pv + \int_{\infty}^{v} [\,T(\frac{\partial p}{\partial T}) - p\,]\,dv + k_1 \qquad (3.5.10)$$

where

H	=	Enthalpy at v,T.
$C_{v\infty}$	=	Isochoric specific heat capacity at infinite volume.
p	=	Pressure.
k_1	=	Arbitrary constant which is chosen to make the value of reduced enthalpy equal to unity at the critical point.

Enthalpy, H, is calculated by working out each term in equation (3.5.10).

An expression for the specific heat of vapour is given by

$$C_v = d_1 + d_2T + d_3T^2 + d_4T^3 \qquad (3.5.11)$$

which is in terms of temperature only and can be integrated easily.

In equation (3.5.10), P and v are the given pressure and specific volume of gas. The value for saturated vapour pressure can be calculated by applying an iterative method to the Beattie-Bridgeman relationship for the vapour pressure given as

$$P = \frac{RT}{v-b}\sum_{j=2}^{5}\frac{C_{1j}+C_{2j}(T-1)+C_{3j}(e^{k(T-1)}-1-kT+k)}{(v-b)^j} + \sum_{j=6}^{7}\frac{C_{1j}+C_{2j}(T-1)+C_{3j}(e^{k(T-1)}-1-kT+k)}{e^{(j-5)\alpha(v-1)}} \qquad (3.5.12)$$

Equation (3.5.12) can also be differentiated with respect to T while keeping v constant to yield the third term in equation (3.5.10).

Details of the above calculations are included as flow charts in Appendix 3. To make the value of reduced enthalpy, unity at the critical point, k_1 was calculated to be -26.339107.

3.5.2.2 Density, Viscosity and Thermal Conductivity of Vapour

Density of the vapour phase of R114 is calculated using

$$\rho_g = \frac{1}{v_g} \qquad (3.5.13)$$

Viscosity is stated again in ASHRAE Guide and Data Book[50] as 1.182×10^{-5} (Ns/m^2), and the value of thermal conductivity is 0.011 (W/mK).

3.5.3 The Mixture of Liquid and Vapour

Once evaporation takes place, then appropriate density and viscosity of the mixture need to be evaluated and used in the equations described earlier. The evaporation phenomenon is determined by comparing locally, in each layer, the enthalpy of the layer at a given radius with the enthalpy of saturated liquid at the same pressure. The flow is treated as two-phase if the enthalpy of the layer is greater than the enthalpy of saturated liquid.

3.5.3.1 Enthalpy

Enthalpy of evaporation is calculated using the Calusius-Clapeyron equation as

$$h_{fg} = T \frac{dp}{dT} (v_g - v_f) \qquad (3.5.14)$$

Calculation of all terms in equation (3.5.14) have already been discussed above when expressing properties for the vapour and liquid phase.

3.5.3.2 Quality

If some vapour forms it becomes necessary to know what proportion of the fluid mass has turned to vapour. The mass fraction, x, of vapour is calculated using

$$x = \frac{h - h_f}{h_g - h_f} \qquad (3.5.15)$$

3.5.3.3 Density

By definition, specific volume in a two-phase mixture is given by

$$v_x = (1-x)\, v_f + x\, v_g \tag{3.5.16}$$

where

v_f, v_g = volumes of liquid and vapour respectively.

Thus, the density of the mixture is given by

$$\rho_x = \frac{1}{v_x} = \frac{1}{\frac{(1-x)}{\rho_f} + \frac{x}{\rho_g}} = \frac{\rho_f \rho_g}{(1-x)\rho_g + x\rho_f} \tag{3.5.17}$$

3.5.3.4 Viscosity

There have been many relations presented by different authors which express the viscosity of a mixture of liquid and vapour, namely those listed in section 2.3.1. Equation (3.5.18), which is Heyward's expression for bubbly oil, is another example.

$$\eta_m = \eta_0 (1 + a\beta) \tag{3.5.18}$$

where

a	=0.0125 for bubbly oil (an experimentally determined constant)
η_m	=Viscosity of the mixture
η_0	=Viscosity of the base liquid
β	=Volume percentage occupied by solid particles/ air bubbles

The above relation indicates that there is an increase in the viscosity of the oil/air mixture due to the presence of air bubbles, in the case of bubbly oil a local increase in the shear forces of the lubricant would occur. The same expression is recommended when solid

particles are present. The limitation with this relation is that it is only valid for values of β not exceeding 30%.

In attempting to represent the variation of viscosity of the liquid/vapour mixture between the limits of saturated liquid and saturated vapour, it is necessary to employ an expression which yields the correct values at these limits and represents the known or accepted variation equally well in all regions close to these extremes. No experimental verification has been found for the expression of Isbin, Cicchitti, Duckler and it is therefore suggested that a logarithmic relation be used to represent viscosity in terms of the volume ratio of vapour to liquid at a given mixture temperature, in such a way that the value and its rate of change are correct at these extremes. The expression should also show a decrease in the viscosity of mixture since in the case of evaporation it is expected that vapour bubbles would cause a decrease in the local shear forces.

Figure 3.5.1. shows the nature of a suggested logarithmic relation for the viscosity of a mixture in terms of the ratio of vapour volume to liquid volume, β', rather than volume proportion as used by Heyward.

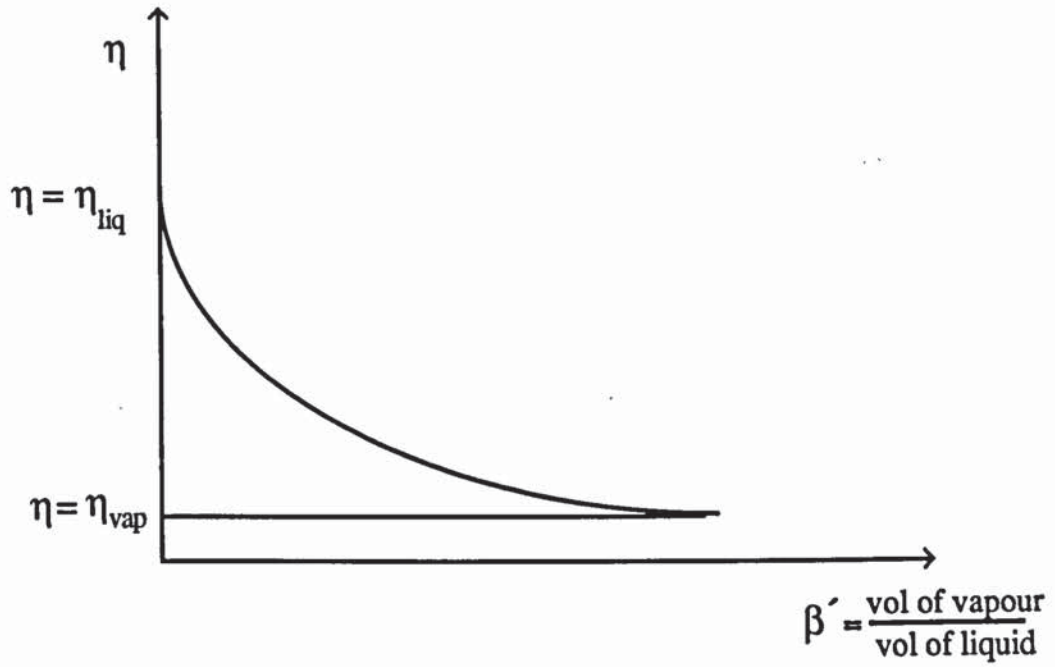

Figure 3.5.1
Viscosity of liquid/vapour mixture with volume ratio of vapour to liquid

If it is assumed that the viscosity of the mixture, η_m, has a logarithmic form, then it can be represented as

$$\frac{\eta_m - \eta_0}{\eta_\infty - \eta_0} = 1 - e^{-\beta'/k} \qquad (3.5.19)$$

where suffices 0 and ∞ refer to liquid and vapour states, respectively, and β' represents the volume ratio of vapour to liquid.

It is required that three boundary conditions are established to enable the solution of constant k as used in equation (3.5.19) From Figure 3.5.1 it is evident that $\eta_0 = \eta_f$ and $\eta_\infty = \eta_g$.

The third boundary condition can be obtained by considering the gradient η_m, given by

$$\frac{d\eta_m}{d\beta'} = (\eta_\infty - \eta_0)\left(\frac{1}{k} e^{-\beta'/k}\right) \qquad (3.5.20)$$

If it is assumed that the magnitude of this gradient is of the same order as the expression developed by Heyward then from equation (3.5.18) the gradient becomes

$$\frac{d\eta_m}{d\beta'} = a\eta_0 \frac{\partial\beta}{\partial\beta'} \qquad (3.5.21)$$

Since β is the volume fraction of vapour and β' is the ratio of volume of gas to the volume of liquid are, related by

$$\beta = \frac{\beta'}{1+\beta'}$$

therefore

$$\frac{\partial\beta}{\partial\beta'} = \frac{1}{(1+\beta')^2},$$

which gives the gradient as shown in equation (3.5.21) in terms of the ratio of the volumes of gas to liquid as

$$\frac{d\eta_m}{d\beta'} = \frac{a\eta_0}{(1+\beta')^2} \qquad (3.5.22)$$

If it is assumed that the ratio β'/k is small so that

$$e^{-\beta'/k} \approx 1 - \frac{\beta'}{k} \qquad (3.2.23)$$

Higher order terms in the series expression of $e^{-\beta'/k}$ are neglected

By equating gradients given by equations (3.5.20) and (3.5.22), the value of k can be determined from the quadratic equation

$$\frac{a\eta_0}{(1+\beta')^2} k^2 - (\eta_\infty - \eta_0)\, k + \beta' (\eta_\infty - \eta_0) = 0 \qquad (3.5.24)$$

therefore k becomes,

$$k = \frac{(\eta_\infty - \eta_0) + \sqrt{c}}{\frac{2\,a\,\eta_0}{(1+\beta')^2}} \quad \text{, where } c = (\eta_\infty - \eta_0)^2 - 4a\,\frac{\eta_0}{(1+\beta')^2}\,\beta'\,(\eta_\infty - \eta_0) \qquad (3.5.25)$$

It was found that constant 'a' is very important in representing the form of relation for the viscosity of the mixture. If this value is taken as 0.0125, analogous to the value suggested by Heyward for bubbly oil, then the variation of mixture viscosity is found to be very similar to that given by Cicchitti's expression, discussed in Chapter 2. This suggests that the viscosity of the mixture remains similar to the liquid viscosity unless very high proportions of vapour are present. However, when 'a' is unity then an intermediate relation is obtained between the extremes predicted by Isbin and Cicchitti[46].

A comparison between the new correlation for the viscosity of mixture and those listed by Feng and Hahn, mentioned in Chapter 2 is presented as Figure 3.5.2.

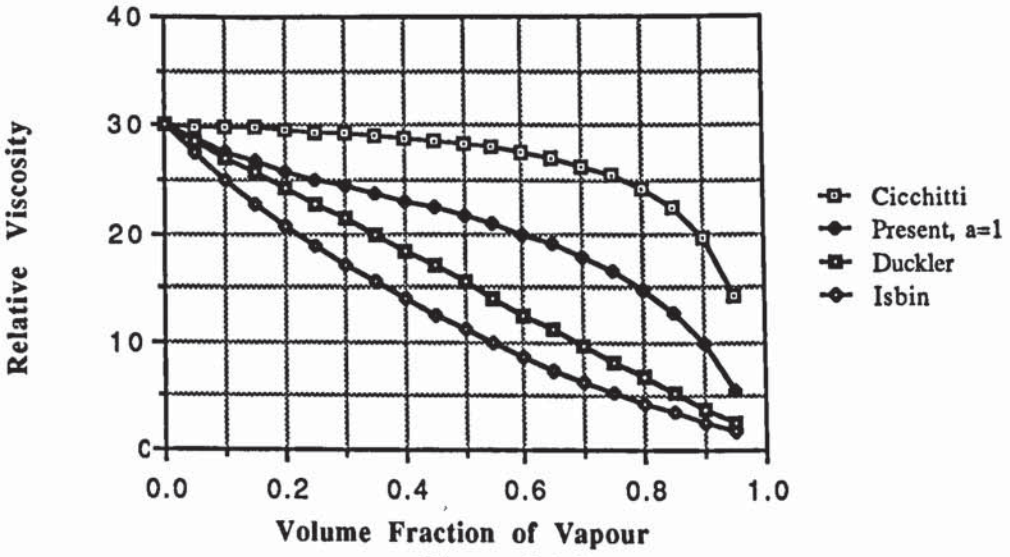

Figure 3.5.2
Comparison of the proposed correlation for the viscosity of a mixture with those listed by Feng and Hahn

The above comparison shows that the proposed correlation predicts a reduction in the viscosity of the mixture as the proportion of vapour is increased. The prediction is similar to Isbin and Duckler for small values of vapour but the rate of decrease is less significant for higher proportions of vapour than by their prediction. A possible

advantage of the logarithmic expression is that constant "a" might be selected to correlate with experimental results to predict more realistic values for the mixture viscosity. Figures 3.5.3 illustrates that the choice of constant "a" enables any correlation to be represented from that of Cicchitti to Isbin.

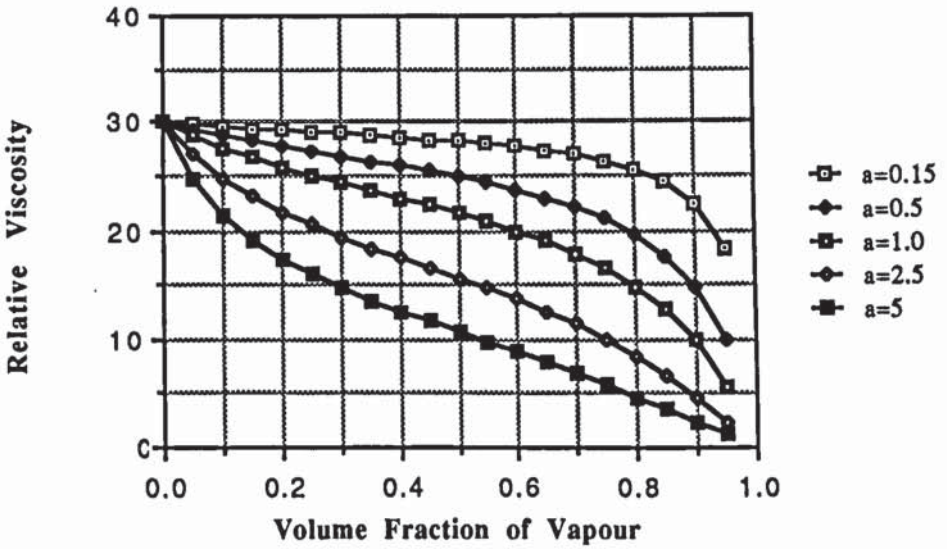

Figure 3.5.3
Selecting the value of constant 'a' would allow the predicted variation of viscosity to correlate with experimental results

3.5.3.5 Temperature

In the two phase region the temperature becomes the saturation temperature corresponding to the local pressure and the Beattie-Bridgeman relationship may be used to evaluate the saturation temperature. Since the pressure is constant across the lubricating film, then the two phase region temperature also remains constant across the film gap.

3.6 Solution of the Equations

The system of equations (3.2.4-5, 3.3.4, 3.4.1) cannot be solved explicitly. Continuity of mass requires the radial velocity gradient, which can be found from the momentum, equation (3.2.4), in terms of the pressure gradient. But the value of pressure gradient for which there is no net change in film thickness while at the same time, the momentum, continuity and energy equation are satisfied is not known, unless the velocity profile can be satisfied. Thus, equations were solved in finite difference form using a 4th order Runge-Kutta process. The thickness of the film is subdivided into a large number of unmixing shear layers and the 'correct' value of the local radial pressure gradient is determined by trial and error using a Newton-Raphson approach. The Newton-Raphson method was used to locate the value for which the predicted overall film thickness at the end of each step was within 0.03% of the actual constant value, while momentum, continuity and energy constraints were satisfied. The residual error of 0.03% was distributed amongst the layers before the next step was taken. The 'correct' pressure gradient normally found gave a total thickness error much better than this limit of 0.03%.

Chapter 5 gives a more detailed description of the program while Appendix 3 includes the flow chart of the program used to solve the equations.

3.7 Simplification Offered by the Assumption of a Parabolic Distribution in the Radial Flow Distribution and Constant Film Viscosity

In an attempt to reduce computation time, an investigation was made to determine if the "correct" radial pressure gradient was amenable to a simplified approach using the average velocity. To do this, the equations of motion, continuity and energy were solved by a fourth order Runge-Kutta procedure to determine the radial pressure gradients which

would arise in different layers within the film for a given initial parabolic velocity distribution. The layers were assumed to be of constant thickness over the radial step. The gradient associated with each individual layer was then used in turn to examine the change of every layer thickness which was predicted for that pressure gradient and the given initial velocity gradient.

The steady flow of a Newtonian fluid in one direction between stationary parallel boundaries gives rise to a parabolic velocity distribution within the gap. For the steady flow situation with a film of thickness Z this leads to

$$u(y) = a\,y^2 - a\,Z\,y \quad \text{and} \quad \frac{\partial^2 u}{\partial y^2} = 2\,a \text{ , where } a = -\frac{3\dot{V}}{\pi Z^3 r} \tag{3.7.1}$$

Using the assumption of laminar flow, the average velocity for a layer of thickness Z in the film can be related to the volume flow rate as

$$u = \frac{\Delta\dot{V}}{2\pi r Z} \tag{3.7.2}$$

Thus within a layer of thickness Z

$$\frac{1}{r}\frac{\partial}{\partial r}\left(r\frac{\partial u}{\partial r}\right) = \frac{1}{r}\frac{\partial}{\partial r}\left\{-r\frac{\Delta\dot{V}}{2\pi r^2 Z}\right\} = \frac{\Delta\dot{V}}{2\pi r^3 Z} \tag{3.7.3}$$

$$\text{and} \qquad -\frac{u}{r^2} = -\frac{\Delta\dot{V}}{2\pi r^3 Z} \tag{3.7.4}$$

The inclusion of terms for inertia requires their summation at all levels within the film. In the case of the parabolic velocity distribution this effect can be related to the average velocity of the film and is 1.2 times the average velocity, as demonstrated by Constantinescu[13]. Thus, for a radially symmetrical hydrostatic thrust bearing with a parabolic velocity distribution in the fluid film and including the effect of inertia forces, the pressure distribution can be written as

$$\frac{\partial p}{\partial r} = \eta\left(\frac{\partial^2 u}{\partial y^2}\right) - 1.2\left(\rho u\frac{\partial u}{\partial r} - \frac{u^2}{2}\frac{\partial \rho}{\partial r}\right) \tag{3.7.5}$$

It is clear that in equation (3.7.5), the constant viscosity form of Navier-Stokes equation is used. However, the way in which the Navier-Stokes equations are derived, involves consideration of a small differential element of volume and the equations may be taken as applicable at any particular point in the field of interest.

Equation (3.7.5) can be solved numerically to give the pressure distribution, provided that further equations for density and velocity distribution are available and solved simultaneously. Before doing so it is necessary to consider the limitations imposed by the assumption of a parabolic velocity distribution and the use of mass average velocity of the flow.

3.7.1 Effect of Viscosity and Density Distribution Across the Film Thickness for the Hydrostatic Thrust Bearing

The assumptions of isoviscous and incompressible flow can apply only to the isothermal flow of a single phase and must require heat transfer to the solid boundary. In the case of the fully developed isothermal, single phase flow there is no further growth of the boundary layer. If dissipation leads to changing values of density and viscosity in adiabatic flow then there must be a continuous development of the boundary layer and of the velocity profile.

In the adiabatic case of uniform radial outward flow of a thin film between two flat plates, it is appropriate to consider the velocity in the transverse direction (normal to flow) to be negligible, in spite of the development of the boundary layer, with the consequence that the pressure gradient exists only in the radial direction. If the film thickness is subdivided into elementary layers and each is assumed to be of constant thickness, then the Navier-Stokes equations would predict a different radial pressure gradient at any given radius.

These predictions are determined by the rate of change of the velocity gradient in the axial direction. This would predict very large gradients in layers adjacent to the walls, and yield the ideal inviscid flow solution at the centre of the film. Since there is no significant transverse component of velocity in adiabatic flow, it is apparent that the thickness of each elementary layer must vary in the axial direction to accommodate the common radial pressure gradient.

If the momentum equation in the radial direction is written to allow the thickness of an elementary layer to vary then it takes the form

$$u\frac{\partial u}{\partial r} + \frac{1}{\rho}\frac{\partial p}{\partial r} = \frac{\eta}{\rho}\frac{\partial^2 u}{\partial y^2} \qquad (3.7.6)$$

The problem of finding the correct value for the pressure gradient is resolved if the summation of all changes in thickness across the film is zero, i.e.

$$\sum_{0}^{Z} (z)_{\text{layer thickness}} = \text{film thickness} \qquad (3.7.7)$$

A further condition is found by considering the total thickness, Z, of the film and the shear forces at the solid boundaries, which leads to

$$-Z\frac{\partial p}{\partial r} + 2\eta \left(\frac{\partial u}{\partial y}\right)_w = \sum_{0}^{Z} \left(\rho z u \frac{\partial u}{\partial r}\right) \qquad (3.7.8)$$

where suffix w refers to the conditions at the wall.

Thus, if momentum changes in all the elementary layers are summed at the correct value of the radial pressure gradient, and the same value of pressure gradient is used for the whole thickness of the layer, then

$$\sum_{0}^{z} \left(\eta \frac{\partial^2 u}{\partial y^2}\right) \delta y = \eta_w \left(\frac{\partial u}{\partial y}\right)_w \qquad (3.7.9)$$

In fact there is only one condition, for examination of equation (3.7.8) shows that the summation of ($p\ \partial z/\partial r$) is zero when ($\sum_{0}^{z} \partial z/\partial r=0$), i.e. when there is no net change in film thickness.

The equation of constraint, equation (3.7.7), was then applied to determine which value of pressure gradient was appropriate to satisfy the general conditions. The results indicated that the pressure gradient was virtually the same as that associated with 1.2 times the mean velocity of flow. In other words, the value which is generally accepted as correct for the parabolic velocity profile in isoviscous flow. This value of pressure gradient is used only for the first radial step and as an initial value in the Newton-Raphson procedure for locating the correct pressure gradient.

CHAPTER FOUR

EXPERIMENTAL TEST RIG

4.1 Introduction

Experimental work conducted to support the theoretical predictions of phase change in a lubricating film has consisted of the construction of a test rig. Chapter 1 and 2 highlighted the lack of experimental data and validation from the literature reviewed. The difficulties of instrumenting a sliding vane compressor to investigate phase change in regions where it might arise were discussed and the decision to use a simple hydrostatic thrust bearing was stated in Chapter 1. The choice of equipment was constrained by the need to obtain accurate measurements of pressure distribution in a thin film. The experimental requirement was to provide not only the bearing but a supply of suitable lubricant under the applied conditions of pressure and temperature which would ensure that phase change would occur, as in Figure 4.1.1.

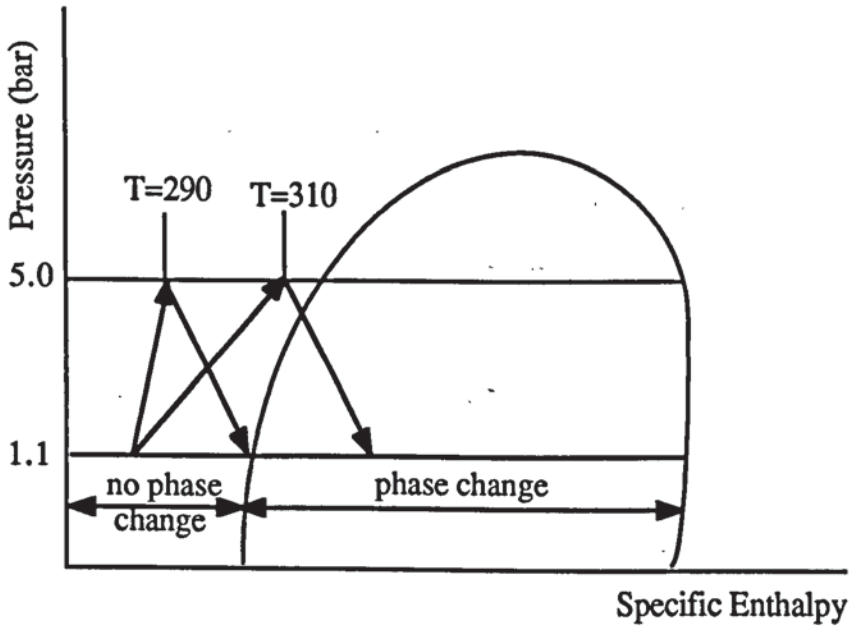

Figure 4.1.1
Pressure-Specific Enthalpy diagram showing a typical condition for evaporation of liquid refrigerant R114

Radially symmetrical flow between flat plates using refrigerant R114 was shown to be a vehicle which would produce sufficient viscous dissipation to cause phase change at moderate pressure and fluid temperatures which were close to the temperature of the surroundings, thus enabling heat transfer to the surroundings be neglected.

The present Chapter reviews a number of circuit designs which were considered for the supply of liquid refrigerant into a hydrostatic bearing and the reason why a particular method was chosen as the most suitable one.

On account of the difficulties of ensuring the uniformity of the gap and measuring the mass flow accurately it was thought better to include a load cell and flow meter to permit as many cross checks as possible between the measured and predicted data. The flow meter and the pump characteristics would provide mass flow rate data and their results should then allow correlation between the theory and the pressure distribution records.

The parameters and method by which they were measured are listed below:-

1. The pressure and temperature at both the inlet and outlet of the pump circulating the refrigerant.

   The pressure readings for this part of the circuit were taken using two dial gauges incorporated in a system analyser used in refrigeration systems for filling or emptying the system. Since the circulating pump used for this purpose was a gear type, this produced pressure pulses at the outlet due to the engagement and disengagement of gears. These pulses caused the pressure gauges to oscillate during the test runs and the average pressure was recorded.

2. Pressure of the refrigerant as it flowed across the surface of the bearing.

   Eight type 24 solid state sensors that utilized a 316 Stainless Steel diaphragm to provide compatibility with refrigerant R114 were used for this purpose. These sensors were connected by PTFE tubes to the pressure tapping points on the underside of the bearing plate (See Figure 4.2.3).

3. Temperature of the refrigerant inside the chamber.

   A sealed ceramic plate with terminals on either side was used to connect the Chromel/ Alumel thermocouples from inside the bearing chamber to the external

readout system. This connector was pressure tested to ensure that there would be no cracking or bursting of the ceramic plate during the experiment.

4. The mass flow rate of the refrigerant.

This was measured using a turbine flow meter which was placed immediately after the pump.

4.2 Test Rig Design

Three possible circuits were investigated. In the first it was proposed to evaporate the mixture of liquid and vapour discharged from the bearing and then use a standard refrigeration compressor and condenser to compress and liquify the refrigerant before returning it to the bearing. This design seems to present no complication, since it is basically a standard circuit used in refrigeration plants.

The second arrangement would be to separate the mixture leaving the bearing surface (Figure 4.2.1). Here the vapour part can be sent directly to the compressor to be compressed and condensed for recirculation, and the remaining liquid can be sent to a Diaphragm or Gear pump which is capable of handling liquid refrigerant and then redirected back to the accumulator.

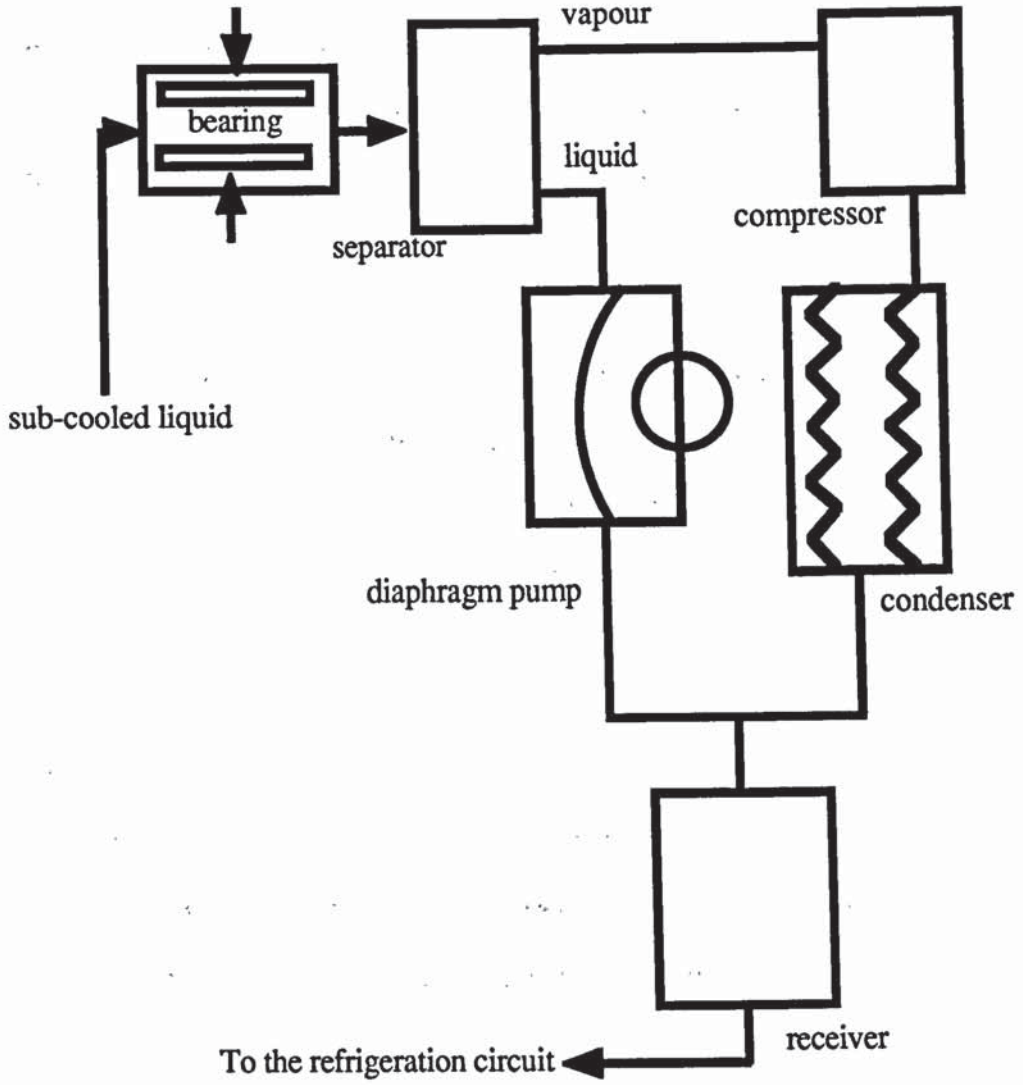

Figure 4.2.1
Details of the system in which mixture leaving the bearing is separated

In the third arrangement considered, the vapour component of the mixture leaving the bearing would be condensed before being sent to a diaphragm or gear pump to be compressed for recirculation. There is one problem associated with this arrangement that is the condensation process of the mixture. The temperature of the refrigerant after leaving the bearing was estimated to be around 15-18°C. If tap water was to be used in the condenser, there would be a problem because the temperature of the water is about 15°C and this relatively high temperature of water cannot effectively cool the mixture which is only 2°C warmer.

However, this problem can be overcome in two ways:

(1) A separate refrigerator can be used to chill the water used in the condenser. In which case the temperature of the water can be dropped to as low as a few degrees above freezing point.

(2) A refrigerator, operating as a slave circuit, can be used to chill the mixture leaving the bearing surface. The necessary control can be achieved by using a standard pressure control valve to switch on/ off the slave refrigeration circuit. With this arrangement the condenser of the bearing circuit and the evaporator of the slave circuit form a heat exchanger.

It is evident from above, that the problem generally was the recompression of a mixture leaving the bearing which would have a high proportion of liquid. Only vapour can be compressed in a standard reciprocating compressor, as commonly used in refrigeration. Liquid only can be compressed in a diaphragm or a gear pump. The gear pump deals very effectively with liquid but not liquid/vapour mixtures, so that no type of pump is suitable for the mixture leaving the bearing. Hence it is necessary to either cool the mixture to condense any vapour before compressing liquid only, or evaporate it completely so as to compress only vapour. The latter is not acceptable since it would require a large heat input to evaporate the remaining liquid and then a great deal more work would be required in compression on account of much greater volume changes during compression of vapour. The third system was selected because the vapour leaving the bearing is less dense than the liquid, the phases separate naturally and it is easier to condense the vapour on its own. Figure 4.2.2 shows the overall arrangement of this circuit.

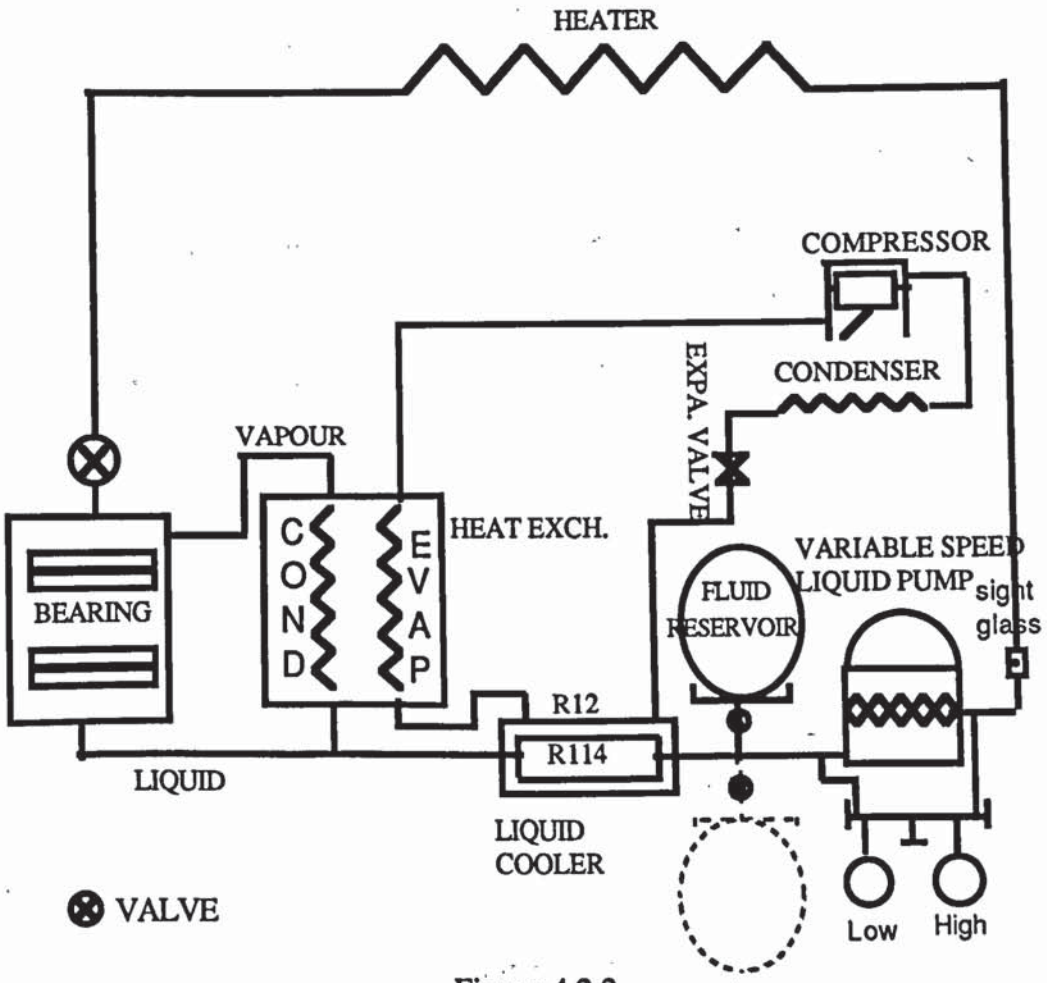

Figure 4.2.2
Details of the system used for the experimental investigation

Liquid refrigerant compressed by the gear pump is fed to the bearing, the vapour part of the refrigerant mixture which leaves the bearing is then directed to a heat exchanger while the liquid is sent back to the pump for recirculation. The heat exchanger serves as a condenser for vapour leaving the bearing chamber and as an evaporator for the liquid refrigerant in the slave circuit where complete vaporization of the refrigerant will not occur in the liquid cooler and since a reciprocating compressor (selected for use in the slave circuit) should strictly be fed with vaporized refrigerant. The heat exchanger ensures that refrigerant from the compressor is fed to the water cooled condenser and back into the accumulator.

Figure 4.2.3 illustrates the details of the bearing and test chamber which was constructed during the present research programme. The liquid refrigerant is fed from the top into the surface of the bearing. After flowing radially outwards the vaporized refrigerant is

collected from the top of the chamber and the remaining liquid flows down the sides as indicated by the arrows. It was decided to attempt to observe any development of vapour bubbles by using a transparent material for the upper bearing surface. The best material, apart from glass which proved to be unsuitable because of breakage after three attempts due to residual stresses at the central hole, was perspex. This material was tested for any possible chemical reaction with Arcton R114 and, once proved satisfactory, it was used. The lower bearing surface was made of mild steel.

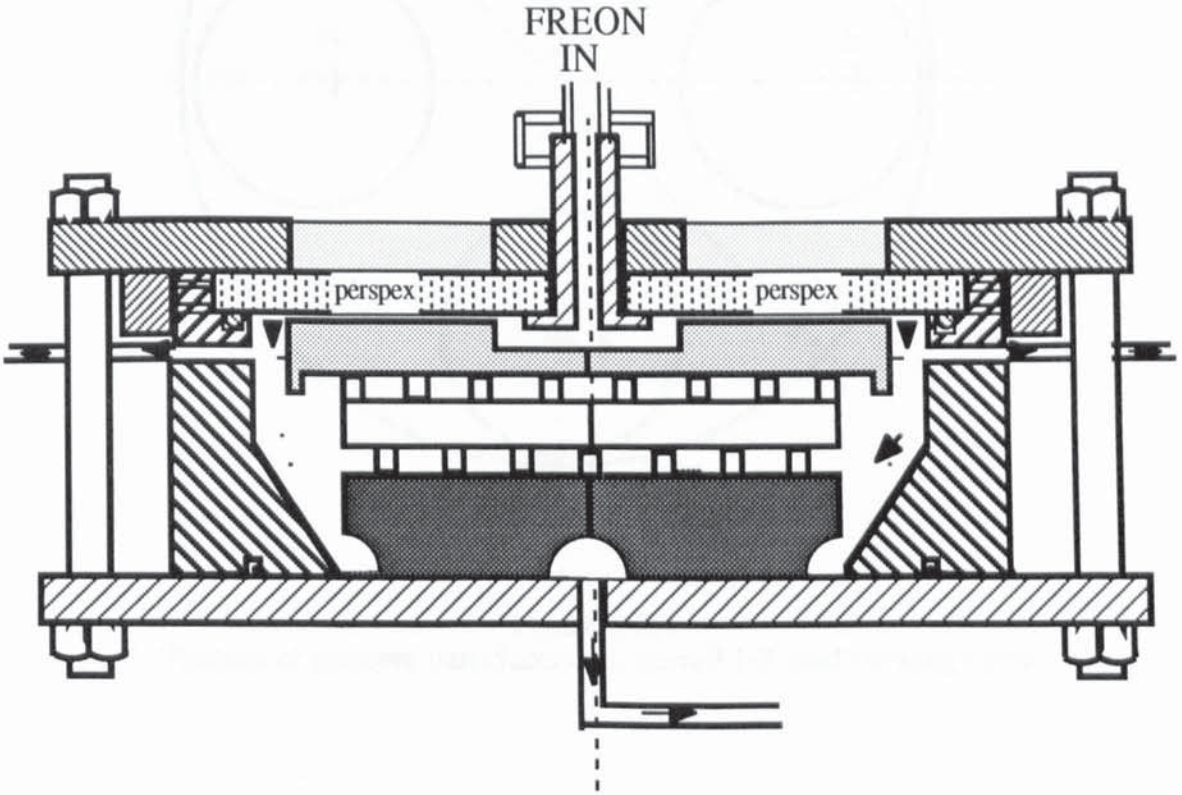

Figure 4.2.3
Arrangement of the bearing assembly

Figure 4.2.4 shows the arrangement of pressure tappings provided on the face of the bearing plate. It would have been preferable to locate the tappings on a single radius, however, the difficulty of accommodating the necessary underside connections to pipes transmitting the signals to transducers outside the chamber prevented this, therefore the layout shown was adapted. The chamber was also provided with thermocouples to measure the temperature of the liquid and vapour refrigerant.

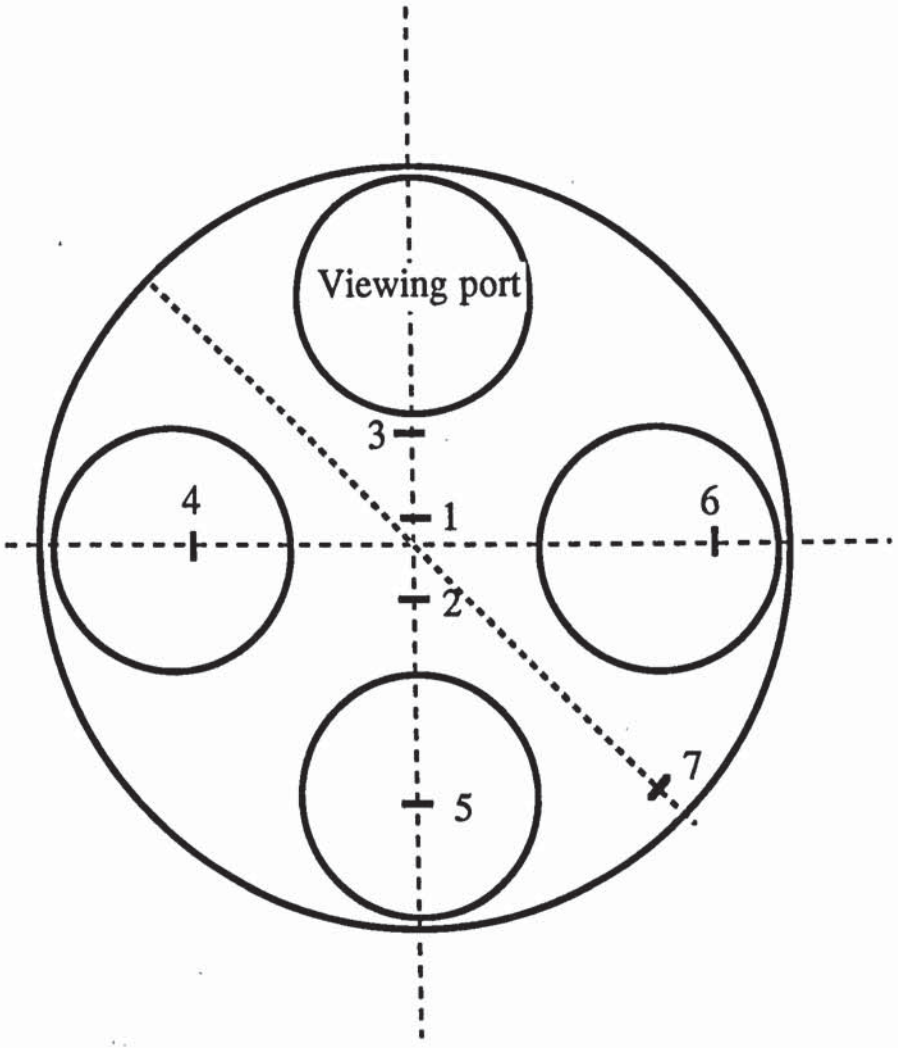

Figure 4.2.4
Position of pressure transducers (numbered 1-7) and viewing ports

4.3 Components for the Main Test Rig

4.3.1 Bearing Chamber

The design of the bearing chamber had to comply with an International standard for pressure vessels. All calculations were based on BS 5500: 1988. Appendix 2 gives details of some sample calculations required to determine the thickness of the cover for the chamber inside which the bearing was to be accommodated. Calculations for determining

the size of the bolts connecting the top and bottom plate have also been included in the same Appendix.

The pressure drop along the radius of the bearing is greatly dependent on the gap, Z, in the bearing. The size of the gap required to be chosen to ensure that a meaningful pressure distribution could be obtained under conditions which would cause evaporation of the lubricant to take place within the bearing. The final choice of the gap size was determined as the result of numerous computer predictions of the performance, assuming Reynolds' equation apply.

4.3.2 Pressure Transducers and their location

Eight pressure transducers were used to measure the pressure of R114. One was placed to measure the pressure at the central inlet port and the remaining seven were placed at the tapping locations shown in Figure 4.2.5, so that the refrigerant pressure would be measured as it flowed outwards through the bearing.

The transducers were tested and calibrated using the standard deadweight pressure testing system and later compared with under static conditions. Appendix 2 contains the calibration curves for these transducers.

Tapping locations were chosen to achieve roughly equal pressure drops along the radius between each pressure transducer. The choice was determined at an early stage in the design process by a simple method based on Reynolds' equation. The calculation has been included in Appendix 2.

4.3.3 Load cell

In order to measure the axial load applied to the bearing during test runs it was decided that a transducer in the form of a circular ring would be used. The design of this type of transducer was described by Baines[57]. It consisted of a continuous annular elastic beam loaded transversely through eight pads equi-spaced on the lower surface and a further eight pads spaced intermediately on the upper surface. Opposite each pad were two strain gauges and the system of gauges was connected in a bridge form to give maximum response and accuracy. Since the bonding material of these gauges would be affected by R114, it was necessary to protect them by using an appropriate protective coating.

A detailed list of calculations for the design of this load cell together with calibration curves has been included in Appendix 2.

Figure 4.3.3.1 shows the load cell in some details.

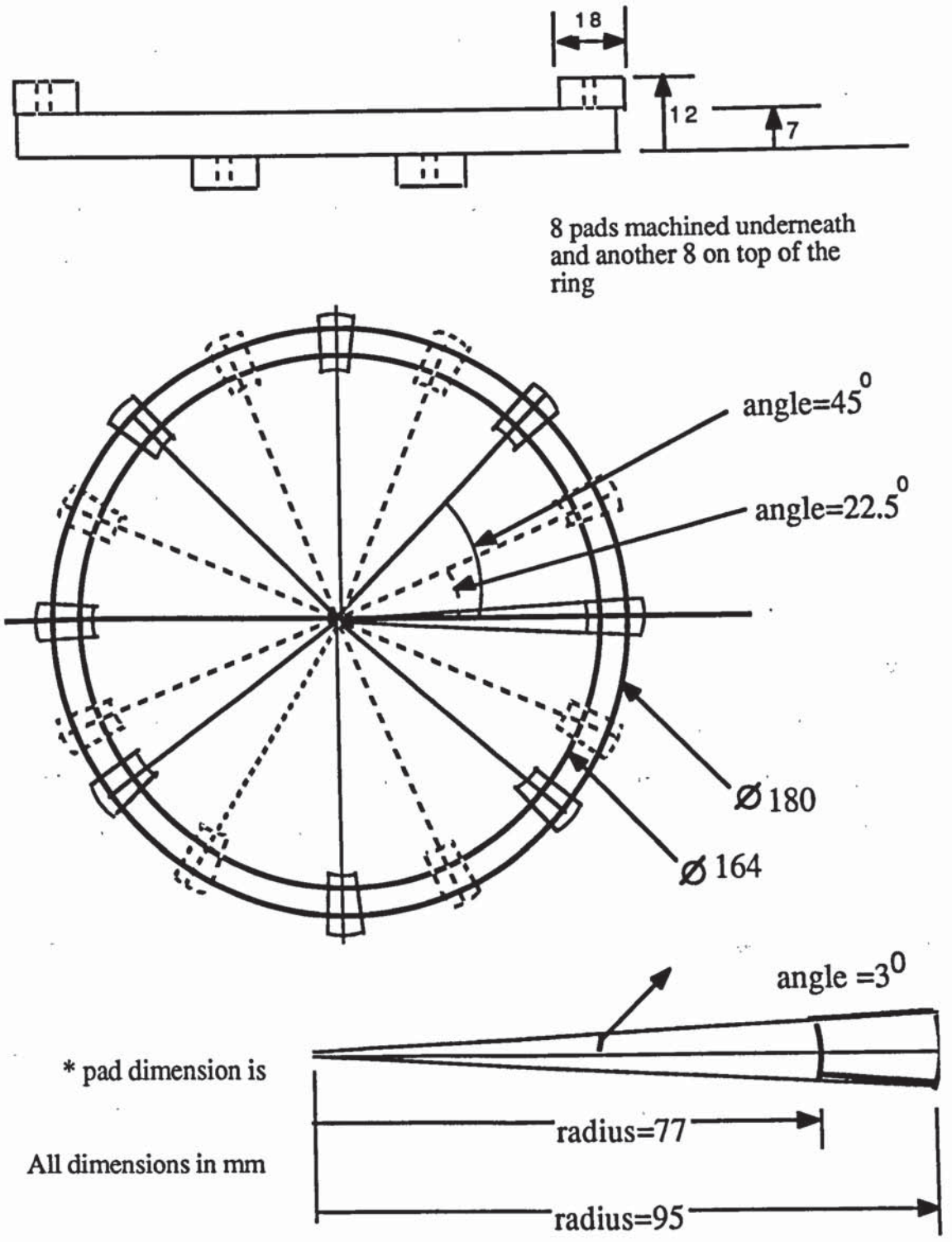

Figure 4.3.3.1
Details of Load Cell

4.3.4 Observation Plate

The deflection of the observation plate, and stress levels under the maximum load during the test run, were determined to ensure an adequate safety margin and to prevent accident or breakage upon subsequent release of the halocarbon refrigerant.

Calculations for the appropriate thickness of the Perspex observation plate were based on BS 65002, "Elastic stresses and deflections for flat circular plates with diameter/thickness>4 under uniform pressure". For a Perspex thickness of 20 mm and diameter of each observation hole 90 mm, the design parameters were considered and the deflection of the Perspex under a load of 10 kN/m^2 was calculated to be 0.035 mm.

Details of the calculation are listed in Appendix 2.

4.3.5 Heater

To promote a degree of phase change within the bearing the temperature of liquid refrigerant at the entry to the region was required to be raised to the point where it would be close to its saturation temperature. Evaporation would then take place due to viscous dissipation and energy in the film as it flowed through the bearing with reducing pressure. This is shown on a sketch of the pressure/ specific enthalpy field as Figure 4.3.5.1.

Two methods were considered by which the temperature could be raised. The first being to use heating tapes wrapped around the pipe carrying the fluid, and the other to use a sheathed heating element located centrally within the pipe conveying the liquid refrigerant. The second method seemed more suitable, in that the length of the standard heating tapes suitable for providing the required heating power would have been excessively large to accommodate.

In choosing the sheethed heating element for this purpose, it was necessary to estimate the heat transfer coefficient on the surface of an annular gap in order to determine the maximum temperature of the sheath surface at the outlet of the heater, where the temperature would be greatest and most likely to cause the refrigerant to break down by thermal cracking. Using the temperature value calculated, a thermistor controlled switching circuit was built to limit the temperature of the heater sheath. Although liquid

R114 has excellent thermal stability and does not crack into simpler components below 120°C [58], it can, under extreme conditions react exothermally with metals and produce metal halides and carbon. The purpose of the above control system was therefore the prevention of any possible decomposition of R114.

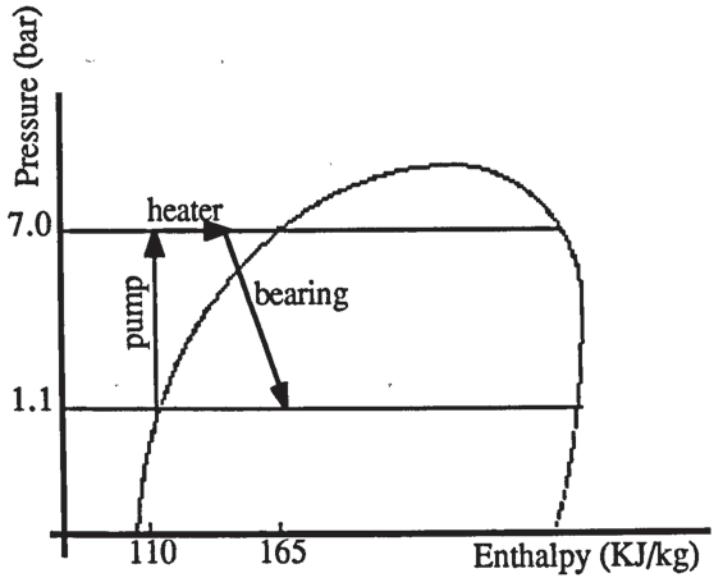

Figure 4.3.5.1
Pressure-specific enthalpy diagram for determination of input power for the heater (assuming ideal conditions)

The calculations detailed in Appendix 3 showed that a suitable design of heater would consist of two electrical sheath heaters, each 1kW connected parallel to give a total of 2kW heat input when using 220V mains supply. Since it was necessary to vary the temperature of the liquid R114 in the circuit, a Variac was employed to vary the voltage supplied to these heaters. Figure 4.3.5.2 shows a block diagram of the control system for the heaters, in which a thermistor in contact with the sheath was used to control the power supply.

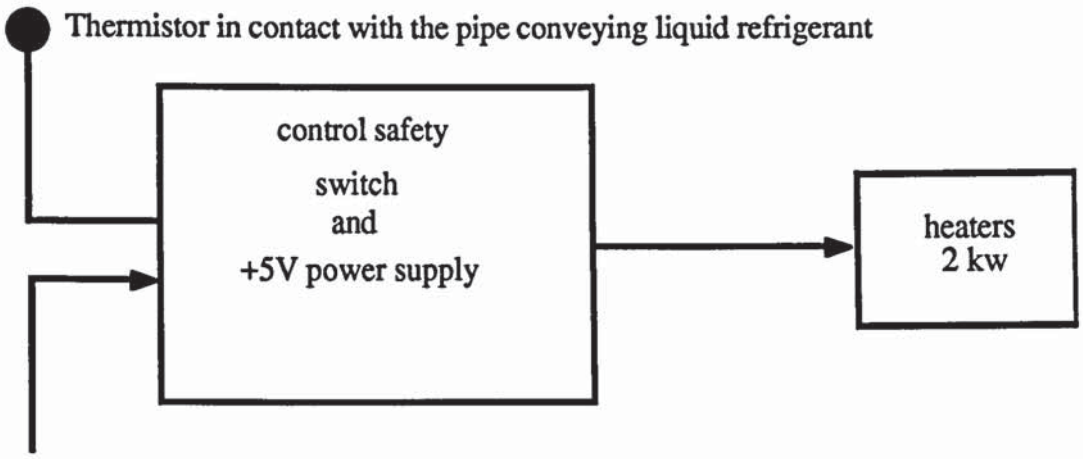

Figure 4.3.5.2
Thermistor block diagram for controlling the heater power

4.4 Components for the slave circuit

As described earlier the test rig consisted of two circuits, the main circuit containing the bearing and a slave circuit whose function was to control the thermodynamic state of the refrigerant flowing in the main circuit. The various components required for the slave circuit are essentially those of a simple refrigerator system, viz

1) Evaporator/ Heat exchanger.

2) Condenser.

3) Reciprocating compressor.

4) Expansion Valve.

The performance requirements of the above components were determined from the predicted heat load and temperature levels, allowing selection of the condenser and compressor. Temperature of the coolant (water), was known, therefore the condensing temperature was selected and subsequently selection of the appropriate condenser. Allowing a suitable pressure drop in suction and deliver lines, the compressor and delivery conditions were selected, using these conditions and the required evaporating heat load, a compressor was selected. Appendix 3 includes details of selection, type and make of these components.

CHAPTER FIVE

PROGRAMMING OF THE THEORETICAL MODEL

5.1 Introduction

This Chapter describes the structure of the computer program which is based on the mathematical model discussed in Chapter 3 to predict the operating characteristics of the test bearing and rotor end face seal of a sliding vane compressor. In Chapter 3, it will be recalled that the lubricating film was divided into a finite number of unmixing shear layers within which the radial change of fluid properties was to be predicted. It was also described that the value of pressure gradient was evaluated which satisfied the momentum, energy and mass conservation equations simultaneously in all layers of the film while also satisfying the constraint of constant film thickness.

The calculation assumes that fluid is supplied entirely in the liquid phase and requires the initial conditions of pressure (p1), temperature (T1) and mass flow rate (m) to be set. Temperature (T1) determines density (ρ) and viscosity (η) while pressure (p1) and temperature (T1) determine the enthalpy (h1) and the enthalpy of saturated liquid corresponding to pressure (p1). Details of the property calculations, which utilise data provided by Imperial Chemical Industries, are included in Appendix 3. Five simultaneous equations (3.2.13, 19, 21, 22 and 26) listed in Chapter 3 are solved using a fourth order Runge-Kutta method to determine changes of enthalpy (Δh), pressure (Δp), temperature (ΔT), velocity (Δu), tangential velocity (Δw), layer thickness (Δz), density ($\Delta \rho$), and viscosity ($\Delta \eta$). These equations are solved over a chosen radial step length for each of the layers in the lubricating film. In order to determine whether evaporation is taking place, the new enthalpy ($h1+\Delta h$) is compared with the enthalpy of the saturated liquid corresponding to the new pressure ($p1+\Delta p$). Taking full account of the vapour component of the mixture once evaporation has commenced, new values of density and viscosity are calculated before proceeding to the next layer in the lubricating film.

The program is constructed as an assembly of four subroutines to allow maximum flexibility during program modification and subroutine development and allow the main program to be independent of changes to the individual subroutines.

The main program organises the sequence in which the subroutines are called and then carries out step by step calculation of the changing values of program variables. The main program reads in the starting values of parameters and physical constants required for the calculation. For the first layer and given initial conditions of pressure, temperature and velocity distribution the 'prop' routine is called. This routine calculates the saturation temperature corresponding to the given pressure, then the volumes of liquid and vapour refrigerant corresponding to the initial conditions are worked out and these parameters are used to calculate the enthalpy of the refrigerant which is then passed to the subsequent routine for further calculation.

Having established the value of enthalpy for all layers in the lubricating film at the first radial step, it is possible to check if there has been any evaporation of the lubricant. Values of density and viscosity are then calculated and 'Runge1' routine is called to evaluate a first estimate of pressure drop, assuming that there is no change in the layer thicknesses. This value of pressure drop is then passed on to the 'Runge2' routine from which other parameters can be calculated, including the 'correct' value for the pressure drop. 'Runge1' is called only for the very first radial step to obtain the initial estimate of pressure gradient.

'Runge2' routine is comprised of two parts. In the first part the initial estimate of radial pressure gradient is used to solve the equations of continuity, momentum and the energy and compute the correct pressure gradient. This is achieved by varying the pressure gradient to satisfy all conservation equations and the film thickness constraint using a simple Newton-Raphson approach, in the 'Locator' routine, to locate the value for which the predicted overall film thickness at the end of each step is within 0.03% of the actual film thickness. This error is then distributed amongst the layers before the next calculation is taken. The second part of the 'Runge2' routine uses this 'correct' value of pressure gradient and for every layer of the lubricating film calculates the radial and tangential velocity, together with the enthalpy and temperature distribution for the lubricant. A check is made to see if there has been any evaporation by comparing locally,

the enthalpy of the layer with the enthalpy of saturated liquid at the same pressure. If there has been some evaporation then the 'Viscosity' routine is called to compute the new density and viscosity of the liquid-vapour mixture, otherwise density and viscosity are calculated using the temperature relationship, before moving to the next layer to continue the calculation.

5.2 Main Program

As stated earlier, the main program has been designed to call different subroutines which perform the actual calculation. A block diagram is given below which indicates the general sequence in which the main program calls the routines. The object of the block diagram is to show the overall procedure of the calculations contained in the program. A detailed flow chart is presented in Appendix 4.

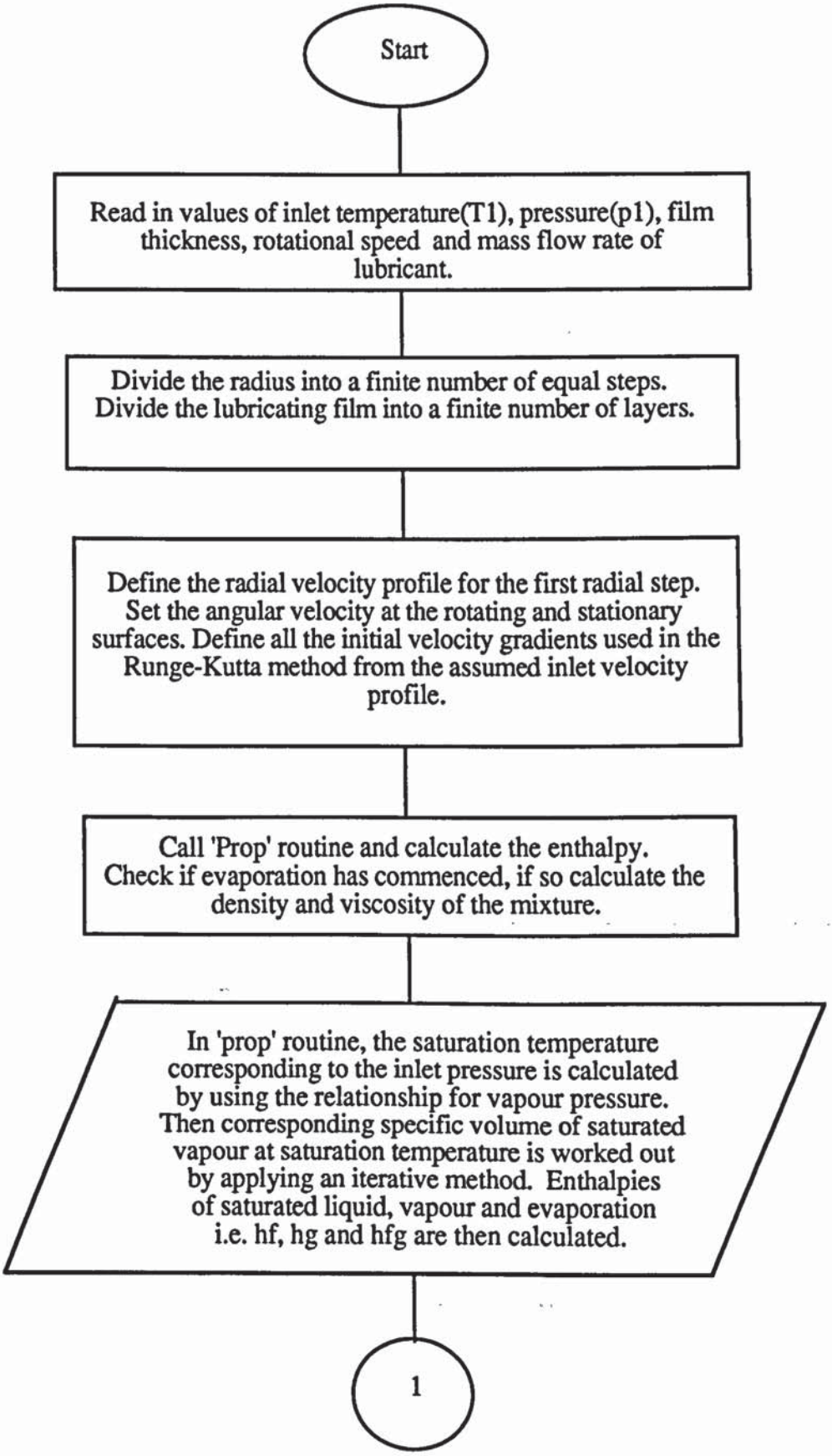
Start
Read in values of inlet temperature(T1), pressure(p1), film thickness, rotational speed and mass flow rate of lubricant.
Divide the radius into a finite number of equal steps. Divide the lubricating film into a finite number of layers.
Define the radial velocity profile for the first radial step. Set the angular velocity at the rotating and stationary surfaces. Define all the initial velocity gradients used in the Runge-Kutta method from the assumed inlet velocity profile.
Call 'Prop' routine and calculate the enthalpy. Check if evaporation has commenced, if so calculate the density and viscosity of the mixture.
In 'prop' routine, the saturation temperature corresponding to the inlet pressure is calculated by using the relationship for vapour pressure. Then corresponding specific volume of saturated vapour at saturation temperature is worked out by applying an iterative method. Enthalpies of saturated liquid, vapour and evaporation i.e. hf, hg and hfg are then calculated.
1

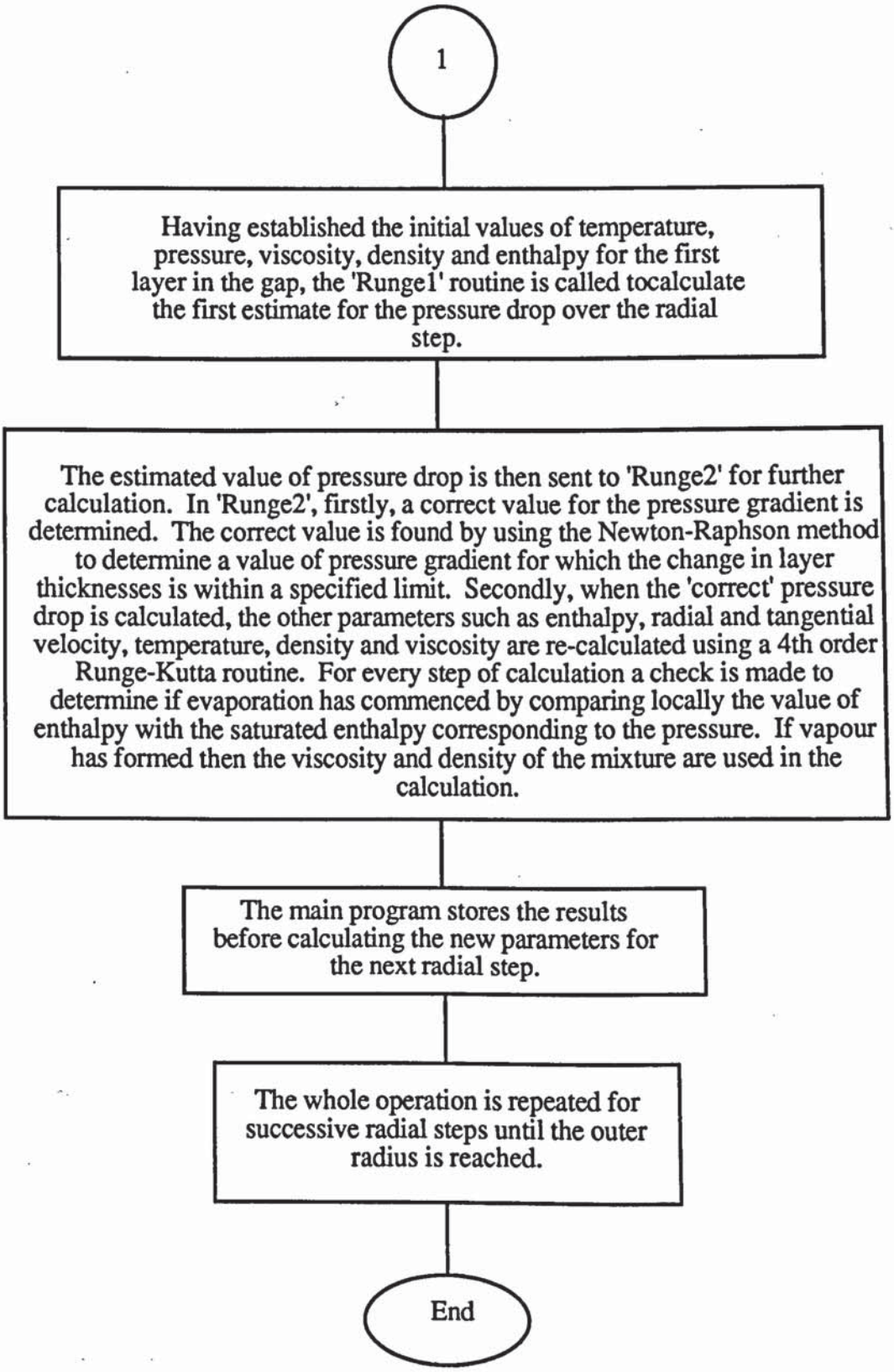
1
Having established the initial values of temperature, pressure, viscosity, density and enthalpy for the first layer in the gap, the 'Runge1' routine is called tocalculate the first estimate for the pressure drop over the radial step.
The estimated value of pressure drop is then sent to 'Runge2' for further calculation. In 'Runge2', firstly, a correct value for the pressure gradient is determined. The correct value is found by using the Newton-Raphson method to determine a value of pressure gradient for which the change in layer thicknesses is within a specified limit. Secondly, when the 'correct' pressure drop is calculated, the other parameters such as enthalpy, radial and tangential velocity, temperature, density and viscosity are re-calculated using a 4th order Runge-Kutta routine. For every step of calculation a check is made to determine if evaporation has commenced by comparing locally the value of enthalpy with the saturated enthalpy corresponding to the pressure. If vapour has formed then the viscosity and density of the mixture are used in the calculation.
The main program stores the results before calculating the new parameters for the next radial step.
The whole operation is repeated for successive radial steps until the outer radius is reached.
End

5.2.1 Presentation of Momentum and Continuity Equations for Runge-Kutta Routine

The equations of momentum, continuity and state are solved numerically using a 4th order Runge-Kutta method, which is one of the popular methods for solving initial-value ordinary differential equations. One reason for its popularity is that it is a self-starting process as the new function value is calculated using only the immediately preceding value and requires that the parameters are expressed as functions of radius as shown below. In calculating all parameters as discussed in Chapter 3, the local value of viscosity and density are used. The radial velocity distribution is calculated using

$$\frac{\partial u}{\partial r}\left(\rho u - \frac{4}{3}\frac{\partial \eta}{\partial r} - \frac{4\eta}{3r}\right) = \frac{\rho w^2}{r} - \frac{\partial p}{\partial r} - \frac{2u}{3r}\frac{\partial \eta}{\partial r} + \frac{\partial \eta}{\partial y}\frac{\partial u}{\partial y} + \eta\left[-\frac{4u}{3r^2} + \frac{4}{3}\frac{\partial^2 u}{\partial r^2} + \frac{\partial^2 u}{\partial y^2}\right] \qquad (5.2.1)$$

The changes of tangential component of velocity is calculated using

$$\frac{\partial w}{\partial r}\left(\rho u - \frac{\partial \eta}{\partial r} - \frac{\eta}{r}\right) = \frac{-\rho u w}{r} - \frac{w}{r}\frac{\partial \eta}{\partial r} + \frac{\partial \eta}{\partial y}\frac{\partial w}{\partial y} + \eta\left[\frac{\partial^2 w}{\partial r^2} + \frac{\partial^2 w}{\partial y^2} - \frac{w}{r^2}\right] \qquad (5.2.2)$$

The changes in enthalpy, are calculated from the dissipation function of the form

$$\frac{\partial h}{\partial r} = \frac{\Phi}{\rho\sqrt{u^2 + w^2}} - u\frac{\partial u}{\partial r} - w\frac{\partial w}{\partial r} + k\frac{1}{\rho u z}\frac{\partial T}{\partial y} \qquad (5.2.3)$$

where

$$\Phi = 2\eta\left\{\left(\frac{\partial u}{\partial r}\right)^2 + \left(\frac{u}{r}\right)^2\right\} + \eta\left\{\left(\frac{\partial w}{\partial y}\right)^2 + \left(\frac{\partial u}{\partial y}\right)^2 + \left(\frac{\partial w}{\partial r} - \frac{w}{r}\right)^2\right\}$$

And $k\frac{\partial T}{\partial y}$ is heat transfer by conduction within the lubricating film

Also the density change is calculated by

$$\frac{\partial \rho}{\partial r} = -\frac{\partial T}{\partial r}\left[C1 + \frac{C2}{2}(1-T_R)^{-1/2} + \frac{C3}{3}(1-T_R)^{-2/3} + 2C4(1-T_R)\right] \qquad (5.2.4)$$

where T_R is the reduced temperature

The change in the elementary layer thicknesses is calculated by using mass continuity of the form

$$\frac{\partial z}{\partial r} = -z \left\{ \frac{1}{r} + \frac{1}{\rho}\frac{\partial \rho}{\partial r} + \frac{1}{u}\frac{\partial u}{\partial r} \right\} \qquad (5.2.5)$$

The above equations are used in the 'Runge2' routine from which pressure, radial and tangential velocity, layer thickness temperature, viscosity and density are obtained for every radial step and each layer within the lubricating film.

The method of locating the onset of possible evaporation is as follows. A check is made to see if the enthalpy of fluid at the entry is greater than that of saturated liquid (corresponding to the input pressure), if so, then it is evident that there has been some evaporation of the fluid. It is then necessary to calculate how much vapour has been generated. This is done by using

$$x = \frac{h - h_f}{h_g - h_f} \qquad (5.2.6)$$

where

x= Mass fraction of vapour generated

h= Enthalpy

Suffices f,g denote liquid and gas respectively

Once vapour has been generated, the density and viscosity of the mixture need to be calculated. The relationships for the density and viscosity of a mixture have already been discussed in Chapter 3, which are

$$\rho_m = \frac{\rho_g \rho_f}{(1-x)\rho_g + \rho_f} \qquad (5.2.7)$$

$$\frac{\eta_m - \eta_f}{\eta_g - \eta_f} = 1 - e^{-\beta'/k} \qquad (5.2.8)$$

where

η = Dynamic viscosity

Suffices f,g,m denote liquid,vapour and mixture respectively.

Parameters β' and k have already been defined earlier in Chapter 3.

5.2.2 Instability in the Solution of Momentum Equations

In the procedure for calculating the pressure drop, the film thickness was subdivided into a finite number of unmixing shear layers as discussed in Chapter 3. The thickness of each layer may vary in the direction of flow, but the sum of the individual layer thickness must equal the local film thickness.

It was stated earlier that equation (5.2.9) gives the radial component of the tangential velocity for use in the Runge-Kutta procedure.

$$\frac{\partial w}{\partial r} = \frac{\frac{-\rho u w}{r} - \frac{w}{r}\frac{\partial \eta}{\partial r} + \frac{\partial \eta}{\partial y}\frac{\partial w}{\partial y} + \eta\left[\frac{\partial^2 w}{\partial r^2} + \frac{\partial^2 w}{\partial y^2} - \frac{w}{r^2}\right]}{\rho u - \frac{\partial \eta}{\partial r} - \frac{\eta}{r}} \qquad (5.2.9)$$

At the wall boundaries velocity u is zero, and thus the denominator of equation (5.2.9) may tend to zero which would cause an overflow. This will mean that the results obtained will be dependent on the mesh size, and as the mesh becomes finer the flow tends to a uniform profile with an infinite velocity gradient at the boundaries.

Applying L'Hôpital's rule to equation (5.2.9) shows that this equation is stable. In addition solutions have been presented in Chapter 7 which show that small mesh sizes have been used and that there is a convergence of the solution with decreasing the mesh size.

CHAPTER SIX

PLANNING AND EXECUTION OF THE EXPERIMENTAL PROGRAMME

6.1 Introduction

This chapter briefly discusses some difficulties which were present during the initial comparison of the practical results with the theoretical predictions.

The computer program described in Chapter 5 was used to determine the operating conditions which should be used in order to be reasonably certain that vapour would be generated within the bearing. As discussed in Chapter 4, the parameters which would have a major effect on the pressure distribution and viscous dissipation of energy in the bearing are, the gap, mass flow rate, inlet pressure and temperature. A series of predictions were carried out to establish the influence of these parameters and the operating limitations which would be imposed by the characteristics of the experimental equipment.

6.2 Prediction of Suitable Test Conditions

The momentum equation takes no account of thermodynamic effects and in the absence of phase change the corresponding prediction of variation of pressure within the bearing is independent of inlet pressure. Phase change within the bearing is determined by the relative values of local enthalpy and the enthalpy of saturated liquid at the local pressure. The combination of momentum and energy equations permits the enthalpy variations to be predicted and the point at which phase change occurs, if at all, is determined by the combined effect of gap, mass flow rate, inlet pressure and inlet temperature.

The momentum equation, equation (3.7.5) indicates that the radial outward flow between parallel plates may result in either an increase or a decrease in fluid pressure, determined by the relative magnitudes of fluid momentum and viscous shear force. Thus for a given gap the resulting pressure distribution is a function of mass flow rate. This effect was investigated for a range of gaps and mass flow rates and compared with mass flow/pressure drop characteristics of the available circulating pump to establish the operating boundaries of the apparatus.

The likely range of appropriate inlet conditions was determined by predicting the pressure and enthalpy distribution as functions of mass flow rate, inlet pressure and inlet temperature for a range of gaps. Some typical output data for pressure is presented graphically in Figure 6.2.1, but the constraints imposed by the circulating pump and remaining parts of experimental equipment are best summarised in tabular form as shown in Table 6.2.1.

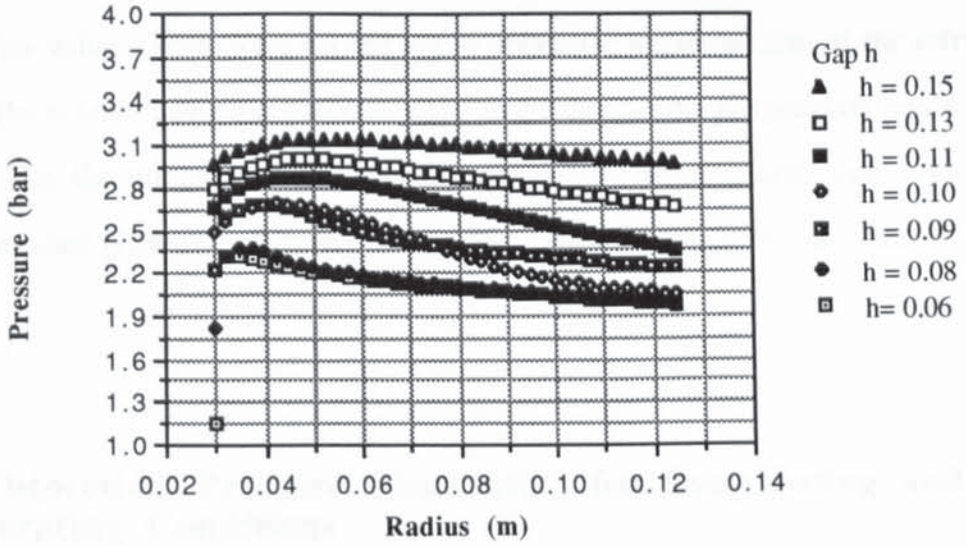

Figure 6.2.1
Typical theoretical pressure distribution curves for constant mass flow, constant inlet conditions and a range of gap sizes

Gap h (mm)	Mass Flow (kg/s)	Port Pressure(bar)	Inlet Temp.(K)	Suitability
0.06	0.26	2.30	292	No
0.06	0.26	2.5	305	No
0.06	0.33	2.8	295	No
0.06	0.33	3.3	306	No
0.08	0.26	2.3	292	No
0.08	0.26	2.5	305	No
0.08	0.33	2.8	295	No
0.08	0.33	3.3	306	No
0.09	0.26	2.3	292	No
0.09	0.26	2.5	305	No
0.09	0.33	2.8	295	No
0.09	**0.33**	**3.3**	**306**	**Yes**
0.1	0.26	2.3	292	No
0.1	0.26	2.5	305	No
0.1	0.33	2.8	295	No
0.1	0.33	3.3	306	No
0.11	0.26	2.3	292	No
0.11	0.26	2.5	306	No
0.11	0.33	2.8	295	No
0.11	0.33	3.3	306	No

Table 6.2.1
Typical data considered in selection of a suitable set of test condition

It is apparent from Table 6.2.1 that a gap of 0.09 mm was predicted the most appropriate size to use for the investigation. It was therefore decided that the gap should initially be

set to this value. Tests were carried out to obtain the vapourisation of the refrigerant within the bearing using a gap of 0.09 mm. The experimental programme was designed to examine the widest possible range of conditions, starting with non-evaporating conditions and gradually advancing to the point at which evaporation commenced.

6.3 Theoretical Pressure Distribution for Evaporating and non-Evaporating Conditions

Theoretical predictions based on the present theory indicated that it should be possible to achieve evaporating conditions simply by increasing the temperature of the refrigerant at the inlet port to the bearing. Two typical predictions are shown in Figures 6.3.1 and 6.3.2. Figure 6.3.1 shows the comparison between, a non-evaporating situation, a partially evaporating situation in which the refrigerant starts to evaporate somewhere within the bearing, and finally a situation of full evaporation where the refrigerant has already begun to evaporate before reaching the bearing. These results correspond to a mass flow rate of 0.08 kg/s and a gap of 0.09 mm. Figure 6.3.2 shows another comparison between non-evaporation, partial evaporation and full evaporation, corresponding to a higher mass flow rate of 0.28 kg/s and the same gap size of 0.09 mm. It is evident from these Figures that in both cases, evaporation causes a decrease in the pressure drop along the bearing.

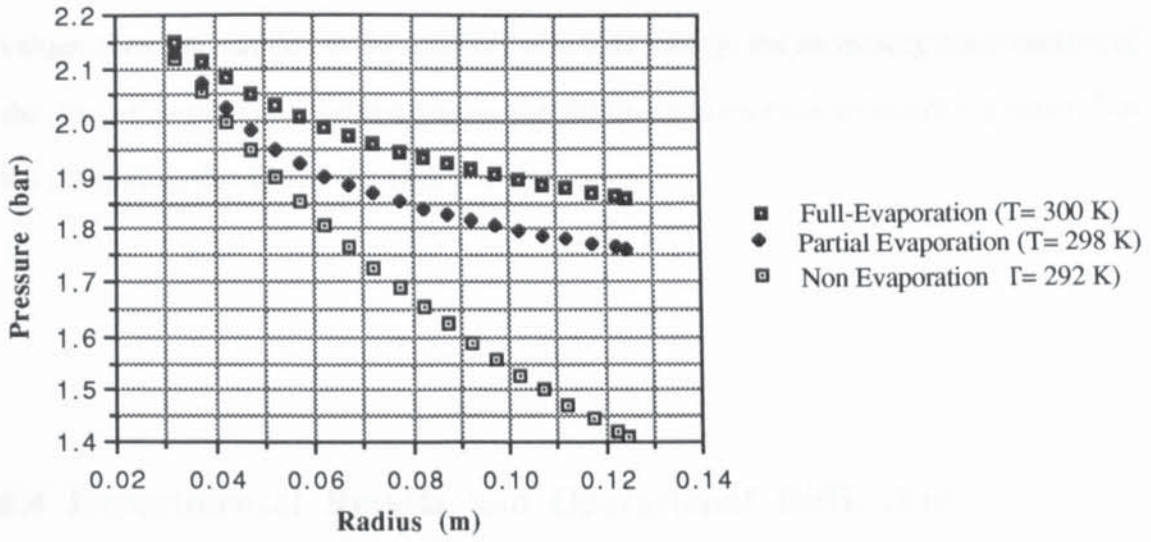

Figure 6.3.1
Theoretical pressure distribution curves for evaporation and non-evaporation conditions, corresponding to a mass flow rate of 0.08 kg/s and a gap of 0.09 mm

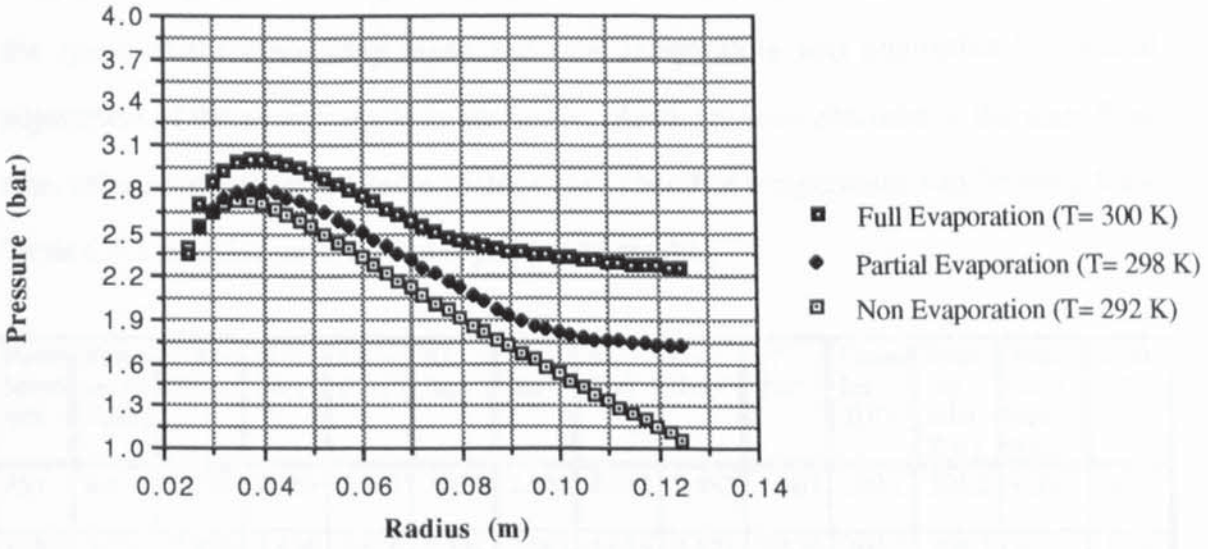

Figure 6.3.2
Theoretical pressure distribution curves for evaporation and non-evaporation conditions, corresponding to a mass flow rate of 0.28 kg/s and a gap of 0.09 mm.

These predictions indicate that evaporation has a considerable effect on the pressure drop through the bearing, causing a marked reduction in the overall pressure drop which would increase the load carrying capacity if the chamber pressure remained unaltered, otherwise it would reduce it. In Figure 6.3.2 the pressure rise within the bearing at low

values of radius was due to the recovery of kinetic energy: the increasing cross section of the flow allows the bearing to act as a radial diffuser and pressure recovery is greater than the dissipation due to viscous effects in this region.

6.4 Experimental Results and Operational Difficulties

A series of tests were performed in which the operation conditions of the experimental equipment corresponded as closely as possible to the theoretical predictions produced by the computer program. The gap was set at 0.09 mm; mass flow was varied by changing the speed of the circulating pump and inlet temperature was controlled by careful adjustment of the power supply to the heater. Readings were obtained of the mass flow rate, inlet temperature, pressure distribution, chamber temperature and bearing load. Table 6.4.1 contains some typical experimental results.

Pump Speed rpm	Pump outlet P(bar)	Port P(bar)	p1 (bar)	p2 (bar)	p3 (bar)	p4 (bar)	p5 (bar)	p6 (bar)	p7 (bar)	Chamber T(K)	Beari-ng inlet T(K)	Mass flow rate kg/s	Load (N)
950	4.63	2.728	2.563	2.537	2.506	2.601	2.532	2.487	2.403	300.1	301.2	0.26	1653
1050	5.25	2.873	2.656	2.626	2.592	2.693	2.625	2.573	2.525	304.2	305.3	0.27	1504
1200	5.65	3.057	2.769	2.742	2.706	2.807	2.738	2.677	2.734	308.5	309.8	0.29	1368
1250	5.94	3.214	2.842	2.802	2.779	2.879	2.818	2.763	2.810	311.9	312.7	0.30	1285
1300	6.25	3.279	2.875	2.809	2.778	2.866	2.824	2.743	2.775	313.1	314.5	0.32	1141
1350	6.78	3.378	2.908	2.844	2.819	2.912	2.865	2.790	2.821	315	317.1	0.33	1083

Table 6.4.1
Typical experimental values of the pressure distribution and load for different mass flow rates.

Table 6.4.1 shows that the measured load decreases while the inlet bearing pressure increases. The load cell measurements could not be regarded to be valid since an increase in the inlet pressure should have caused a rise in the bearing load. It was therefore apparent that the performance of the load cell required investigation which is discussed later in this chapter.

The principle operating difficulty which had been exposed from the first series of tests related to the control of chamber pressure, which rose rapidly when the bearing inlet temperature was increased to try to obtain conditions in which evaporation had been predicted. A further cause for concern was the lack of agreement between predicted and measured mass flow rates. Problems relating to the load cell and mass flow rate were resolved as follows.

6.4.1 Load Cell

Figure 6.4.1.1 is a sectional representation of the bearing chamber indicating the relative position of important features. Refrigerant flows radially outwards through the gap (1), between the bearing surface(2) and the perspex(4). The Figure is not to scale.

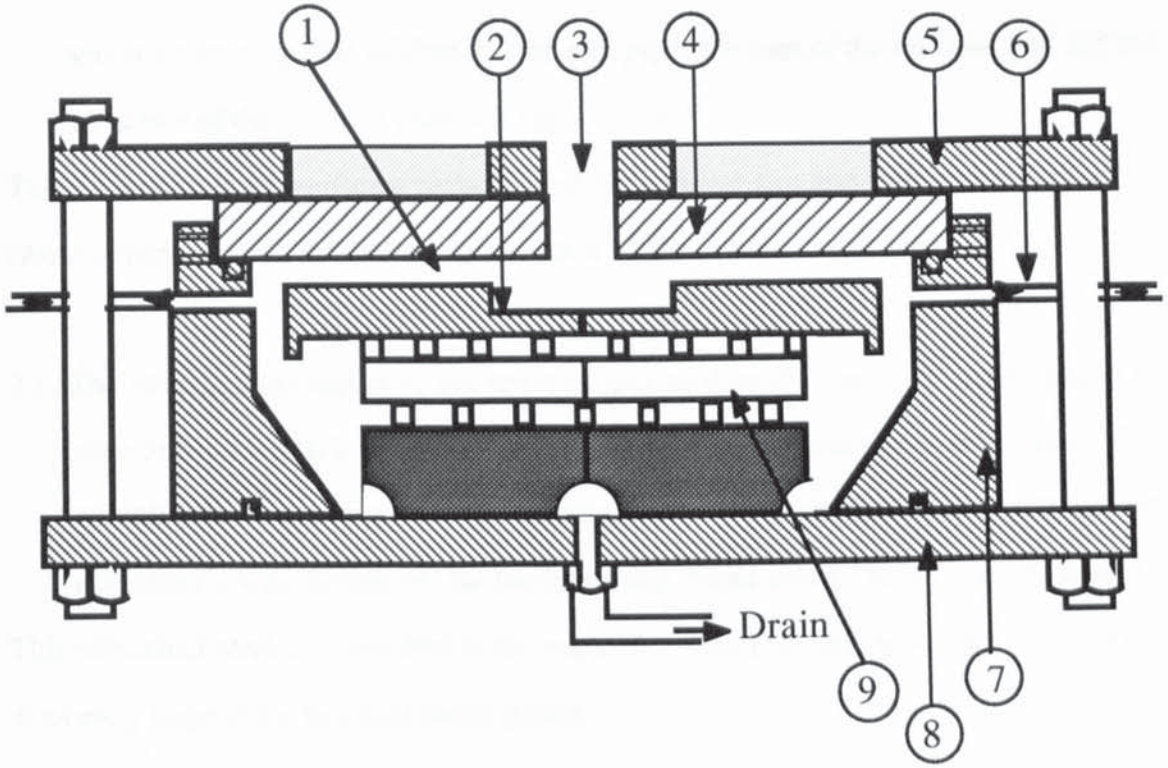

Figure 6.4.1.1
Details of the gap in the bearing

where

1. Gap in the bearing
2. Bearing plate
3. Inlet port
4. Perspex
5. Top flange
6. Vapour discharge to condenser
7. Chamber wall
8. Bottom flange
9. Load cell

Problems associated with the load cell are summarised as:-

1) Since the principle by which the load cell would operate was the deflection of the beam, as described earlier in section 4.3.3, Chapter 4, and the value of the gap is a function of the response of the cell to the load generated by the pressure distribution

within the bearing, it is evident that the true gap is the sum of the nominal gap and the deflection of the load cell under the applied load.

This deflection is a significant proportion of the nominal gap and is dependent upon the chamber pressure and the pressure distribution on the bearing surface.

2) The electrical insulation of the strain gauges used on the load cell was found to be susceptible to attack by refrigerant R114 despite manufacturers assurance. The assembly had been protected by coating with the recommended silicon product but when the rig was dismantled the insulation was found to have failed in many places.

This effect had obviously resulted in the output from the load cell becoming meaningless at an early stage in the practical investigation.

Subsequently the load cell was replaced with a solid annular ring support giving a fixed gap. The value of this gap was chosen from the prediction of pressure drop to provide phase change within the bearing as discussed earlier.

6.4.2 Measurement of Mass Flow Rate

The narrow range of mass flow indicated in Table 6.4.1 was first thought to be caused by some malfunction of the flowmeter, but when the data was compared with the values obtained by interpolation from the mass flow rate and pressure rise characteristics of the circulating pump, it was apparent that there was reasonable agreement.

A cross check between the values obtained from the flow meter and those available from the pump characteristics is shown in Table 6.4.2.1 which contains some typical values and shows a close agreement, confirming that the flowmeter readings were reliable.

Test	Speed (R.P.M)	Pressure Rise (bar)	Mass (Pump) (kg/s)	Mass(Meter) (kg/s)
1	950	2.1	0.265	0.26
2	1050	2.41	0.28	0.27
3	1200	2.75	0.295	0.28
4	1250	2.90	0.30	0.29
5	1300	3.10	0.31	0.30
6	1400	4.0	0.34	0.32

Table 6.4.2.1
Comparison of some typical measured values of mass flow rate and those available from the circulating pump characteristics.

6.4.3 Control of Chamber Pressure

During early use of the equipment it was apparent that pump inlet pressure was effectively determined by the saturation pressure of the mixture in the bearing chamber which is a unique function of temperature in the chamber. Consequently, when the temperature of the liquid refrigerant at the inlet to the bearing was increased to encourage evaporation within the bearing the chamber temperature and pressure also increased. Now because the pressure rise in the circulating pump is a function of rotational speed and mass flow

rate, any attempt to increase the liquid temperature at the inlet to the bearing while keeping mass flow rate constant resulted in a corresponding pressure rise at the inlet port. This had the effect of suppressing the formation of vapour within the bearing, as illustrated on the pressure-specific enthalpy diagram in Figure 6.4.3.1.

This interaction severely limited the possibility of obtaining two phase operation within the bearing and is discussed fully in Chapter 8.

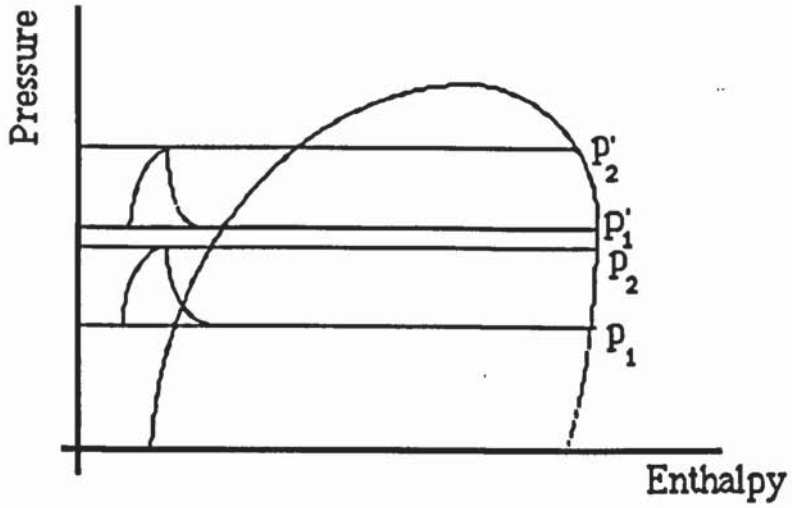

Figure 6.4.3.1
Pressure-Specific enthalpy illustrating that increased pump inlet pressure p_1 results in the suppression of vapour formation for a constant mass flow rate

6.5 Revised Comparison of the Theoretical Predictions with the Measured values.

Having replaced the load cell with a solid annular ring support to achieve a fixed gap, and confirmed the measurements of mass flow rates, a further series of experimental results were obtained with a fixed gap set nominally at 0.09 mm employing the available range

of mass flow rate. Table 6.5.1 contains values of temperature, pressure and mass flow rates while Figure 6.5.1 shows the corresponding pressure distribution curves.

Mass flow rate kg/s	Pump speed (rpm)	Beari -ng inlet T (K)	Cham ber Temp (K)	pump inlet P(bar)	pump outlet P(bar)	port P(bar)	p1 (bar)	p2 (bar)	p3 (bar)	p4 (bar)	p5 (bar)	p6 (bar)	p7 (bar)
0.26	950	292.8	291.9	1.83	3.76	2.31	2.010	2.011	2.012	2.103	2.024	2.060	2.007
0.27	1050	293.7	292.5	1.83	4.10	2.41	2.080	2.085	2.088	2.152	2.110	2.122	2.062
0.29	1200	294.4	293.2	1.83	4.21	2.52	2.145	2.154	2.161	2.234	2.196	2.188	2.138
0.30	1250	295.2	293.7	2.03	4.62	2.69	2.259	2.262	2.274	2.310	2.317	2.303	2.289
0.32	1300	296.1	294.6	2.03	4.86	2.93	2.425	2.439	2.468	2.524	2.509	2.462	2.455
0.33	1350	297.9	296.0	2.03	5.83	3.24	2.650	2.669	2.695	2.779	2.741	2.717	2.703
0.35	1450	300.2	298.2	2.03	6.52	3.69	2.995	3.009	3.043	3.103	3.094	3.069	3.041

Table 6.5.1
Experimental values of the pressure distribution for different mass flow rates

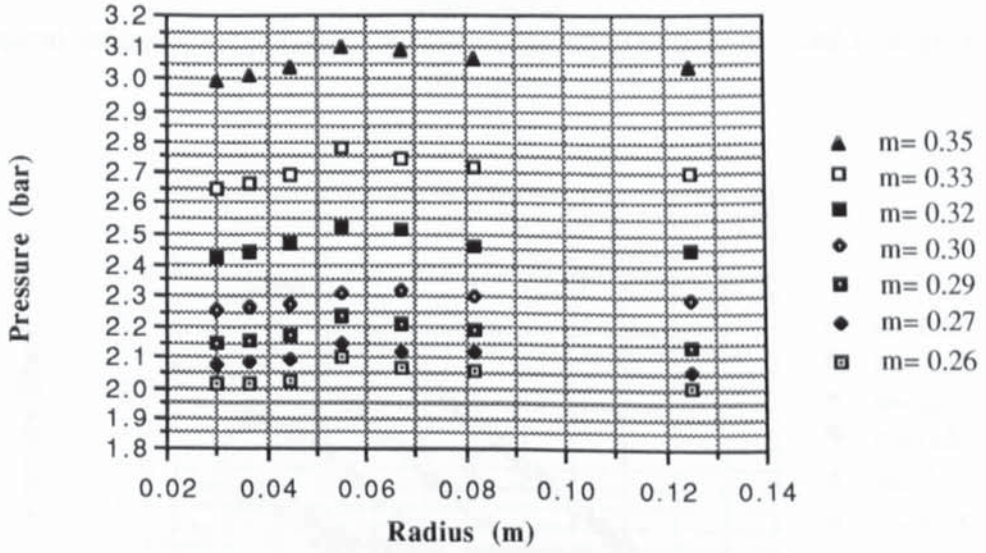

Figure 6.5.1
Measured pressure distribution curves for several mass flow rates

Theoretical predictions corresponding to these inlet conditions are presented as Table 6.5.2 and Figure 6.5.2. The measured pressure distribution curves presented as Figure

6.5.1 indicate that the overall pressure drop across the bearing has a very small magnitude compared to the predicted pressure drop as indicated in Figure 6.5.2.

Radius (m)	Pressure (bar) (m= 0.26)	Pressure (bar) (m= 0.27)	Pressure (bar) (m= 0.29)	Pressure (bar) (m= 0.30)	Pressure (bar) (m= 0.32)	Pressure (bar) (m= 0.33)
0.03	1.6019	1.6035	1.6386	1.9464	2.181	2.5069
0.0323	1.6315	1.6487	1.7018	2.0436	2.3051	2.677
0.0398	1.5872	1.6122	1.6754	2.0421	2.3214	2.7216
0.0448	1.5025	1.532	1.6016	1.9874	2.2786	2.6957
0.0498	1.3949	1.4318	1.5004	1.9048	2.2047	2.632
0.0548	1.28	1.3941	1.4389	1.805	2.1146	2.5479
0.0598	1.2427	1.3802	1.4214	1.6949	2.0146	2.4531
0.0648	1.2316	1.3693	1.4096	1.5786	1.9079	2.353
0.0698	1.2232	1.3595	1.3994	1.4586	1.7974	2.251
0.0748	1.2156	1.3506	1.39	1.3572	1.6847	2.1473
0.0798	1.2086	1.3422	1.3813	1.324	1.5709	2.0421
0.0848	1.202	1.3345	1.3732	1.3112	1.4565	1.9365
0.0898	1.1957	1.3271	1.3656	1.3028	1.3697	1.831
0.0948	1.1898	1.3202	1.3548	1.2958	1.337	1.7257
0.0998	1.1841	1.3136	1.3515	1.2893	1.3222	1.6209
0.1048	1.1787	1.3072	1.3449	1.2832	1.313	1.5165
0.1098	1.1734	1.3012	1.3386	1.2773	1.3059	1.4145
0.1148	1.1684	1.2953	1.3326	1.2717	1.2996	1.3541
0.1223	1.161	1.2869	1.3238	1.2636	1.291	1.3172
0.1248	1.1586	1.2841	1.321	1.261	1.2883	1.3104

Table 6.5.2
Theoretical values of the pressure distribution for a gap of 0.09 mm and a range of mass flow rates

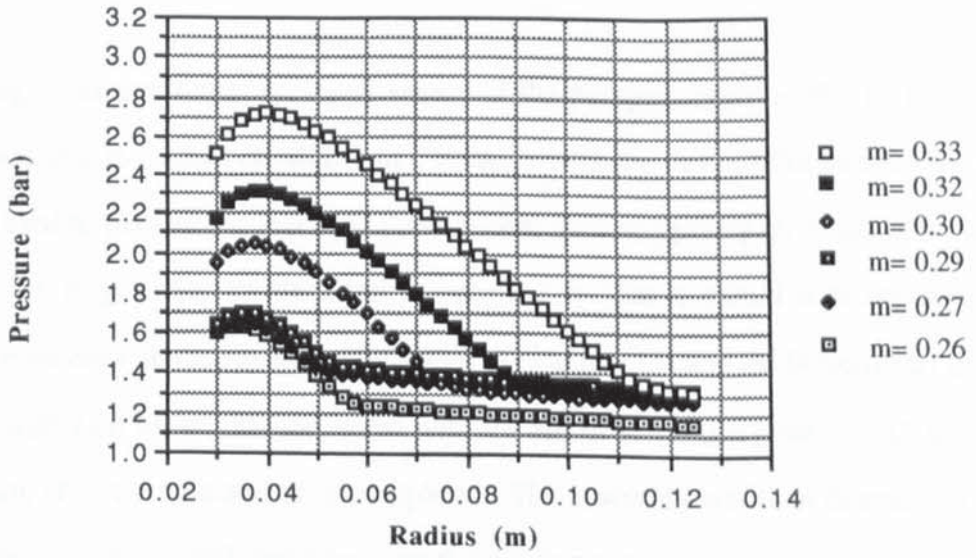

Figure 6.5.2
Theoretical pressure distribution curves for a gap of 0.09 mm and the range of mass flow rates and inlet conditions corresponding to Table 6.5.1

It is apparent that evaporation was predicted to occur at different radii depending upon the mass flow rate and, more importantly, inlet temperature. When the theoretical predictions shown in Figure 6.5.1 are compared with the experimental pressure distribution presented in Figure 6.5.1, it is evident that there is no correlation between the results. This finding was regarded as symptomatic of deeper problems either with the mathematical model, the computer program or the experimental apparatus.

It had already been established that the flowmeter readings were reliable and that gap size was no longer dependent on the deflection of load cell. Strain in the bolts retaining the cover plate and in other components of the chamber and bearing support assembly was predicted to add only 0.0004 mm under the load which arose during the tests discussed in 6.5.1, a change which did not affect the predicted pressure distribution significantly. The only factor which could explain the discrepancy was the size of the gap in the bearing which may not have been set correctly to the nominal value during assembly.

6.6 Investigation of Gap Size

Referring to Figure 6.6.1, it can be seen that the perspex overlaps the main chamber, which was due to the unavailability of a perspex with the desired thickness. An 'O' ring (2) was used to prevent the leakage of refrigerant. In setting the gap, it had been assumed that the 'O' ring would be flattened completely so that it would seal correctly. The clearance between the top surface of the wall of chamber (3) and the bottom part of the top plate as indicated by 'c', was measured with the aid of some slip gauges with the 'O' ring in position after the tests had been completed. The assembly was then dismantled and the clearance again measured, this time with the 'O' ring removed. It was discovered that the 'O' ring had not been flattened completely during the initial assembly and there was a

difference of 0.08 mm between the two readings, this meant that the true gap (1) in the bearing was 0.17 mm.

This value of 0.17 mm was considered in further theoretical predictions, (presented in Chapter 7) and a good correlation was obtained with the measured pressure distribution, indicating that there had been no evaporation during any of the inlet conditions which had been employed in the tests.

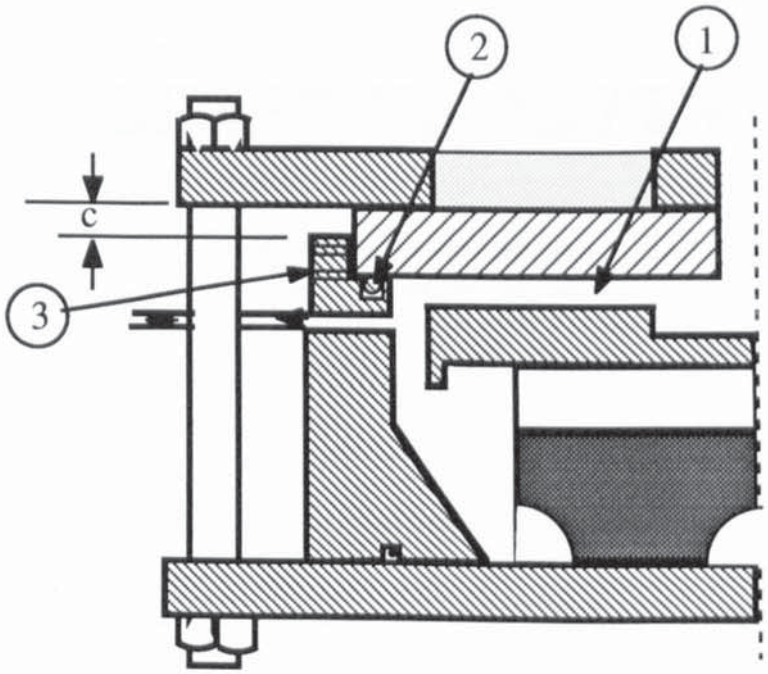

Figure 6.6.1
Details of the gap in the bearing

CHAPTER SEVEN

RESULTS

7.1 Introduction

The experimental results discussed in this chapter are those which were finally obtained when the operational difficulties of the equipment had been largely resolved. The operating characteristics of the test rig prevented the desired control of inlet pressure from being achieved because of the dependence of pump delivery pressure upon chamber pressure and pump speed, as mentioned in Chapter 4.

Five sets of typical results are presented and where applicable, in each case the experimental data are compared with predicted data for the same mass flow rate, inlet temperature and pressure at station 1. Early predictions were made using the constant viscosity form of the Navier-Stokes equations. Although viscosity values were updated continuously within the Runge-Kutta process, this form of the equations omits the effect of the transverse gradient of viscosity across the film and the predictions are, therefore, lacking in precision. The full variable viscosity form of the equation was employed at a later stage in the research when the effect of phase change within a rotating face seal was predicted, where the transverse viscosity gradients are greater due to the effect of rotation. When later used for the hydrostatic thrust bearing prediction, the full equations produced results which were not significantly different from those obtained with the constant viscosity form of the Navier-Stokes equations.

The first set of results covers the range of mass flow rate originally predicted to show evaporation, but with the larger gap of 0.17 mm, as mentioned in Chapter 6; the next utilised increased temperature to try and encourage evaporation. Further predictions indicated that a gap of 0.12 mm and a suitable condition of mass flow rate and inlet temperature should give two phase flow in the outer regions, despite the severe limitations imposed by the interaction between liquid temperature, chamber pressure, pump speed and mass flow rate. Results are presented to show this effect.

Before any result is presented the accuracy of the measurement technique and equipment used in the experimental test rig is considered and presented in section 7.2.

The experimental and theoretical results with initial comments are presented in the following sections:

Section 7.3 - The first series of tests to investigate the effect of varying mass flow rate in the range predicted to demonstrate both single phase and two phase flow with minimum changes in supply pressure and temperature.

Section 7.4 - The effect of varying inlet temperature with restricted changes in supply pressure and a comparison with theoretical predictions using the model based on the constant viscosity form of the Navier-Stokes equations.

Section 7.5 - The effect of a lower mass flow rate with a higher inlet temperature and the predicted values using the constant viscosity model.

Section 7.6 - Results corresponding to evaporating conditions and a comparison with predictions from the constant viscosity model.

Section 7.7 - Results for the prediction of the rotor end face seal characteristics obtained from a more accurate analysis in which the variable viscosity form of the Navier-Stokes equation was used.

7.2 Accuracy of Experimental Measurements

7.2.1 Effect of inaccuracy in measurement of the gap

The metal surface of the test bearing was ground carefully to an average roughness of 0.40 μm while the opposing perspex surface was shown to be even smoother. Since a large diameter of the surface was used to accommodate the necessary instrumentation, the flatness was less precise than this. Although great care was taken during the assembly to ensure that a uniform gap was obtained around the periphery, it was not possible to achieve a variation of less than 12 μm. It has to be accepted that the exact size of the gap

and its possible variation within the bearing was not known to the same degree of accuracy.

The discrepancy between the theoretically predicted and experimentally determined pressure distribution can be related to the possible lack of uniformity of the gap and small variation which existed at the periphery.

7.2.2 Accuracy of Pressure Distribution

Measurement of pressure on any surface is greatly influenced by the condition and precision of sensing points. Errors can occur in the measurement of local static pressure if any slight recess or protuberance exists on the surface, since these may cause the fluid to accelerate. In the present work this was minimised by a precise grinding of the surface. In selecting the pressure transducers, consideration was given to the types which would operate within the full range of anticipated pressure , a maximum range of a approximately 4 bar, which arose during the test runs and stand-by conditions. The transducers were found to be accurate within ± 500 N/m^2 when calibrated, which was better than the manufacturers guarantee of accuracy as a percentage of full scale response. Appendix 1, contains the calibration curves for the pressure transducers. In the case of the first test series the pressure variation across the bearing surface was much less than expected, on account of the excessive gap, the consequence of which produced an effective error band of pressure measurement as high as 5% of the total variation. Nevertheless, the discrepancy between the recorded and the predicted distribution was seldom greater than half the width of the error band and represented the form of the experimental distribution very closely.

7.2.3 Mass Flow Measurement

The measurement of volumetric flow through the bearing was carried out by use of a turbine flow meter. Due to the nature of the refrigerant no simple and direct volumetric calibration of the meter was possible. The meter was calibrated using first water and then paraffin, the latter having a viscosity close to that of the refrigerant, and then dimensional analysis was used to deduce the performance when metering R114. The accuracy of turbine flow meters is generally quoted as 5%, and the method of calibration would possibly widen that value.

The circulating pump used for the liquid refrigerant was a gear pump and as such, there should exist a distinct volume flow rate, and pressure rise characteristic at a given speed when pumping fluids of a given kinematic viscosity. The manufacturer's published calibration of this characteristic must always be equalled or improved by the unit actually supplied and is therefore not necessarily correct, although modern manufacturing methods ensure that the variation from the guaranteed performance is not significant. When the values of volumetric flow rate recorded by the turbine meter were compared with the pump characteristic the discrepancy was found to vary by approximately ±8%. The effect which this level of uncertainty has, when comparing measured and predicted pressure distributions is illustrated for one typical non-evaporating situation by the prediction shown in Figure 7.2.1. It can be seen from this Figure that the discrepancy which results is of the same order as the error band width associated with measurement by the pressure transducers.

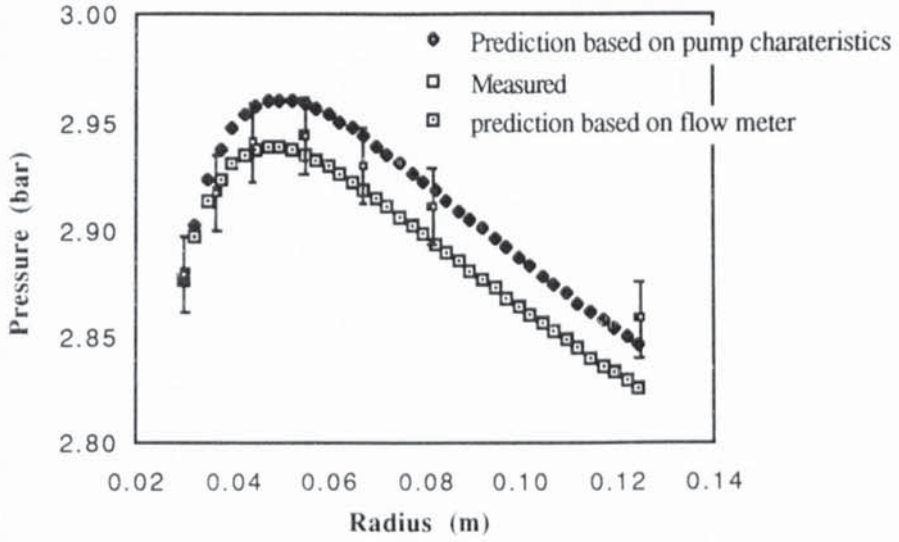

Figure 7.2.1
Predicted discrepancy due to a mass flow error of 8%

7.2.4 Temperature Measurement

Temperatures were recorded at the pump inlet and exit, bearing port inlet, and within the bearing chamber. The records were obtained using Chromel/ Alumel thermocouples, and values were shown on a digital indicator reading to 0.1 K. Temperature measurements were found to affect two aspects of the experimental programme and proved to be very important in determining whether or not evaporation could be achieved within the bearing. Assuming the theoretical approach to be correct it was shown in Chapter 6 that very small changes in temperature at the bearing port caused relatively large changes in the location at which evaporation commenced within the bearing. These small changes were within the accuracy of the digital indicator, but the indication itself relies on the accuracy of the reference datum within the thermocouple amplifier unit, which was ±1 K.

Temperature measurement was also the basis on which the pressure in the bearing chamber was determined, since saturation pressure of the liquid/ vapour mixture is a fundamental characteristic of the temperature of a given fluid.

7.3 First Series of Tests For the Planned range of Mass Flow Rate

In this series of experiments the gap in the model bearing was set to 0.17 mm on the basis of theoretical predictions obtained using the constant viscosity form of the Navier-Stokes equations. The corresponding theoretical results in this section were determined using 50 layers in the lubricating film. Initial program proving was carried out using 10 then 20 and later larger number of layers in the film. The effect of mass flow rate in non-evaporating conditions was measured for a range of values from 0.26 kg/s to 0.35 kg/s corresponding to the required mass flow rates initially predicted to show evaporating conditions while the inlet temperature was maintained as closely as possible to a constant value of 293 K.

7.3.1 Experimental Results

The results shown in Table 7.3.1.1 were obtained using what were predicted to be non-evaporating conditions. No vapour bubbles were observed in the flow passing across the observation points in the cover plate of the bearing chamber.

Mass flow rate kg/s	pump speed (rpm)	Beari-ng inlet T (K)	Cham-ber Temp T (K)	pump inlet P(bar)	pump outlet P(bar)	port P(bar)	p1 (bar) r=.03	p2 (bar) r=.037	p3 (bar) r=.045	p4 (bar) r=.055	p5 (bar) r=.067	p6 (bar) r=.08	p7 (bar) r=.12
0.26	950	292.8	291.9	1.83	3.76	2.31	2.010	2.048	2.051	2.046	2.016	1.970	1.860
0.27	1050	293.7	292.5	1.83	4.10	2.41	2.080	2.109	2.132	2.110	2.089	2.024	1.942
0.29	1200	294.4	293.2	1.83	4.21	2.52	2.145	2.175	2.188	2.171	2.139	2.123	2.012
0.3	1250	295.2	293.7	2.03	4.62	2.69	2.259	2.292	2.328	2.289	2.291	2.241	2.141
0.32	1300	296.1	294.6	2.03	4.86	2.93	2.425	2.465	2.521	2.501	2.472	2.441	2.331
0.33	1350	297.9	296.0	2.03	5.83	3.24	2.650	2.699	2.755	2.732	2.698	2.682	2.565
0.35	1450	300.2	298.2	2.03	6.52	3.69	2.995	3.045	3.119	3.103	3.064	3.045	2.941

Table 7.3.1.1
Measured radial pressure distribution. Mass flow rate 0.26 to 0.35 kg/s. Gap 0.17 mm

7.3.2 Theoretical Results

The corresponding predicted values of pressure distribution are shown in Table A4.3.1, in Appendix 4.

Figures 7.3.1.1-2 overleaf compare the measured and predicted pressure distribution and it is evident that there is now reasonably close agreement whereas Table 6.4.1 in Chapter 6 contained results which were much less satisfactory. The corresponding prediction for the enthalpy distribution under these inlet conditions indicates that no evaporation takes place at any radius.

It is apparent from the shape of the pressure distribution curves in Figure 7.3.1.1 and 7.3.1.2 that 35% variation in mass flow rate has little effect on the rate of change of pressure with radius.

With non-evaporating flow the principal determinant of absolute pressure values is the pressure at the inlet to the bearing. The pressure rise across the circulating pump is a function of speed and the mass flow rate so that the bearing inlet pressure is determined by chamber pressure if speed and mass flow rate are constant. Because the chamber contains a mixture of liquid and vapour the pressure is determined by saturation temperature. If the smooth uniform slopes of the pressure distribution curves indicated by the theoretical predictions of Chapter 6, section 6.3 are correct then there has been no evaporation in all of these tests. The changing inlet temperatures would otherwise have led to different pressure distributions in each case, assuming that the theoretical predictions provide a reliable indication of trends.

Figures 7.3.1.1-2 show the corresponding measured and predicted pressure distribution curves for the same range of mass flow rates and a gap of 0.17 mm.

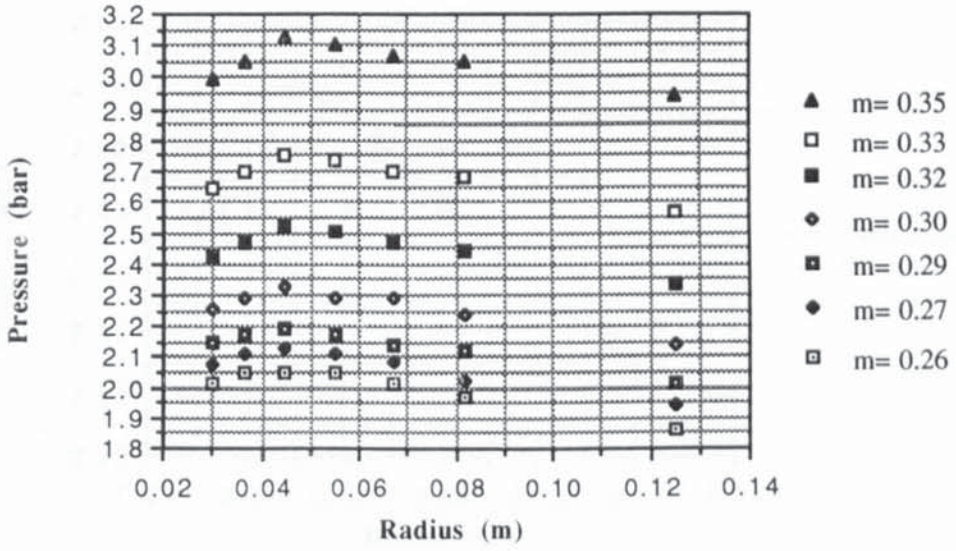

Figure 7.3.1.1
Measured pressure distribution curve for several mass flow rates and a bearing gap of 0.17 mm

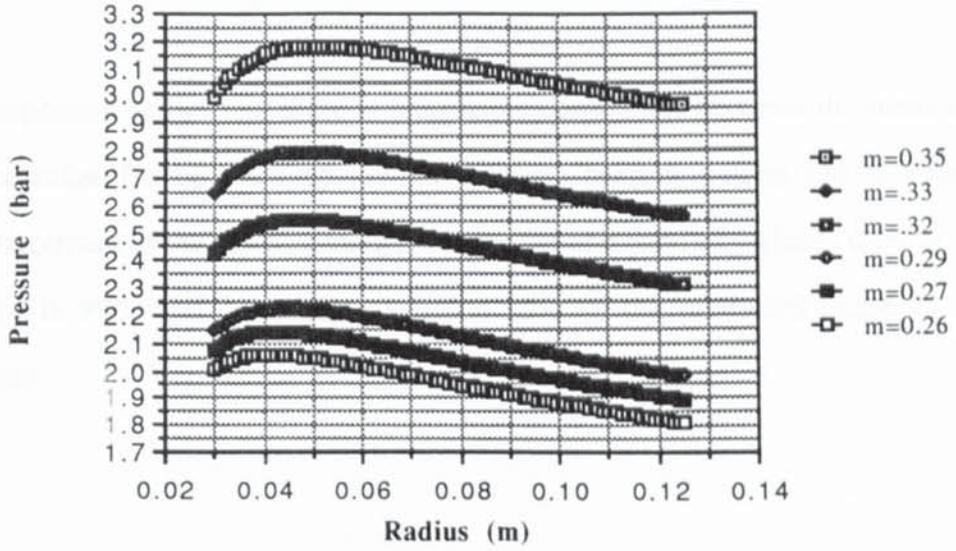

Figure 7.3.1.2
Theoretical pressure distribution curves for corresponding mass flow rates and bearing gap of 0.17 mm

7.3.3 Comparison of Measured and Predicted Pressure Distribution

Figure 7.3.3.1 shows a typical direct comparison between the measured values of the pressure and the predicted values corresponding to a mass flow rate of 0.32 kg/s and a gap of 0.17 mm. Error bands for the measured values have been included in this Figure.

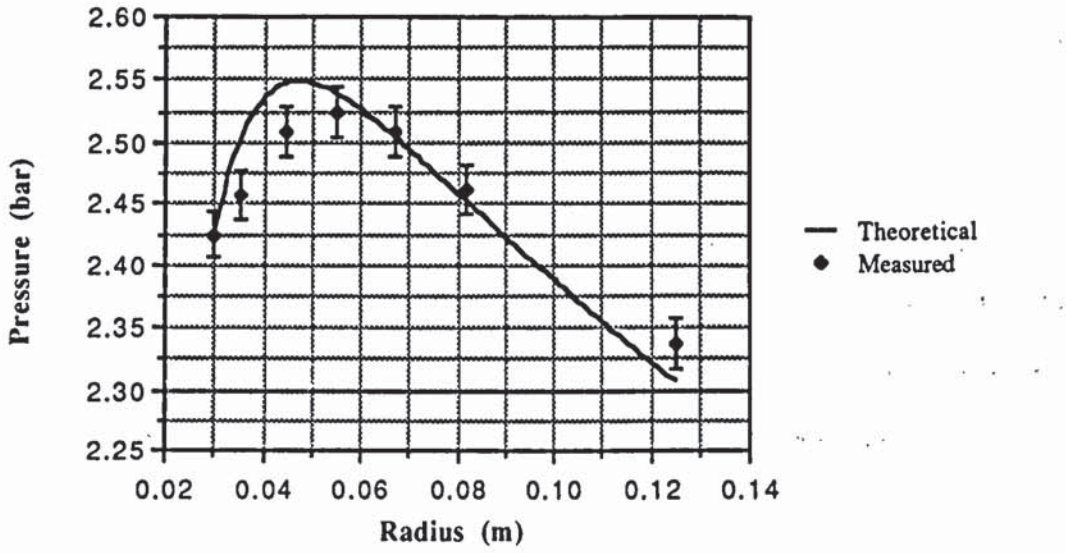

Figure 7.3.3.1
Comparison of the predicted and measured pressure distribution. Mass flow 0.32 kg/s; gap 0.17 mm; inlet temperature 296 K

The comparison shows that there is reasonable correlation between the measured and predicted values for the non-evaporating conditions, bearing in mind that the accuracy of the measurement of the gap assuming perfectly flat and parallel surfaces is ±7%, of mass flow rate is ±5% and of pressure itself is ±2% of the predicted range of the test conditions.

7.3.4 Predicted Radial Distribution of Density and Enthalpy

As described in Chapter 3, the gap was divided into a finite number of layers (in this particular case, 50) for which the variation of the properties was predicted assuming a parabolic velocity profile at the inlet. The pressure distribution is determined principally by the variation of lubricant density and viscosity at any given mass flow rate. The results indicate that viscous dissipation within the lubricant film entering the bearing leads to increasing temperature, reduced density and reduced viscosity. The temperature dependence of lubricant density and viscosity was included in the solution of the momentum, energy and continuity equations, as described in Chapter 3.

The predicted radial distribution of density, enthalpy, enthalpy of saturated liquid at local pressure, temperature and viscosity are presented graphically as Figures 7.3.4.1-6.

Figure 7.3.4.1 shows the density distribution for a typical non-evaporating condition. It can be seen that only the layers near the wall exhibit some changes in density but the subsequent layers show a minimal change. The overall decrease in density of the lubricant between the inlet and the outlet of the bearing chamber corresponds to the layer near the wall and for this typical test is less than 0.1%. However, a layer at the centre of the gap shows no change in the density.

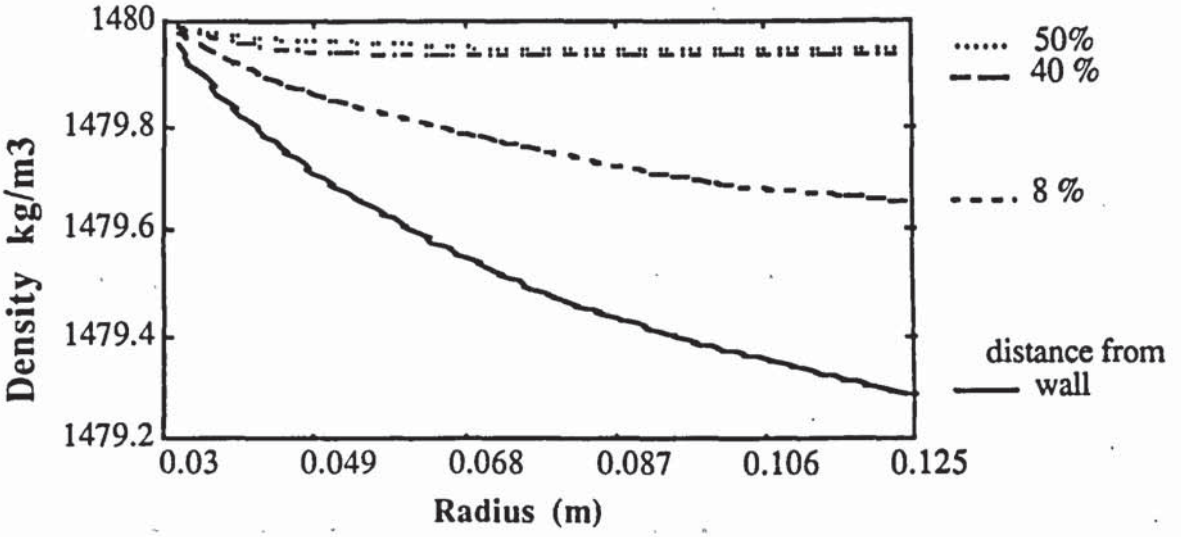

Figure 7.3.4.1
Radial Density Distribution at 0.26 kg/s; gap 0.17 mm; inlet temperature 293 K; inlet pressure 2.01 bar. Non-evaporating flow. The % sign indicates the percentage of the distance away from the wall

Figure 7.3.4.2 shows the radial enthalpy distribution for the same non-evaporating conditions whose density distribution was considered above as Figure 7.3.4.1. Again it can be seen that the only layers whose enthalpy undergo any small changes are those near the walls and the minimum changes correspond to the layer midway across the gap. It should be noted that the distribution of all parameters such as density, temperature etc. is always symmetrical across the gap as will be shown by the velocity profile on the following pages.

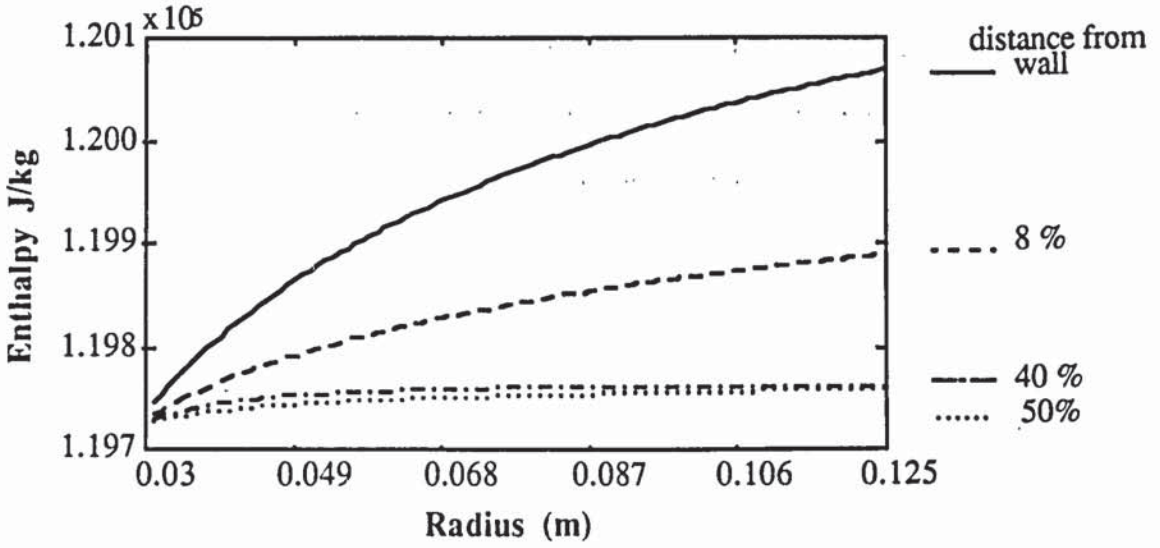

Figure 7.3.4.2
Radial Enthalpy Distribution at 0.26 kg/s; gap 0.17 mm; inlet temperature 293 K; inlet pressure 2.01 bar. Non-evaporating flow

Figure 7.3.4.3 shows the radial distribution of the enthalpy of saturated liquid at local pressure which is compared with the predicted enthalpy in the layers to determine if evaporation has taken place. This Figure corresponds to the same non-evaporating conditions considered above.

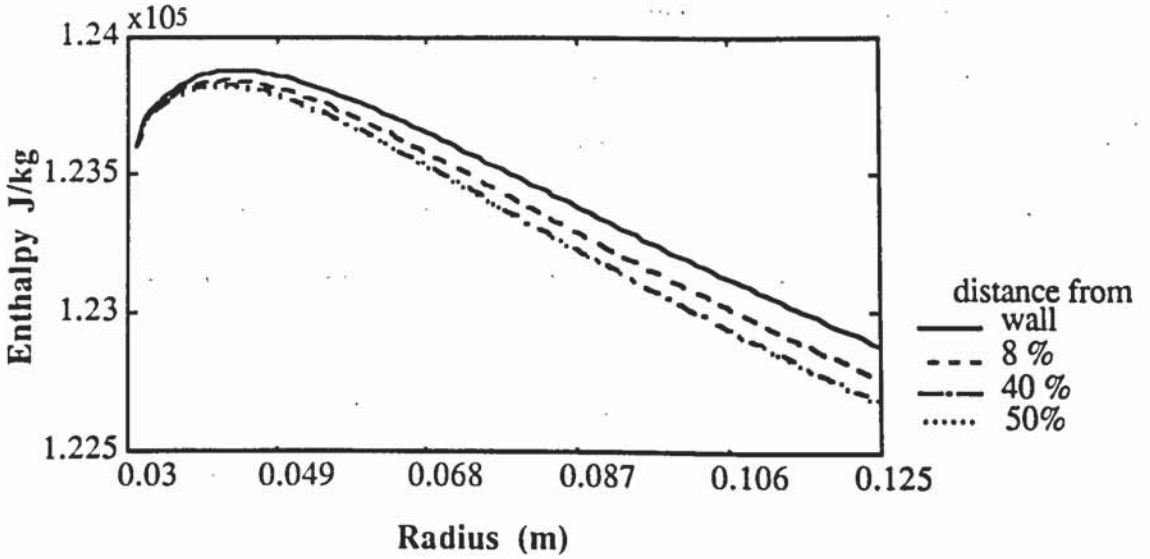

Figure 7.3.4.3
Radial Enthalpy Distribution at 0.26 kg/s; gap 0.17 mm; inlet temperature 293 K; inlet pressure 2.01 bar. Non-evaporating flow

A typical plot of the predicted radial distribution of temperature in selected layers is included as Figure 7.3.4.4 and indicates that temperature changes are very small in the non-evaporating case. Even the temperature of the layers near the walls increases by less than 0.5 K in the radial direction whereas for the central layer within the gap there is a totally negligible change.

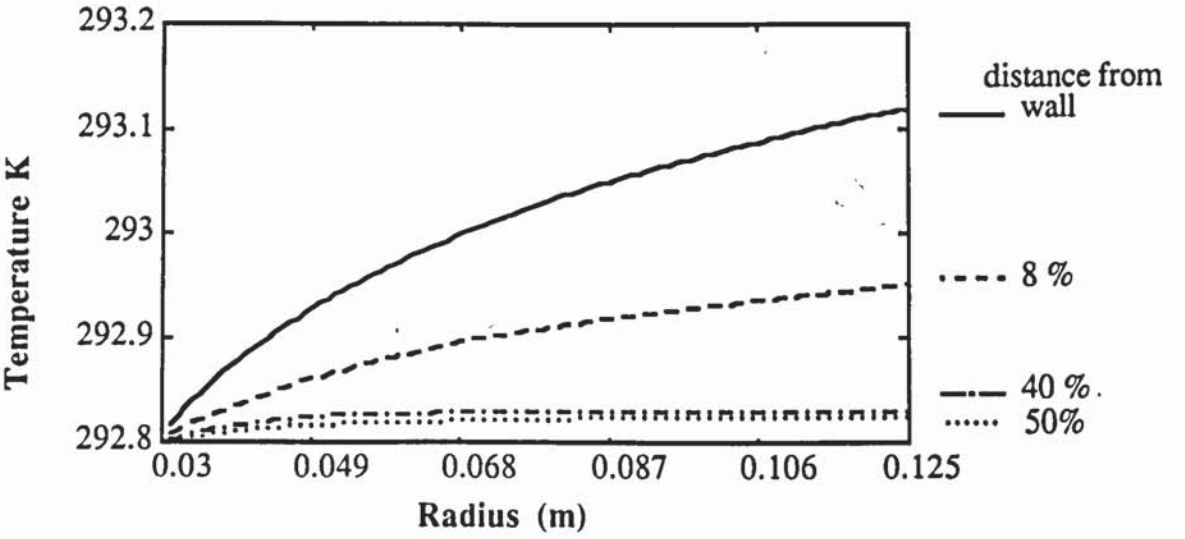

Figure 7.3.4.4
Radial Temperature Distribution at 0.26 kg/s; gap 0.17 mm; inlet temperature 293 K; inlet pressure 2.01 bar. Non-evaporating flow

Figure 7.3.4.5 shows the velocity profiles across the gap rather than the radius. There are two reasons for presenting the velocity profiles across the gap. First to show that there was symmetry of solutions within the gap, as expected, and secondly to show that the velocity distribution across the gap virtually remained parabolic at all radii, despite the greater dissipation of energy in layers of high shear near the walls.

Figure 7.3.4.6 shows the radial viscosity distribution for the non-evaporating conditions. Again it is evident that the viscosity of the layers near the walls exhibits some decrease which is due to an increase in the temperature, whereas the central layers within the gap experiences very little change in viscosity. The overall viscosity change for the non-evaporating condition is not sufficient to cause abrupt changes in the pressure distribution

but, as will be shown later, that change can be substantial in an evaporating condition and leads to a decrease in the slope of pressure distribution curve.

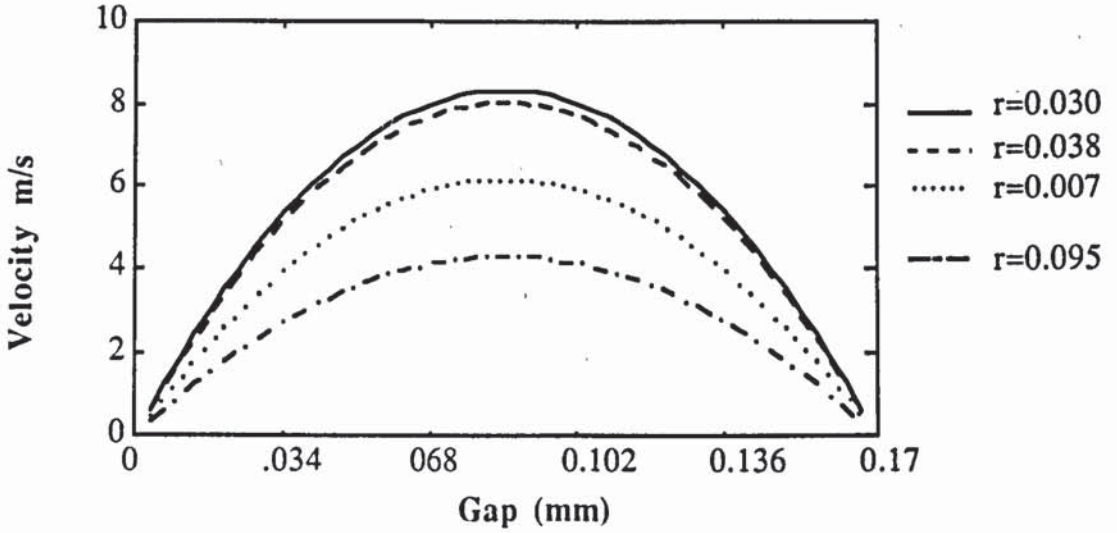

Figure 7.3.4.5
Velocity profiles at 0.26 kg/s; gap 0.17 mm; inlet temperature 293 K; inlet pressure 2.01 bar. Non-evaporating flow

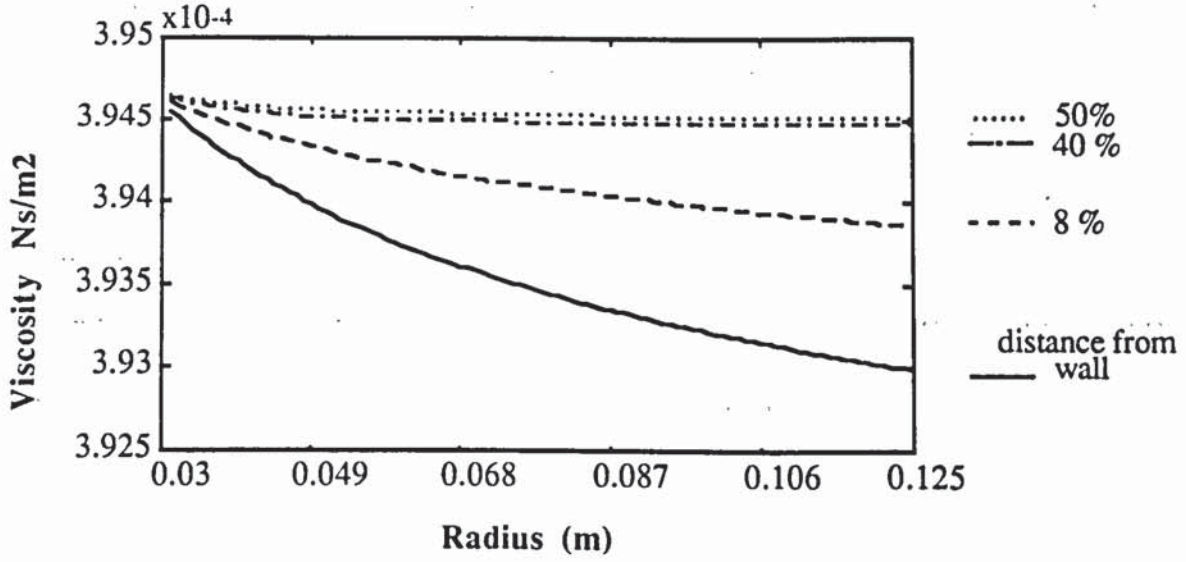

Figure 7.3.4.6
Radial Viscosity Distribution at 0.26 kg/s; gap 0.17 mm; inlet temperature 293 K; inlet pressure 2.01 bar. Non-evaporating flow

7.4 Effect of Varying Inlet Temperature

7.4.1 Experimental Results

In an attempt to achieve some evaporation during the tests with a gap of 0.17 mm, the temperature of the refrigerant was increased at the inlet to the bearing, while keeping the mass flow rate constant. Table 7.4.1.1 contains the measured values of pressure and temperature for these tests at a nominal measured mass flow rate of 0.30 kg/s, nominal gap of 0.17 mm and a range of inlet temperatures for the refrigerant. Figure 7.4.1.1 shows the values of pressure plotted against the radius of the bearing. Figure 7.4.1.2 shows the corresponding predicted pressure distribution.

pump inlet P(bar)	pump outlet P(bar)	port P(bar)	p1 (bar) r=.03	p2 (bar) r=.037	p3 (bar) r=.045	p4 (bar) r=.055	p5 (bar) r=.067	p6 (bar) r=.082	p7 (bar) r=.125	Liq. Ref. Temp (K)	Vap. Ref. Temp (K)	Beari-ng inlet T (K)	Mas flow rate kg/s
2.379	5.137	3.328	2.791	2.866	2.879	2.877	2.854	2.824	2.733	303.9	303.8	306.4	0.30
2.586	5.482	3.492	3.010	3.049	3.086	3.103	3.089	3.056	2.957	305.7	305.6	308.1	0.30
2.655	5.827	3.627	3.112	3.165	3.189	3.212	3.187	3.152	3.072	306.1	306.0	309.4	0.30
2.724	5.931	3.728	3.190	3.241	3.303	3.292	3.273	3.234	3.153	307.5	307.3	310.7	0.30
2.862	6.172	3.895	3.385	3.447	3.462	3.486	3.466	3.416	3.354	309.7	309.5	312.1	0.30
3.069	6.689	4.141	3.595	3.646	3.675	3.698	3.689	3.638	3.575	312.0	311.8	314.3	0.30
3.207	6.862	4.344	3.785	3.839	3.868	3.891	3.858	3.849	3.767	312.7	312.7	315.0	0.30

Table 7.4.1.1
Radial pressure distribution as a function of inlet temperature. Experimental values. Gap 0.17 mm; pump speed 1250 rev/min and mass flow 0.30 kg/s

The theoretical and experimental pressure distribution curves are shown as Figures 7.4.1.1 and 7.4.1.2 on the following page. The theoretical results were obtained using the constant viscosity form of the Navier-Stokes equation and 50 layers in the fluid film.

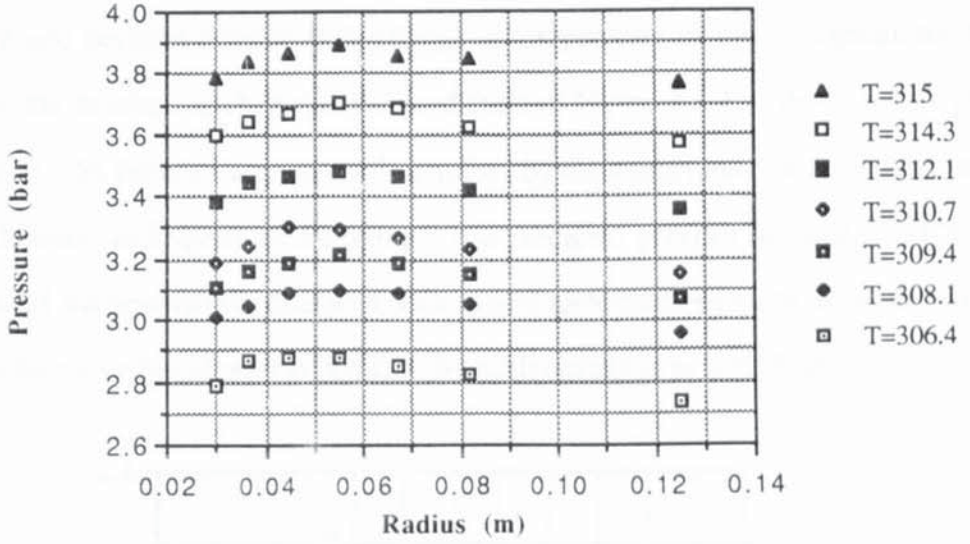

Figure 7.4.1.1
Radial pressure distribution as a function of inlet temperature. Measured values, Gap 0.17 mm; pump speed 1250 rev/min and mass flow 0.3 kg/s

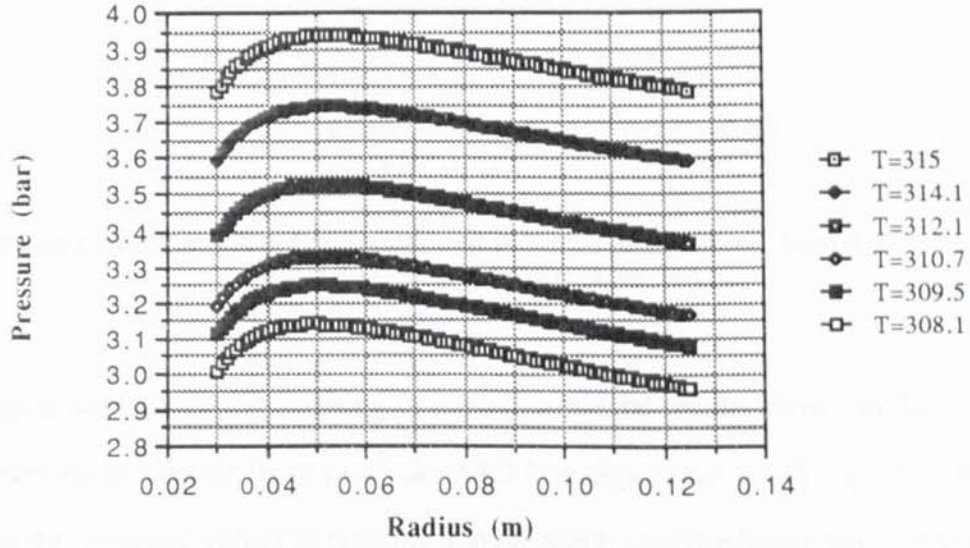

Figure 7.4.1.2
Radial pressure distribution as a function of inlet temperature. Predicted values, Gap 0.17 mm; pump speed 1250 rev/min and mass flow 0.30 kg/s

It is evident that the most significant influence is the inlet pressure. The pressure profiles are virtually identical but displaced by the change in port pressure from one test to the next. As described in Chapter 6, the pressure rise across the pump is related to speed and

mass flow rate, and the pump inlet pressure is determined by the saturation pressure in the bearing chamber. Because saturation pressure is related directly to the temperature of the mixture and because there is little change in temperature of the refrigerant as it flows through the bearing, as shown in the prediction of Figure 7.3.4.4, the chamber pressure and pump inlet pressure are largely determined by the temperature of the fluid at the inlet to the bearing and speed of the pump. The predicted profiles indicated in Chapter 6, section 6.3 suggest that the characteristics should have changed quite markedly with inlet temperature if evaporation was present. No such change is evident here.

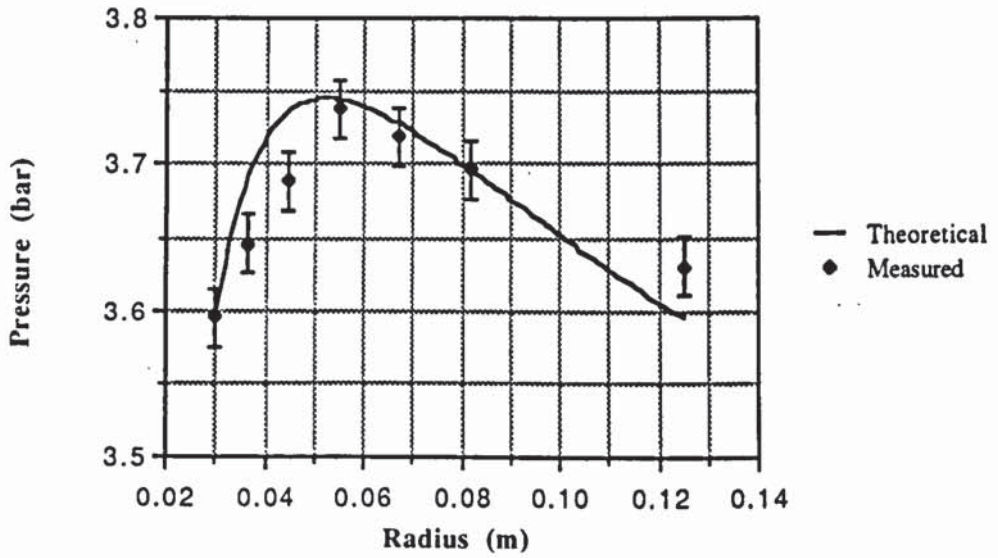

Figure 7.4.1.3
Comparison of the predicted and measured pressure distribution. Gap 0.17 mm; mass flow 0.3 kg/s; inlet temperature 314 K

Theoretical solutions corresponding to the experimental results shown in Table 7.4.1.1 are presented in tabular form in Table A4.3.2 in Appendix 4. A direct comparison between the measured values of pressure and the theoretical prediction was made which is presented as Figure 7.4.1.3. Error bands for the measured values are also included, as before.

In none of the theoretical predictions of enthalpy variation associated with the pressures listed in Table 7.4.1.1 was there any evidence of evaporation despite an increase in the inlet temperature of the refrigerant.

7.5 Effect of Low Mass Flow Rate

Critical examination of the experimental results discussed above and consideration of the inlet pressures and temperatures likely to promote evaporation with a gap of 0.17 mm led to the conclusion that the lower inlet pressure which could be employed by using a lower pump speed and mass flow rates might be combined with an inlet temperature which would lead to two phase operation in the outer regions of the bearing. In these conditions the initial rise in pressure due to changes in kinetic energy of the flow would be reduced, with a corresponding reduction in the tendency to suppress evaporation on account of the saturation temperature/ pressure relationship.

A further series of tests was carried out at significantly reduced pump speeds but still failed to achieve the desired effect. The results are shown below as Table 7.5.1.1 and Figure 7.5.2.1. The corresponding predicted pressure distribution curves are presented as Figure 7.5.2.2. The predictions were based on the model in which the constant viscosity form of the Navier-Stokes equations was used.

7.5.1 Experimental Results

Mass flow rate kg/s	pump speed (rpm)	Beari-ng inlet T (K)	Cham-ber Temp T (K)	pump inlet P(bar)	pump outlet P(bar)	port P(bar)	p1 (bar) r=.03	p2 (bar) r=.037	p3 (bar) r=.045	p4 (bar) r=.055	p5 (bar) r=.067	p6 (bar) r=.08	p7 (bar) r=.12
0.2	460	308.1	305.7	2.75	3.90	3.50	3.103	3.118	3.112	3.104	3.092	3.071	2.989
0.21	540	302.7	301.7	2.38	3.34	2.97	2.579	2.586	2.614	2.608	2.584	2.542	2.501
0.21	540	304.6	302.8	2.38	3.42	3.08	2.703	2.721	2.733	2.721	2.698	2.652	2.612
0.22	510	307.9	305.5	2.73	3.80	3.38	3.0	3.035	3.041	3.030	3.021	3.002	2.922
0.23	600	307.7	305.4	2.72	3.76	3.27	2.876	2.883	2.926	2.923	2.912	2.891	2.812

Table 7.5.1.1
Radial pressure distribution as function of inlet temperature. Experimental values.
Gap 0.17 mm; varying pump speed and mass flows.

7.5.2 Theoretical Results

Theoretical predictions corresponding to the inlet conditions of Table 7.5.1.1 are shown in tabular form in Table A4.3.3 in Appendix 4. The predictions do not indicate any evaporation

Visual inspection of the test run gave rise initially to the hope that two phase operation might first have been achieved in the outer regions. And it should be commented that all measured results presented above suggest a change of pressure slope in the outer region. This must be attributable to the small variation in the gap across the whole surface. Measurements of the gap variation across the surface showed that pressure sensing point 7 was located at an angular position at which the gap was about 15% greater than used in the prediction.

As in the case of results presented in section 7.4.1, the only significant change was due to the change in the inlet pressure arising from the relationship between chamber pressure and liquid temperature. The resulting pressure profiles were identical but displaced by the change in port pressure as a result of increasing the temperature. It is apparent that there was no indication of evaporation during these tests, nor was evaporation predicted in the corresponding computed pressure distributions.

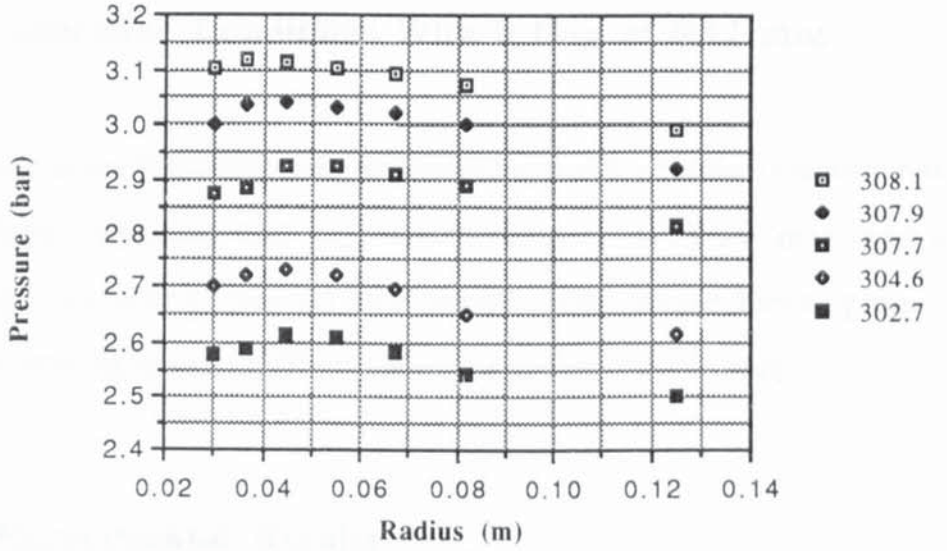

Figure 7.5.2.1
Measured pressure distribution. Mass flow rate 0.20 to 0.23 kg/s; Gap 0.17 mm

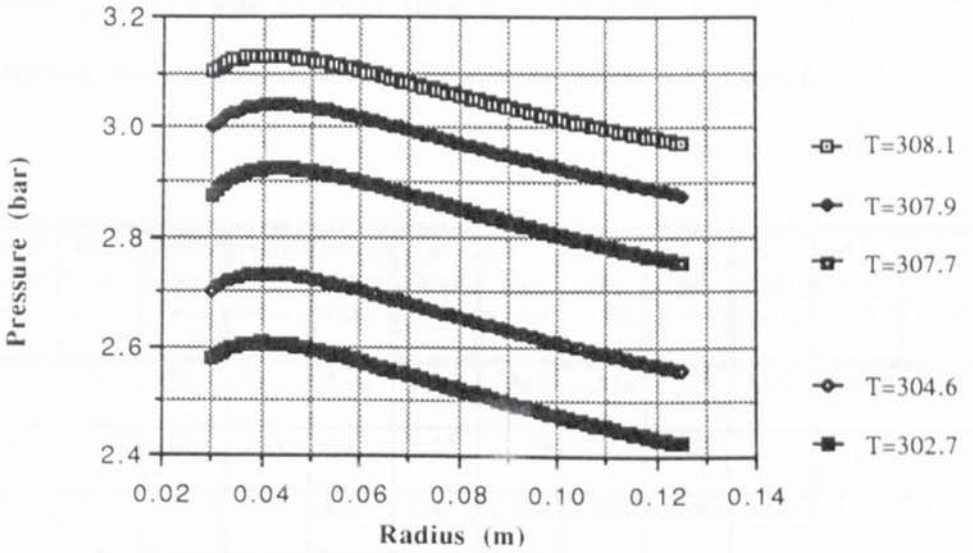

Figure 7.5.2.2
Predicted pressure distribution. Mass flow rate 0.2 to 0.23 kg/s; Gap 0.17 mm

7.6 Evaporating Conditions With a Gap of 0.12 mm

Following further predictions using the model based on the constant viscosity form of the Navier-Stokes equation which suggested that evaporation should arise using a gap of 0.12 mm, tests were carried out with increased inlet temperature to promote some evaporation of refrigerant as it flowed along the surface of the bearing.

7.6.1 Experimental Results

Table 7.6.1.1 contains measured values of pressure distribution and temperatures corresponding to a range of mass flow rates with the reduced gap of 0.12 mm. Corresponding predicted values are tabulated in Appendix 4 as Table A4.3.4.

Mass flow rate kg/s	pump speed (rpm)	Beari-ng inlet T (K)	Cham-ber Temp T (K)	pump inlet P(bar)	pump outlet P(bar)	port P(bar)	p1 (bar) r=.03	p2 (bar) r=.037	p3 (bar) r=.045	p4 (bar) r=.055	p5 (bar) r=.067	p6 (bar) r=.082	p7 (bar) r=.12
0.26	950	296.1	295.4	2.03	4.10	2.75	2.663	2.714	2.705	2.680	2.662	2.631	2.509
0.26	950	310.5	308.4	2.24	4.45	3.22	3.109	3.168	3.182	3.173	3.142	3.097	3.062
0.27	1050	296	294.9	1.89	4.10	2.69	2.612	2.657	2.686	2.658	2.653	2.593	2.465
0.27	1050	311	309.5	2.45	4.93	3.28	3.151	3.215	3.250	3.232	3.212	3.157	3.091
0.28	1200	298.1	296.8	2.03	5.13	2.87	2.791	2.858	2.865	2.860	2.840	2.751	2.665
0.28	1200	310.8	309.4	2.17	4.79	3.244	3.113	3.178	3.215	3.268	3.181	3.137	3.041
0.31	1350	298.1	296.8	2.03	5.13	2.87	2.791	2.858	2.865	2.860	2.840	2.751	2.665
0.31	1350	311.0	309.6	2.31	5.34	3.25	3.122	3.179	3.212	3.194	3.173	3.147	3.069

Table 7.6.1.1
Measured pressure distribution. Mass flow rate 0.26 to 0.31 kg/s
Gap 0.12 mm

7.6.2 Visual Observation

The viewing ports described in Chapter 4 were used in all tests in an effort to observe the presence of vapour bubbles in the flow across the lower metal surface of the bearing. The liquid film in non-evaporating conditions was found to be completely transparent. On account of the high velocity of the flow it was not anticipated that bubbles would be seen with the naked eye in evaporating conditions, rather the presence of bubbles might make the film somewhat opaque. No significant change in the character of the film was detected with the naked eye, but a distinct change was noted in the nature of the flow as it streamed into the chamber at the exit from the bearing.

The chamber contains a mixture of liquid and vapour under all operating conditions and the chamber pressure is determined by the saturation temperature of the mixture. Because there is no heat transfer to the surroundings the specific enthalpy of the mixture in the chamber must be the same as that of the fluid at the exit from the bearing. Under many conditions of inlet pressure, temperature and mass flow rate, the pressure at the exit from the bearing is significantly greater than in the chamber, with the result that vapour will flash from the liquid stream at the exit from the gap. This phenomenon produced a visible effect and was observed on many occasions, but the presence of bubbles causing a degree of reflection which might have been visible within the film in the outer regions of the bearing was never seen convincingly. Indeed it might only have been imagined in the strong reflection of light from the polished metal of the lower plate.

Stroboscopic illumination was used in an attempt to make any bubbles more visible, but this did not improve matters for the naked eye and a number of still photographs were taken using high speed film to 'freeze' the motion. These photographs illustrated clearly a difference in the character of the flow as vapour flashes from the liquid at exit from the bearing. Three photographs are included as Plates PI.7.6.2.1-3 to illustrate this in non-evaporating, incipient evaporation and evaporating conditions respectively.

In plate PI.7.6.2.1, the non-evaporating situation, the outer edge of the bearing is clearly visible since no vapour bubbles exist to reflect any light in this region. Plate PI.7.6.2.2, the partial evaporating situation, exhibits a dark narrow band beyond the outer edge of the bearing, which probably represents the distance which the flow has travelled into the chamber before tiny bubbles have been generated. The outer edge seems clearly delineated, but the dark band displays a varying width. This is attributed to a varying proportion of vapour present in this region. Plate PI.7.6.2.3 was obtained under evaporating conditions. In this case the dark narrow band beyond the outer edge of the bearing seems much more uniform.

Both the pure liquid and pure vapour will be completely transparent, so the opacity of the liquid/vapour mixture must display a maximum value at some intermediate mixture quality. The degree of reflection will depend on the size and distribution of the individual bubbles of vapour, which have the effect of diffracting the incident and reflected light seen by the eye or the camera lens. It is possible that the degree of reflection had reduced in the situation where there were vapour bubbles already in the flow at the exit from the bearing.

Plate PI 7.6.2.1
Non- Evaporating Condition

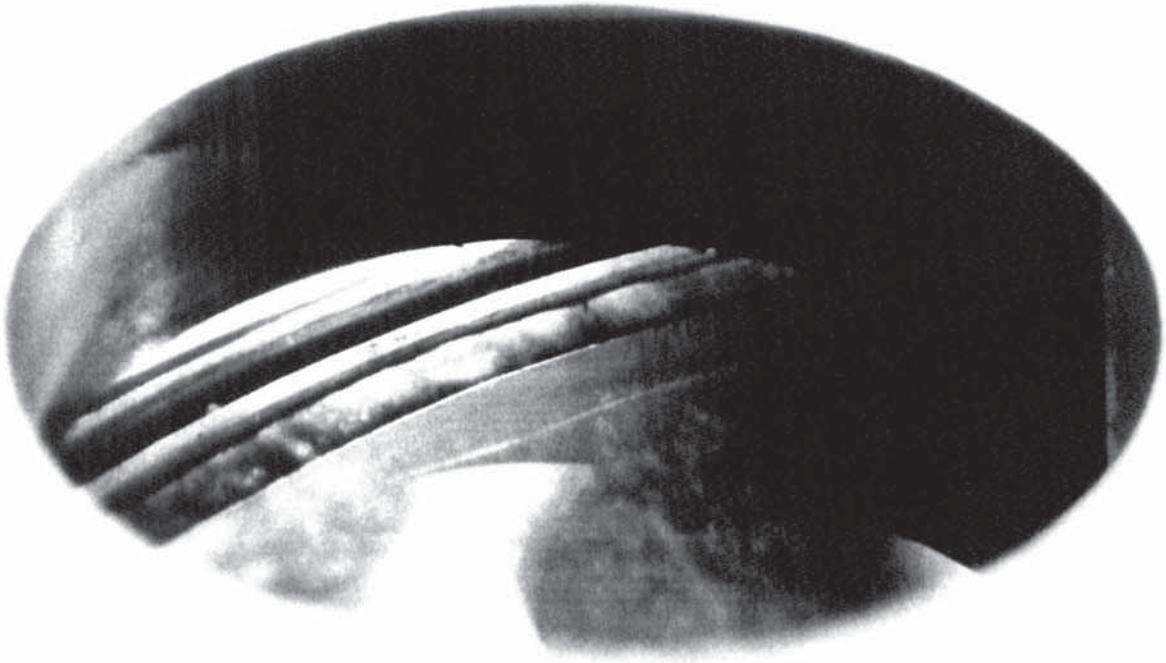

Plate PI 7.6.2.2
Partial Evaporating Condition

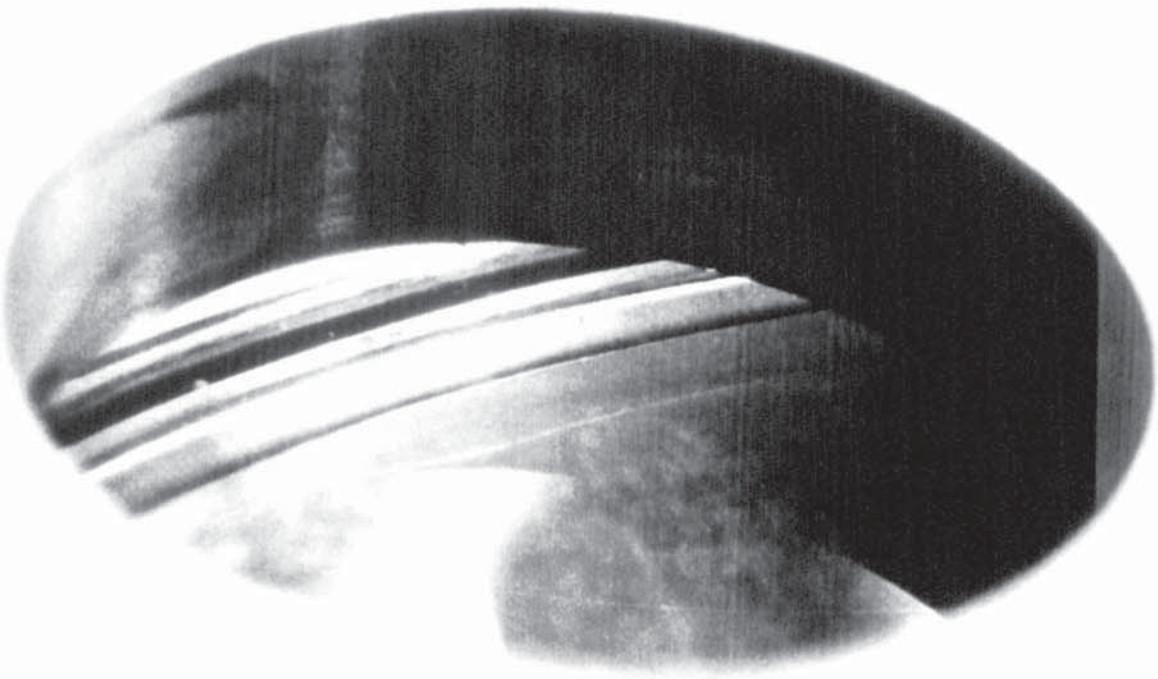

Plate PI 7.6.2.3
Evaporating Condition

7.6.3 Comparison of Measured and Predicted Results

The experimental and predicted pressure distributions corresponding to evaporating and non-evaporating conditions are presented graphically as Figures 7.6.3.1 and 7.6.3.2 below.

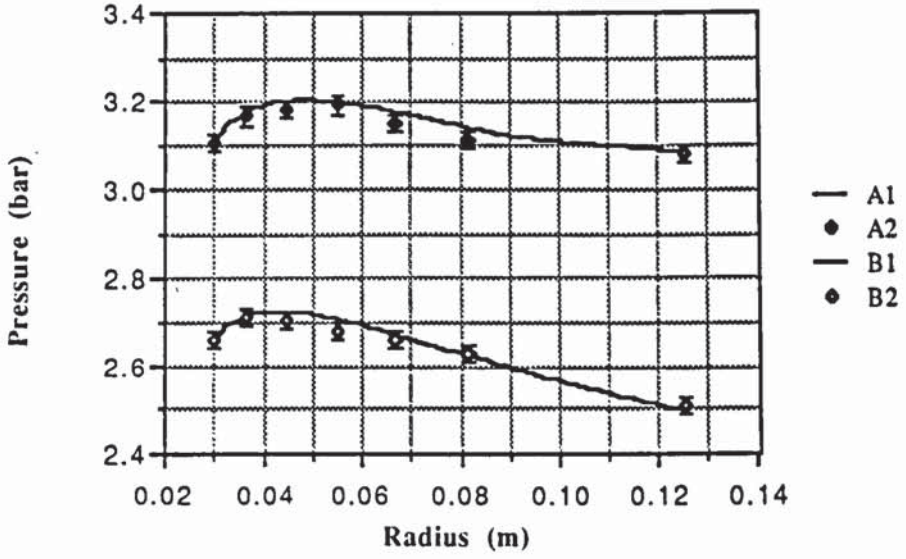

Figure 7.6.3.1
Comparison of pressure distribution curves for evaporating and non-evaporating condition. Mass flow rate 0.26 kg/s; Gap 0.12 mm

A1) Prediction, evaporating condition, inlet temperature of 310.5 K
A2) Measured, evaporating condition, inlet temperature of 310.5 K
B1) Predicted, non-evaporating condition, inlet temperature of 296.1 K
B2) Measured, non-evaporating condition, inlet temperature of 296.1 K

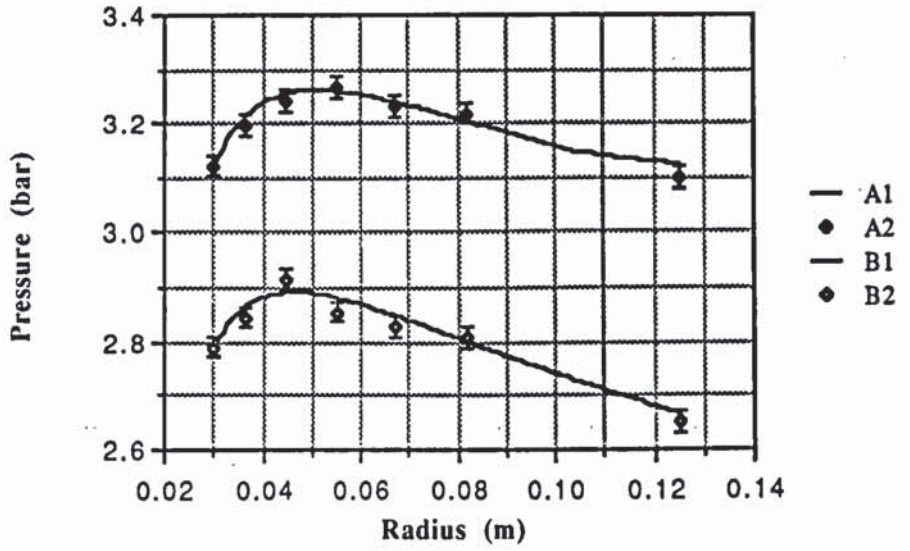

Figure 7.6.3.2
Comparison of pressure distribution curves for evaporating and non-evaporating condition. Mass flow rate 0.30 kg/s; Gap 0.12 mm

A1) Prediction, evaporating condition, inlet temperature of 311 K
A2) Measured, evaporating condition, inlet temperature of 311 K
B1) Predicted, non-evaporating condition, inlet temperature of 298.1 K
B2) Measured, non-evaporating condition, inlet temperature of 298.1 K

The evidence of evaporation is identified by the change in the slope of the pressure distribution curve. The mass fractions of vapour predicted here are within the limits of volume fractions for which the unsubstantiated viscosity correlations of Isbin and Duckler might be accepted and consequently the predicted values might be considered as reliable. The adequacy of the theoretical approach is verified by the excellent correlation shown above and implies that the Duckler and Isbin correlations are indeed acceptable over the limit range of liquid/vapour fractions which were present during these tests.

7.6.4 Prediction of Radial Density and Enthalpy Distribution

The predicted radial density and enthalpy distribution together with saturated enthalpy, temperature, velocity and viscosity for a typical set of conditions corresponding to a mass flow rate of 0.26 kg/s and a gap of 0.12 mm are presented graphically as Figures 7.6.4.1-6.

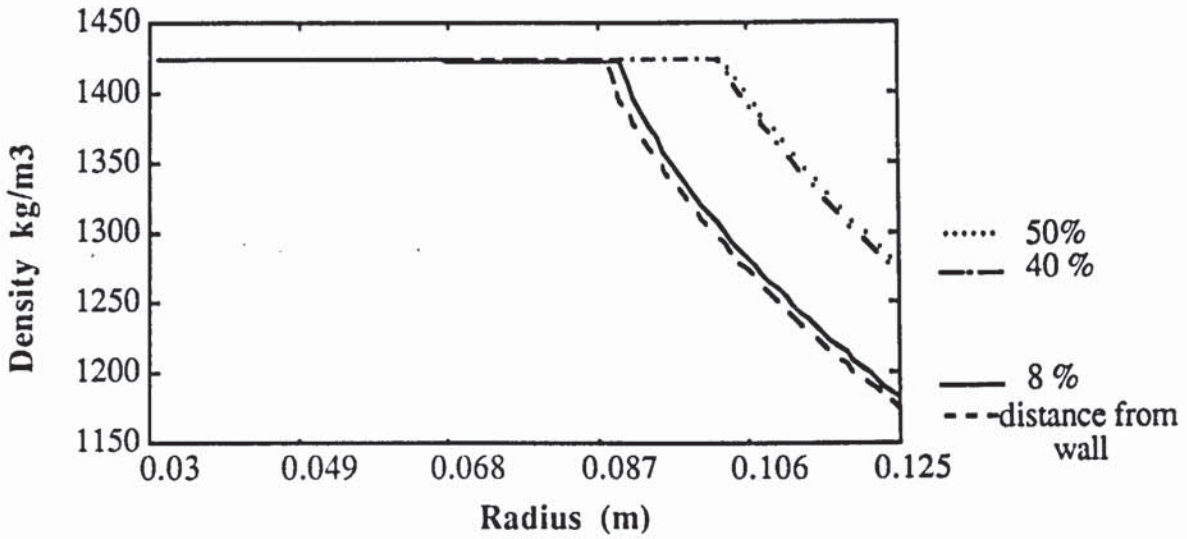

Figure 7.6.4.1

Radial Density Distribution at 0.26 kg/s; gap 0.12 mm; inlet temperature 310.5 K; inlet pressure 3.109 bar. Evaporating flow

Figure 7.6.4.1 shows the radial density distribution for a typical evaporating condition. It can be seen that before any evaporation takes place there is virtually no change in the density for any layer of the lubricant but as soon as some vapour is formed then the density starts to decrease. The decrease in the density for the layers near the walls is more significant than for the more central layers. The overall decrease in the density for layers near the wall in this test was about 250 kg/m^3 whereas a layer midway along the gap exhibits only a decrease of 50 kg/m^3.

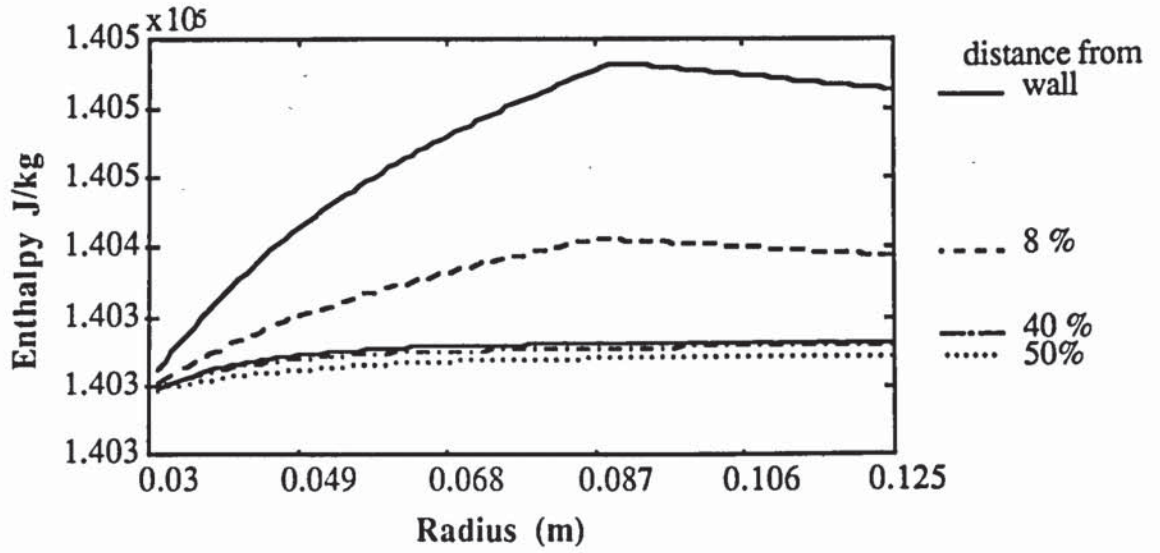

Figure 7.6.4.2

Radial Enthalpy Distribution at 0.26 kg/s; gap 0.12 mm; inlet temperature 310.5 K; inlet pressure 3.109 bar. Evaporating flow

Figure 7.6.4.2 shows the radial distribution of enthalpy for the same evaporating conditions considered in the preceeding graphs. Comparison of this distribution with that of the non-evaporating condition shows that the enthalpy of the lubricant increases due to viscous dissipation until some vapour has been formed. But as soon as evaporation takes place both density and viscosity of the lubricant start to decrease which reduces the effect of viscous dissipation, and as the result the enthalpy gain reduces slightly as vapour formation penetrates further into the film. Again it can be seen that the layers near the walls are mostly influenced by the evaporation, where the temperature is the highest. (See Figure 7.6.4.4).

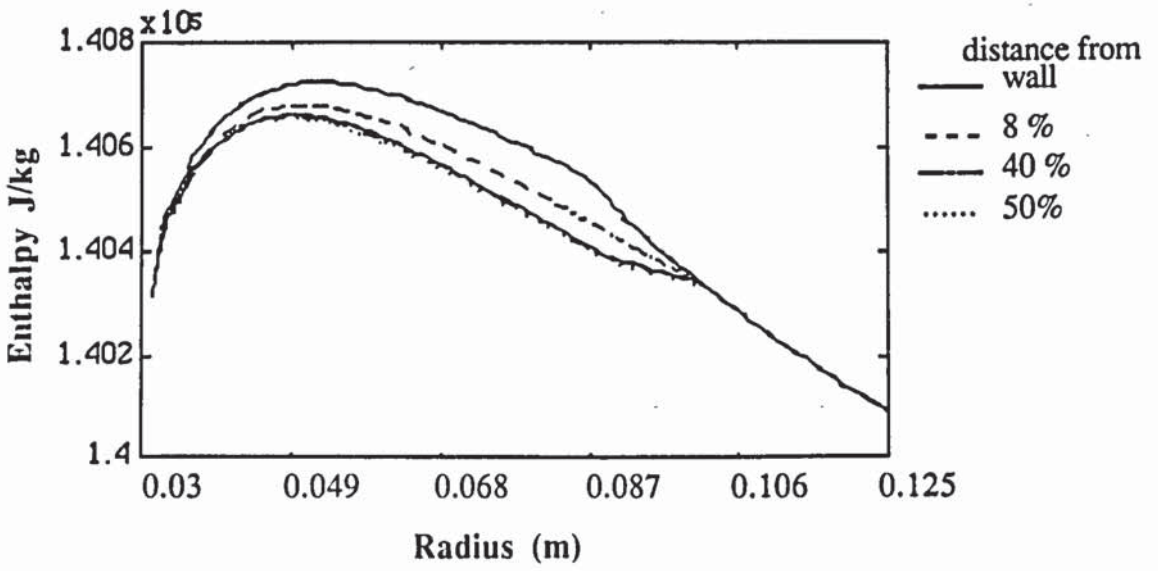

Figure 7.6.4.3

Radial Enthalpy of saturated liquid Distribution at 0.26 kg/s; gap 0.12 mm; inlet temperature 310.5 K; inlet pressure 3.109 bar. Evaporating flow

Figure 7.6.4.3 shows the radial liquid enthalpy distribution for the same evaporating condition. The presence of vapour phase has been determined by comparing locally, in each layer, the enthalpy of the layer at a given radius with the enthalpy of saturated liquid at the same pressure. If the enthalpy of the layer is greater than the enthalpy of saturated liquid then the flow in that layer is treated as two-phase with corresponding treatment of density and viscosity functions. Comparison of Figures 7.6.4.2 and 7.6.4.3 shows that at a radial position of 0.087 m, for this typical result the enthalpy exceeded that of the enthalpy of saturated liquid at the local pressure and therefore evaporation took place. It is interesting to note that once evaporation commences the enthalpy of saturated liquid remains constant for all layers in the gap as shown in Figure 7.6.4.3. This is due to the fact that in the two-phase region the saturated enthalpy is a function of pressure only which is constant for all layers.

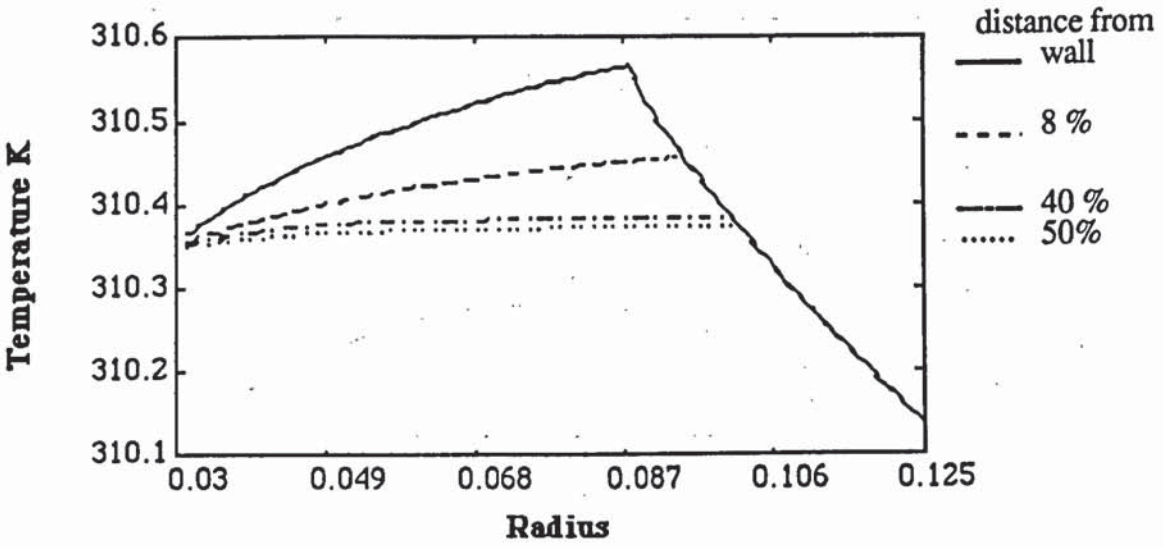

Figure 7.6.4.4

Radial Temperature Distribution at 0.26 kg/s; gap 0.12 mm; inlet temperature 310.5 K; inlet pressure 3.109 bar. Evaporating flow

Figure 7.6.4.4 shows the radial distribution of temperature for the same evaporating conditions considered above. Comparison of this distribution with that of the enthalpy distribution shows that before any vapour is formed an increase in temperature has caused the enthalpy to increase proportionately. But as soon as evaporation takes place the temperature which is the saturation temperature drops as a consequence of a decrease in pressure. This decrease in temperature then causes the total enthalpy to decrease as has already been shown in Figure 7.6.4.2.

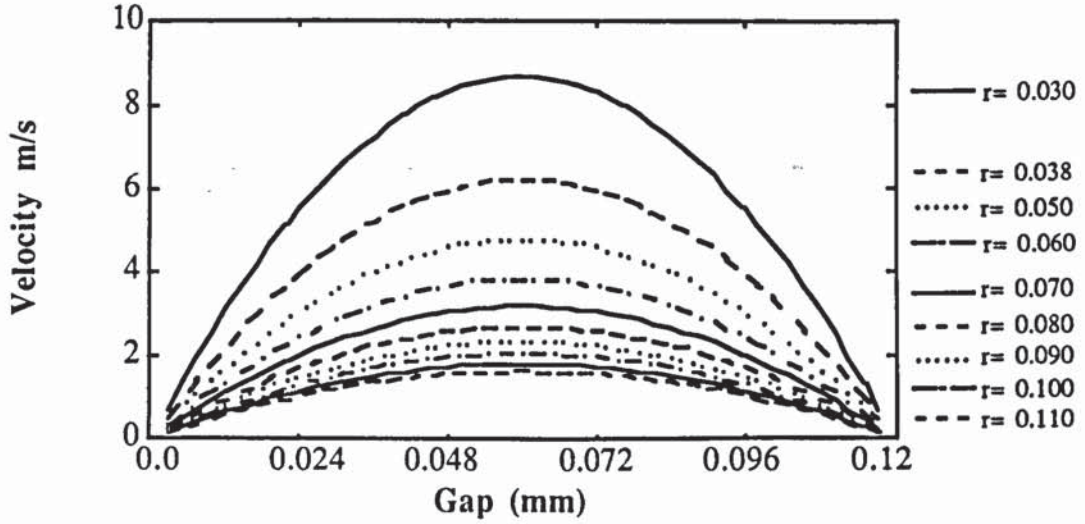

Figure 7.6.4.5

Velocity profiles at 0.26 kg/s; gap 0.12 mm; inlet temperature 310.5 K; inlet pressure 3.109 bar. Evaporating flow

Figure 7.6.4.5 shows the velocity profiles along the gap rather than the radius. As mentioned already in section 7.3.4 there are two reasons for presenting the velocity profiles along the gap as oppose to the radius. First to show that there was symmetry of solutions about the gap as expected and secondly to show that velocity remained parabolic at all radii. In this case evaporation has had no visible effect on the parabolic nature of the velocity distribution, but this is probably due to the limited region over which evaporation has been predicted: one might expect the distribution to change towards the form generally regarded as resembling a turbulent profile if the evaporation region was not limited to a small region. Since the central core of the flow would be subjected to only small values of transverse velocity gradient and shear forces while layers close to the solid surfaces would be under high velocity gradients but low viscosity, resulting in low shear forces.

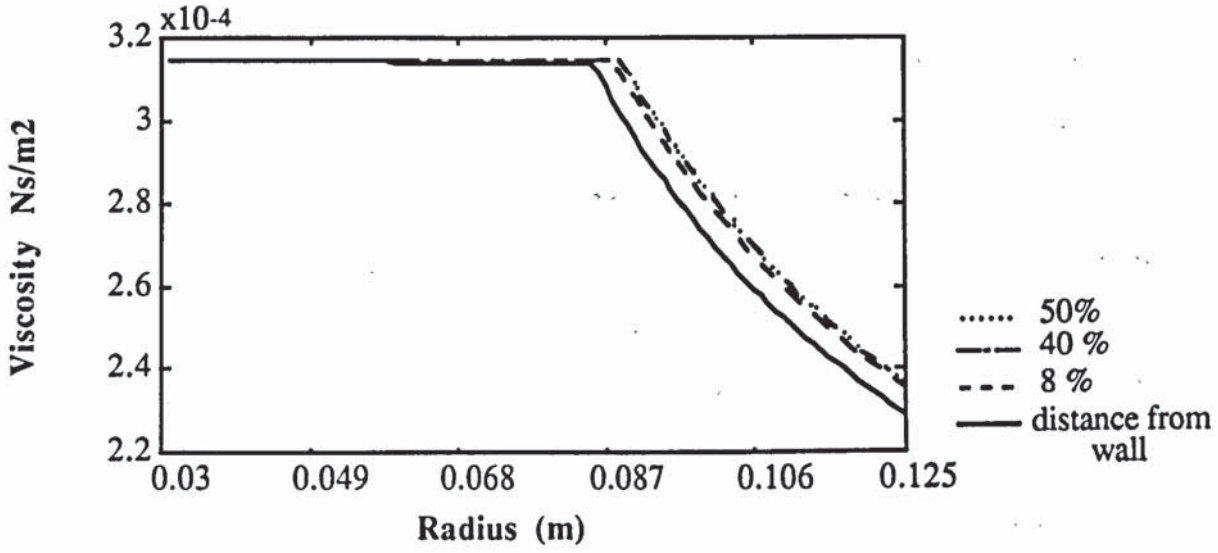

Figure 7.6.4.6

Radial Viscosity Distribution at 0.26 kg/s; gap 0.12 mm; inlet temperature 310.5 K; inlet pressure 3.109 bar. Evaporating flow

Figure 7.6.4.6 shows the viscosity distribution for the evaporating condition. It should be noted that computer plots can represent the variation only to the nearest pixel height. The apparent step in value of the wall layer at r= 0.06 is not truly a step change. Again it is evident that the viscosity of the layers near the walls decrease very little due to an increase in the temperature prior to the evaporation. But once evaporation takes place the viscosity of the mixture decreases in proportion to the volume of vapour produced and this decrease in viscosity accompanies a change of slope in the pressure distribution i.e. it reduces the rate of decrease of the pressure as shown earlier in section 7.6.3.

7.7 Results Obtained From the Variable Viscosity Form of the Navier-Stokes Equation

The theoretical model based on the variable viscosity form of the Navier-Stokes equations was developed to give a more accurate prediction of radial pressure distribution and is first compared in this section with the experimental results obtained in purely radial flow. The model has also been applied to predict the distribution of pressure on the rotor end face, using rotor dimensions and fluid conditions met with during a parallel investigation into the possible use of the liquid injected sliding vane compressor to improve the coefficient of performance of a heat pump, but neglecting the circumferential variation of exit pressure caused by the compression process. Results for both situations are presented and discussed in the following pages.

7.7.1 Hydrostatic Thrust Bearing

7.7.1.1 Parabolic Velocity Profile

Figure 7.7.1.1 overleaf compares a typical measured and predicted pressure distribution corresponding to an evaporating condition with a mass flow rate of 0.27 kg/s and an inlet temperature of 311 K. The measured values of pressure are taken from Table 7.3.1.1. It is evident from Figure 7.7.1.1 that with the assumption of a parabolic velocity profile at the inlet to the gap, there is good correlation between the measured values and those predicted. The corresponding radial velocity profiles are included as Figure 7.7.1.2 which shows the profiles at selected radii across the lubricating film. After the first radius, where the profile is defined, the subsequent profiles remain effectively parabolic. This supports the assumptions used in the earlier prediction, presented as Figure 7.6.4.5, where the simplified method had been used.

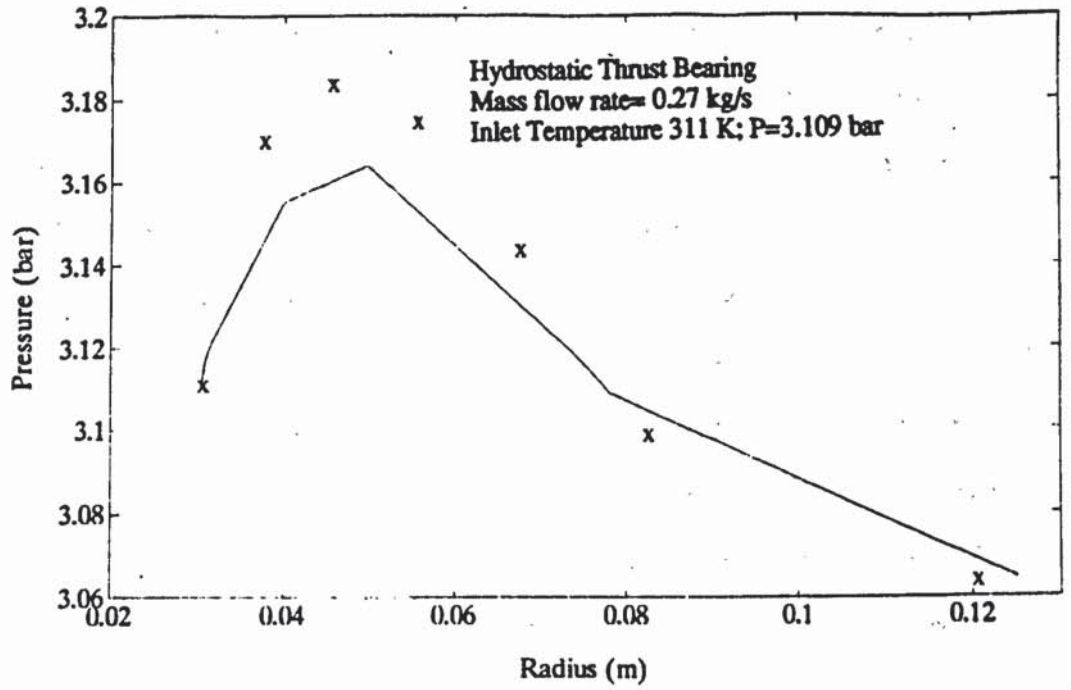

Figure 7.7.1.1. Comparison between measured and theoretical pressure distribution

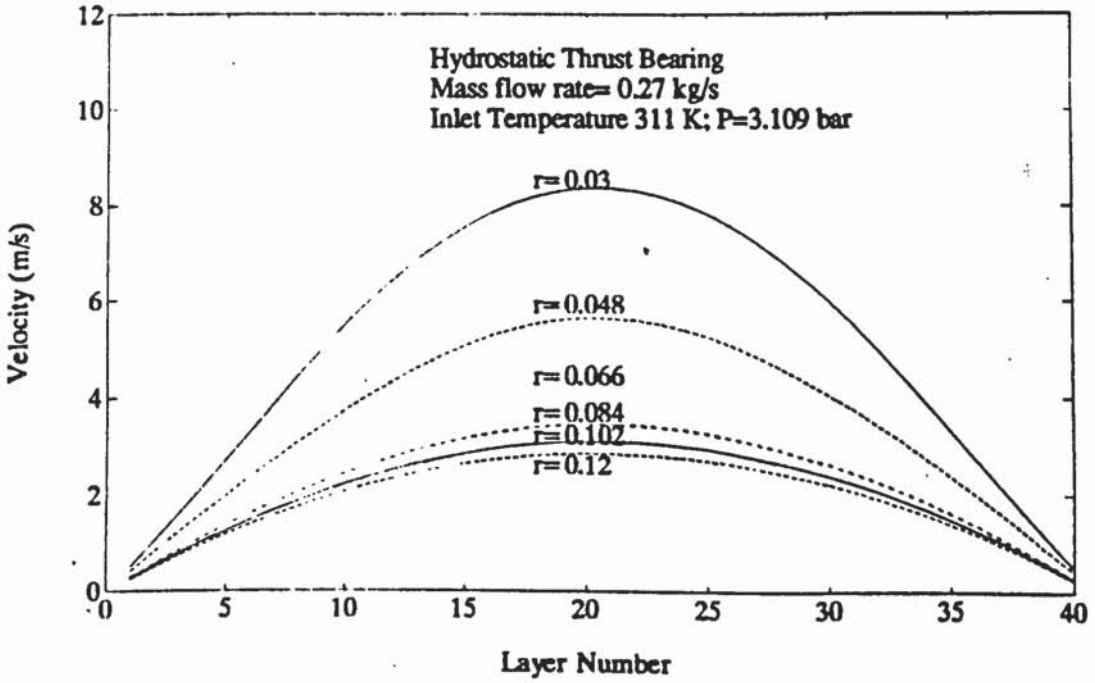

Figure 7.7.1.2. Transverse distribution of radial velocity

Figures 7.7.1.3-4 show the corresponding radial density and quality distribution. As explained earlier, the presence of vapour has been determined by comparing locally, in each layer of the lubricating film, the enthalpy of the layer at a given radius with the enthalpy of saturated liquid at the same pressure. If the value of local enthalpy is greater than the enthalpy of saturated liquid then that layer is treated as two-phase, which involves the application of appropriate viscosity and density functions. It is noted that the change in density is negligible in all layers until a radius of 0.079 m is reached, when evaporation commences. The curves which are presented are for the layer of fluid adjacent to the solid surface and the central layer within the gap. These curves indicate that for the given hydrostatic thrust bearing with fluid entering in the liquid phase with a parabolic velocity profile, the quality and density of the fluid are each virtually constant across the thickness of the film at any given radius. Recalling that the predicted velocity profiles are parabolic at all radii in this case, it is apparent that the earlier analysis in which the constant viscosity form of the Navier-Stokes equations was employed, can be considered to be an adequate representation of the situation in these specific circumstances.

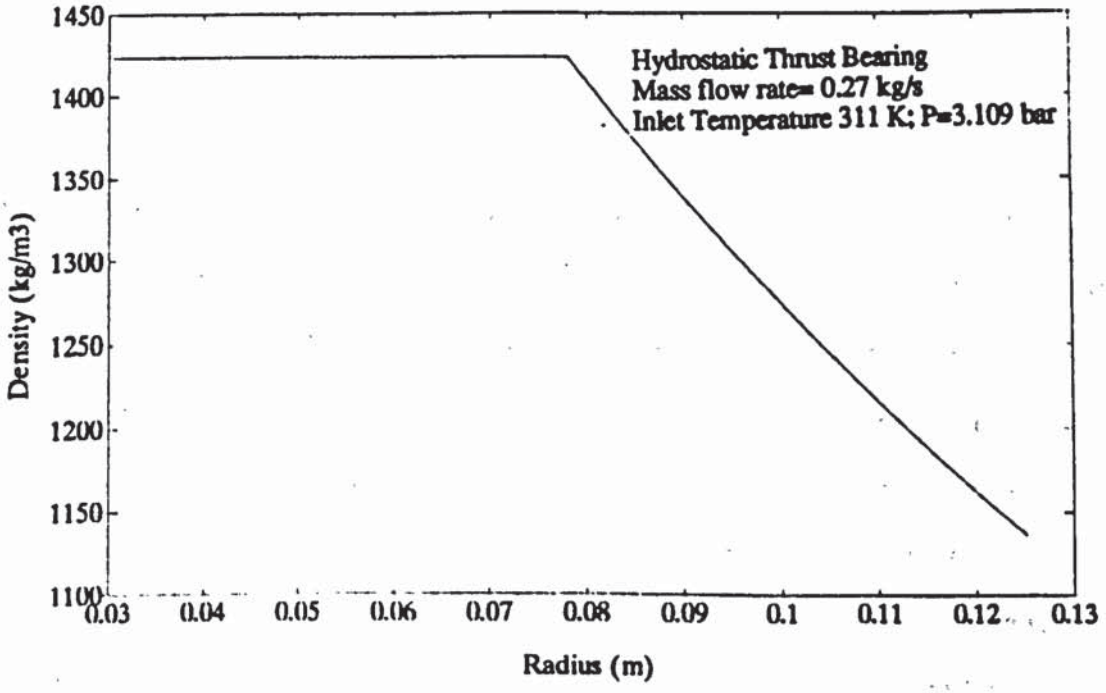

Figure 7.7.1.3. Radial distribution of Density. Note that all layers are coincident

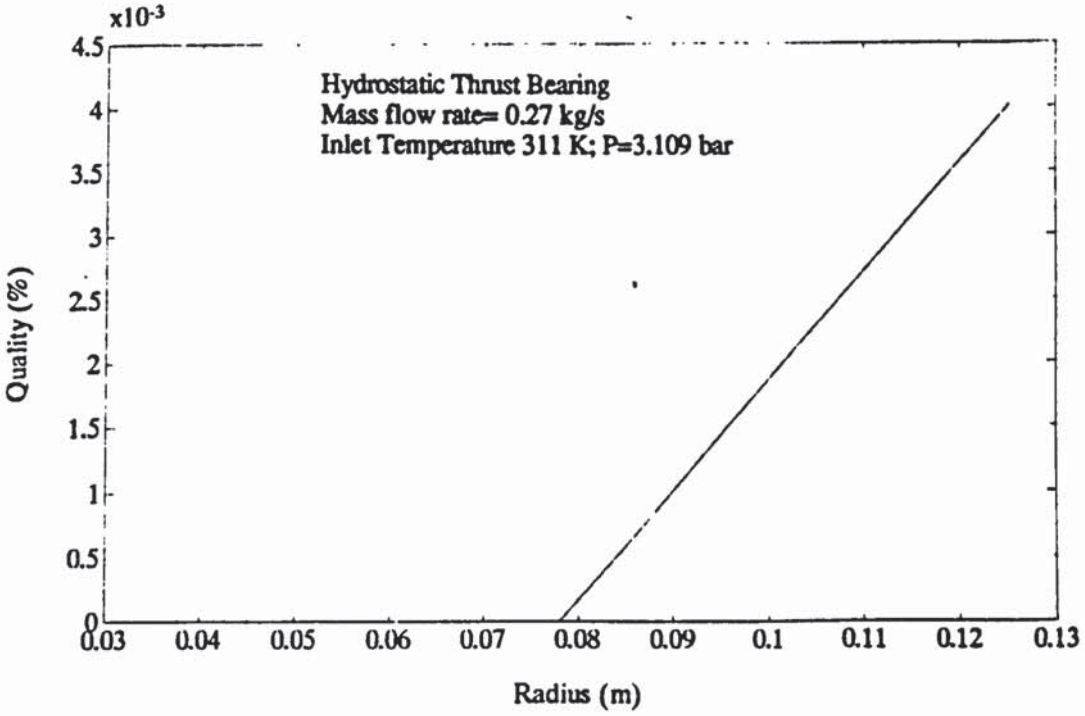

Figure 7.7.1.4. Radial distribution of Quality. Note that all layers are coincident

7.7.2 Rotor End Face and Rotating Seals

7.7.2.1 Uniform Velocity Profile

The sealing fluid supply pressure and temperature used in this prediction were those which would arise in a typical heat pump application using R114 in a sliding vane machine, while the radial dimensions correspond to those of the compressor used in the parallel research programme referred to in section 7.7. The machine used in the heat pump research programme was driven by a four-pole motor, giving a rotational speed of approximately 150 rad/s. A suitable value for the clearance between end covers and end faces of the rotor was assumed to be 0.05 mm. It is assumed that the lubricant/sealing fluid would be supplied at 5 bar and 325 K. The supply groove is at a radius of 30 mm and the rotor surface radius is 65 mm. The exit pressure is assumed to be equal to the

suction pressure between 1.5 and 1.0 bar, which takes place over the compression arc of approximately 130 degrees. The geometrical details are represented in Figure 7.7.2.1.

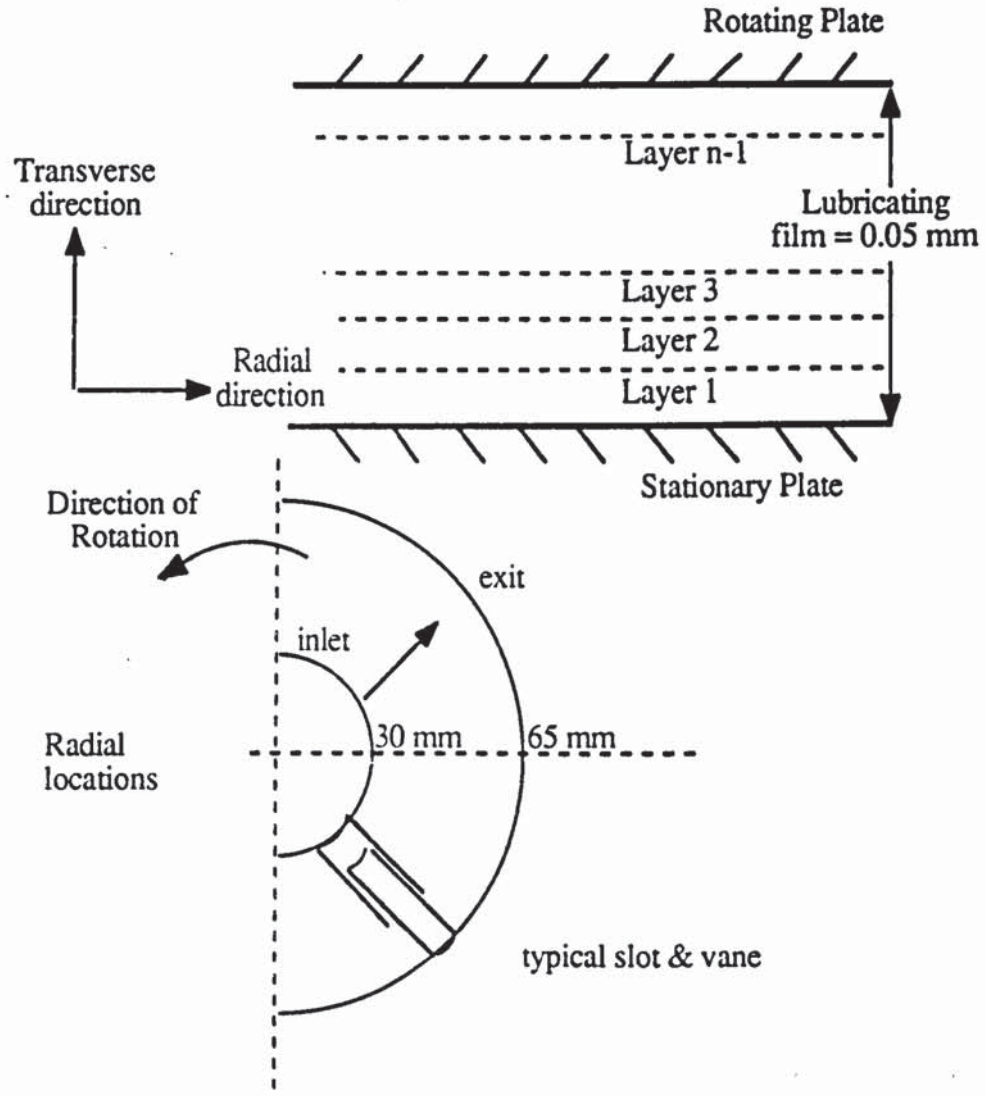

Figure 7.7.2.1
Dimension of the rotor end face

In the sliding vane compressor, the pressure at the surface of the rotor is the pressure in the compression cells and varies with angular position of the cell. This pressure variation was not accounted for in the present analysis, where considerable difficulty arose in prescribing a mass flow rate which corresponded to the simple assumption of a uniform pressure at the exit equal to the pressure existing over the suction arc of the machine. Such difficulties in determining the 'correct' mass flow are described by Yasuna and Hughes[34] in their less rigorous treatment of the changing conditions in a rotating seal in which the fluid is evaporating.

Supply temperature has also a significant effect on the pressure drop, since it determines the location at which phase change commences. Evaporation will begin first in the layer adjacent to the moving surface, since the rate of dissipation of energy must be greatest in this layer. The effect which this has on pressure gradient cannot be found analytically but is determined by successive approximation, as explained in Chapter 3.

Figures 7.7.2.1 to 7.7.2.10 show the predicted radial and transverse distribution of pressure, velocity, enthalpy, quality, tangential velocity, density and viscosity in the lubricating film under the conditions set out above and summarised as:

Film thickness= 0.05 mm
Angular velocity= 150 rad/s
Lubricant= R114
Supply pressure= 5.0 bar
Supply temperature= 325 K
Exit pressure= 1.50 bar

The solutions for the hydrostatic thrust bearing with purely radial flow, which is essentially of one dimensional flow, have already been compared with experimental data and it was shown that good correlation existed. For the rotor end face seal, however, since the tangential component flow must now be taken into account, the flow becomes two dimensional in the theoretical sense.

The effect of mesh size was examined by considering different number of layers in the lubrication film. Solutions were obtained for 40, 50, 60, 70, 80 and 90 layers in the lubrication film. In these predictions it is assumed that the velocity at the inlet has a uniform profile. Figure 7.7.2.2 shows typical pressure distributions for these solutions which correspond to a seal with the same inlet condition in each case. It can be seen that there is a clear convergence of the solution and therefore in considering the rotor end face seal, solutions were obtained for 80 layers in the lubricating film rather than 40 as in the case of hydrostatic thrust bearing.

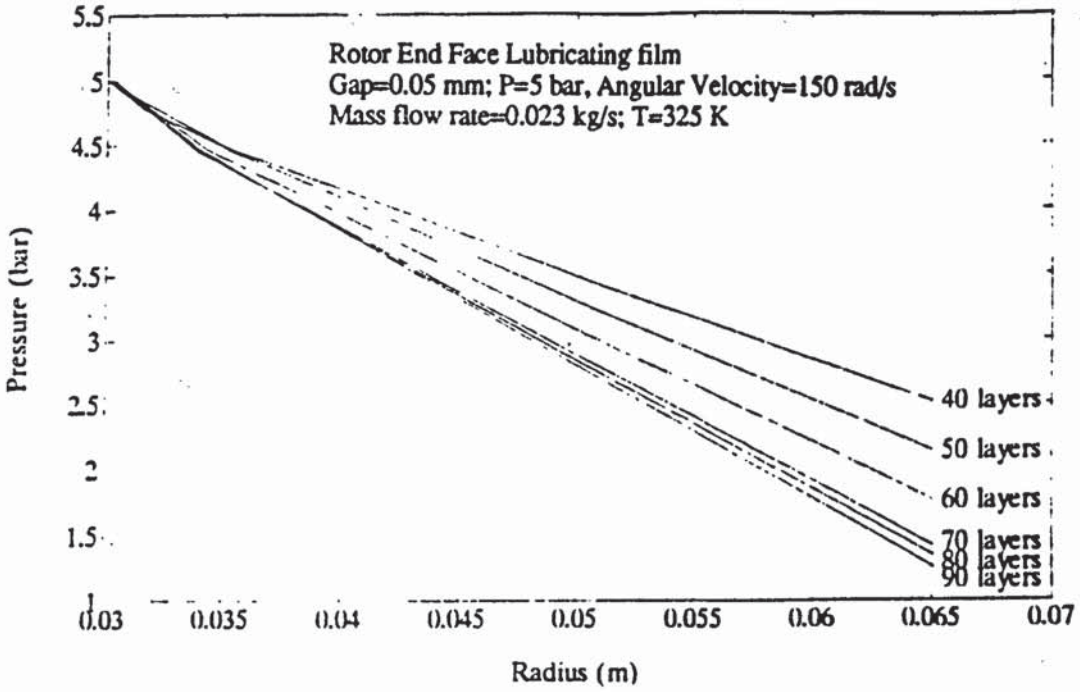

Figure 7.7.2.2. Comparison between solutions for different number of layers in the lubricating film

Figure 7.7.2.3 shows three typical pressure distribution curves corresponding to different mass flow rates, indicated on the graph. It can be seen from the curves that a mass flow rate of 0.012 kg/s resulted in an exit pressure of 2.5 bar at a radius of 58.00 mm, whereas a mass flow rate of 0.018 kg/s resulted in an exit pressure of 2.1 bar at a radius of 60 mm. However, mass flow rate of 0.023 kg/s resulted in the exit pressure of 1.4 bar at a radius of 65.00 mm. The early termination of the curves representing flows of 0.012 and 0.018 kg/s was caused by the prediction of flow reversal in layer 1, adjacent to the stationary wall. This situation might be interpreted as indicating flow break-away, induced by the rotation, although it must be accepted that if the pressure reduced in the sudden manner predicted, then the whole flow would flash completely to vapour. Reduction of the radial step size used in the Runge-Kutta process did not alter the prediction; consequently the suggestion of flow break-away is favoured as an explanation for the predicted reversal.

The lower pressure gradients are caused by a combination of early onset of evaporation reducing viscosity in the layers near the walls and lower velocity gradients reducing dissipation even further at lower values of mass flow rates.

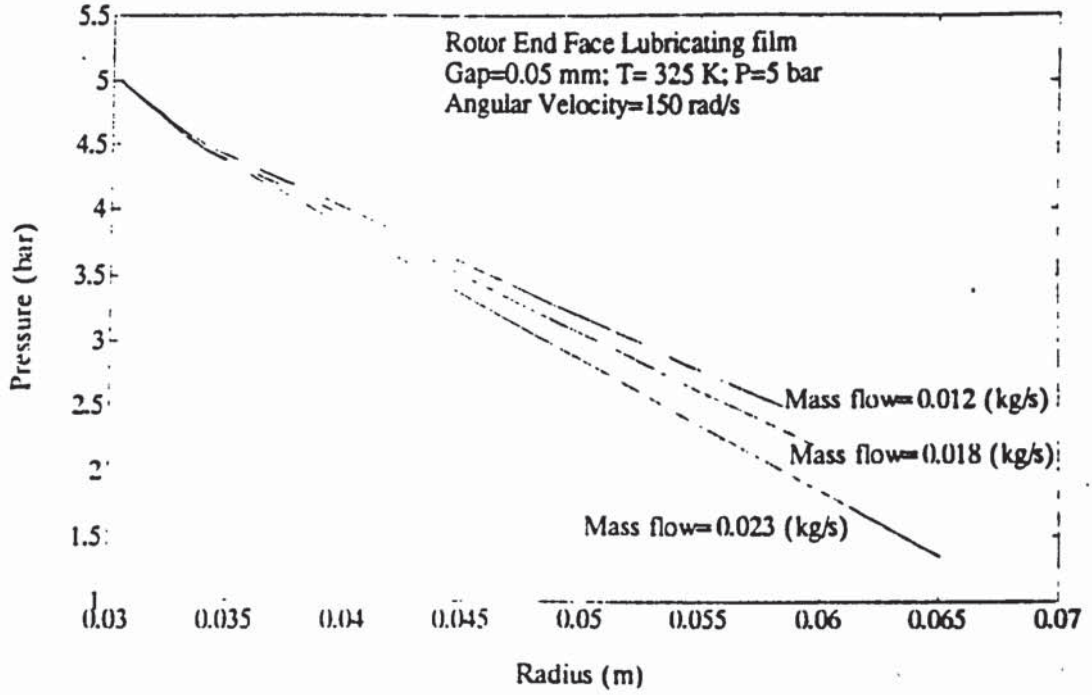

Figure 7.7.2.3. Comparison between radial distribution of pressure for different mass flow rates and the same inlet conditions with 80 layers in the film

Having established a suitable mass flow rate, the effect of inlet temperature was examined. Figure 7.7.2.4 shows three pressure distribution curves corresponding to different inlet temperatures. As shown by the pressure distribution curves the different inlet temperatures caused the evaporation to take place at different radial locations. The higher inlet temperature of 325 K results in evaporation taking place earlier and causing a more gradual decrease in the rate of pressure drop, as indicated by the curve.

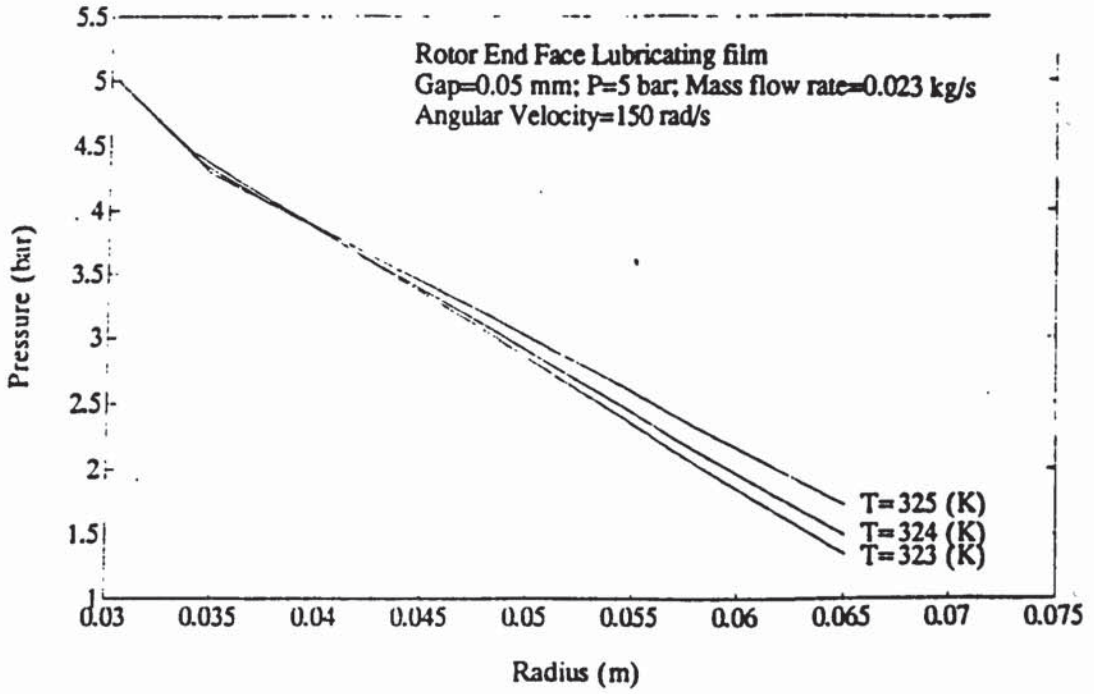

Figure 7.7.2.4. Comparison between radial distribution of pressure for different inlet temperature and the same mass flow rate with 80 layer

The results which are presented in Figures 7.7.2.5 to 7.7.2.12 show the radial distribution of radial and tangential velocity, enthalpy, quality, density and viscosity in selected layers of the flow when the seal is supplied with liquid R114 at 325 K. Transverse distributions of these quantities are also shown at selected radii, to indicate the development of the changes taking place. Figures 7.7.2.5 and 6 show the distribution of radial velocity component of the fluid flow. It is noted that velocity in layers 5 to 80 is almost constant. This is due to the evaporation taking place initially at the rotating surface, caused by the much higher dissipation and lowering the density. It is also evident that initially the velocity of fluid decreases due to increasing flow cross-section with constant density until evaporation commences. Beyond this point at a radius of 0.034 mm, the density decreases when some vapour bubbles are formed and, because of conservation of mass, the velocity of the fluid/vapour mixture starts to increase.

Figures 7.7.2.7-8 show the radial and transverse enthalpy distribution. The greatest increase in enthalpy is seen to arise in layer 80, in which the dissipation is greatest due to the rotational shear coming from the adjacent solid surface.

Figures 7.7.2.9 show the radial variation of quality. It will be recalled from earlier comments that the presence of vapour phase has been determined by comparing locally, in each layer, the enthalpy of the layer at a given radius with the enthalpy of saturated liquid at the same pressure. If the enthalpy in any layer is predicted to be greater than that of saturated liquid at the predicted pressure then evaporation is deemed to have commenced and the quality is determined.

It is evident from Figure 7.7.4.9 that layers 79 and 80, at the rotating surface have the highest vapour generated, as expected.

Figure 7.7.2.10 shows the transverse angular velocity distribution. Again it can noted that only in layers 76 to 80 is any significant additional tangential component of velocity predicted. Also the transmission of tangential shear is restricted to these layers which must be attributed to the great reduction in viscosity caused by progressive phase change. The graph indicates that the assumption of a linear tangential velocity distribution made by Lau *et al.* [59] in their in their investigation of a simplified model for two-phase face seals design is called into question.

Figures 7.7.2.11-12 represent the radial density and viscosity. The evidence of evaporation is again demonstrated by the sudden decrease in the values of both density and viscosity at layers on the rotating surface, i.e layers 79 and 80, at a radius of .05 mm.

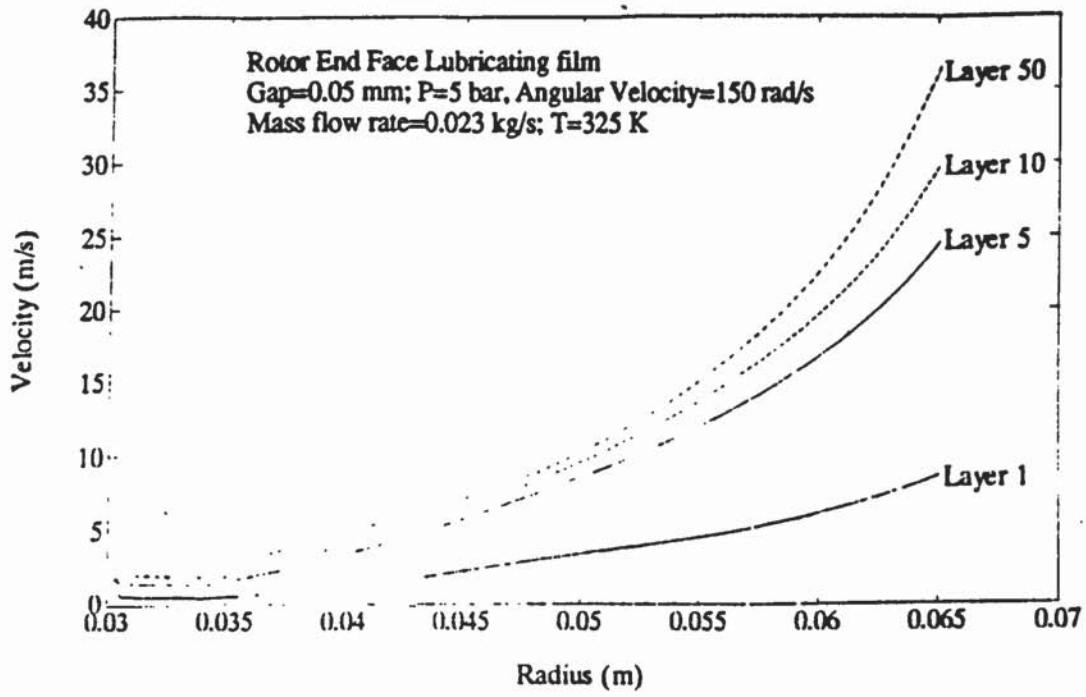

Figure 7.7.2.5. Radial distribution of velocity for a typical solution with 80 layers in the film

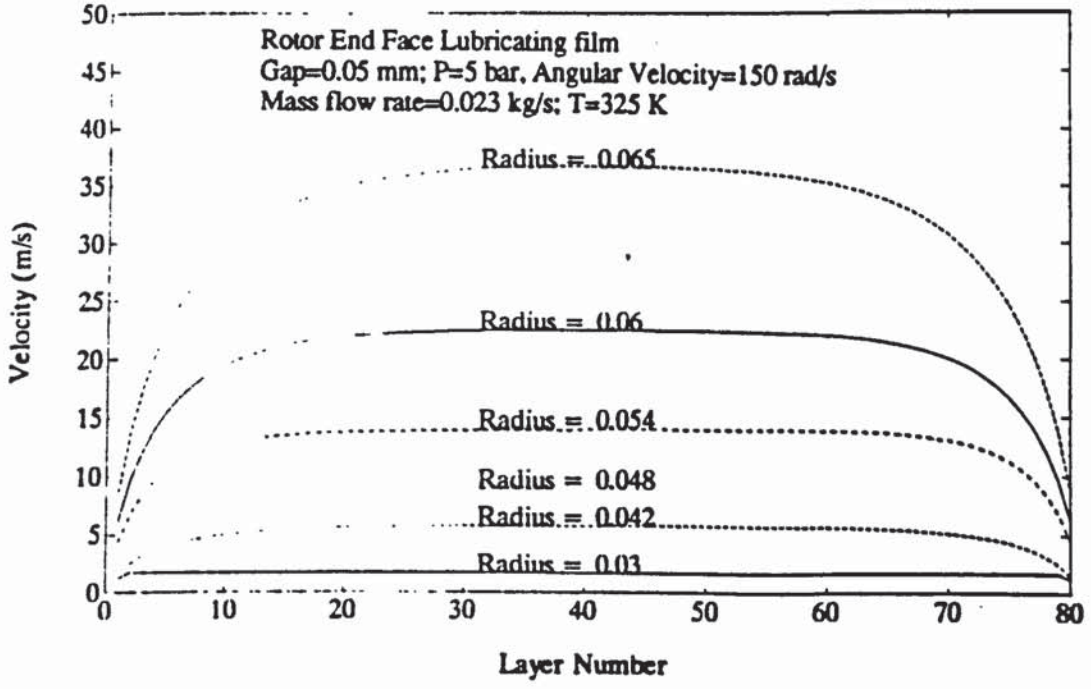

Figure 7.7.2.6. Transverse distribution of radial velocity component

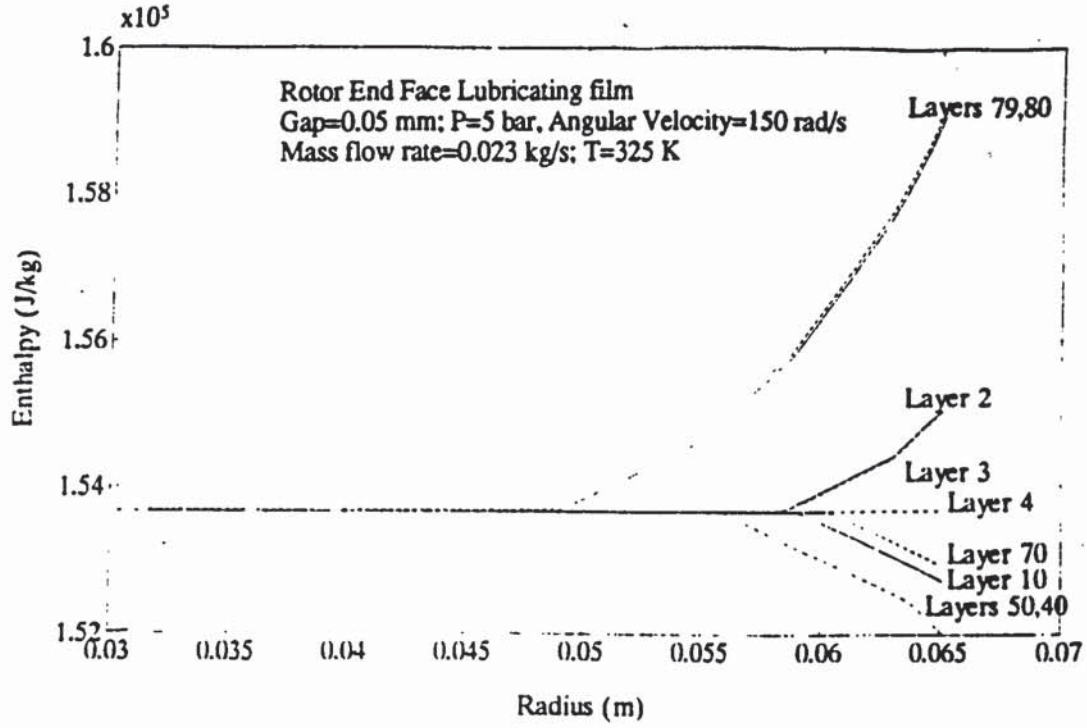

Figure 7.7.2.7. Radial distribution of Enthalpy

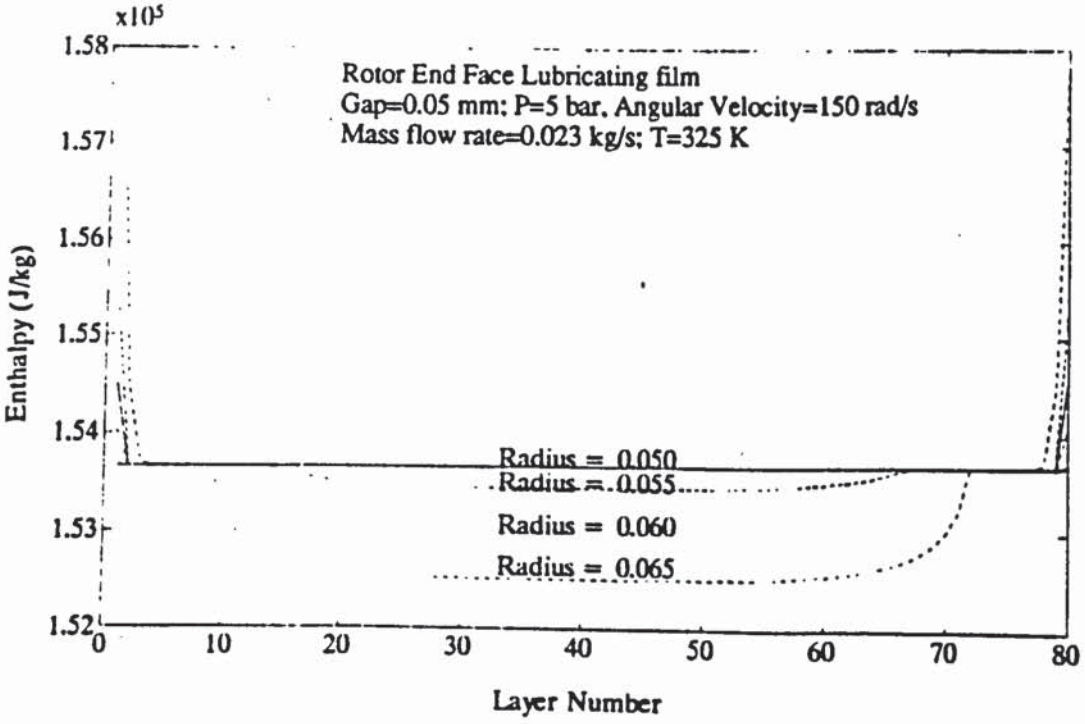

Figure 7.7.2.8. Transverse distribution of enthalpy

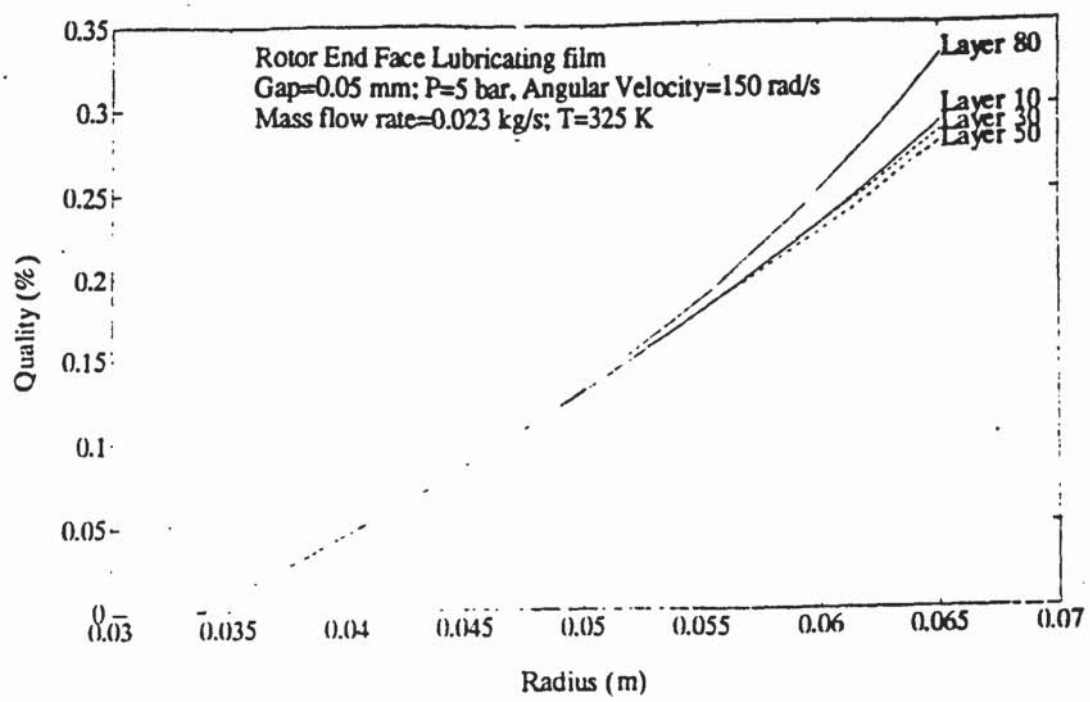

Figure 7.7.2.9. Radial distribution of Quality

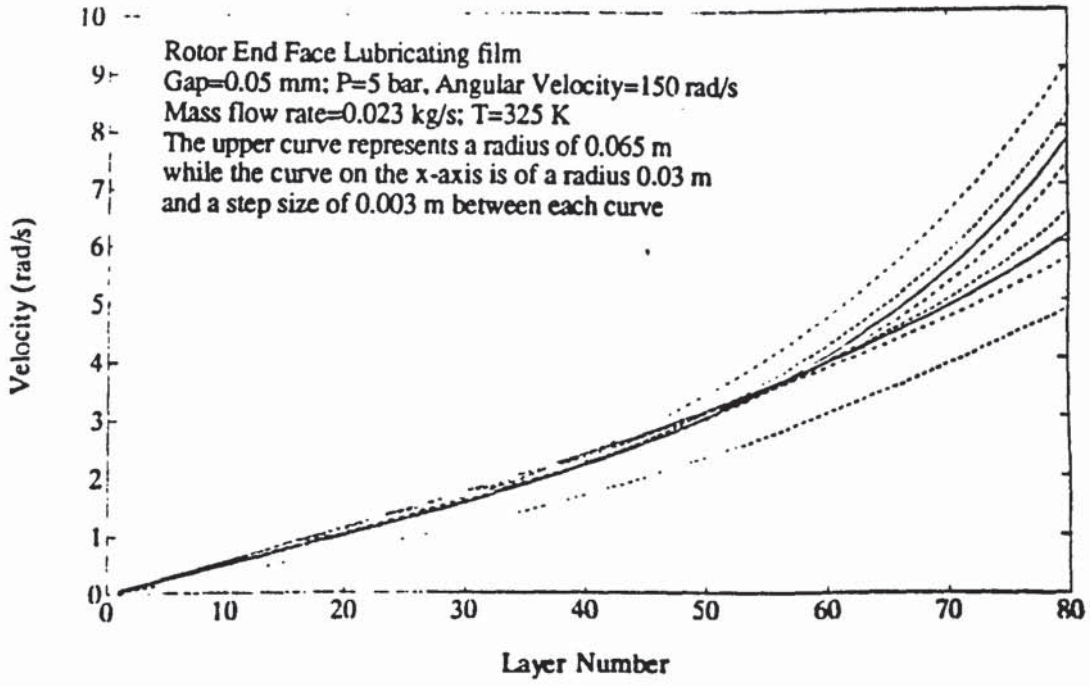

Figure 7.7.2.10. Transverse distribution of angular velocity at different radial positions

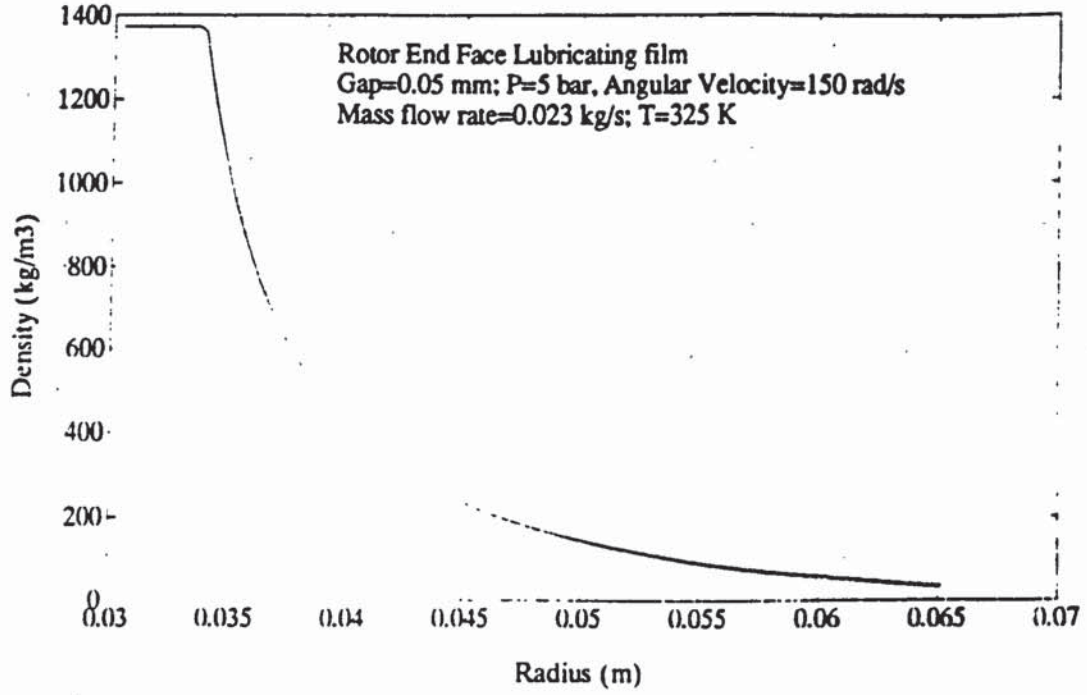

Figure 7.7.2.11. Radial distribution of density for all layers in the film

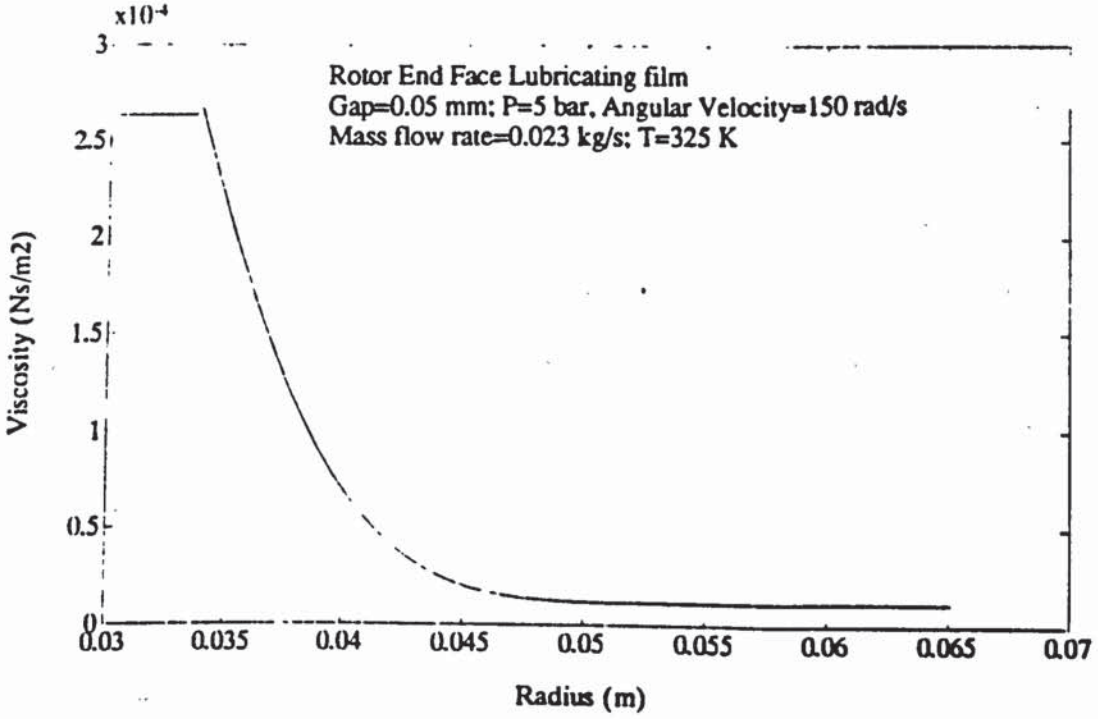

Figure 7.7.2.12. Radial distribution of viscosity for all layers in the film

7.7.2.2 Effect of Parabolic Velocity Profile at Inlet to the Seal

It seems appropriate to make a comparison between the predictions obtained from the assumption of a uniform velocity at the inlet and those which arise if the distribution of radial velocity component is assumed to be parabolic at the inlet to the seal. Figures 7.7.2.13 to 7.7.2.16 show the predicted radial and transverse distribution of pressure, velocity, density, viscosity, enthalpy and quality in the lubricating film under the same conditions corresponding to Figures 7.7.2.5-12 but with the assumption of parabolic velocity at the entry.

Figure 7.7.2.13 represents the radial pressure distribution. A comparison between this curve and that presented earlier as Figure 7.7.2.3, for the uniform entry velocity, corresponding to a mass flow rate of 0.023 kg/s and inlet temperature of 325 K shows that in the case where the velocity is assumed to be parabolic at the entry, evaporation has commenced at a later radial position of 0.042 m. This caused the pressure at the exit to be lower than that the exit pressure in the case of uniform velocity at the entry. As was noted in Chapter 3, increasing evaporation of the fluid in layers close to the solid surfaces leads to a significant reduction in viscosity and hence the rate of pressure drop. The sudden drop of pressure at a radius of 52 mm was attributed to flow separation. Figure 7.7.2.14 shows the transverse velocity distribution across the lubricating film. It is evident from the graph that apart from the first profile at a radius of 30 mm, where a parabolic profile is defined the subsequent profiles change to a turbulent type profile within a very small radial distance. This would indicate that the assumption of a parabolic profile for the radial velocity by Hughes *et al.*[31] and Lau *et al.* [59] in their investigation of a simplified model for two-phase face seals design is not justified.

Figure 7.7.2.15 shows the radial distribution of enthalpy for some selected layers in the lubricating film. It is evident again, that there is more dissipation at the rotating surface, i.e. layer 80, as expected.

Figure 7.7.2.16 represents the radial distribution of quality for selected layers in the lubricating film. The graph shows that the highest proportion of vapour is generated at the rotating surface as it was in the case where a uniform velocity profile had been assumed for the radial velocity at the entry.

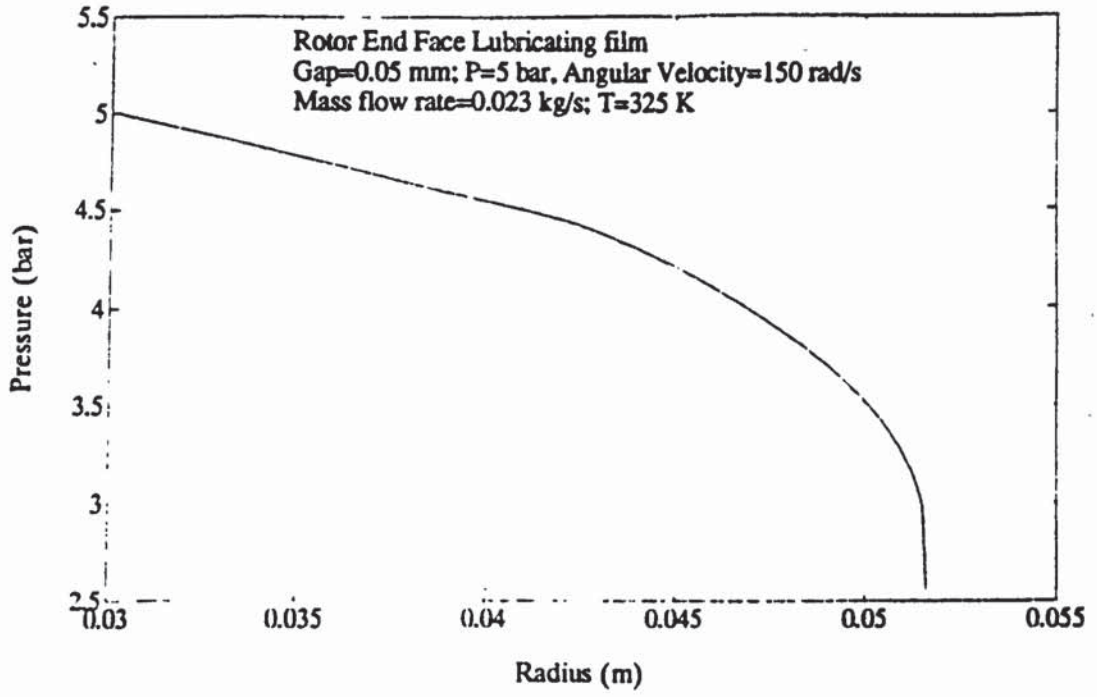

Figure 7.7.2.13. Radial distribution of pressure

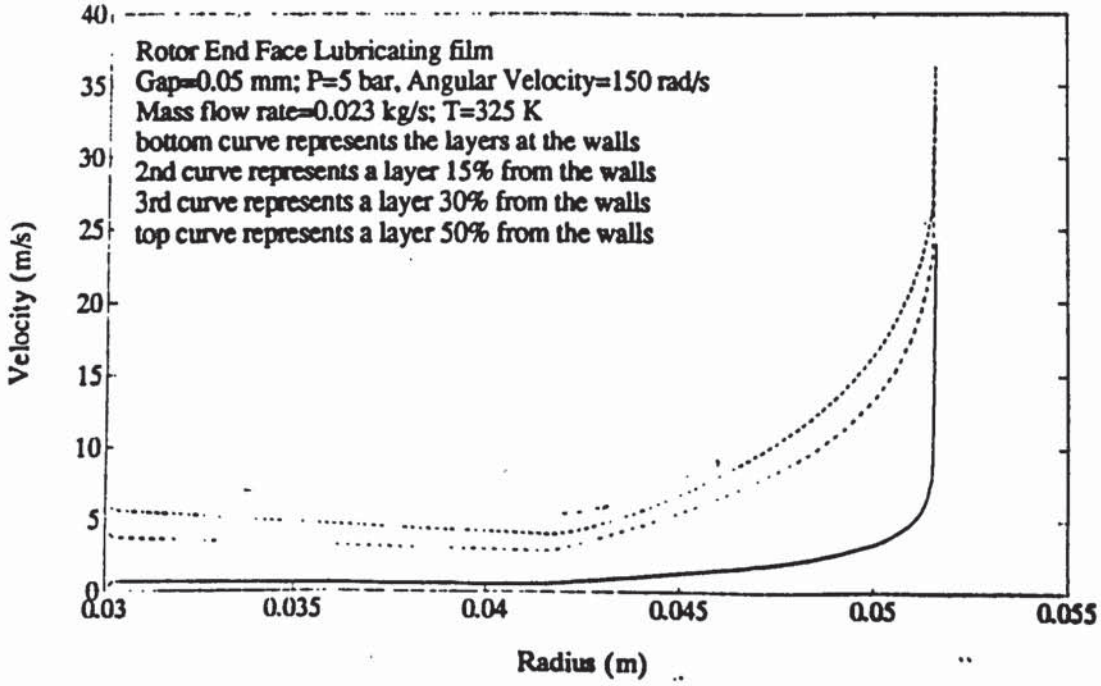

Figure 7.7.2.14. Radial distribution of velocity

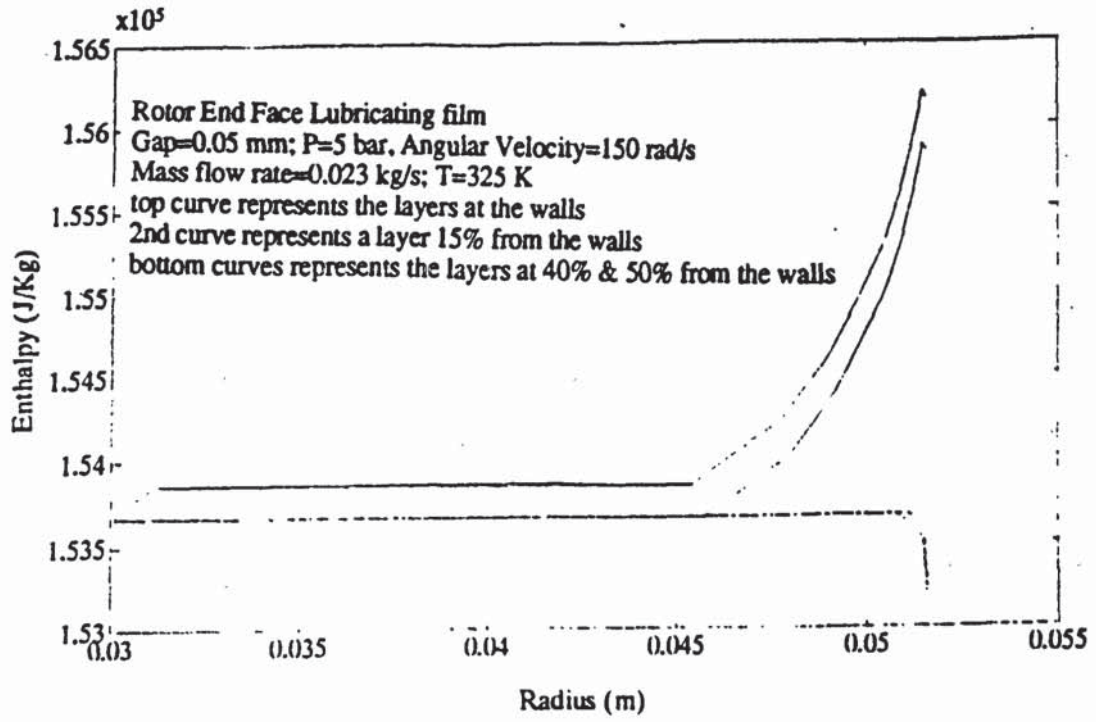

Figure 7.7.2.15. Radial distribution of enthalpy

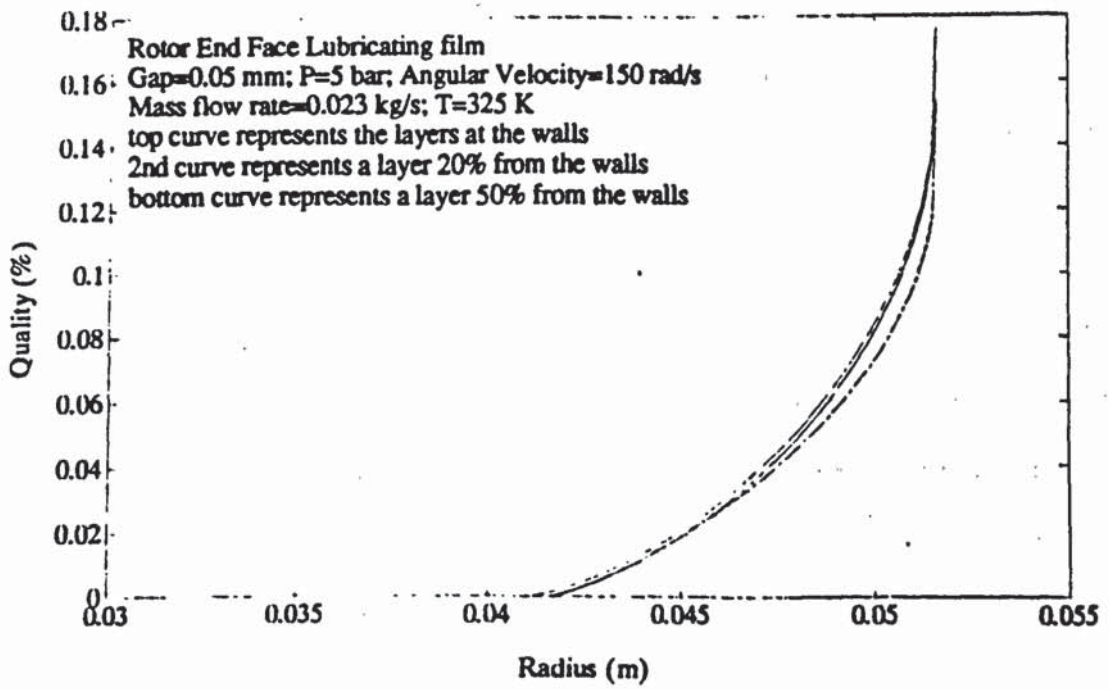

Figure 7.7.2.16. Radial distribution of quality

7.8 Summary of Predicted Results

The first set of results considered were those corresponding to a varied range of mass flow rate with minimum changes in supply pressure and temperature. Both the measured and predicted pressure distribution indicated that no evaporation of the refrigerant took place.

By increasing the inlet temperature of the refrigerant it had been hoped to achieve promotion of vapour formation but as the result of operational limitations relating to an interaction between the liquid temperature, chamber pressure and mass flow rate no evaporating condition were obtained. The comparison of measured and predicted pressure distribution, however, showed good correlation.

After further predictions it became evident that the bearing gap had to be reduced to 0.12 mm to ensure the possibility of vapour formation. The bearing gap was adjusted to this value and further results obtained which showed evaporation of the refrigerant in the outer regions of the bearing plate. Again, good correlation existed between the measured and predicted values of pressure. Operational difficulties of the test rig mentioned earlier prevented any possibility of achieving two phase flow with formation of vapour at an earlier radial position in the bearing.

Predictions concerned with the rotor end face include the variation of pressure, radial and tangential velocity, enthalpy, temperature, viscosity and density. The results indicate that that the nature of the velocity profiles assumed at the entry exerts a great influence on, the location at which evaporation is predicted to commence and as a consequence on, the rate of enthalpy generation and pressure drop. Comparison between these theoretical predictions and those published by other authors are presented in Chapter 8.

CHAPTER EIGHT
DISCUSSION

8.1 Introduction

The objective of the research programme described in the foregoing chapters has been to determine the extent and effect of phase change which might occur in bearings and seals of a sliding vane machine compressing refrigerant fluid and using the liquid phase of that fluid as a lubricant. An extensive literature search has revealed that numerous researchers have examined aspects of related problems but that no experimental measurements existed to test the adequacy of the theoretical predictions which have been made: supporting evidence was purely circumstantial.

The most pertinent studies examined were those of Hughes and co-researchers[31,32,33,34] and of Lau *et al*[60]. In each case the investigators had assumed that the fluid might be treated as a continuum and that profiles of velocity components in the flow could be represented simply. This enabled the effects of viscous dissipation to be predicted for the whole film progressively in the principal direction of flow. The computational difficulties were further eased by, averaging the distributed effect of dissipation across the whole thickness of the film and employing the consequent average values of thermodynamic and transport properties of the fluid to predict the developing phase change situation, although a complete phase change is assumed with the exception of the investigation by Hughes and Chao[32].

The present investigation has aimed to achieve a solution more in keeping with the physical reality of energy dissipation and phase change, and to test the predictions against experimental data as far as possible. No prior assumptions have been made concerning the profiles of fluid velocity components: these have been allowed to develop in accordance with the physical laws governing the motion of the fluid, treated as a continuum, using the Navier-Stokes equations and the laws of mass and continuity conservation.

Fluid properties have been correctly represented at all times, using the Beattie-Bridgman equations to determine the thermodynamic properties together with accepted empirical correlations to represent transport properties, in particular the viscosity of the liquid/vapour mixture. The only major assumption employed was that the flow remained laminar as phase change developed. The assumption of laminar flow allowed the film to be represented as a series of unmixing fluid layers and enabled the Navier-Stokes equations to be solved iteratively across the film thickness to determine the correct value of local pressure gradient, using a 4th order Runge-Kutta process applied in the flow direction. From this, the transverse and streamwise property changes could be predicted and the whole process repeated progressively in the flow direction.

The experimental programme had some restrictions but yielded sufficient data to confirm that the mathematical model gave an acceptable representation of developing phase change in a radial flow hydrostatic thrust bearing. The form of the model bearing was unusual in that it comprised a uniform gap over the whole face of the bearing, rather than the commercial hydrostatic bearing which employs a narrow annular gap to control the leakage rate. This allowed the pressure distribution to be measured accurately, but the extent to which vapour could be generated by viscous dissipation was severely limited by the performance of auxiliary plant items and by the design of the bearing itself as described in Chapter 6.

Details of the experimental equipment had to be established at an early stage in order that construction might proceed. Many decisions were required to be taken before the computer model could be developed to predict the behaviour of the fluid film; in particular the full thermodynamic behaviour of the refrigerant had to be modelled before predictions could be made. This led to problems during the final stages of experimental investigation. For instance, although it was clear from the beginning that auxiliary heating and cooling surfaces needed to be incorporated in the circuit to give the necessary degree of control over test variables, it became apparent only during the final stages that the basic design was somewhat inadequate. Attempts to achieve evaporation of liquid refrigerant indicated

that it would be desirable to incorporate additional cooling surfaces within the bearing chamber itself.

The development of the computer program involved various cross checks between the standard thermodynamic properties of R114 and those predicted by the program. Tables A4.2.1 and A4.2.2 included in Appendix 4 show that the predicted properties of refrigerant R114 are in close agreement with those available in the literature.

The reliability of the computer prediction depends upon two important factors which require practical verification. The first is the validity of the assumptions that under conditions of laminar flow enthalpy generation by viscous dissipation in each 'layer' of the laminar flow might be related to the local velocity of the layer. The second is the suitability of the expression devised to represent the viscosity of the liquid/ vapour mixture produced by evaporation. Results obtained during the experimental investigation for the hydrostatic thrust bearing operating both with and without phase change are in good agreement with the corresponding predictions of the computer model, which suggests that both assumptions are valid. It has to be admitted that the implied quality of the liquid vapour mixture produced during the experimental programme never exceeded 0.2% by mass, equivelant to 10% by volume under the given operating conditions, so that the adequacy of the viscosity relationship for a mixture has not been fully established.

8.2 Validity of Theoretical Assumptions

8.2.1 Laminar Flow and Parabolic Velocity Distribution

The onset of flow instabilities associated with turbulence in a journal bearing is generally related to a Reynolds' number based on the peripheral velocity of the shaft and the radial clearance between the shaft and bearing. The critical value is then taken to be that

established by G.I Taylor[60], who examined the flow between rotating concentric cylinders and established that stable flow exists provided that

$$\frac{\rho U c}{\eta} < 41.3 \sqrt{\frac{R}{c}}$$

where

U = Peripheral velocity of the shaft whose radius is R

c = Radial clearance

Constantinescu[61] debates this point and concludes that a realistic value for the standard hydrostatic thrust bearing would be

$$\frac{\rho U_r Z}{\eta} = 1000$$

For the non-evaporating situation, the maximum value of Reynolds' number at the inlet to the bearing under the operating conditions used in the experimental programme did not exceed 950.

The tendency for the flow to become turbulent in the case of possible evaporation would be determined by the relative rates of change of the product ρU_r and the viscosity η. Any assessment in the present circumstances is complicated by the inter-relationships between viscosity, the consequent rate of change of pressure and rate of generation of enthalpy relative to the value of the enthalpy of saturated liquid at a given radius. Underlying these relationships is their dependence upon the assumption made regarding the viscosity of the liquid/ vapour mixture.

In the conventional analysis of fluid film bearings it is normally assumed that the flow is laminar within the thickness of the lubricating film. This assumption, on which the present theoretical analysis is based, made it possible to employ a simple expression for the distribution of velocity at the first radial position, while the distribution for the subsequent radial steps was evaluated using equation (3.2.2), stated in Chapter 3.

The pressure distributions predicted, show close agreement with those obtained in the experimental programme indicating that the assumption of laminar flow is valid even at the relatively high flow velocities which were involved in the present work. As stated earlier the maximum value of Reynolds' number in the present test was evaluated as 950.

Figure 8.2.1 shows the parabolic velocity profile for the first radial step of the hydrostatic thrust bearing, together with profiles corresponding to some further radial positions. It is evident from the correlation factors obtained by analysing the profile, that the velocity profile remains parabolic at all radial positions. The assumption of a parabolic velocity profile has been practiced by many investigators, including Hughes *et al* [31] who considered the radial velocity to be of parabolic form when analysing phase change of lubricant in liquid face seals even in rotating conditions. The acceptability of this assumption is discussed later.

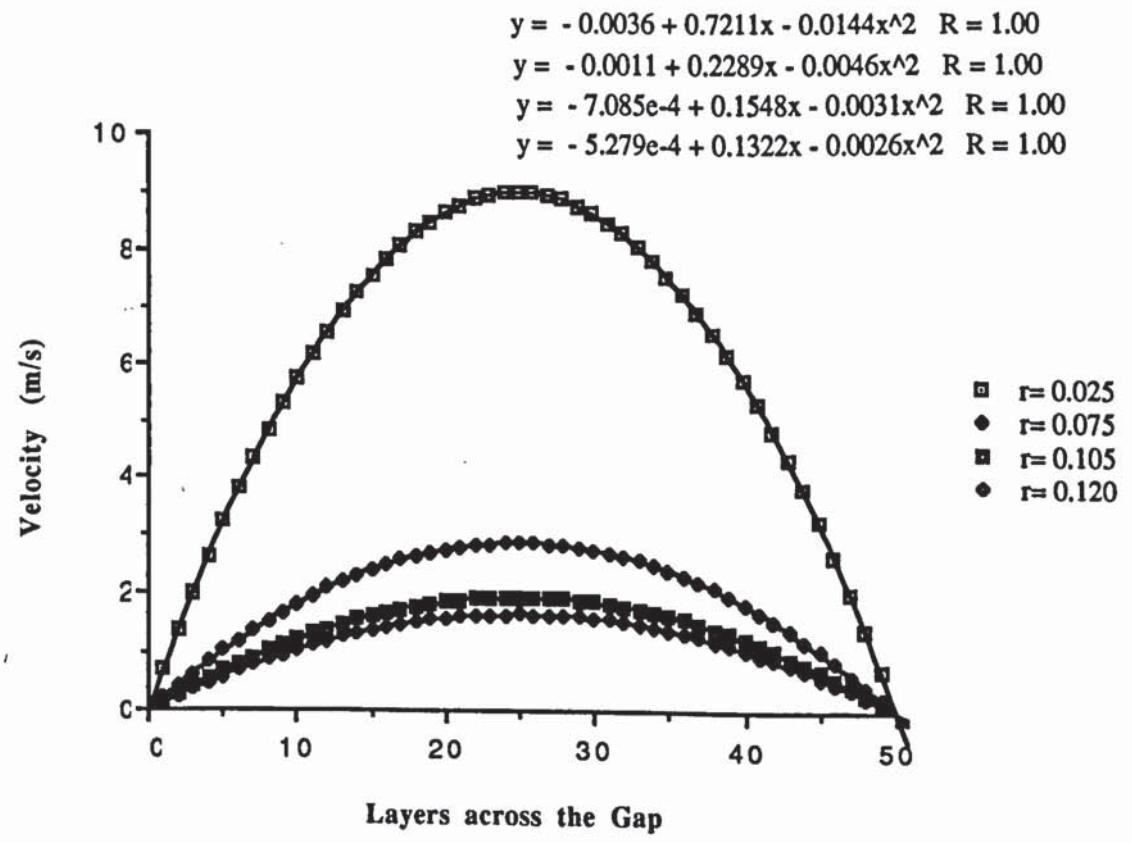

Figure 8.2.1
Velocity profiles corresponding to a typical evaporating condition with respective correlation factor (R)

8.2.2 Viscosity of the Liquid/Vapour Mixture

As mentioned in Chapter 3, all the expressions representing the viscosity of the liquid/vapour mixture predicted a reduction in the viscosity of the mixture as the proportion of vapour was increased, but the prediction varied considerably. As discussed in Chapter 2, Feng and Hahn[46] considered four different relationships but showed no comparison of the quoted relationships with experimental results. It was therefore not possible to form any conclusion as to which relationship would be most reliable.

Within the limited range of measurement obtained during the present investigation it has been possible to make a comparison between these relationships and the proposed correlation. Figure 8.2.2 shows the pressure distribution curves obtained using Cicchitti, Isbin and the present relationship for the viscosity of the mixture and compares this with the measured values of pressure. It may be concluded from the graph that Cicchitti's relationship seems to give a better correlation. However, it can also be concluded from an examination of the slope of pressure curve, that the present logarithmic relationship proposed in Chapter 3 with the coefficient 'a' as unity, results in a better correlation. It is important to note that although the measured data were limited due to the physical constraint of the experimental apparatus, nevertheless the discrepancy between different correlations is clearly evident.

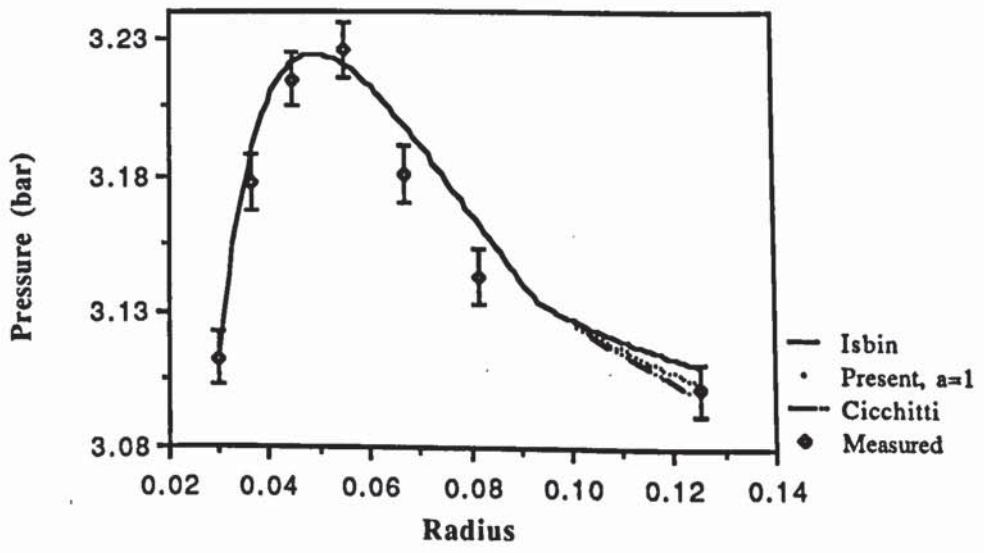

Figure 8.2.2
Comparison of predicted pressure distribution

Theoretical predictions using the proposed correlation showed good agreement with all the results obtained experimentally, as presented in Chapter 7. This means that the expression could be assumed to be valid in predicting the pressure distribution in two-phase flows at least within the liquid/vapour value and ratio range covered by the experimental work. It should also be noted that the expression shows the same values as Isbin and Duckler when the proportion by volume of vapour is small and yields the correct value for the viscosity of pure liquid and pure vapour. A possible advantage of the proposed expression is that coefficient 'a' might be selected to correlate with experimental results to predict a more realistic value for the mixture viscosity, as demonstrated in Chapter 3, section 3.5.3.4. If, during the experimental investigation, conditions of full evaporation had been obtained, then it should have been possible to establish a limiting liquid/ vapour ratio beyond which the expression would not be suitable to describe the viscosity of the mixture. Such a limit is to be expected, as inhomogeneity develops in the mixture in the presence of a significant proportion of vapour by volume.

8.2.3 Consideration of Kinetic Energy

Figure 8.2.3 shows how consideration of kinetic energy and the possible evaporation, affect the pressure distribution in a radially symmetric hydrostatic bearing. The pressure distribution curves in this figure correspond to a bearing with the same inlet conditions, but with three different assumptions. Reynolds' analysis predicts a logarithmic decrease in the pressure of the lubricating film between the port pressure at the inner radius and exit pressure at the perimeter. Consideration of kinetic energy would, however, alter the pressure distribution significantly. The increasing radial cross-section of the flow path acts as a diffuser which causes a rise in the pressure until shear forces become more dominant, and produces a decrease in pressure. Evaporation would lead to a reduction in the shear forces which would reduce the rate of decrease in pressure.

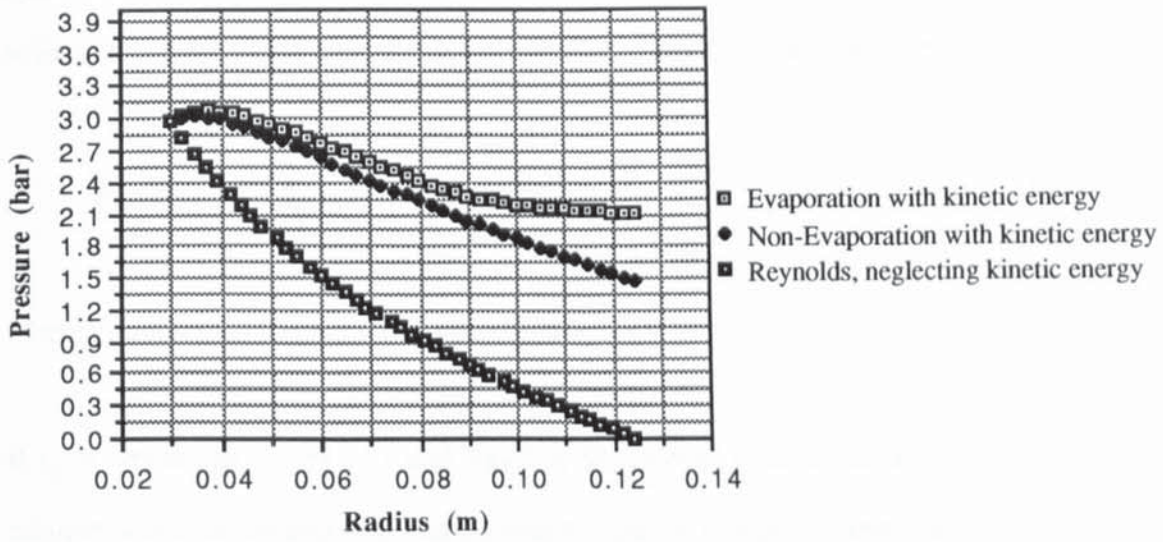

Figure 8.2.3
Comparison of predicted pressure profiles between the solution of Reynolds and the present work with particular reference to the kinetic energy of the lubricant

It is evident from the above comparison that evaporation of the lubricant would lead to a significant change in the load carrying capacity of a bearing of the form investigated. This form of bearing is not truly representative of the standard hydrostatic bearing, which is normally designed to carry a high load by use of a large port diameter, which transmits port pressure over the greatest possible area enclosed within a narrow annular gap to restrict the lubricant flow. The hydrostatic thrust bearing incorporated in the present work was selected to ensure some means by which evaporation of the lubricant could be achieved while providing a means of measuring the pressure distribution reliably.

The effect of kinetic energy of a lubricant is briefly discussed by Cameron who quotes the work of Osterle *et al* [62]. In their work, which is related to journal bearings, they state that "the acceleration of the fluid when it first comes into the bearing might be expected to affect the oil pressure to a negligibly small amount", even at high Reynolds' numbers. The effect of kinetic energy in the context of single phase flow in the hydrostatic thrust bearing can be assessed by re-arrangement and manipulation of the equation for the pressure distribution.

The equation of motion, describing the pressure distribution in the lubricating film of a hydrostatic thrust bearing with isoviscous and laminar flow, can be re-written in a manner which relates the magnitude of viscous effects and kinetic energy changes, viz

$$\frac{p_2 - p_1}{\rho} = \frac{6\eta \dot{V}}{\pi\rho Z^3} \ln\frac{r_1}{r_2} \{ 1 + \frac{\rho Z \dot{V}}{48 \pi \eta r_1^2} \frac{\{1 - (\frac{r_1}{r_2})^2\}}{\ln\frac{r_1}{r_2}} \} \qquad (8.2.3.1)$$

where r_1 and r_2 are the inner and outer radius, respectively.

If r_1 is written as $r_1 = r_2 - \Delta r$ and Taylor's theorem is used to expand the logarithmic relation while neglecting small terms then the rate of change of pressure along the radius can be expressed as

$$\frac{\Delta p}{\Delta r} = \frac{6\eta \dot{V}}{\pi\rho Z^3 r^2} \{ \frac{\rho Z \dot{V}}{24 \pi \eta r^2} - 1 \} \qquad (8.2.3.2)$$

Equation (8.2.3.2) contains the dimensionless group

$$\frac{\rho Z \dot{V}}{24 \pi\eta r^2} \qquad (8.2.3.3)$$

The group is effectively a Reynolds' number, but its importance lies in its magnitude. According to the classical Reynolds' analysis this parameter should have a zero value. However, equation (8.2.3.2) shows that, if its value is unity then the pressure gradient at the radius r will have a zero value, rather than the gradient predicted by Reynolds. Cameron does not define the appropriate parameters of a Reynolds' number in the context of fluid film bearings but the present argument suggests that this should be zero in the case of the circular hydrostatic thrust bearing and that the relative importance of kinetic energy may be determined as

$$(\frac{\rho Z \dot{V}}{24 \pi\eta r^2} - 1) \times 100\% \qquad (8.2.3.4)$$

The nominal value of the above dimensionless number gives no indication as to the laminar or turbulent nature of the flow, but if the local velocity at radius r is used in place of the volume flow rate, then the modified parameter is more clearly recognised as a Reynolds' number, i.e.

$$\frac{\rho u_r Z^2}{12 \eta r} \qquad (8.2.3.5)$$

This suggests that there is a critical value above which the core of the flow becomes turbulent, but the literature does not seem to have established such a value in the case of the circular thrust bearing. The value of the above number was estimated to be between 0.175 and 0.36 for the two values of the bearing gap, 0.08 mm and 0.12 mm as used during the present experimental tests. These values were detrmined at the radius corresponding to the maximum value of pressure.

8.2.4 Energy Dissipation

Comparison between enthalpy distribution curves corresponding to a typical evaporating and non-evaporating condition in Chapter 7, showed that the enthalpy of the lubricant increases due to viscous dissipation. However, as soon as evaporation takes place both density and viscosity of the lubricant decrease, reducing the effect of viscous dissipation and as a consequence, the rate of enthalpy gain reduces slightly as vapour formation increases. The results also indicated that the enthalpy generation was most dominant in the layers near the walls where the temperature was the highest and the velocity was lowest. The supposition that the bubbles of vapour formed and carried with the stream in their own streamlines could only apply while the size of the individual bubbles remained very small in relation to the gap and it must be expected that this would not be the case once the volume proportion of vapour became significant.

8.2.5 Heat Transfer

In the analysis presented in Chapter 3, the heat transfer by convection and conduction between the refrigerant and the bearing surfaces was neglected. The heat flux considered included only the dissipation term and heat transfer by conduction within the fluid film. This can be justified since the temperature gradient between the bearing surfaces and the refrigerant is negligible. During the experimental phase of the research programme the highest temperature difference noted between the bearing chamber and the refrigerant was no more than 2°C. The heat transfer coefficient of a condensing vapour is very high so a very small temperature difference between the adjacent fluid and the bearing surface gave a very high rate of heat transfer. In the experimental test rig there was a wet mixture of liquid/vapour with a high proportion of liquid in the gap, while outside in the chamber there was a saturated mixture with vapour only in the upper region where the bearing was located. A calculation of the heat transfer by conduction between the refrigerant and the bearing surfaces was carried out using the measured maximum temperature difference of 2 degrees. At the same time the heat transfer by conduction within the refrigerant film was calculated for a typical prediction in which the thickness of the film was taken to be 0.12 mm and a maximum temperature difference of 0.5 K. Comparison between these two calculations showed that the heat transfer by conduction within the film was much greater than that between the bearing surfaces and the refrigerant.

Heat transfer by conduction through the bearing plate with 2 K temperature difference across the 25 mm thickness is

$$\frac{Q}{A} = -k\left(\frac{dT}{dz}\right) = -47\left(\frac{2}{.025}\right) = -0.37\ (kW/m^2)$$

And the heat transfer by conduction for one layer in the refrigerant is

$$\frac{Q}{A} = -k\left(\frac{\Delta T}{\Delta z}\right) = -0.058\left(\frac{0.5}{0.00012/50}\right) = -12.1\ (kW/m^2)$$

Predictions presented in Chapter 7 have shown that under the experimental conditions full evaporation did not take place. This justifies the reason for not including the heat transfer to the solid boundaries, despite the high values of heat transfer for condensing vapour since when there is vapour present it is always in contact with the fluid and this is taken care of by including the conduction within the fluid film.

8.2.6 Layer Thickness Changes

It will be recalled that in the procedure for calculating the pressure drop, the film thickness was subdivided into a finite number of unmixing shear layers. The thickness of each layer may vary in the direction of flow, but the sum of the individual layer thickness must equal the local film thickness. In the majority of predictions this criterion was applied successfully, assuming that adequate accuracy had been obtained over a radial step when the error was less than 0.03% and that the error was distributed proportionately among the layers before proceeding to the next radial step.

The dependence of the method for solving the Navier-Stokes and continuity equations on the mesh size was mentioned in Chapter 5, where it was shown that the equation did not become indefinite as number of layers increased to 80. Figure 7.6.2.2 in Chapter 7 was presented to show how the solution converged as the number of layers increased. It has been confirmed, that the model is capable of dealing with very small mesh sizes. However, the important factor to remember is that although the film thickness can be divided into many layers, the possibility of the layer thickness becoming less than the molecular spacing of the fluid is always a danger which should be born in mind, as well as the computational time necessary to obtain a solution.

Under certain inlet conditions of mass flow rate, temperature and pressure, the thickness of the layer next to the solid surface was predicted to become very large leading to

negative values elsewhere in the film and causing the program to terminate. In some instances the predictions were found to be of a reversal of flow in the layer adjacent to the wall immediately prior to the step at which the program aborted.

The flow reversal prediction might be taken to indicate detachment of the flow, as suggested in Chapter 7 but it was not possible to conclude this with any degree of certainty. The computer program contained conditional statements which caused termination, e.g. on the detection of flow reversal, or when the predicted pressure gradient over a step length led to the use of a negative value of absolute pressure entering the Beattie-Bridgeman routine for property calculation. In general the negative pressure prediction could be overcome by increasing the value of supply pressure or, by reducing the rate of mass flow.

The prediction of flow reversal was less readily avoided on account of the interactions between inlet pressure and temperature, and the dependence of the dissipative effect on the rate of mass flow entering the bearing or the rotating seal. Hughes *et al*[31] determined a 'stable' mass flow for a given pressure drop by assuming that phase change was instantaneous and complete at some intermediate radius within the face seal, and using momentum, continuity and energy equations in the single phases flowing in each zone to iterate towards the 'correct' mass flow for the given pressure drop. As has been discussed in Chapter 3, these researchers also assumed the profiles of both the radial and tangential velocity components of flow in the lubricant film and thereby were able to determine the rate of energy dissipation. This rate was then used to yield an average change in properties of the whole film thickness at a given radius.

There are several critisisms concerning these assumptions, since they do not conform to the physical reality:

1) Instantaneous phase change from liquid to vapour is possible only when the liquid reaches its critical temperature at critical or supercritical pressure.

2) At pressures below the critical, phase change requires a finite energy input: at normal pressure the requirement is substantial and certainly could not arise as the result of dissipation over a very small distance.

3) The major contribution to the dissipation is the local transverse velocity gradient in the film, which is greatest at the solid boundaries enclosing the flow. Consequently phase change commences in those 'layers' of the film adjacent to the boundaries.

8.3 Significance of Results for Rotor Ends and Vane Ends of a Sliding Vane Compressor

It has been established in Chapter 1, that the only part in a sliding vane compressor where it is possible that phase change would seriously affect the bearing or seal performance is the rotor end faces. This was stated to be due to the rotor ends having a small clearance within which the fluid flows outward and its pressure reduces, so that energy dissipation may cause evaporation of the fluid.

If the rotor and vane portions within the rotor are taken together, they then combine to form a rotating thrust bearing which might be considered as the system discussed by Hirano and Sakitani[63]. If rotation and the true path of the lubrication are neglected then the assembly resembles the model bearing tested in the present work, from which it would seem probable that two phase conditions would arise at some radius in the region. The rotor end clearances of practical machines are small and consequently pressure would drop as the film flowed outwards, with enthalpy generation leading rapidly to the evolution of vapour within the lubricant film.

8.3.1 Rotor Ends and Rotating Face Seals

Since good correlation for the predictions representing the behaviour of the hydrostatic bearing with the experimental measurements was achieved, the method was extended to assess the effect of phase change on the performance of rotor ends. The dimensions employed were those likely to arise in the end faces of the rotor of a sliding vane compressor. The mass flow through the seal, fluid pressure and temperature at entry and the rotational speed of the shaft were set at appropriate values and led to the prediction of profiles of the form shown in Figures 7.7.2.3, Chapter 7 the characteristics of developing phase change already discussed.

8.3.1.1 Pressure Distribution and Velocity Profiles

The present approach to the prediction of phase change has allowed for the local effects upon fluid properties of energy dissipation and heat transfer within the fluid film under laminar flow conditions. The theoretical prediction for the rotor end face indicates clearly that phase change does not occur uniformly across the film but predominantly in the highly sheared layers adjacent to the solid boundaries. Figure 7.7.2.3 in Chapter 7, shows the radial distribution of pressure in the film, and in Figure 7.7.2.7 the corresponding transverse distribution of enthalpy is shown. For these particular predictions, the film was divided into 80 layers. It can be seen that there is a significant enthalpy change only in the layers lying closest to either the stationary or the rotating boundary. It must be noted that the enthalpy axis of Figure 7.7.2.7 does not start from zero and that substantial changes nowhere exceed 7%. At first glance it may seem peculiar that effects are not greater at the rotating face, but examination of Figure 7.7.2.10 shows that the tangential velocities are much lower than the radial velocities in these layers

so that rotation has only a secondary effect on the generation of enthalpy under these particular circumstances.

The resulting distributions of fluid quality, density and viscosity were shown in Figures 7.7.2.7,11-12. Figure 7.7.2.9 indicates that there is not a large variation of quality across the film at any given radial location, despite the apparently large variation of enthalpy generation. It must be noted, however, that the refrigerant is assumed to enter the rotor end face seal at a temperature which is already close to the saturation temperature and that pressure reduces as the fluid flows radially outwards through the seal. The combination of pressure reduction and temperature increase in all layers of the liquid is seen to lead to the nearly simultaneous start of vapour generation throughout the flow at a radius of 0.035 m (approximately). It is therefore only at greater radii that the effect of dissipation in layers close to the solid boundaries become significant.

The apparently constant value of enthalpy at all radii in central layers, despite energy dissipation and heat transfer within the film, may be accounted for by the density changes and changes in the increased kinetic energy of fluid in these layers.

Referring again to the velocity distribution of Figure 7.7.2.5, it is apparent that the radial component of velocity achieves high values and that significant transverse gradients of the radial component exists only in layers adjacent to the walls. This is more clearly illustrated in Figure 7.7.2.6, where the development of the transverse profile is shown at selected radii. The shape of this profile is of particular interest, since the major past contributors to the analysis of phase change in face seals have assumed that the transverse profile remains parabolic. With the exception of the first profile which is defined as uniform, the subsequent profiles do resemble a parabolic form. It should, however, be noted that in this particular prediction the rotational speed was assumed to be 150 rad/s which is not a particularly high speed. It will be shown later in section 8.4 that the profiles can be skewed as the result of high rotational speeds. The results also showed that viscosity of layers adjacent to the solid boundaries was reduced as evaporation

proceeded. Consequently the core of the flow was subjected to shear effects which were considerably reduced from those which would arise in an isoviscous situation, or where the energy dissipation was assumed to affect the average properties of the film.

The transverse distribution of the tangential velocity component shown in Figure 7.7.2.10 is also of interest insofar as previous authors have assumed a linear variation of angular velocity between the rotating and stationary boundaries. The present prediction indicates that the reduced fluid viscosity in layers adjacent to the moving boundary and the greater density of the mixture in the core of the flow alter the profile considerably from the linear variation which would characterise isoviscous shear with the film.

8.3.1.2 Performance of Rotating Face Seals

The discrepancy between the forms of profiles employed by earlier researchers and those obtained by the present solution procedure suggests that the pressure distribution and leakage mass flow rate determined by the two approaches would also differ. Figures 8.3.1-2 compare the radial distribution of pressure and temperature obtained by Hughes and Chao[32] for a water pump seal with that predicted by the present theoretical approach. A parallel type seal was used with a film thickness of 0.0229 mm, the temperature and pressure of water being 383 K and 3.1 bar respectively while the rotational speed of the shaft is 4000 rad/s (38197 rpm). Hughes and Chao obtained their solution by trial and error, assuming uniform properties in the film at any given radius. In the present case the value of mass flow rate quoted by Hughes and Chao has been used together with the quoted inlet conditions and plane seal geometry. In addition the corresponding pressure distribution has been computed for water flow with varying thermodynamic and transport properties of water and steam fully accounted for.

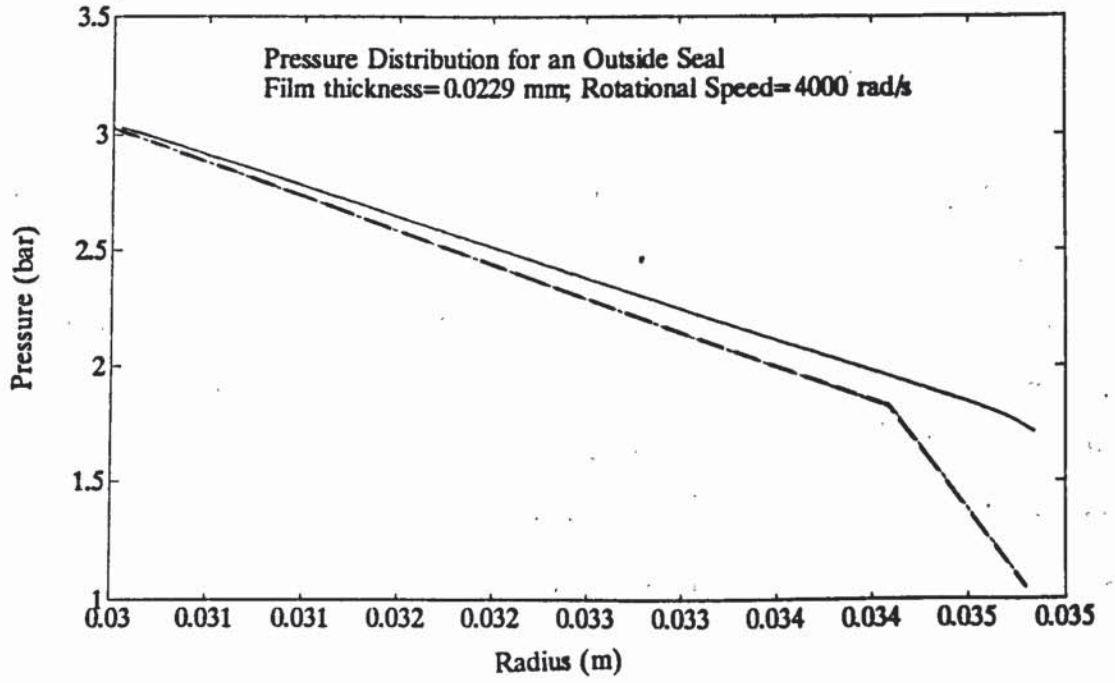

Figure 8.3.1. Comparison of pressure distribution between Hughes and Chao with the present analysis The upper curve corresponds to the present analysis while the lower curve shows the prediction by Hughes and Chao

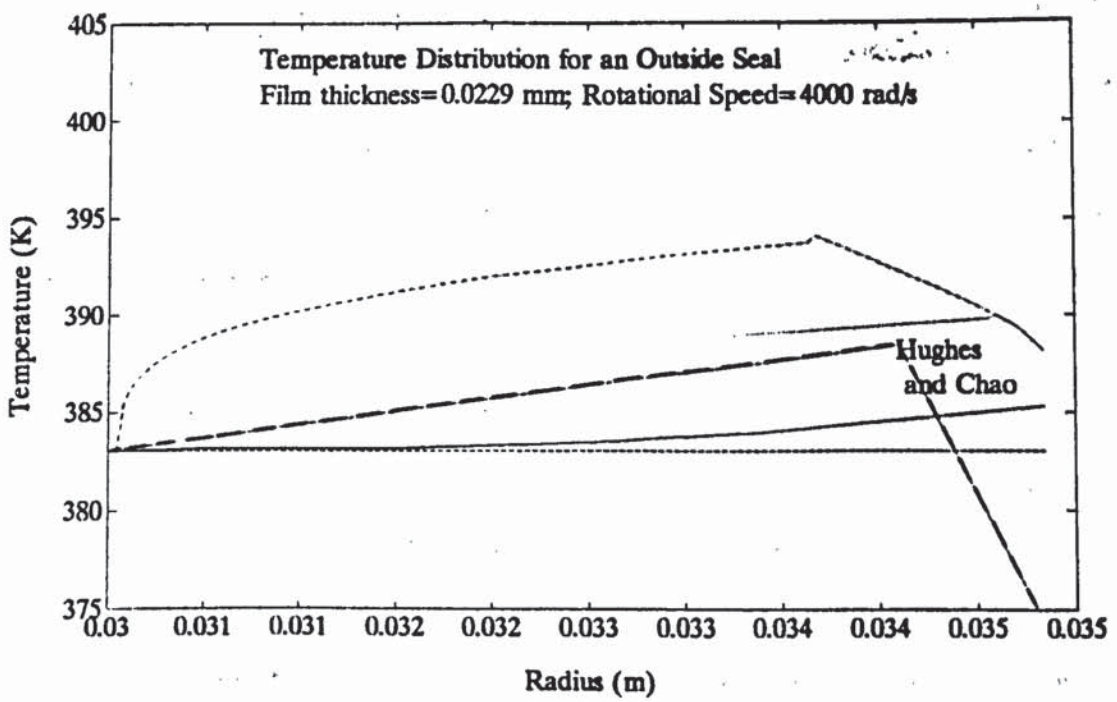

Figure 8.3.2. Comparison of temperature distribution between Hughes and Chao with the present analysis. The dashed curve represents the prediction by Hughes and Chao. The horizontal, 2nd, 3rd and 4th curve correspond to the temperature at the stationary surface and at 20% , 50% and 100% away from the stationary surface, predicted using the present analysis

Examination of Figure 8.3.1 shows that the discrepancy appears to remain small until the radius at which Hughes and Chao show phase change taking place. The present method predicts a smaller pressure drop due to the partial evaporation of the fluid in layers of the film adjacent to the solid boundaries and the resulting reduction in viscosity and wall shear forces. A greater discrepancy arises in the outer regions of the seal where the assumption by Hughes and Chao of average fluid properties leads to their use of reduced values of fluid density and viscosity at the boundaries, which must lead to the prediction of substantially increased fluid momentum changes. These effects combine to conclude that much greater rate of pressure drop is required and that the load carrying capacity of the seal is much less than is presently predicted provided the supply conditions were similar, free expansion existed at the exit and that the pressure outside the bearing was the same as that used by Hughes and Chao. It should be noted that the load carrying capacity of the seal is related to the pressure distribution within the seal which is a function of supply conditions, the gap and mass flow rate.

The effect of two phase flow on load carrying capacity has been investigated by other researchers, namely Orcut[27], as mentioned when reviewing the literature discussed in Chapter 2. When investigating the load carrying capacity of a steam lubricated bearing with conditions of two phase flow, Orcutt concluded that the load carrying capacity of the bearing was lower than with single phase conditions.

Examination of Figure 8.3.2 also reveals that Hughes and Chao predicted a single profile for the temperature of the fluid which starts to increase and, as evaporation takes place, will decrease due to the saturation pressure reducing. The present prediction, however, indicates that there is a big difference between the layers of the film on the moving surface and those on the stationary surface due to the very high rotational speed of 4000 rad/s. This temperature difference is approximately 5 K for this type of seal and inlet conditions. However, if a higher rotational speed were to be considered it is expected that the difference could be much higher than this value.

8.3.2 Vane Ends

In discussing lubrication of the vane ends two separate situations need to be considered.

1 The zone extending beyond the body of the rotor which is lubricated by the fluid which is a mixture of vapour and injected liquid and rests on the cell walls.

2 The portion of the vane end which lies within the radius of the rotor is lubricated by fluid which will have been delivered directly to the zone via appropriate supply ports, or have leaked into the region as a discharge from the journal bearings.

Rotary motion is involved in both zones. Hirano and Sakitani[63] examined the lubrication of the rotor ends. They tried to account for the variation of exit pressure around the periphery of the end face in the sliding vane machine, using a heat transfer analogy, but assuming isoviscous flow. The difficulties which rotary motion introduces will not be considered in the present discussion.

If the outer region is considered as, flow between parallel plates then it will have the traditional Couette solution, so long as the flow is laminar and there is no phase change. Thus there will be a continuous pressure drop in the rearward direction and the strong possibility that evaporation would take place. This would not cause problems if the axis of the machine was horizontal and assuming identical events at both ends of the vane. If the resulting forces were not in balance on account of non-identical events then it is likely that axial oscillatory motion could be induced, although there would be very high damping forces due to the shearing of the fluid film between the vanes and the rotor slots in which they move.

8.3.3 Leakage Flow

Hughes *et al.* also made extensive[31,32,33] theoretical investigations into the potential of two phase flow as a leakage control mechanism rather than its effect on the load carrying capacity. There were no direct comparisons with experimental results in any of these investigations.

In comparing the present predictions with those of Hughes and Chao (Figures 8.3.1-2) it is apparent that the mass flow rate was associated with a greater pressure drop using Hughes and Chao's analysis than indicated by the present method. This does not necessarily imply that the present method would predict a greater mass flow rate for the same pressure drop. If the supply conditions were the same and pressure outside the bearing was that pertaining to Hughes and Chao's exit pressure and providing sonic conditions were reached at some radius within the seal then the mass flow rate would govern the pressure drop within the bearing and pressure equilibrium would be achieved through sudden expansion at the point of discharge. Thus the mass flow rate would be unchanged, depending only on inlet conditions, seal geometry and rotational speed. In addition, the load carrying capacity would be then greater than suggested by Hughes and Chao.

If the film is completely in the vapour phase then sonic conditions may occur and there could be free expansion of the flow at exit from the seal, but this can never be the case in the liquid phase, since the flow is virtually incompressible. The situation is less certain if a liquid vapour mixture is present because the sonic velocity of a liquid/vapour mixture is generally lower than that of either the liquid or the vapour alone. Evidence suggests a value which is only some 10% of the corresponding sonic velocity in the vapour, dependant upon the proportions of liquid and vapour in the mixture. Moody[65] determined the accoustic velocity of a homogeneous mixture using equation (8.3.1)

$$C = \frac{C_g}{\alpha} \sqrt{\frac{1}{1 + \frac{1-\alpha}{\alpha}\frac{\rho_f}{\rho_g}}} \qquad (8.3.1)$$

where
C =Accoustic velocity
α =proprtion of vapour generated
ρ =Density
Suffices f and g refer to fluid and vapour phase respectively

This suggests that the limiting flow will be significantly less than would be predicted using sonic velocity of the vapour as the criterion. The present experimental programme yielded no evidence of limiting flow conditions during any of the tests which were undertaken.

The suggestion by Hughes and Chao that phase change might provide a method of leakage control appears to have some merit. Examination of Figure 8.3.1 indicates that the same mass flow rate requires a greater pressure drop when there is no evaporation taking place than when there is partial evaporation in the same bearing. What is important to the designer of face seals is to ensure that the dimensions and gap provide the required load carrying capacity and yet limit the leakage of fluid to an acceptable level.

It is the interaction between the fluid supply conditions, seal geometry and shaft speed which prevents the establishment of a direct relationship between the mass flow rate and pressure drop in the phase change situation as investigated by Hughes and Chao and the present solution. Solutions can be achieved only by trial and error: the satisfactory matching of the design to the working conditions of the fluid will be a difficult process.

8.3.4 Shaft Vibrations and Seal/Thrust Bearing Characteristics

Some authors[33,64] have considered the mechanical stability of the rotor to be affected by possible evaporation of the lubricant in a face seal or thrust bearing. A frequency of oscillation can be predicted on the basis of load carrying capacity characteristics estimated from equilibrium theory, and then applied over a range of seal gaps under non-equilibrium conditions. Their conclusions have not been tested by direct experimental measurement but do indicate that axial stability of the shaft may be a problem in these circumstances. Although instability is frequently observed to arise on shafts employing seals and thrust bearings, the sliding vane compressor employs identical seals at each end and is not known to exhibit shaft instabilities.

The solution routine explained in this thesis assumes thermodynamic equilibrium to exist at all times in all layers of the fluid. Evaporation is not an instantaneous effect and its correct representation would be achieved by introducing the appropriate rate equation, of the Arrenhius type. This has not been considered in the present investigation.

8.4 Effect of Centrifugal Forces

It has been mentioned in Chapter 3 that some authors have considered the effect of centrifugal forces in the past. These include the investigation by Fog[6] into the fluid film lubrication of parallel surfaces, under a high-speed rotating member. His conclusions indicated that the centrifugal forces were important to produce positive pressure in high rotational speeds. The present prediction was applied to the case of high rotational speed to examine the effect which it may have on the parameters such as enthalpy, radial velocity and so on. Figure 8.4.1 through 8.4.3 presented earlier showed the distribution of transverse angular velocity, radial velocity, mass fraction of vapour,x, and the viscosity corresponding to angular velocity of 700 rad/s. Examination of these graphs

reveals that, in the case of the transverse distribution of radial velocity the profiles are skewed as a result of the high angular velocity of the moving part. It is also evident from Figure 8.4.3 that there is approximately a 9% difference of quality between the layers at the walls and those in the middle of the film. It can be said that the assumption which Hughes and Chao have made on averaging the variation of properties across the lubricating film is acceptable when the rotational speed of the shaft is low, although the assumption leads to a different pressure distribution because the outer layers are predicted to be less viscous than shown by the present method. Further predictions with higher rotational speed showed that the difference in quality across the film between different layers was much greater than 9%. This is an indication that a very high rotational speed does affect the operating conditions of a rotating seal.

The profiles of Figures 8.4.1-3 show that the rotating member of a face seal imparts angular velocity to the adjacent layer of the fluid film, as would be expected, but that angular acceleration imparted to the fluid also causes it to accelerate in the radial direction. Thus the transverse velocity profiles are skewed substantially for the symmetric form predicted for the hydrostatic bearing, indicating a 'pumping effect' on the rotating surface.

Figure 8.4.1 and 8.4.2 represent a face seal in which the fluid is evaporating progressively. It can be observed that the transverse profiles for the radial component of velocity exhibit the same tendency towards the shape normally associated with turbulent flow, rather than the parabolic form of single phase laminar flow but have superimposed on them the increasing radial velocity in layers adjacent to the rotating surface, caused by the pumping effect. This is entirely in agreement with the comments made by Fog[6] concerning centrifugal forces in rotating seals.

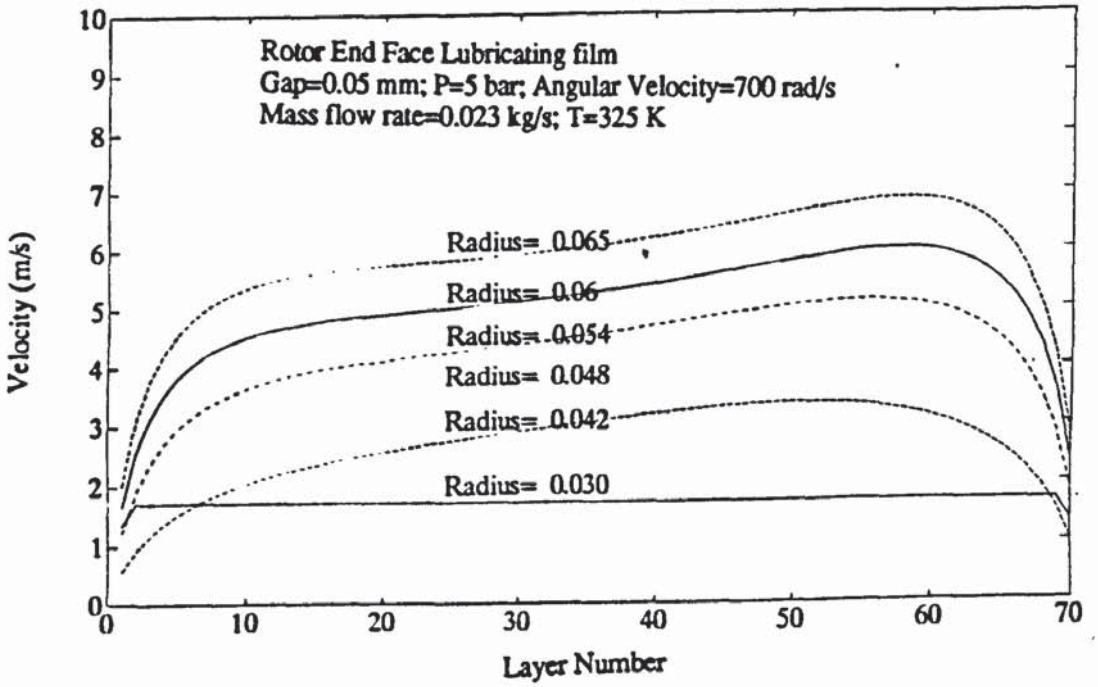

Figure 8.4.1. Transverse distribution of radial velocity corresponding to a high angular velocity of 700 (rad/s)

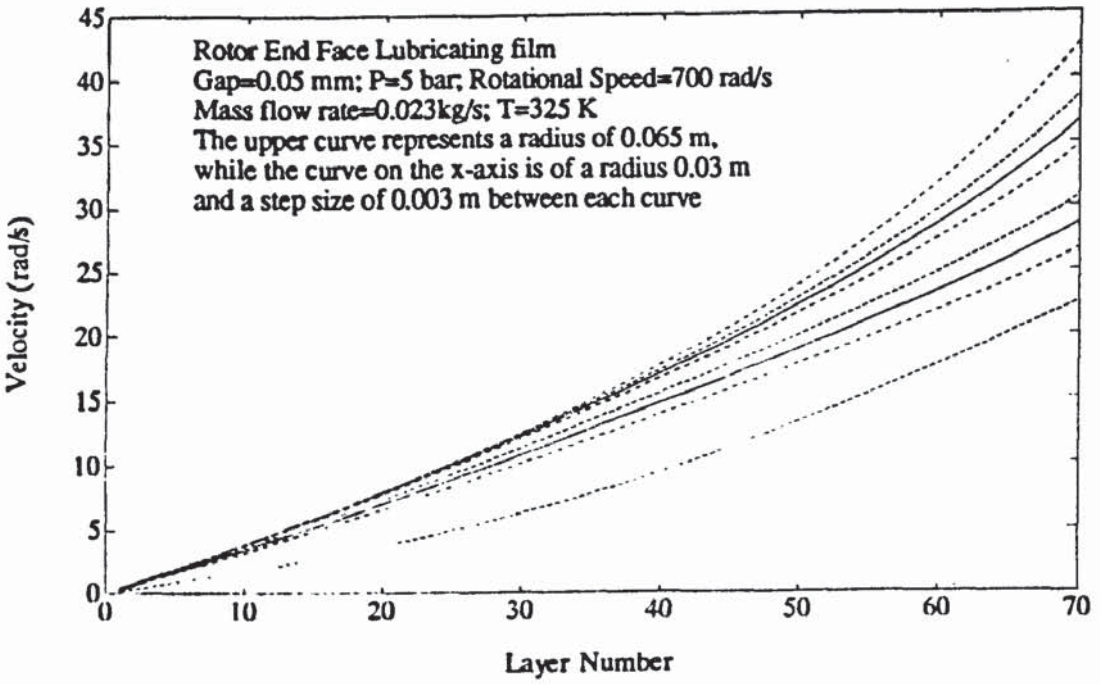

Figure 8.4.2. Transverse distribution of angular velocity corresponding to a high angular velocity of 700 (rad/s)

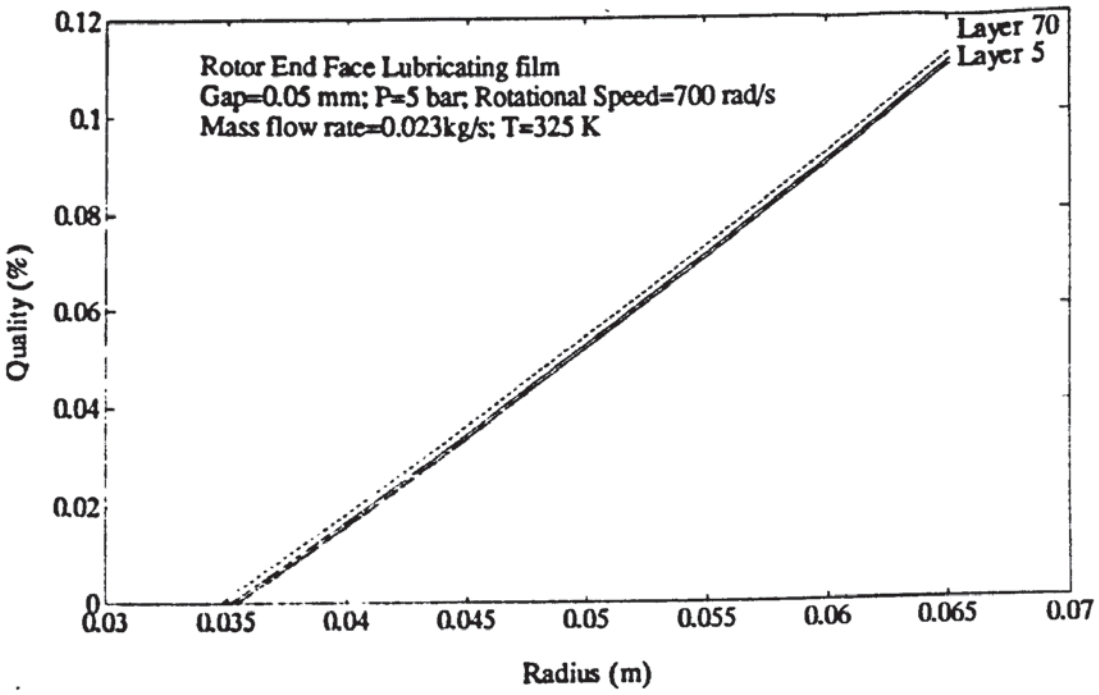

Figure 8.4.3. Radial distribution of quality corresponding to a high angular velocity of 700 (rad/s). The curves correspond to all layers across the film

Conclusions have been drawn from the this discussion chapter which have been presented in Chapter 9, together with suggestions for further work to state aspects of the research which remain uncertain or in need of further research.

CHAPTER NINE
CONCLUSION AND SUGGESTION FOR FURTHER WORK

9.1 Conclusions

A number of useful conclusions have been reached through the practical and theoretical investigations conducted on the consequences of evaporative phase change within the lubricant of thin film bearings and face seals. The conclusions are as follows:

1 The literature search revealed that few authors have investigated two phase flow in bearings or rotating face seals. The review paper on Mechanical Seals by Nau[30] listed 104 references of which approximately 10% relate to phase change, but there is no evidence of direct comparison of experimental measurements with theory to support the findings in any of these papers.

2 The present theoretical model has examined the transverse variation of fluid properties in the developing flow within both radially symmetric hydrostatic thrust bearings and shaft end face seals employing a constant film thickness. Phase change was shown to arise when the temperature at which the lubricant is supplied is close to saturation temperature.

3 The effect of viscous dissipation is greater at the interface between the fluid and the wall than within the core of the flow and initial generation of vapour takes place in the layer of the fluid film in contact with the wall. Dissipation in the core of the film is significantly less, evaporation in the core taking place progressively by the combination of viscous dissipation and the conduction of energy from layers where partial evaporation has already occurred.

4 In the radially symmetric hydrostatic thrust bearing lubricated by a Newtonian fluid, the velocity profile of the film is parabolic until evaporation commences. Viscous dissipation within the liquid causes the fluid temperature to increase. The parabolic velocity distribution resulted in a uniform film temperature at a given radius, and

thus vapour generation commenced at the radius where the local enthalpy first exceeded that of the saturated liquid.

5 The experimental programme yielded results which correlated well with predictions of radial pressure distribution in both single phase flow and partial evaporation. Practical operating limitations prevented the quality of the mixture exceeding a calculated value of 0.2% by mass corresponding to 10% by volume in average conditions. Nevertheless distinct photographic evidence was obtained of the presence of a liquid/vapour mixture at the exit from the test bearing.

6 A computational fluid dynamic analysis of the flow of R114 in the rotor end face seals of a typical sliding vane compressor confirmed that viscous dissipation in the fluid film adjacent to the rotating solid surface would cause vapour generation, reducing the fluid density and viscosity. The resulting profiles of radial and tangential velocity at a given radius were considerably different from those which have been assumed by previous investigators. The reduced viscosity in layers near the rotating surface severely limited the effect of rotational shear within the film and tangential velocity appeared to decay very rapidly across the gap.

7 It was also confirmed that the load carrying capacity of a bearing is reduced when evaporation takes place as found by Orcut[27]. In addition it was confirmed that evaporation can lead to a reduced leakage rate for a face seal as concluded by Hughes *et al.*[31].

8 The predicted pressure drop characteristics were influenced considerably by the nature of the velocity distribution assumed for the flow entering the bearing or seal. A uniform velocity leads to the earlier generation of vapour in the fluid layers close to the solid boundaries, reducing viscosity and density, and hence reducing the rate of pressure drop in relation to that predicted for the case of parabolic velocity profile at entry.

9 The results have indicated that for the case of the hydrostatic thrust bearing, the kinetic energy of the fluid needs to be taken into account when predicting the pressure distribution characteristic.

10 The comparison between the predictions based on the constant viscosity form of the Navier-Stokes equation and the variable viscosity form has shown that there is virtually no difference between the two methods.

11 A good correlation between the experimental results and theoretical predictions indicate that the expressions for the viscosiy of liquid/vapour mixture suggested by Isbin and Duckler[46] provided an adequate representation of the effect of evaporation up to 10% vapour volume in the mixture. An alternative and more flexible expression has been suggested which showed equally good correlation and was used in all theoretical predictions.

12 The radial and transverse profiles of velocity components of the flow in face seals are influenced strongly by the shear forces transmitted from the rotating face. The radial velocity profile exhibited considerable skewing from the parabolic form used in the theoretical predictions of earlier researchers, due to the centrifugal pumping effect, suggested by Fogg[6]. The predicted tangential component did not show a linear variation between the stationary and rotating faces: the tangential shearing effect was observed to decay rapidly, particularly at high rotational speeds.

9.2 Suggestions for Further Work

The experimental equipment should be modified to enable two phase operation to be achieved with the greatest possible range of variables. This would then determine more clearly the adequacy of the computer model, and possibly establish the limitations of the new correlation suggested for the viscosity of a homogeneous two phase mixture. The theoretical model should be extended to include the heat transfer between the surroundings and the lubricant.

A clearer understanding of events experienced during the test programme showed that there is a need to achieve independent control of the pressure in the bearing chamber. This would enable port inlet conditions to be adjusted to values of pressure and temperature, which would ensure a wider range of evaporation within the bearing by means of the appropriate combination of pump speed and bearing gap.

A further suggestion is that the theoretical analysis be extended to represent the rate of vapour generation in order to overcome the errors introduced by assuming the existence of equilibrium condition. The real problem is of a dynamic thermodynamic nature in which non-equilibrium conditions are taken into account and only in the light of such an analysis would an investigation of rotor stability become meaningful.

The desirability of correctly representing the circumferential pressure variation at the exit from the rotor end face seals suggests another area for further work, although the distortion that this would introduce into the flow within the seals would lead to great difficulties obtaining a converging solution.

REFERENCES

1. Cameron, A. (1966), *Principles of Lubrication* , London: Longman.

2. Cameron, A. (1981), *Basic Lubrication Theory*, London: Longman.

3. ASHRAE Handbook (1984), "Tests for Boundary Lubrication", pp. 29.1

4. Lewis, G.K. (1986), Lecture notes, University of Aston, Birmingham.

5. Dowson, D. (1979), *History of Tribology*, London: Longman.

6. Fogg, A. (1946), "Fluid film lubrication of parallel thrust surfaces", Proceedings of Institution of Mechanical Engineers. Vol. 155, pp.49-67

7. Shaw, C. and Strang, J. R. (1948), "The Hydrosphere- A New hydrodynamic bearing.", ASME Journal of Applied. Mechanics. Vol. 70, pp. 137-145

8. Blok,H. and Cameron, A. (1949), "Discussion of Reference (3)", Transactions of ASME Journal of Applied Mechanics. Vol. 71, pp.93

9. Dowson, D. and Taylor, C.M. (1967), "Fluid-inertia effects in Spherical Hydrostatic thrust bearing.", Transactions of ASLE , Vol. 10, pp.316-324

10. Dowson, D. and Taylor, C.M. (1967), "A re-Examination of Hydrosphere performance", Transactions of ASLE , Vol. 10, pp.325-333

11. Gupta, R.S. and Kapur, V.K. (1982), "Inertia effects on pressure depressions in gas lubricated thrust bearings", Wear, Vol. 77, pp.203-216

12. Hasegawa, E. and Izuchi, H. (1982), "Inertia effects due to lubricant compressibility in a sliding externally pressurized gas bearing", Wear, Vol. 80, pp. 207-220

13. Constantinescu V. N. (1970), "On the Influence of Inertia Forces in Turbulent and Laminar Self-Acting Films", Transactions of ASME, Journal of Lubrication Technology, Vol. 92, pp. 473-481

14. Smalley, A.J., *et al.*, "Liquid Metal Bearings Technology for Large, High-Temperature, Sodium Rotating Machinery. An Analytical and Experimental Investigation of Turbulent Flow in Bearing Films, Including Convective Fluid Inertia Forces", MTI Report 68TR80

15. Constantinescu, V.N. and Galetuse, S. (1974), "On the Possibilities of Improving the Accuracy of the Evaluation of Inertia Forces in Laminar and Turbulent Films", Transactions of ASME, Journal of Lubrication Technology, Vol. 96, No.1, pp. 69-79

16. Constantinescu, V.N., Galetuse, S. and Kennedy, F. (1975), "On the Comparison between Lubricating Theory, Including Turbulence and Inertia Forces, and some Existing Experimental Data", Transactions of ASME, Journal of Lubrication Technology, Vol. 97, No.3, pp. 439-449

17. Kennedy, F.E., Constaninescu, V.N. and Galetuse, S. (1975), "A Numerical Method for Studying Inertia Effects in Thin Film Lubrication", Proceedings of the 1975 Symposium (Leeds -Lyon) Super Laminar Flow in Bearings, Institute of Mech. Engrs. Publication.

18. Hashimoto, H., Wada, S. and Sumitomo, M. (1988), "The Effect of Fluid Inertia Forces on the Dynamic Behaviour of Short Journal Bearings in Superlaminar Flow Regime", Transactions of ASME, Journal of Tribology, Vol. 110, pp-539-547

19. Sinha Roy, J. and Izuch, H. (1981), "The effect of lubricant inertia in externally pressurised bearing using a viscoelastic lubricant", Wear, Vol. 71, pp. 45-54

20. Brand, R.S. (1955), "Inertia forces in lubricating films", Transactions of ASME Journal of Applied Mechanics Vol. 22, pp.363-364

21. Macken, N.A. and Saibel, E.A. (1972), "Turbulence and inertia effects in bearings", ASME Journal of Tribology, pp. 155-159

22. Chowdhury, S.J. and Ahmadi, G. (1988), "Thermodynamic analysis of wide thrust bearings operating in turbulent inertial flow regimes", ASME Journal of Tribology, Vol. 110, pp. 327-334

23. Platt, H. (1972), "Hydrodynamic lubrication of sliding vane compressors", Proceedings of Purdue University compressor conference, Purdue University.

24. Tonder, K. (1975), "Parallel surfaces lubricated by bubbly oil", Wear, Vol. 35, pp.23-34

25. Tonder, K. (1976), "Thermal model of effect of gas bubbles on the lubrication of parallel surfaces", Wear, Vol. 40, pp.37-50

26. Tonder, K. (1977), "Effect of gas bubbles on behaviour of isothermal Mitchell bearings", Transactions of ASME, pp. 354-358

27. Orcutt, F.K. (1964), "Experimental investigation of condensing vapour lubricated thrust bearing", ASLE Transactions, Vol. 7, pp.168-179

28. Zuber, N. and Dougherty, D.E. (1982), "The field equations for two-phase Reynold's film flow with a change of phase", ASLE Transactions, Vol. 25, no. 1, pp.108-115

29. Orcutt, F.K., (1969), "An Investigation of the Operation and Failure of Mechanical Face Seals", Transactions of ASME, Journal of Lubrication Technology, Vol. 91, No.4, pp. 713-725

30. Nau, B.S., (1990), "Research in Mechanical Seals", Proceedings of Inst. of Mech. Engrs., Vol. 204

31. Hughes, W.H., Winowich, W.S., Birchak, M.J., Kennedy, W.C., (1978), "Phase Change in Liquid Face Seals", Transactions of ASME, Journal of Lubrication Technology, Vol. 100, pp. 75-81

32. Hughes, W.F. and Chao, N.H., (1980), "Phase Change in Liquid Face Seals II-Isothermal and Adiabatic Bounds With Real Fluids", Transaction of ASME, Journal of Lubrication Technology, Vol. 102, pp. 351-359

33. Beatty, P.A. and Hughes, W.F., (1987), "Turbulent Two-Phase Flow in Shaft Face Seals", Transactions of ASME, Journal of Tribology, Vol. 109, pp. 91-99

34. Yasuna, J.A. and Hughes, W.F., (1990), "A continuous Boiling Model for Face Seals", Transactions of ASME, Journal of Tribology, Vol. 112, pp. 267-274

35. Rajalingham, C. and Prodhu, B.S. (1987), "The influence of variation of viscosity with temperature on the steady state characteristics of journal bearings- Simplified analysis", Tribology International, Vol. 20, no. 5, pp.261-267

36. Jain, S.C. ; Sinhasan, R. ; Singh, D.V. (1983), "Consideration of viscosity variable in determining the performance characteristics of circular bearings in the laminar and turbulent regimes.", Wear, Vol. 86, pp.233-245

37. Tipie, N. and Deguerge, B. (1974), "A solution of thermodynamic problems for exponential lubricating film", Transactions of ASLE, Vol. 17, p.84-91

38. Shukla, J.B. and Kumar, S. (1975), "Effect of viscosity variation and surface roughness in lubrication : effect of viscosity variation in stochastic lubrication.", Journal of Mechanical Engineering Science, Vol. 17, no. 5, pp.256-263

39. Nikolajsen, J.L. (1973), "The effect of variable viscosity on the stability of plain journal bearings and floating-ring journal bearing", Transactions of ASME Journal of tribology, pp.447-455

40. Dowson, D. and Hudson, J.D. (1963), "Thermo-hydrodynamic analysis of the finite slider-bearing :Paper 1 The plane inclined slider-bearing", Journal of Institution of Mechanical Engineers, Lubrication & Wear Convention pp.34-44

41. Dowson, D. and Hudson, J.D. (1963), "Thermo-hydrodynamic analysis of the finite slider-bearing :Paper 2 The parallel surface bearing", Journal of Institution. of Mechanical Engineers, Lubrication & Wear Convention pp.41-45

42. Hahn, E.J. ; Kettleborough, C.F. (1976), "Solution for the pressure and temperature in an infinitely slider bearing of an arbitrary profile.", ASME. J. of Lub. Tech. Series F. Vol. 89, pp.445-454

43. Ezzat, H.A. and Rhode, S.M. (1973), "A study of the thermodynamic performance of finite slider bearings", Transactions of ASME, Journal of Lubrication Technology, pp.298-307

44. Huebner, K.H. (1974), "A three dimensional thermohydrodynamic analysis of sector thrust bearing", ASLE Transactions, Vol. 17, pp.62-73

45. Lotfie Ahmad Abdel-Latiff; Peeken, H. and Benner, J. (1985), "Thermohydrodynamic analysis of thrust-bearing with circular pads running on bubbly oil", Journal of Tribology, Vol. 107, pp.527-537

46. Feng, N.S. and Hahn, E.J. (1985), "Density and viscosity models for two-phase homogeneous hydrodynamic damper fluid", ASLE Transactions, Vol. 29, no. 3, pp.361-369

47. Gill, L.E., Hewitt, G.F, and Lacey, P.M.C. (1965), "Data on Upwards Annular Flow of Air-Water Mixture", Chemical Engineering Science Vol. 20, pp. 71-88

48. Ruttledge, D.C. (1983), "Viscosity of oils diluted with refrigerants", Refrigeration Engineering Vol. 35, pp. 31-36

49. Beerbower, A. and Greene, D.F. (1961), "The behaviour of lubricating oils in inert gas atmosphere", ASLE Transactions Vol. 4, pp. 87-96

50. ASHRAE Handbook (1984), " Lubricant in Refrigerant Systems", pp.29.9

51. Kodayashi, H. and Murata, N. (1985), "The effect of refrigerant dissolved in oil on journal bearings reliability", Transactions of Japanese Society of Mechanical Engineers. Vol 51, no. 472, pp. 1010-1019

52. Murray, S.F.; Johnson, R.L. ; Swiket, (1956), "Difluorodichloromethane as a boundary lubricant for steel and other metals", Mechanical Engineering, Vol. 78, no. 3, pp.23-236

53. Sanvordenker, S.; Kenshav; Gram Warren, J. (1974), "Laboratory testing under controlled environment using a falex machine", Purdue University compressor technology conference, Purdue University, pp.61-71

54. Kloos, H.K. ; Broszeit, E. and Hess, F.J. (1978), "Tribological effect of different fluorocarbon refrigerants", Journal of Material Technology, Vol. 9, pp.445-451

55. Byron Bird, R.; Stewart, W.E.; Lightfoot, E.N. (1960), "Transport Phenomena", New York,Chichester, Brisbane,Toronto,Singapore: John Wiley & Sons.

56. Muneer and Scott, (1991), " The calculation of thermodynamic properties of steam for minimum computer access time", Proceedings of Institute of Mechanical Engineers, Vol. 205, pp. 25-29

57. ASHRAE (1990) ," Refrigerant System Chemistry", Chapter 6.4

58. Bains, K. (1986), Ph. D. Thesis, Aston University, Birmingham

59. Lau, S.Y., Hughes, W.F., Basu, P., Sealol, E.G&G. and Beatty, P.A. (1990), "A Simplified Model for Two Phase Face Seal Design", Tribology Transactions, Vol. 33, No. 3, pp.315-324

60. Taylor, G.I. (1923), "Stability of a viscous liquid contained between two rotating cylinders", Trans of Royal Society, London , Ser. A, pp.223-289

61. Constantinescu, V.N. (1965), "Theory of lubrication", Proceedings of International Conference on Lubrication and wear, pp.161, Mustrand and Strenlicht (ed)

62. Osterle F. ; Saibel E. (1957), " The effect of lubricant inertia in hydrodynamic lubrication", Transactions of ASME, Journal of Applied Mechanics, Vol. 79, pp.494-496

63. Hirano, T. and Sakitani, K. (1976), "Finite Element Analysis of leakage flow in the narrow clearance between the rotor and plates of a sliding vane" Compressor technology conference, Purdue University, , pp.306

64. Beeler, R.M. and Hughes, W.F. (1984), "Dynamics of Two-Phase Face Seals", ASLE Transactions, Vol. 27, pp 146-153

65. Moody, F. (1973), "Time Dependent Forces Caused by Blowdown and Flow Stoppage" Transactions of ASME, Journal of Fluids Engineering, vol 95, pp.422-428

66. Walton II, J.F. ; Walowit, J.A. ; Zorzi, E.J. ; Schrand, J. (1987), "Experimental observation of cavitating squeeze film dampers", Transactions of ASME, Journal of Tribology, vol. 109, pp.290-294

APPENDIX 1

AN INVESTIGATION INTO THE DIFFERENT BEARING SURFACES IN A SLIDING VANE COMPRESSOR

A1.1 Examination of Some Bearing Parts in the Sliding Vane Compressor

The main reason for investigating the performance of bearings operating under the condition of vaporization of lubricant was the fact that certain bearing surfaces of the sliding machine might operate in such conditions, should it be used for vapour compression refrigeration applications. In such applications the recirculated liquid supplied to the bearing surfaces would be at a pressure only marginally greater than saturation pressure and possibly lead to phase change within certain parts of the bearings.

There are five different and important bearing types to consider:

1 The vane tip, which has been modelled as a simple inclined slider bearing by H. Platt[23] as discussed in Chapter 2.

2 Vane slots, which are likely to behave as inclined sliders as the vanes move radially in and out of the slots.

3 The vane ends, which are similar to parallel sliders, but are subject to rotary motion.

4 The rotor ends, which are somewhat similar to rotating shaft hydrostatic thrust bearings.

5 Journal bearings, which support the rotor and vane assembly.

The above surfaces will be considered in sequence. The location of lubricant supply points and the lubricant path through the journals, across the rotor ends and into the compression cells introduces a range of complexities of flow in the real machine which are outside the scope of the present work. At the outer radius of the rotor end face the pressure varies between suction and delivery pressure as a function of angular position. In the present analysis this variation is neglected and it is assumed that a constant pressure exists at the outer radius, independent of angular position.

A1.2 Vane Tips and Journal Bearings

Figure A1.1 shows details of the vane tip. This can be considered as an inclined slider bearing which prevents metal to metal contact due to hydrodynamic pressure generated by the relative motion of the stator and the rotor.

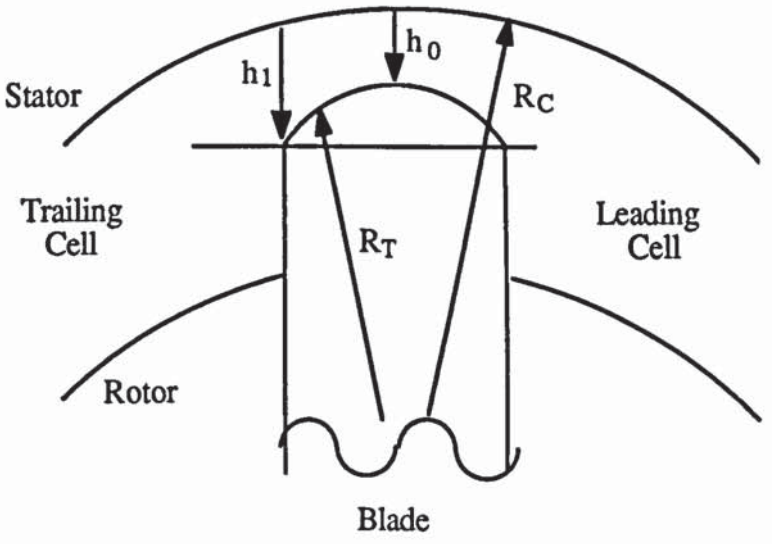

Figure A1.1
Details of the blade tip of a Sliding Vane Compressor

Figure A1.2 shows how the blade tip moves over the cylinder radius with relative velocity U. Platt [23] employed a simplified model by considering a flat surface and an equivalent tip curvature equal to the difference in curvature of the tip radius and cylinder wall.

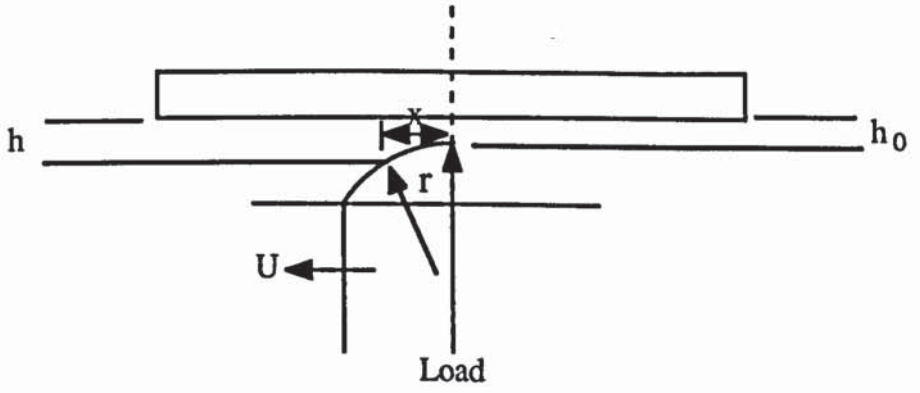

Figure A1.2
Blade tip considered as an inclined slider bearing

By solving the equation for the pressure build-up in a wedge type fluid film, Platt derived an expression for the pressure in the form given as equation (A1.1).

$$p = \frac{2 \mu U x}{\left(h_0 + \frac{x^2}{2r}\right)^2} \qquad \text{(A1.1)}$$

where

U= Relative velocity of blade.
h_0 = Minimum film thickness.
x = Co-ordinate of the lubricating film.

r = equivalent radius defined as: $r = \frac{R_c R_T}{R_c - R_T}$

The author presented a graph of the pressure distribution for some typical solutions. The graph showed that there was a rapid rise in pressure as fluid entered the leading portion of the blade tip indicating that this region of the tip carried the majority of the load. This increase in the pressure would tend to occur faster than the corresponding increase of saturation pressure caused by enthalpy generation in the shear flow of liquid refrigerant between the vane tip and the stator of the compressor. There would be a tendency for phase change to occur only in the trailing portion of the tip, where the flow cross-section increases and causing the pressure to reduce to that found in the trailing cell of the machine.

Cameron[1] has discussed the pressure variation in the trailing edge region of the bearing pad, and suggests that flow separation may arise. This would certainly promote evaporation in the present situation and would not only reduce the load carrying capacity of the tip, which is required to generate the radial force needed to accelerate the blade into the rotor slot during compression, but would also result in a reduction in the volumetric efficiency of a vapour compression machine, since the vapour produced would be equivalent to a leakage flow across the vane tip.

In the real machine it is likely that the injection of liquid refrigerant into the compression cells would result in a liquid/ vapour mixture forming on the stator walls and such mixture would enter under the vane tip. The pressure rise in the leading edge would cause the vapour bubbles to collapse. The process is not instantaneous as was found by Walton II *et al.*[66] when investigating the experimental observation of cavitating squeeze-film dampers and the time constant may be so large as to prevent the total collapse of bubbles, leading to serious difficulties in maintaining adequate lubrication of the vane tips.

As in the case of the vane tips, the changing clearance of the journal, due to the eccentricity, will cause a build-up of pressure as the gap decreases. This will suppress any tendency for vapour to be generated until the film reaches beyond the minimum clearance point. There should not be any operational difficulty on this account.

A1.3 Vane Slot

As shown in Figure A1.3 the vanes of the compressor are normally tilted within the slots in which they move. This is the result of the combination of radial reaction from the stator to acceleration of the vane, the friction force acting at the point of contact between vane and stator and the pressure difference which exists between adjacent cells. The combination of these forces will tilt the vane in the slot in a manner which inclines the leading side of the vane adversely as a bearing, i.e. the gap will decrease in the direction of relative motion, while the trailing side will be tilted in the opposite sense and be capable of acting correctly to generate the necessary load carrying capacity. The distribution of pressure in an inclined slider is well understood, rising to a maximum value at a location determined by the initial gap, the angle of inclination to the stationary surface and the length of the pad. Again it is to be anticipated that there will be vapour generated under the trailing portion of the slider, and that this will reduce the load carrying capacity; the reduction is not likely to

prove serious, since the greatest proportion of load is carried on the forward end of a slider.

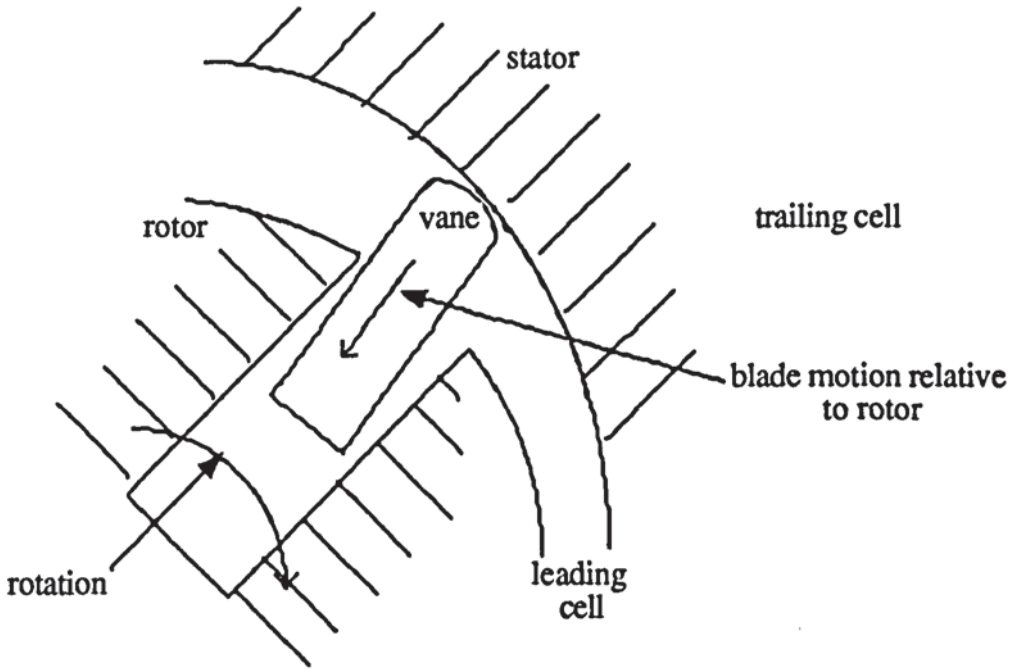

Figure A1.3
Tilting of vane within slot due to pressure and frictional forces at the vane tip

APPENDIX 2

DETAILS OF PRESSURE VESSEL AND LOAD CELL

A2.1 Plate Thickness

This appendix contains details of some sample calculations required for determining the thickness of the cover for the chamber, inside which the bearing was to be accommodated has been listed. Calculations for determining the size of the bolts have also been given. Calculations are in accordance with specifications required by BS 65002. For details refer to Figure A.2.1

G=300 mm, P=1 N/mm^2, m=1.0, S_b=139 (BS 3692) h_G=25 mm, S_{F0}=120 N/mm^2 ,b=4 mm, S_{b1}=120 N/mm^2

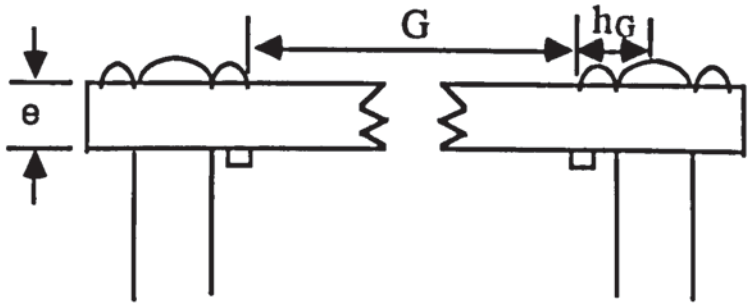

Figure A.2.1
Details of cover plate for the bearing chamber

A2.1.2 Loads and Area of the Bolts

The minimum bolt load W_{m1} is H+Hp

where H=0.785 G^2.P

and

Hp=6.286 G.m.P

Hp=7536

load, W_{m1}=706500+7536=714036

The thickness of the plate will have to be:

$$e=\sqrt{\frac{0.3G^2p}{S_{F0}}+\frac{1.909\,W_{m1}\,h_G}{G\,S_{F0}}}$$

$$e \approx 18 \text{ mm}$$

A2.1.3 Bolt area

$$A_b=\frac{W_{m1}}{S_{b1}}$$

$$A_b=\frac{78186}{120}=651 \text{ mm}^2$$

A2.1.4 Flange Moment

$$M_{op} = H_D\,h_d + H_T\,h_T + H_G\,h_G$$

where $H_D = 0.785\,B^2\,p$; $H_T = H - H_D$; $H_G=H_p$

$$h_d=\frac{C-B}{2} \quad ; \quad h_T=\frac{h_D+h_G}{2} \quad ; \quad h_G=\frac{C-G}{2}$$

$$h_d=\frac{25-400}{2}=187.5 \quad ; \quad h_T=\frac{1187.5+25}{2}=-81.3 \quad ; \quad h_G=\frac{25-300}{2}=-137.5$$

$H_D=0.785*(400)^2*1=125600$

$H_T=70650-(0.785B^2P)=70650-(0.785*400^2*1)$

$H_T=-54950$

$H_G=7536=H_p$

$M_{op}=20$ KN.m

A2.2 Pressure Transducers

Eight pressure transducers were used to measure the pressure of R114 as it flowed along the radius of the bearing. These transducers were tested and calibrated. The current appendix contains the calibration curve for these transducers.

In order to achieve an equal pressure drop along the radius between each pressure transducer, a simple method was employed to determine the position of the tapping points.

Let n= Number of pressure transducer.

p= Pressure on the bearing surface.

c= Constant.

r= Radius of the plate.

Then for a constant pressure drop

$$\frac{dp}{dn} = c \qquad \text{(A2.2.1)}$$

Also for a Hydrostatic bearing

$$\frac{dp}{dr} = \frac{k}{r} \qquad \text{(A2.2.2)}$$

where k is a constant.

Equation (A2.2.2) can be written as

$$\frac{dp}{dn} \cdot \frac{dn}{dr} = \frac{k}{r} \qquad \text{(A2.2.3)}$$

From equations (A2.2.1) and (A2.2.3) , c becomes

$$c = k \frac{dr}{r} \cdot \frac{1}{dn} \qquad \text{(A2.2.4)}$$

i.e.

$$c\, dn = k \frac{dr}{r} \qquad \text{(A2.2.5)}$$

or

$$c\,(n_2 - n_1) = k \log \frac{r_2}{r_1} \qquad \text{(A2.2.6)}$$

Now for a hydrostatic thrust bearing, the value of k is

$$k = \frac{p_p}{\ln\left(\frac{R_p}{R}\right)} \qquad \text{(A2.2.7)}$$

Assuming a port pressure of 5 bar, port radius, R_p, of 25 mm and outside radius, R, of 125 mm then the value of k= -310700.

i.e equation (A2.2.6) becomes

$$c\,(n_2 - n_1) = -310700 \log \frac{25}{125} \qquad \text{(A2.2.8)}$$

By assuming the position of the first pressure of the tapping to be 30 mm from the centre of the plate then the position of the remainder taping can be found easily using equation (A2.2.8).

Pressure transducers were all calibrated using a static weight tester within the pressure range likely to exist during both test runs and stand-by operation. The calibrations curves for 8 transducers are presented graphically as follows.

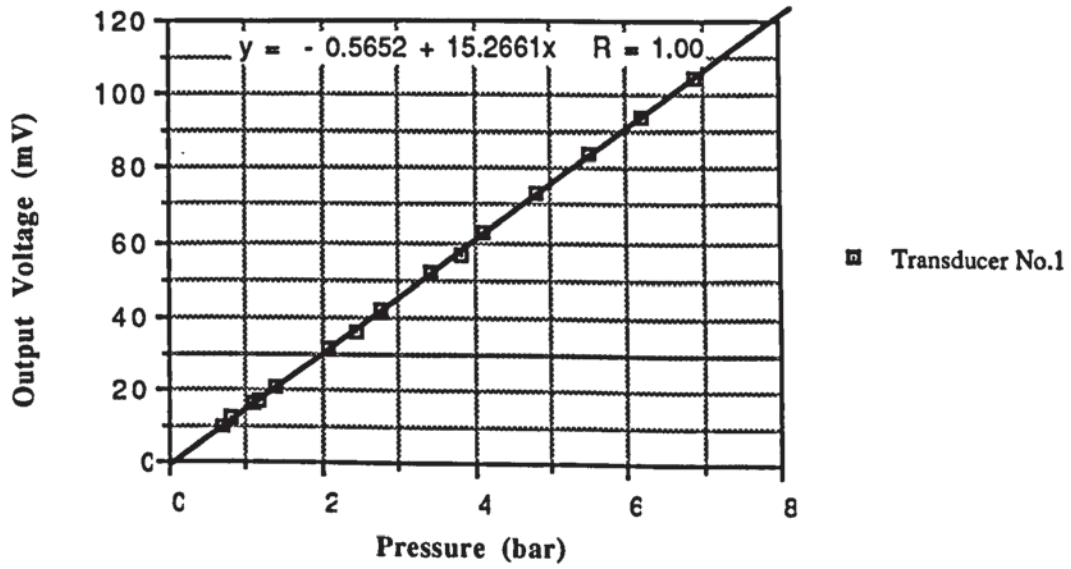

Figure A2.2.1
Calibration curve corresponding to pressure transducer No.1

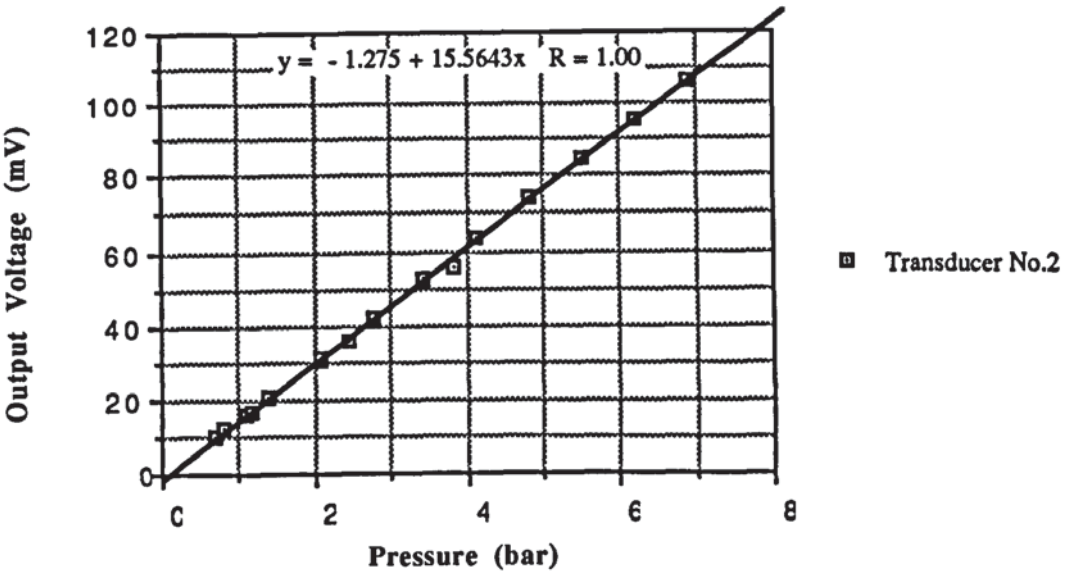

Figure A2.2.2
Calibration curve corresponding to pressure transducer No.2

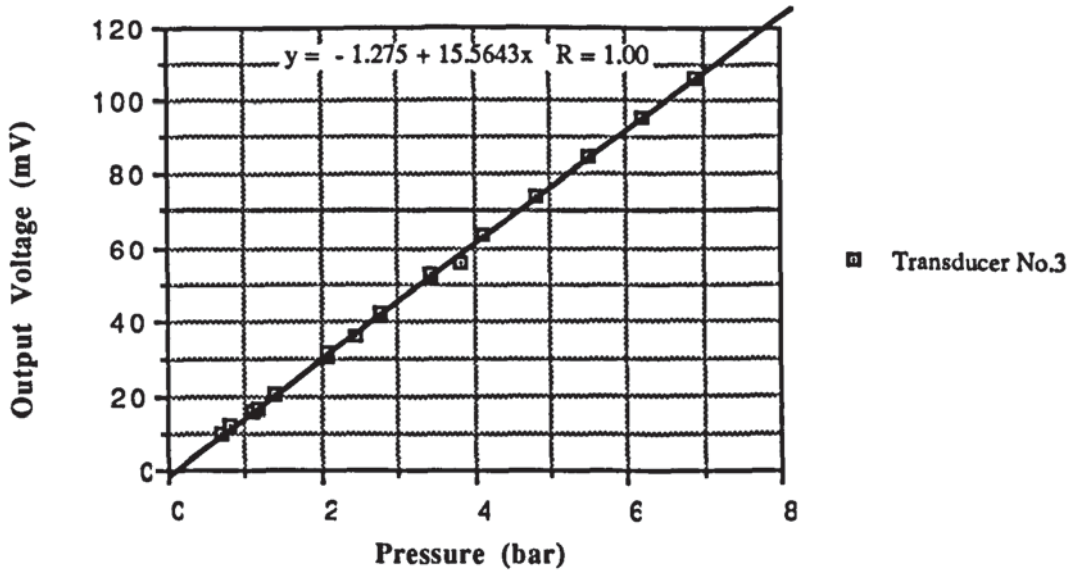

Figure A2.2.3
Calibration curve corresponding to pressure transducer No.3

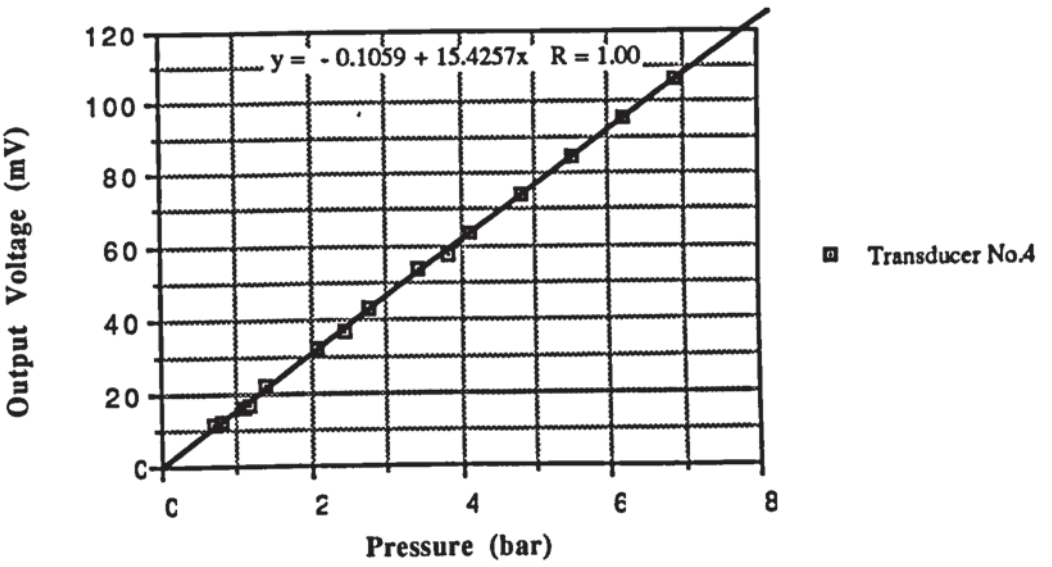

Figure A2.2.4
Calibration curve corresponding to pressure transducer No.4

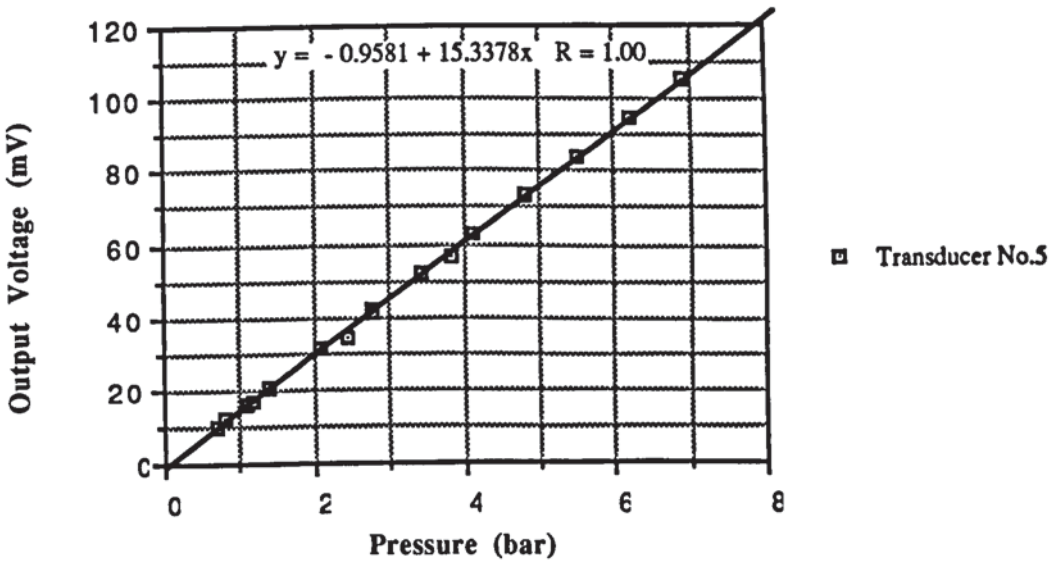

Figure A2.2.5
Calibration curve corresponding to pressure transducer No.5

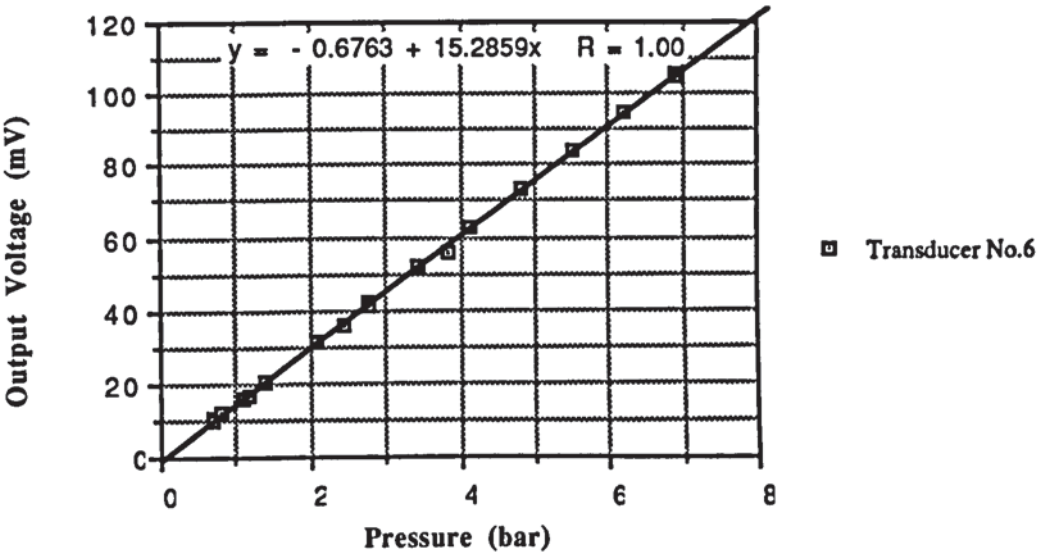

Figure A2.2.6
Calibration curve corresponding to pressure transducer No.6

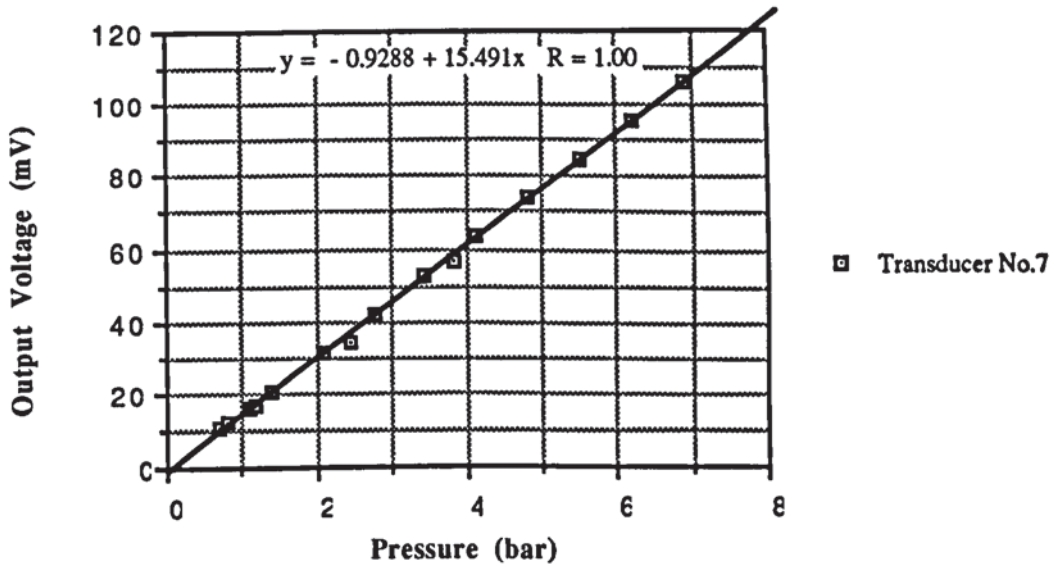

Figure A2.2.7
Calibration curve corresponding to pressure transducer No.7

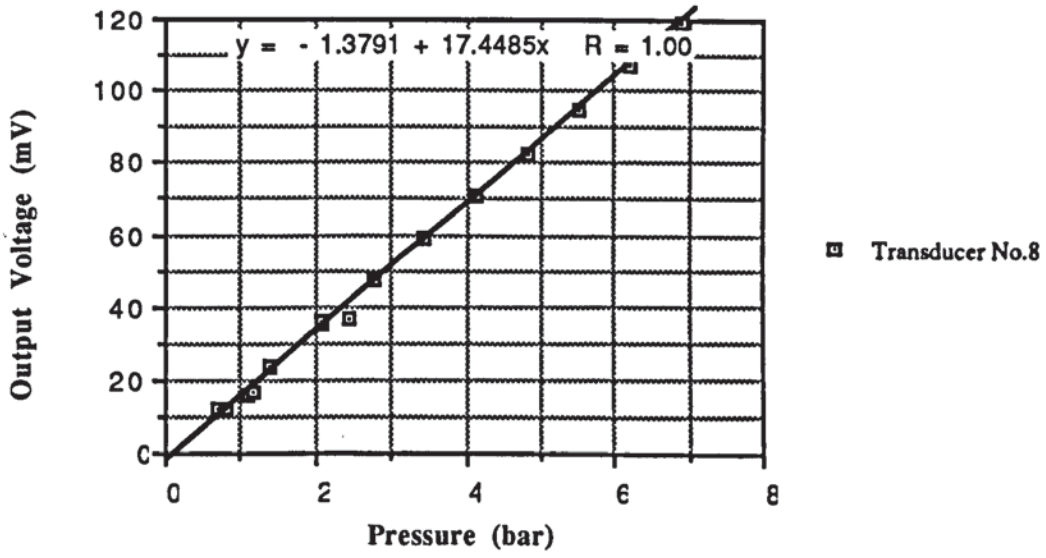

Figure A2.2.8
Calibration curve corresponding to pressure transducer No.8

A2.3 Load Cell Calculation

For a simply supported beam, the maximum stress is

$$\sigma = \frac{3WL}{4Z} \qquad \text{(A2.3.1)}$$

where

$$Z = \frac{bd^2}{3} \qquad \text{(A2.3.2)}$$

i.e

$$\sigma = \frac{3WL}{4bd^2} \qquad \text{(A2.3.3)}$$

and also

$$I = \frac{bd^3}{12} \qquad \text{(A2.3.4)}$$

But the maximum allowable stress for mild steel is σ=300 MN/m^2

For a total load of 3 KN and 8 supports, each load will be, W=375 N

Substitute into equation (A2.3.2), it gives

$b\,d^2 = 6.56*10^{-8}$

choosing b=6 mm gives d=3.5 mm

Allowing for safety factor results

b=7 mm and d= 5 mm

N.B. for L, the circumference S=2*(3.1415)*90=570 mm

If eight strain gauges are used then L=570/8= 70 mm

Substituting back into equation (A2.3.3) gives

$\sigma = 112.5\ MN/m^2$

which is almost a third of the maximum allowable stress.

Consideration of the deflection and/ or strain can be carried out as follows:

For the same beam the maximum deflection is

$$y = \frac{W L^3}{48 E I} \qquad \text{(A2.3.5)}$$

$I = 2.92*10^{-10}\ m^4$, $E = 210\ GN/m^2$

$y = 4.37*10^{-5}\ m$

therefore the strain will be ; $\varepsilon = 4.37*10^{-5}/0.07$

$\varepsilon = 6.24*10^{-4}$

Or $\varepsilon = 0.06\%$

A2.4 Observation Plate (Perspex)

Parameters necessary for this part of calculation are listed as follows:

D=0.09 m ; t=0.02 m ; (D/t)=4.5 ; $P = 10*10^5\ N/m^2$; $E = 3\ GN/m^2$

where D, t, E ,p are the diameter, thickness, modulus of elasticity and pressure acting on the perspex, respectively.

Also the following parameters had to be calculated to help in using the graphs included in the British Standard BS 65002.

$$\frac{p}{E}\left(\frac{D}{t}\right)^4=0.137$$

$$E\left(\frac{t}{D}\right)^2=148*10^6$$

$$\frac{t}{D}=0.22$$

$$\frac{\lambda D}{Et^3}=1.0$$

From Figure 2 in BS 65002

$$\frac{p}{E}\left(\frac{D}{t}\right)^4=0.137$$

which results

$$\frac{f_T}{E}\left(\frac{D}{t}\right)^2=0.0118$$

and from Figure 3 in BS 65002

$$\frac{t}{D}=0.22$$

which gives

$$f_T=0.118*1.4*148*10^6 \ N/m^2$$

or

$$f_T= 2.4*106 \ N/m^2$$

which is the maximum total stress due to bending and memberance tension effects at centre.

Similarly with $k_{Tr}=0.75$ and at

$$\frac{f_{Tr}}{E}\left(\frac{D}{t}\right)^2=0.0116$$

$$f_{Tr}=1.3*106 \ N/m^2$$

which is the maximum total radial stress due to bending and membrance tension effect at edges. Also with $k_{t\theta}=0.35$ and

$$\frac{f_{Tt}}{E}\left(\frac{D}{t}\right)^2=0.01$$

then

$$f_{T\theta}=518*10^3\ N/m^2$$

which is the maximum total tangential stress due to bending and membrance tension effects at edges.

Again with $k_e=0.9$ and at

$$\frac{f_e}{E}\left(\frac{D}{t}\right)^2=0.0114$$

$$f_e=1.52*10^6\ N/m^2 \quad \text{(Von Mises stress *)}$$

From Figure 1 in BS56002

$$\frac{P}{E}\left(\frac{D}{t}\right)^4=0.137$$

which gives d/t= 0.0014

At t/D=0.22 from Figure 4 in BS56002 $k_E=1.21$ and $k_\Delta=1.6$

Hence $\delta=0.0014*1.6*1.21*0.02$

or

$$\delta=5.42*10^{-5}\ m$$

i.e. deflection of the Perspex will be 0.054 mm

*Von Mises-Henckey equivalent stress=$\{1/2\{f_1-f_2)^2+(f_2-f_3)^2+(f_3-f_1)^2\}\}^{1/2}$

where f_1, f_2, f_3 are the principal stresses.

APPENDIX 3

CALCULATION OF HEATER and DETAILS OF SLAVE CIRCUIT COMPONENTS

A3.1 Heater Calculations

Assuming a mass flow rate of 0.2 kg/s and taking the appropriate enthalpy values, then the heat transfer by R114 is

$$Q = \dot{m}\,\Delta h \qquad \text{(A3.1.1)}$$

i.e.

$$Q = 0.2 * (130 - 120) = 2000\ (W)$$

But the governing equation for the heat transfer in the pipe carrying the fluid is

$$Nu = 0.023\ Re^{0.8}\ Pr^{0.23} \qquad \text{(A3.1.2)}$$

or

$$\frac{h\,d}{k} = 0.023\ (\frac{\rho\,u\,d}{\mu})^{0.8}\ (\frac{c_p\,\mu}{k})^{0.23} \qquad \text{(A3.1.3)}$$

By choosing a range of pipe diameters, it became evident that a pipe of 9.5 mm i.d. allowed the necessary heating rate to be achieved with the lowest level of heater sheath temperature. The calculation for this pipe is shown as follows

$$\dot{m} = \rho\,A\,u \qquad \text{(A3.1.4)}$$

$$u = 0.97\ (m/s)$$

By substituting for u into equation (A2.1.3) Nusselt Number will be

$$Nu = 159$$

Which would result in a coefficient of heat transfer of h=1085 W/m K

But

$$Q = h\,\pi\,d\,L\,(T_f - T_w) \qquad \text{(A3.1.5)}$$

By substituting the value of h into equation (A3.1.5) then

$$(T_f - T_w) = 34\ ^\circ C$$

Two electrical sheath heaters, each 1 KW were connected in parallel to give a total of 2 KW heat input when using 220 V mains supply. Since it was necessary to vary the

temperature of the liquid R114 in the circuit, a variac was employed to vary the voltage supplied to these heaters.

Figure A3.1 shows a block diagram of the control system for the heaters.

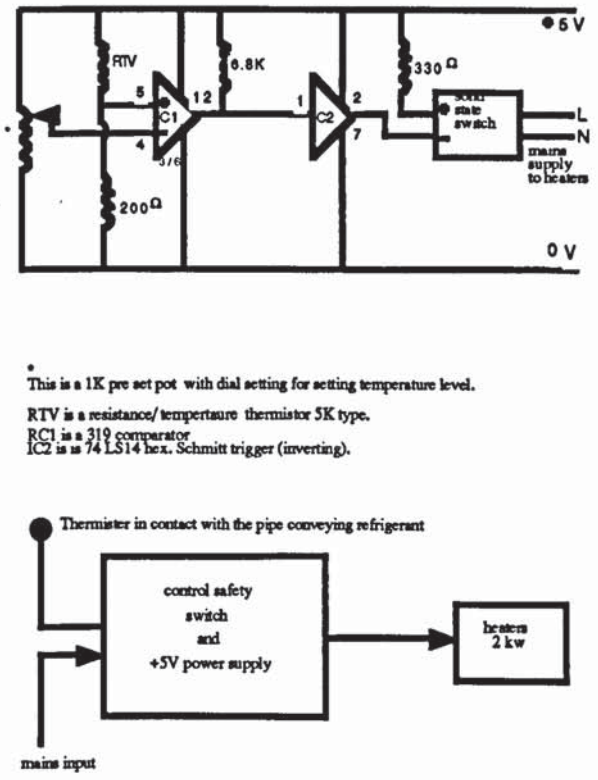

Figure A3.1
Thermistor block diagram for controlling the heater power

A3.2 Slave Circuit Components

A3.2.1 Heat Exchanger

This was a condenser for vapour in the main circuit and evaporator for the R12 in the slave circuit. The load design and operating temperature were predicted to be approximately 2 kW and 40°C for which a K1-3WT Schmole coiled annular type was suitable.

A3.2.2 Condenser

Since the refrigerating load was predicted to be low and temperatures suitable then the most economical condensing coolant was the mains water. A 3.5 KW Schmol K1-3WT condenser was incorporated. This type of condenser is equipped with internally fluted tubes which result in a good heat transfer on the refrigerant side.

A3.2.3 Compressor

A hermetically sealed compressor with motor and compressor contained in welded steel shell was selected. The unit was a Danfoss compressor model SC15A with a capacity of 675 W corresponding to an evaporating temperature of -5°C. The evaporating temperature range for this pump is between -5 to -40°C.

A3.2.4 Expansion Valve

A thermal expansion valve was selected. This type of valve maintains a constant superheat in the vapour at the evaporator outlet, this is achieved by transmitting the evaporating pressure to the diaphragm at the valve outlet, which is the evaporator inlet. This was a Danfoss model TF 2 with an orifice capable of providing 1KW for evaporator load.

APPENDIX 4

FLOW CHART

A4.1 Introduction

A full flow chart of the computer program developed for the analysis is presented in the following pages. The main program is used to initials and input various parameters while five subroutines, Prop, Rung1, Locator, Rung2 and viscosity are used to evaluate the fluid properties and solve the differential equations simultaneously.

alpha,a,b,c,d,E,k	= Constants used in the equation of state for refrigerant.
c1	= Constant chosen to make enthalpy equal unity at the critical point.
cc	= Flag used for indicating if evaporation has occured.
cp	= Specific heat capacity of Refrigerant.
delh	= Difference in enthalpy of saturated vapour and saturated liquid.
etain	= Viscosity of vapour refrigerant.
eta0	= Viscosity of liquid Refrigerant.
f(1)	= Rate of change of pressure.
f(2)	= Rate of change of radial velocity
f(3)	= Rate of change of enthalpy.
f(4)	= Rate of change of elementary thickness.
f(5)	= Rate of change of tangential velocity.
ff	= Flag used for changing the step size once the evaporation starts.
film	= Thickness of lubricating film.
grad	= Pressure gradient.
h	= Enthalpy of lubricant at a given volume and temperature.
hg	= Enthalpy of saturated vapour.
htotal	= Enthalpy of Refrigerant at a given radius.
hl	= Enthalpy of saturated liquid.
mdot	= Mass flow rate of lubricant.
mu	= Dynamic Viscosity of liquid Refrigerant.
mux	= Dynamic Viscosity of liquid-vapour mixture.
nf	= Number of functions used in the Runge-Kutta routine.
nl	= Number of layers in the lubricating film.
nr	= Number of radial steps used in the computation.
Omega	= Rotational speed.
p( )	= Array used for storing the calculated pressure.
pint	= Integral part of the enthalpy.
psat	= Saturation pressure of refrigerant corresponding to its temperature.
r1	= Inner radius.
rho	= Density of liquid refrigerant.
rhox	= Density of liquid-vapour mixture.
satt	= Saturation temperature of refrigerant at a given pressure.
sigma	= Thickness of an elementary lubricant layer.
T,T1	= Absolute and Reduced temperature of refrigerant respectively.
u	= Radial velocity
v,vg	= Volume of vapour lubricant.
vdot	= Volume flow rate of lubricant .
vf	= Volume of liquid lubricant.
w	= Angular velocity
x( )	= Array used for storing quality.
zeta	= Summation of elementary layer thickness.

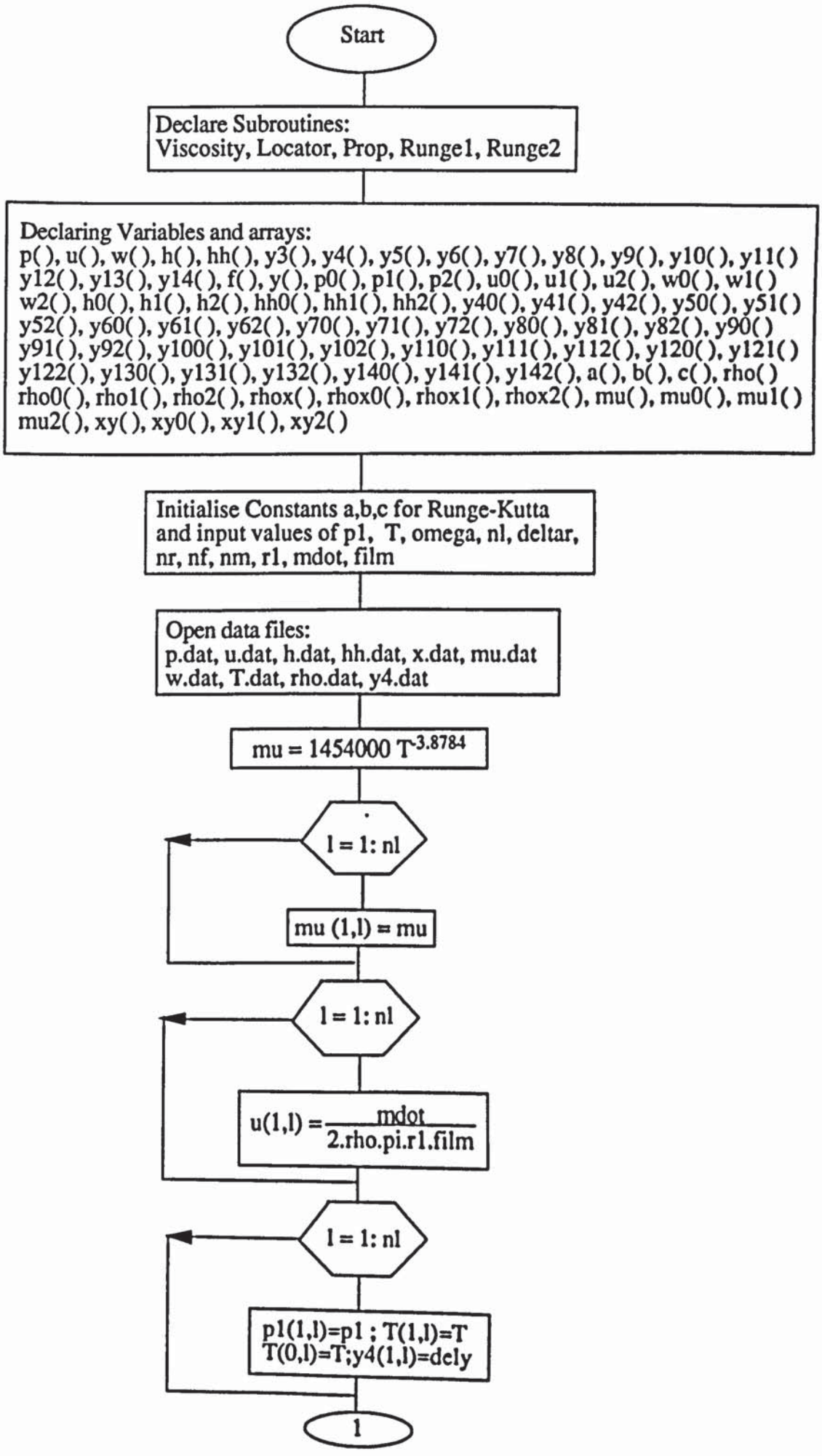
Start
Declare Subroutines:
Viscosity, Locator, Prop, Runge1, Runge2
Declaring Variables and arrays:
p( ), u( ), w( ), h( ), hh( ), y3( ), y4( ), y5( ), y6( ), y7( ), y8( ), y9( ), y10( ), y11( )
y12( ), y13( ), y14( ), f( ), y( ), p0( ), p1( ), p2( ), u0( ), u1( ), u2( ), w0( ), w1( )
w2( ), h0( ), h1( ), h2( ), hh0( ), hh1( ), hh2( ), y40( ), y41( ), y42( ), y50( ), y51( )
y52( ), y60( ), y61( ), y62( ), y70( ), y71( ), y72( ), y80( ), y81( ), y82( ), y90( )
y91( ), y92( ), y100( ), y101( ), y102( ), y110( ), y111( ), y112( ), y120( ), y121( )
y122( ), y130( ), y131( ), y132( ), y140( ), y141( ), y142( ), a( ), b( ), c( ), rho( )
rho0( ), rho1( ), rho2( ), rhox( ), rhox0( ), rhox1( ), rhox2( ), mu( ), mu0( ), mu1( )
mu2( ), xy( ), xy0( ), xy1( ), xy2( )
Initialise Constants a,b,c for Runge-Kutta
and input values of p1, T, omega, nl, deltar,
nr, nf, nm, r1, mdot, film
Open data files:
p.dat, u.dat, h.dat, hh.dat, x.dat, mu.dat
w.dat, T.dat, rho.dat, y4.dat
mu = 1454000 T-3.8784
l = 1: nl
mu (1,l) = mu
l = 1: nl
u(1,l) = mdot / 2.rho.pi.r1.film
l = 1: nl
p1(1,l)=p1 ; T(1,l)=T
T(0,l)=T;y4(1,l)=dely
1

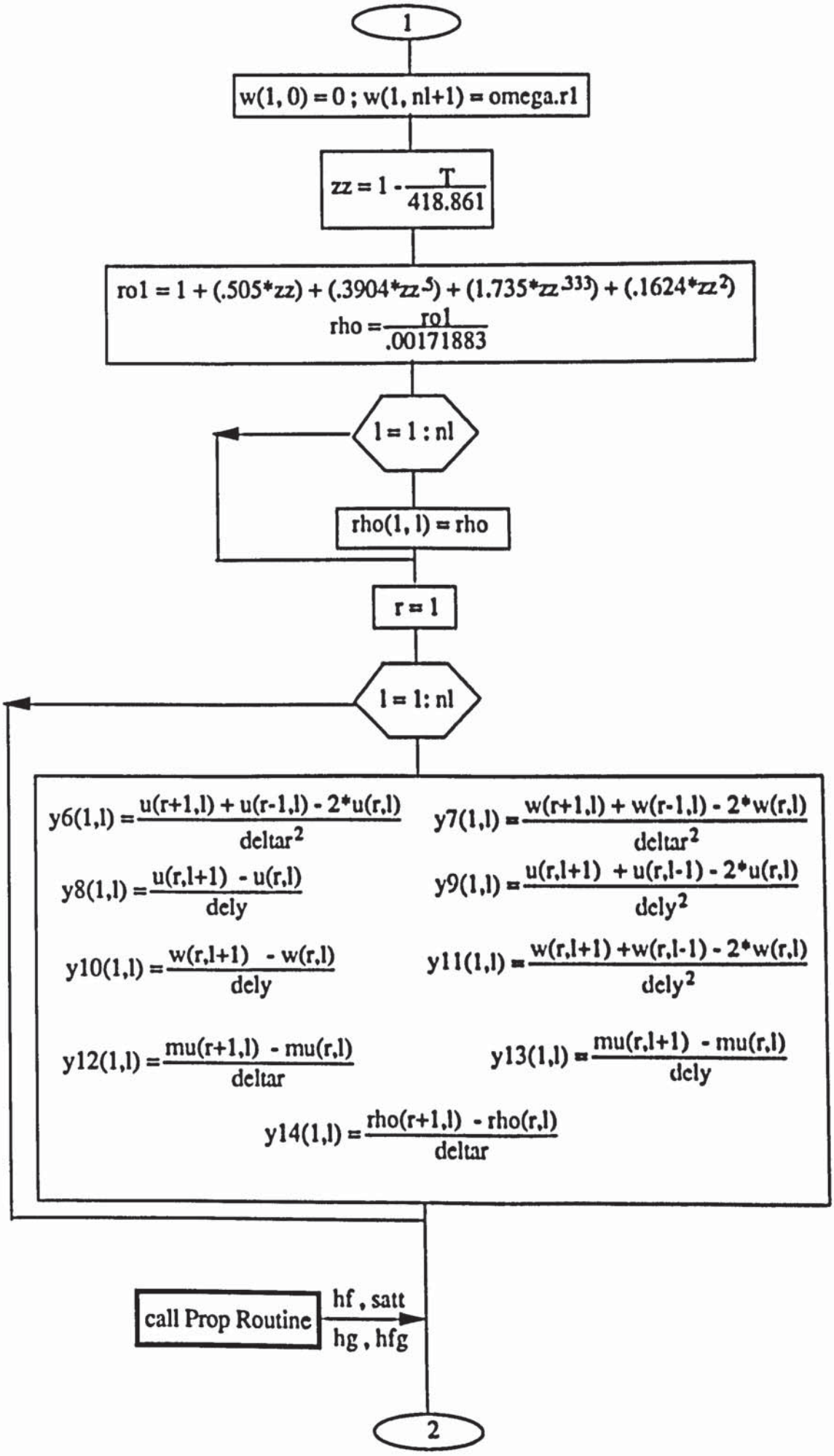
1
w(1, 0) = 0 ; w(1, nl+1) = omega.r1
zz = 1 - T / 418.861
ro1 = 1 + (.505*zz) + (.3904*zz^-5) + (1.735*zz^.333) + (.1624*zz^2)
rho = ro1 / .00171883
l = 1 : nl
rho(1, l) = rho
r = 1
l = 1: nl
y6(1,l) = (u(r+1,l) + u(r-1,l) - 2*u(r,l)) / deltar^2
y7(1,l) = (w(r+1,l) + w(r-1,l) - 2*w(r,l)) / deltar^2
y8(1,l) = (u(r,l+1) - u(r,l)) / dely
y9(1,l) = (u(r,l+1) + u(r,l-1) - 2*u(r,l)) / dely^2
y10(1,l) = (w(r,l+1) - w(r,l)) / dely
y11(1,l) = (w(r,l+1) + w(r,l-1) - 2*w(r,l)) / dely^2
y12(1,l) = (mu(r+1,l) - mu(r,l)) / deltar
y13(1,l) = (mu(r,l+1) - mu(r,l)) / dely
y14(1,l) = (rho(r+1,l) - rho(r,l)) / deltar
call Prop Routine
hf , satt
hg , hfg
2

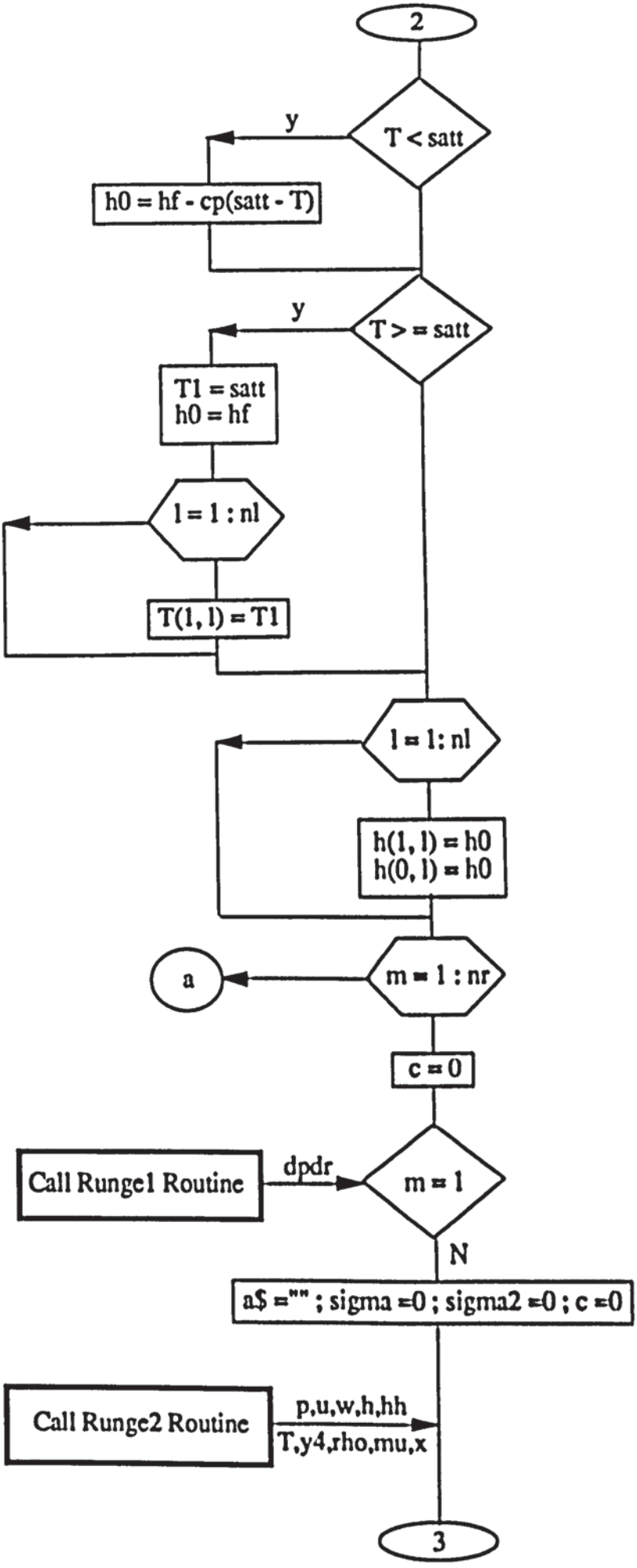
2
T < satt
y
h0 = hf - cp(satt - T)
T > = satt
y
T1 = satt
h0 = hf
l = 1 : nl
T(1, l) = T1
l = 1: nl
h(1, l) = h0
h(0, l) = h0
m = 1 : nr
a
c = 0
Call Runge1 Routine
dpdr
m = 1
N
a$ = "" ; sigma =0 ; sigma2 =0 ; c =0
Call Runge2 Routine
p,u,w,h,hh
T,y4,rho,mu,x
3

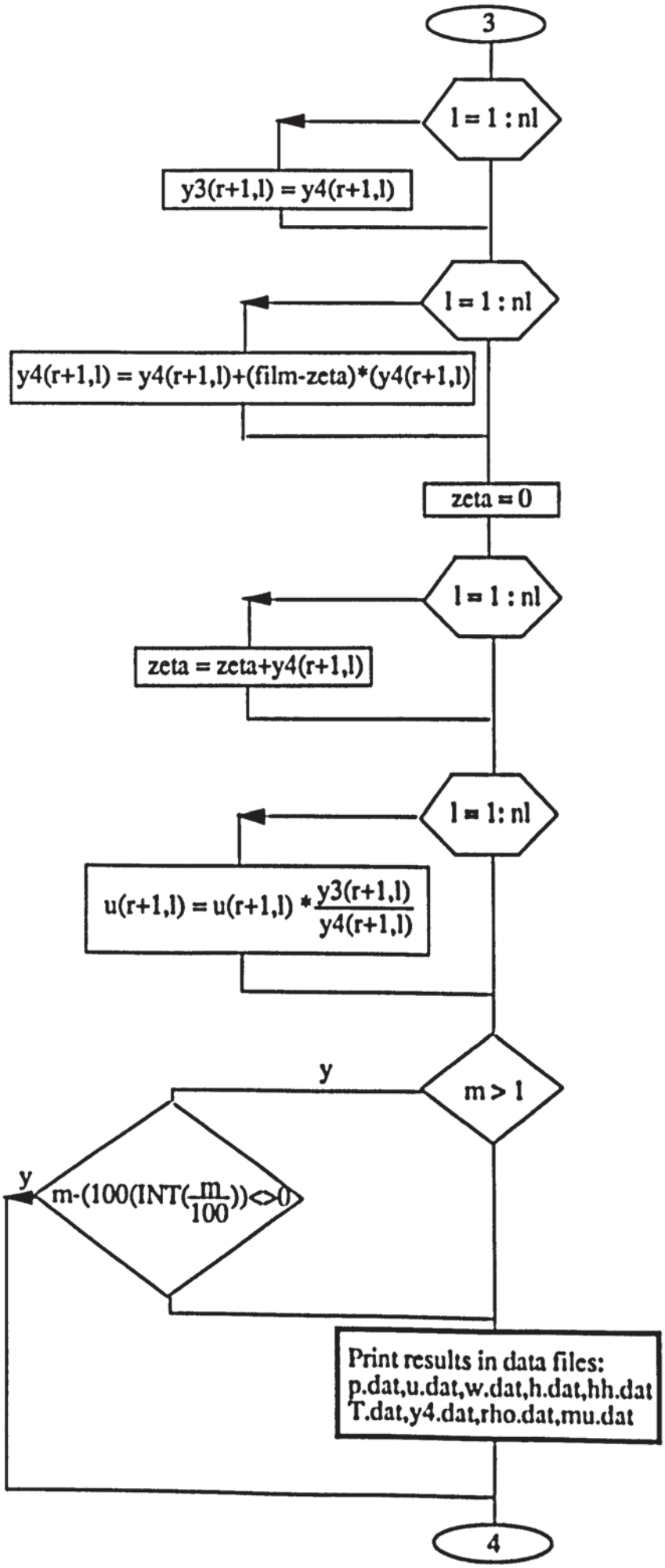
3
l = 1 : nl
y3(r+1,l) = y4(r+1,l)
l = 1 : nl
y4(r+1,l) = y4(r+1,l)+(film-zeta)*(y4(r+1,l)
zeta = 0
l = 1 : nl
zeta = zeta+y4(r+1,l)
l = 1: nl
u(r+1,l) = u(r+1,l) * y3(r+1,l) / y4(r+1,l)
m > 1
y
y
m-(100(INT(m/100))<>0
Print results in data files:
p.dat,u.dat,w.dat,h.dat,hh.dat
T.dat,y4.dat,rho.dat,mu.dat
4

SUBROUTINE LOCATOR

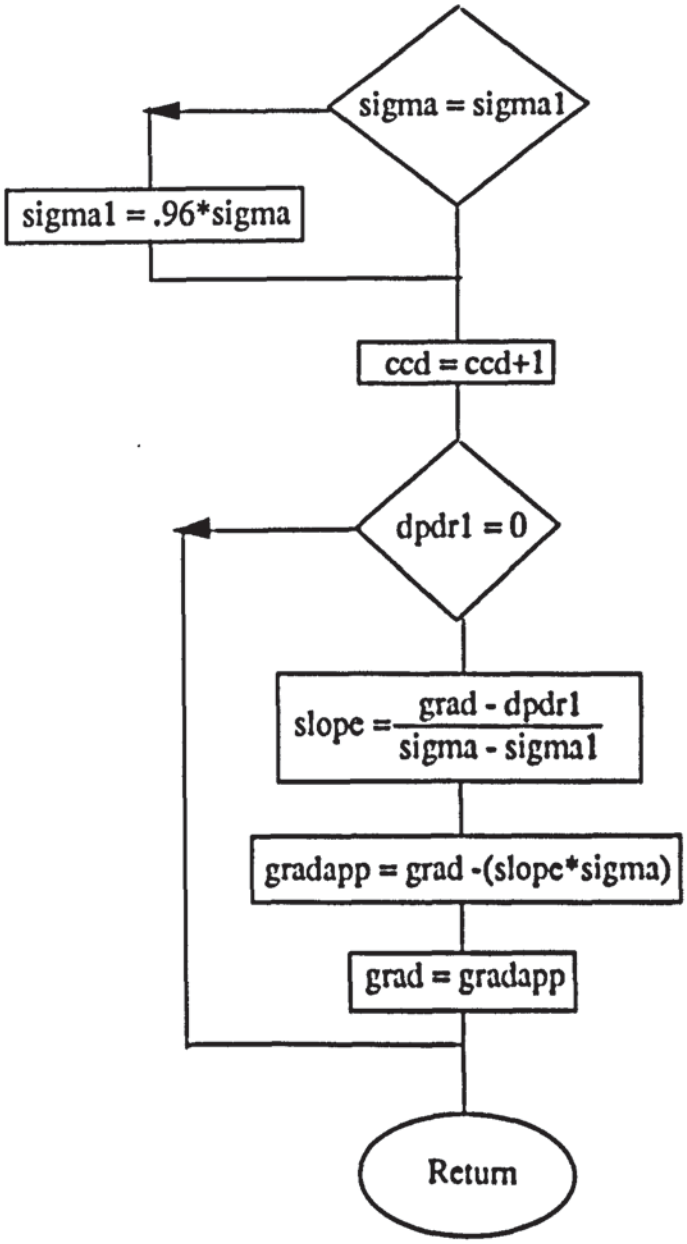

SUBROUTINE PROP

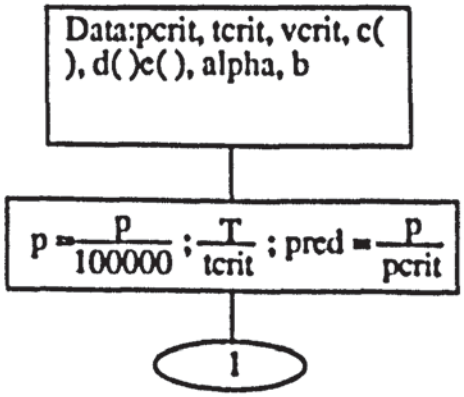

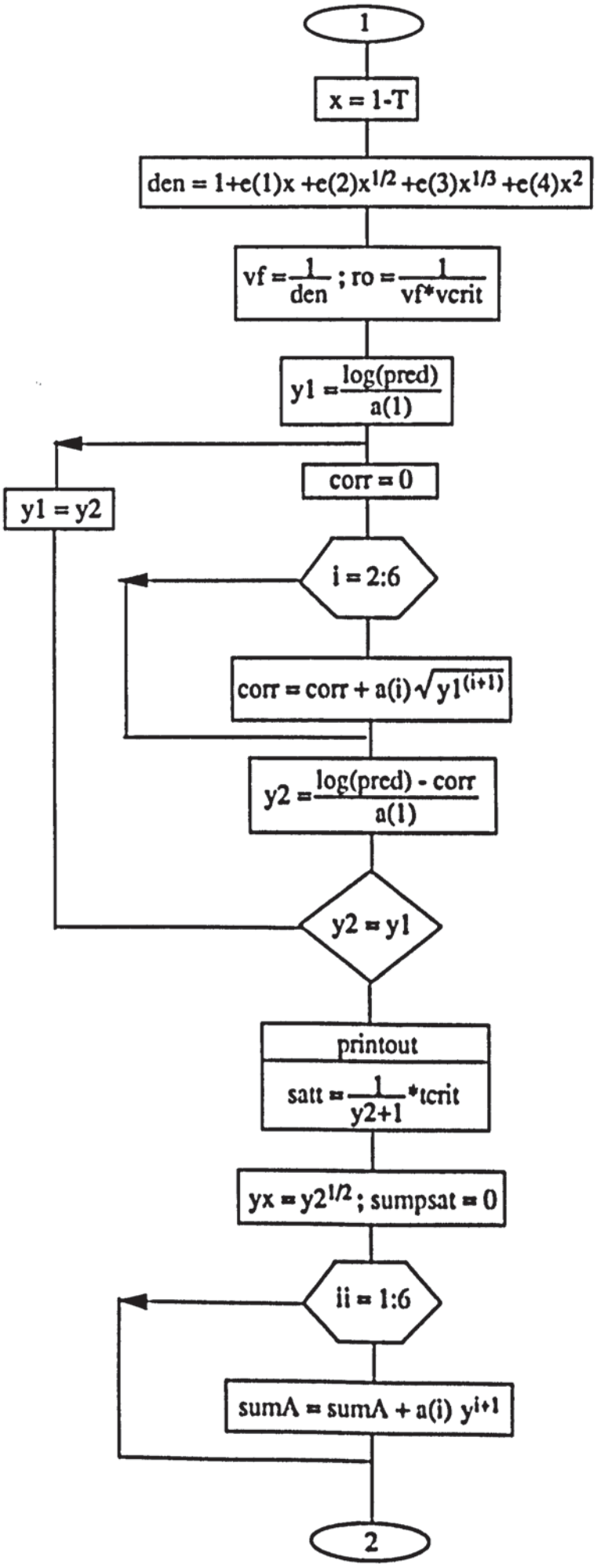
1
x = 1-T
den = 1+e(1)x +e(2)x^1/2 +e(3)x^1/3 +e(4)x^2
vf = 1/den ; ro = 1/vf*vcrit
y1 = log(pred)/a(1)
corr = 0
y1 = y2
i = 2:6
corr = corr + a(i)√y1^(i+1)
y2 = log(pred) - corr/a(1)
y2 = y1
printout
satt = 1/y2+1 *tcrit
yx = y2^1/2 ; sumpsat = 0
ii = 1:6
sumA = sumA + a(i) y^i+1
2

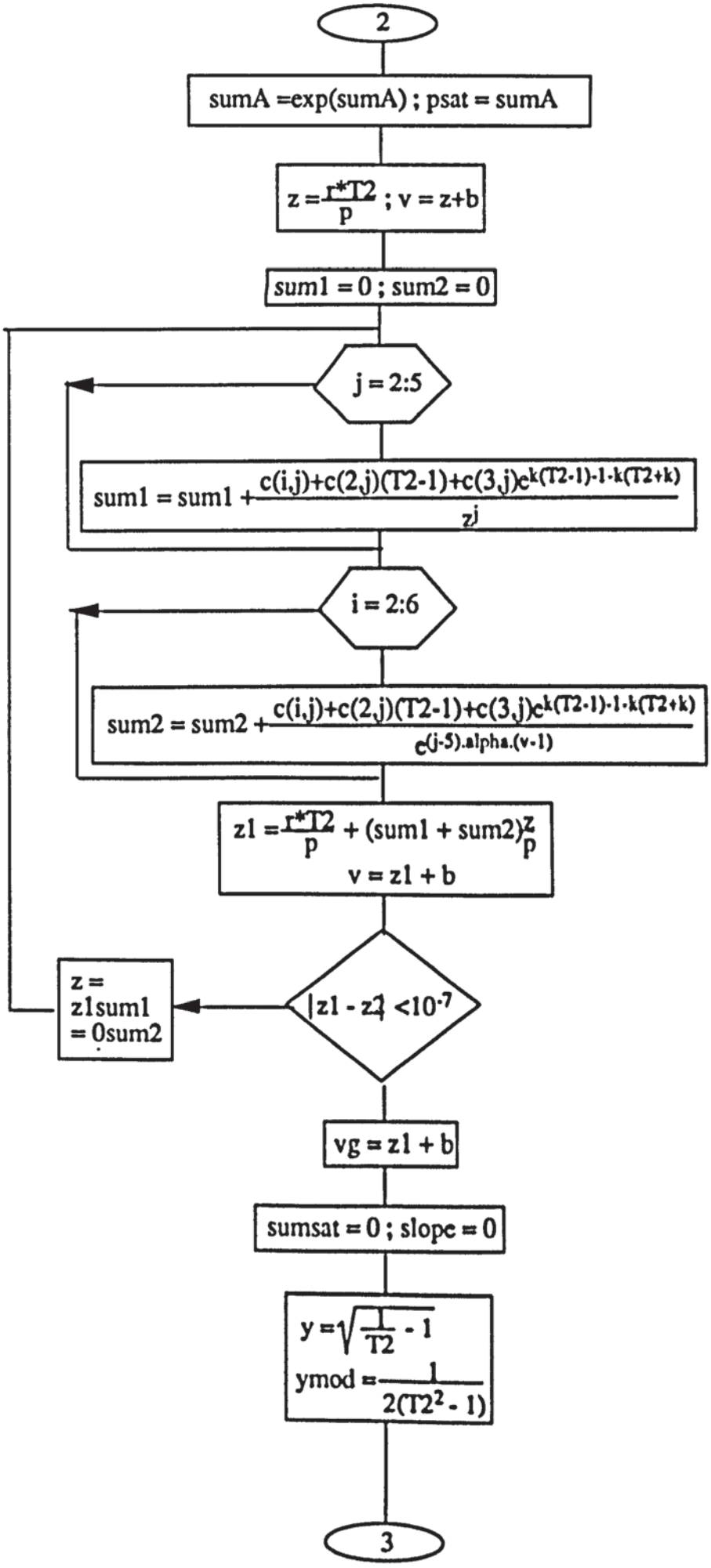
2
sumA =exp(sumA) ; psat = sumA
z = r*T2/p ; v = z+b
sum1 = 0 ; sum2 = 0
j = 2:5
sum1 = sum1 + (c(i,j)+c(2,j)(T2-1)+c(3,j)e^k(T2-1)-1-k(T2+k)) / z^j
i = 2:6
sum2 = sum2 + (c(i,j)+c(2,j)(T2-1)+c(3,j)e^k(T2-1)-1-k(T2+k)) / e^(j-5).alpha.(v-1)
z1 = r*T2/p + (sum1 + sum2)z/p
v = z1 + b
|z1 - z| <10^-7
z = z1sum1 = 0sum2
vg = z1 + b
sumsat = 0 ; slope = 0
y = sqrt(1/T2 - 1)
ymod = 1/(2(T2^2 - 1))
3

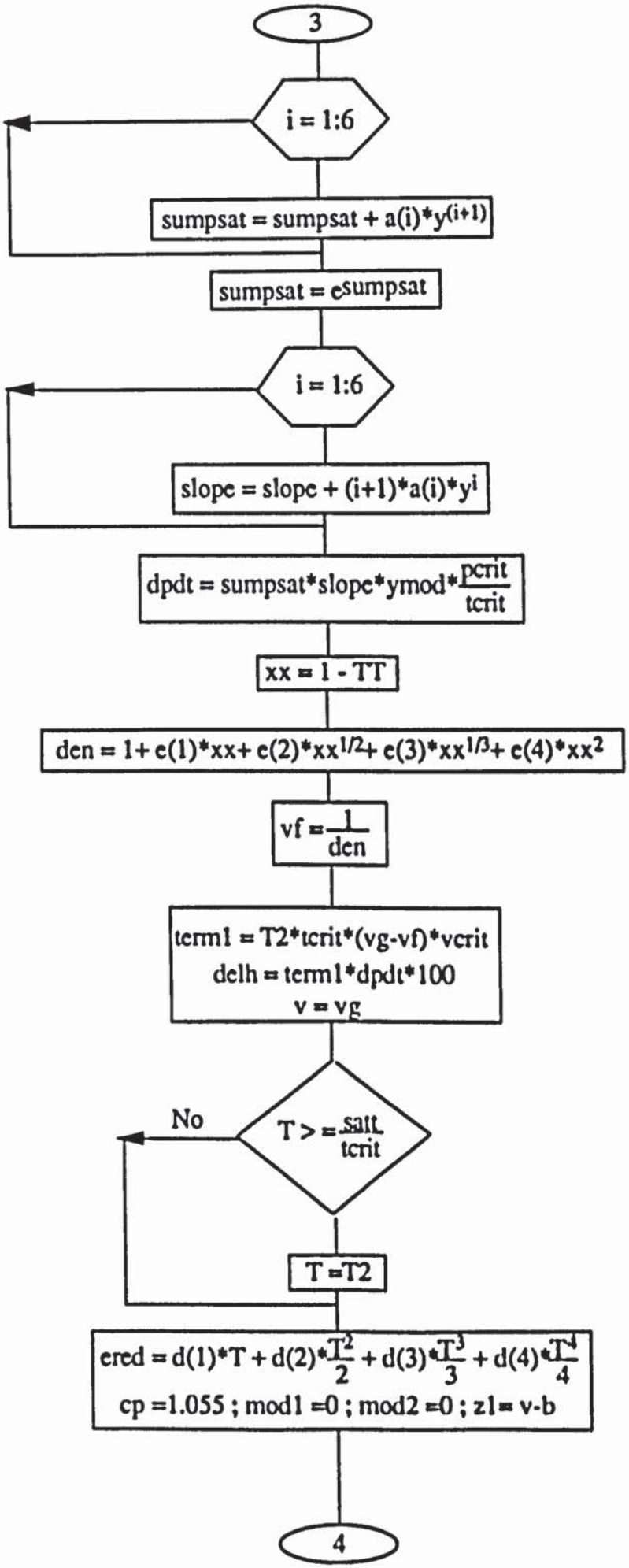
3
i = 1:6
sumpsat = sumpsat + a(i)*y(i+1)
sumpsat = esumpsat
i = 1:6
slope = slope + (i+1)*a(i)*y^i
dpdt = sumpsat*slope*ymod*pcrit/tcrit
xx = 1 - TT
den = 1+ e(1)*xx+ e(2)*xx^1/2+ e(3)*xx^1/3+ e(4)*xx^2
vf = 1/den
term1 = T2*tcrit*(vg-vf)*vcrit
delh = term1*dpdt*100
v = vg
No
T > = satt/tcrit
T =T2
ered = d(1)*T + d(2)*T^2/2 + d(3)*T^3/3 + d(4)*T^4/4
cp =1.055 ; mod1 =0 ; mod2 =0 ; z1= v-b
4

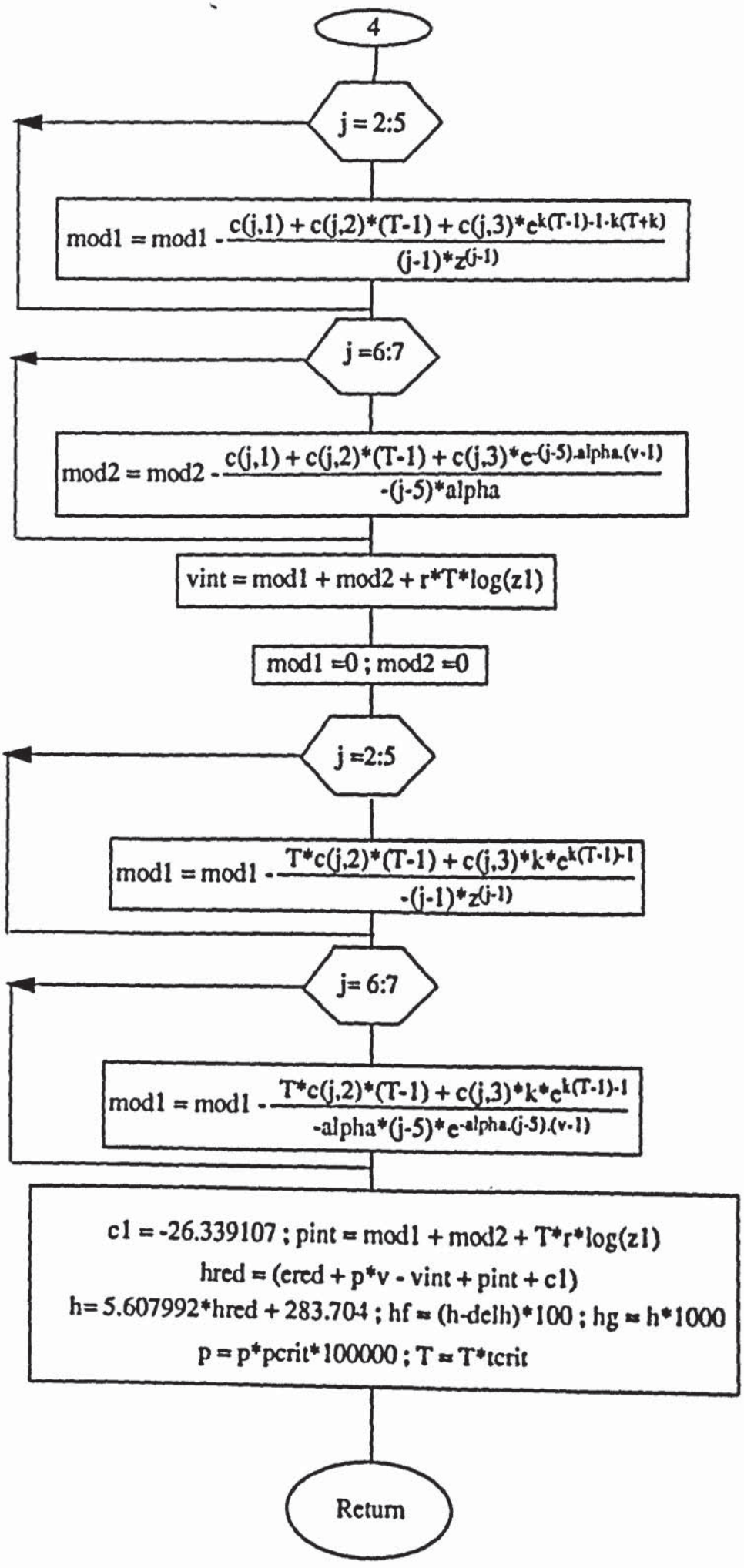
4
j = 2:5
mod1 = mod1 - c(j,1) + c(j,2)*(T-1) + c(j,3)*e^k(T-1)-1-k(T+k) / (j-1)*z^(j-1)
j =6:7
mod2 = mod2 - c(j,1) + c(j,2)*(T-1) + c(j,3)*e^-(j-5).alpha.(v-1) / -(j-5)*alpha
vint = mod1 + mod2 + r*T*log(z1)
mod1 =0 ; mod2 =0
j =2:5
mod1 = mod1 - T*c(j,2)*(T-1) + c(j,3)*k*e^k(T-1)-1 / -(j-1)*z^(j-1)
j= 6:7
mod1 = mod1 - T*c(j,2)*(T-1) + c(j,3)*k*e^k(T-1)-1 / -alpha*(j-5)*e^-alpha.(j-5).(v-1)
c1 = -26.339107 ; pint = mod1 + mod2 + T*r*log(z1)
hred = (ered + p*v - vint + pint + c1)
h= 5.607992*hred + 283.704 ; hf = (h-delh)*100 ; hg = h*1000
p = p*pcrit*100000 ; T = T*tcrit
Return

SUBROUTINE RUNGE1

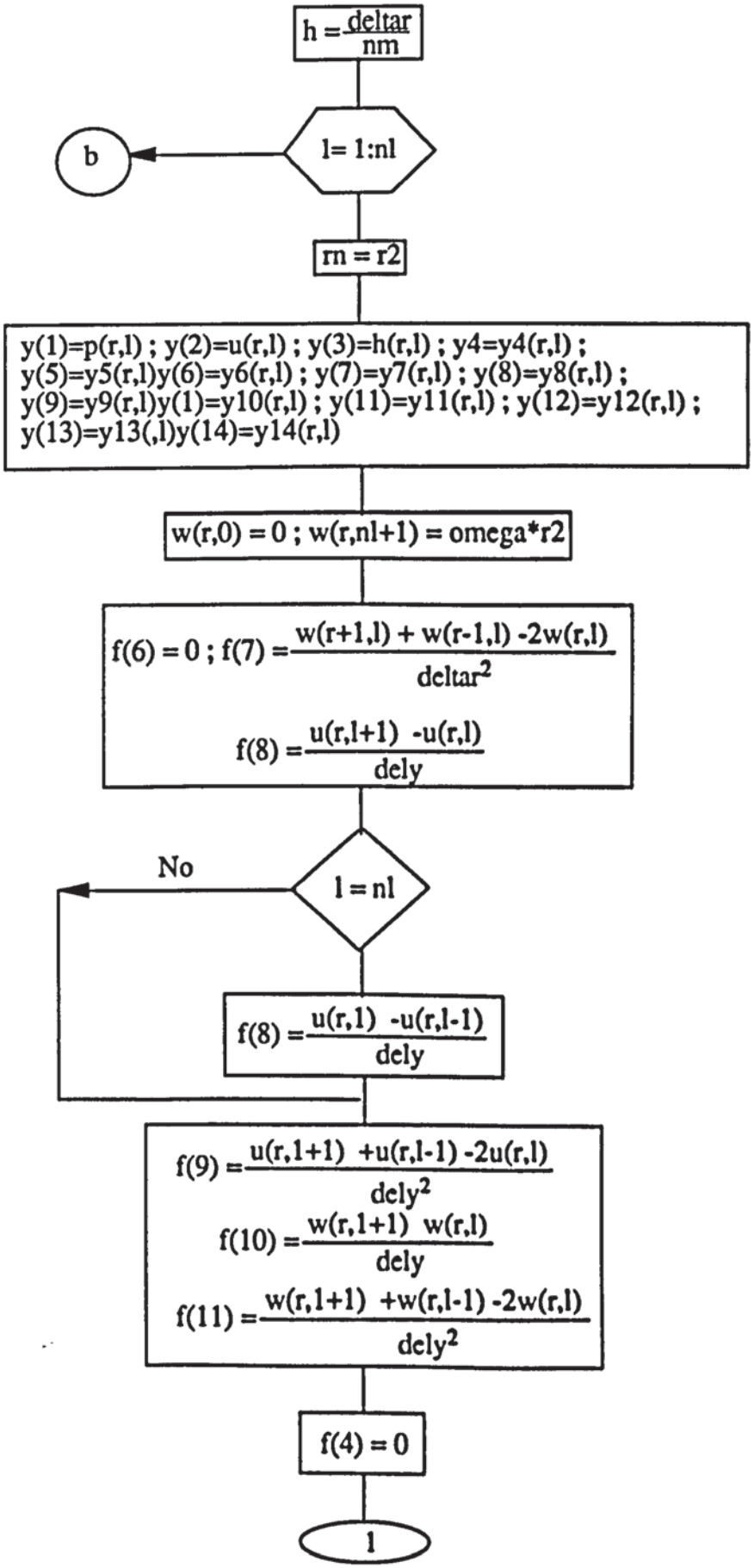

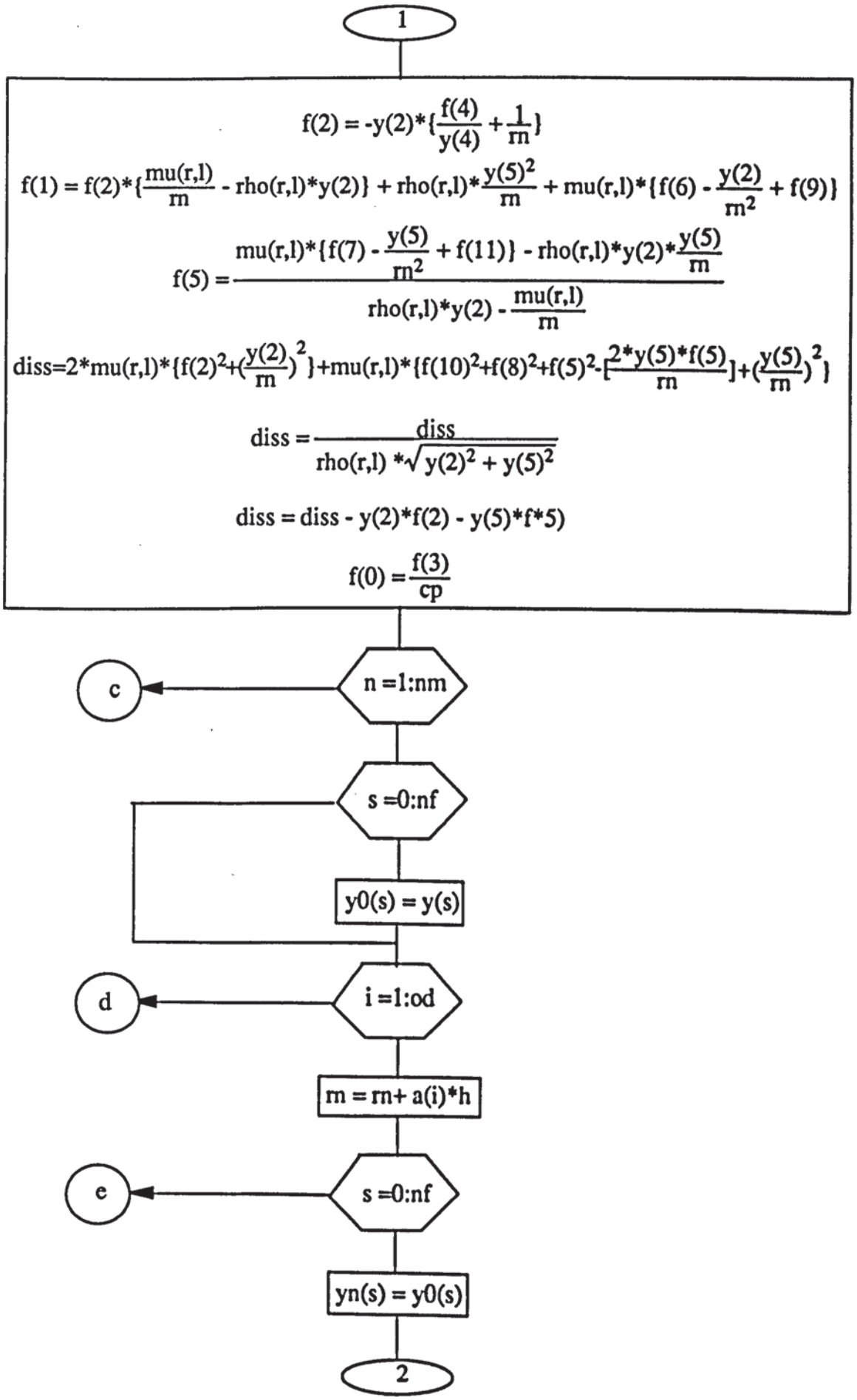
1
$f(2) = -y(2)*\{\frac{f(4)}{y(4)} + \frac{1}{rm}\}$
$f(1) = f(2)*\{\frac{mu(r,l)}{rm} - rho(r,l)*y(2)\} + rho(r,l)*\frac{y(5)^2}{rm} + mu(r,l)*\{f(6) - \frac{y(2)}{rm^2} + f(9)\}$
$f(5) = \frac{mu(r,l)*\{f(7) - \frac{y(5)}{rm^2} + f(11)\} - rho(r,l)*y(2)*\frac{y(5)}{rm}}{rho(r,l)*y(2) - \frac{mu(r,l)}{rm}}$
$diss=2*mu(r,l)*\{f(2)^2+(\frac{y(2)}{rm})^2\}+mu(r,l)*\{f(10)^2+f(8)^2+f(5)^2-[\frac{2*y(5)*f(5)}{rm}]+(\frac{y(5)}{rm})^2\}$
$diss = \frac{diss}{rho(r,l)*\sqrt{y(2)^2 + y(5)^2}}$
diss = diss - y(2)*f(2) - y(5)*f*5)
$f(0) = \frac{f(3)}{cp}$
n =1:nm
c
s =0:nf
y0(s) = y(s)
i =1:od
d
rm = rm+ a(i)*h
s =0:nf
e
yn(s) = y0(s)
2

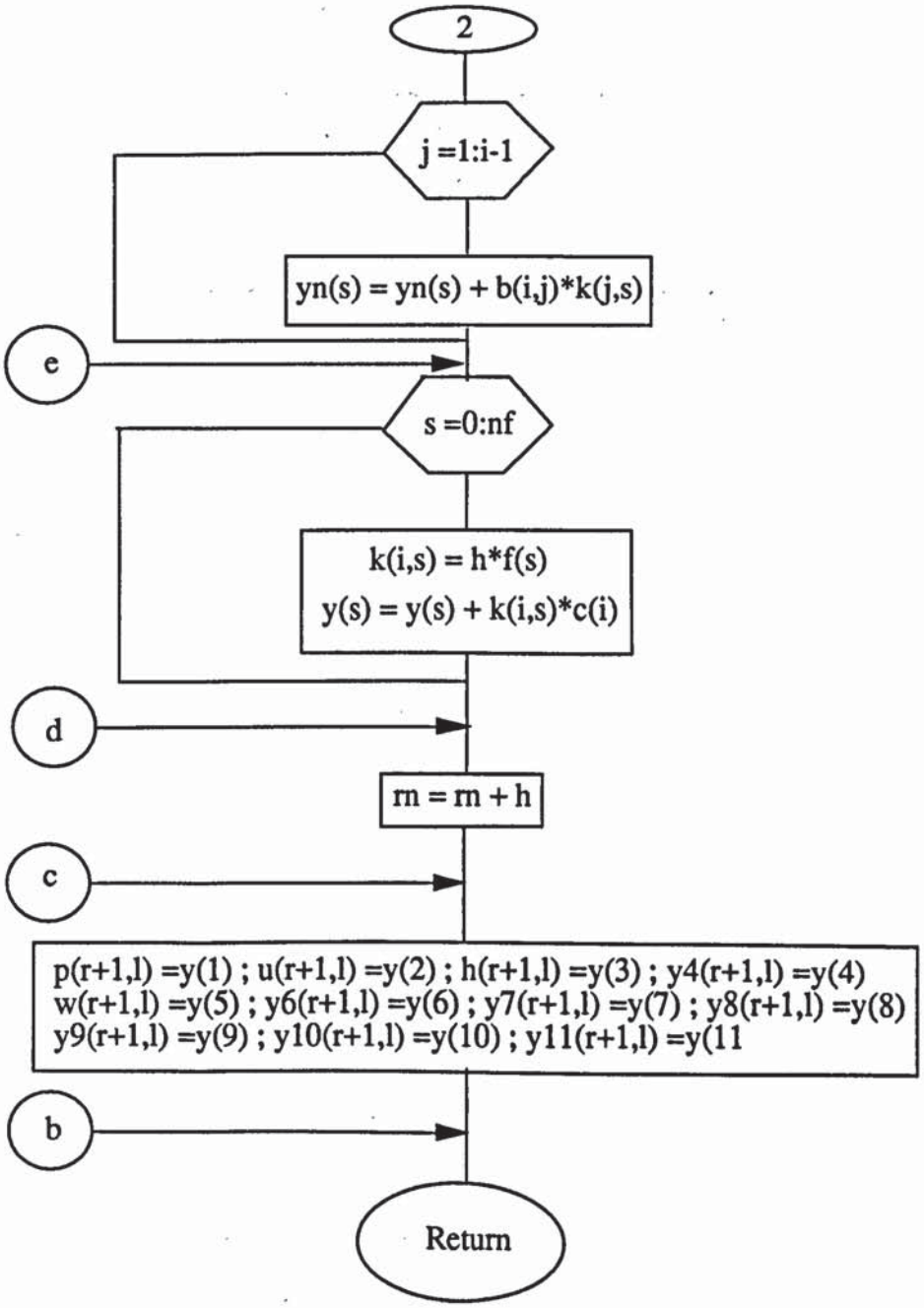
2
j =1:i-1
yn(s) = yn(s) + b(i,j)*k(j,s)
e
s =0:nf
k(i,s) = h*f(s)
y(s) = y(s) + k(i,s)*c(i)
d
rn = rn + h
c
p(r+1,l) =y(1) ; u(r+1,l) =y(2) ; h(r+1,l) =y(3) ; y4(r+1,l) =y(4)
w(r+1,l) =y(5) ; y6(r+1,l) =y(6) ; y7(r+1,l) =y(7) ; y8(r+1,l) =y(8)
y9(r+1,l) =y(9) ; y10(r+1,l) =y(10) ; y11(r+1,l) =y(11
b
Return

SUBROUTINE RUNGE2

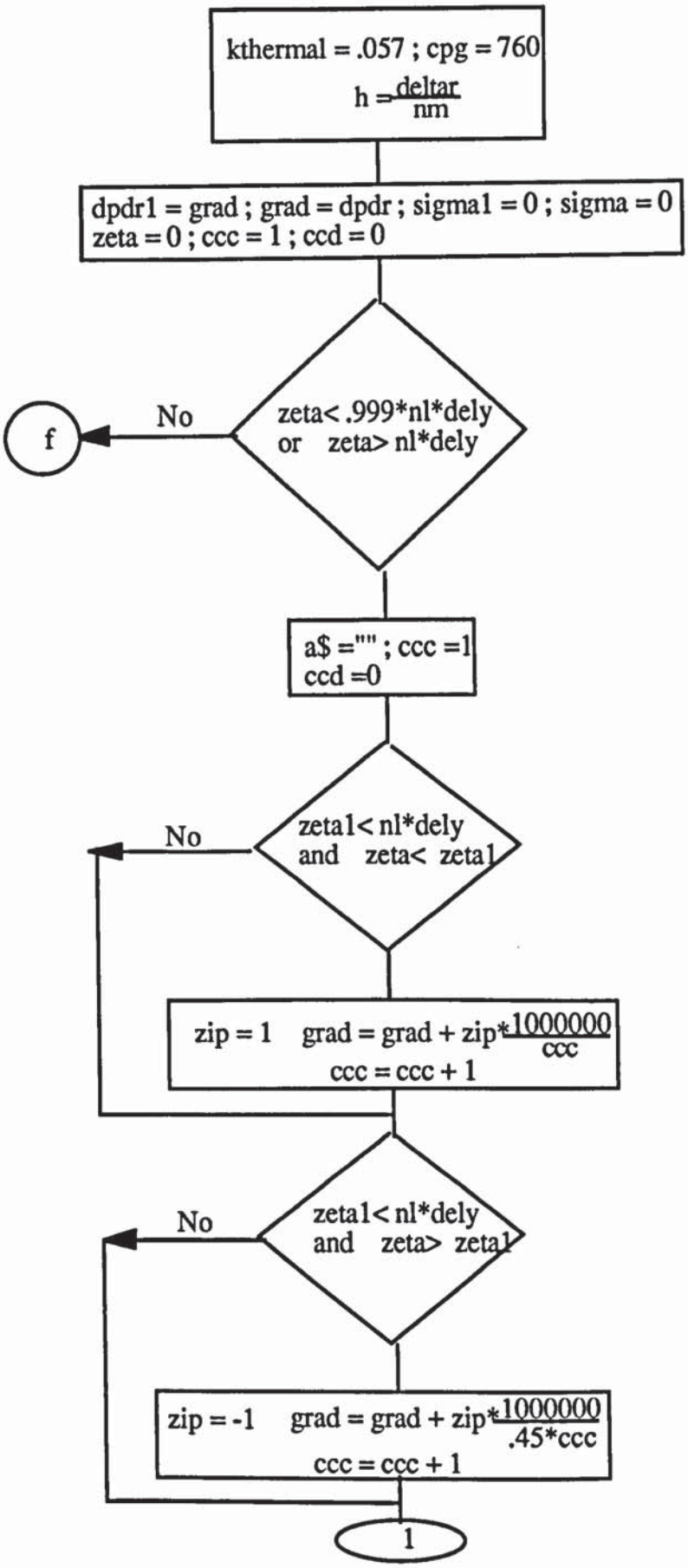

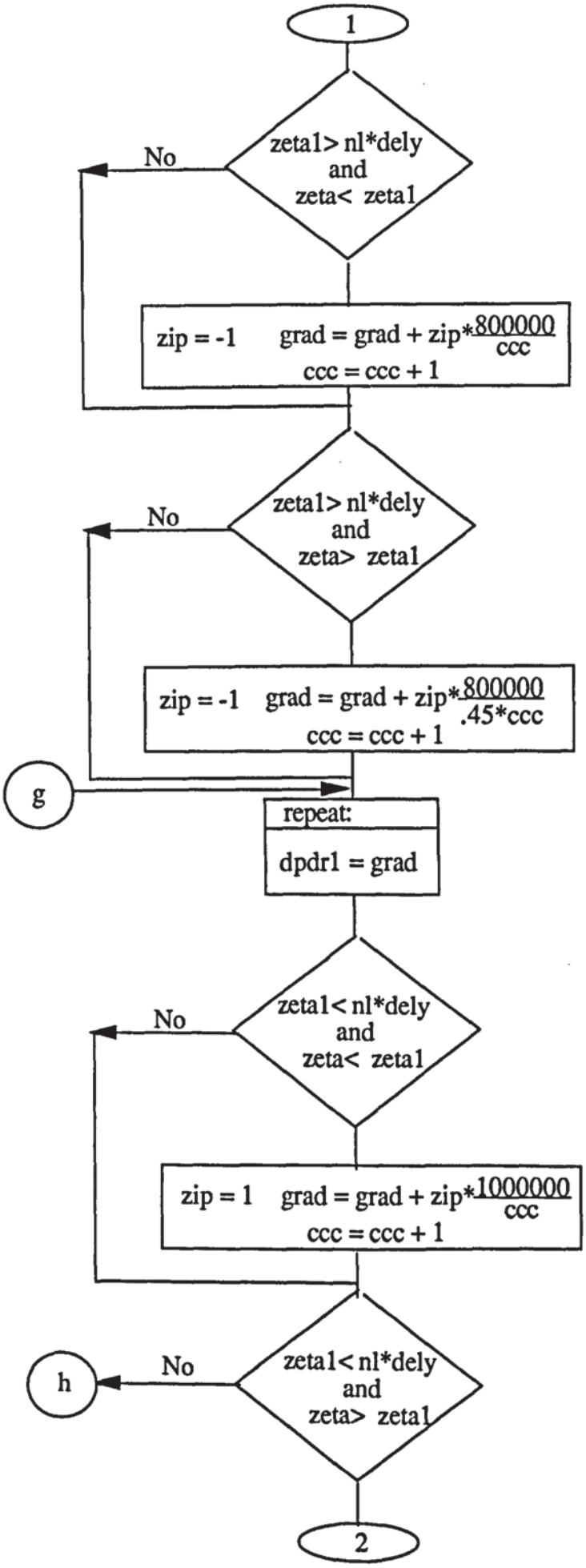
1
zeta1> nl*dely
and
zeta< zeta1
No
zip = -1 grad = grad + zip*800000/ccc
ccc = ccc + 1
zeta1> nl*dely
and
zeta> zeta1
No
zip = -1 grad = grad + zip*800000/.45*ccc
ccc = ccc + 1
g
repeat:
dpdr1 = grad
zeta1< nl*dely
and
zeta< zeta1
No
zip = 1 grad = grad + zip*1000000/ccc
ccc = ccc + 1
zeta1< nl*dely
and
zeta> zeta1
No
h
2

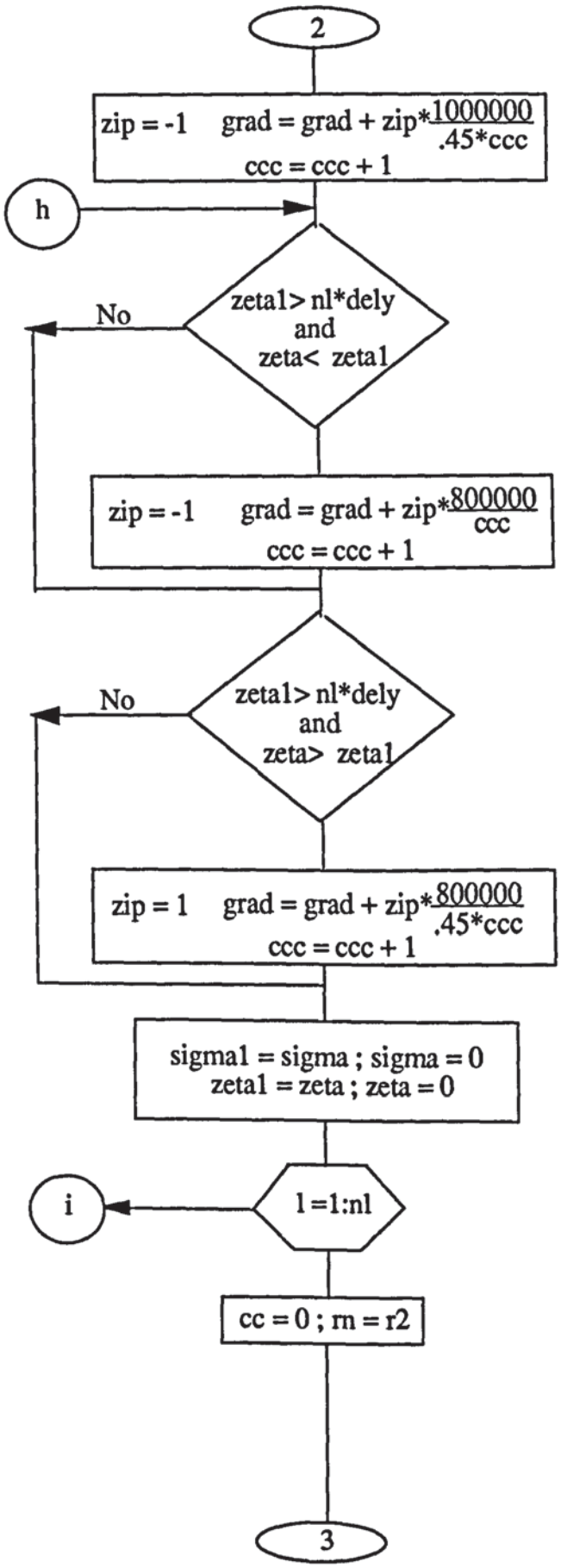
2
zip = -1 grad = grad + zip*1000000/.45*ccc
ccc = ccc + 1
h
zeta1> nl*dely and zeta< zeta1
No
zip = -1 grad = grad + zip*800000/ccc
ccc = ccc + 1
zeta1> nl*dely and zeta> zeta1
No
zip = 1 grad = grad + zip*800000/.45*ccc
ccc = ccc + 1
sigma1 = sigma ; sigma = 0
zeta1 = zeta ; zeta = 0
i
l =1:nl
cc = 0 ; rn = r2
3

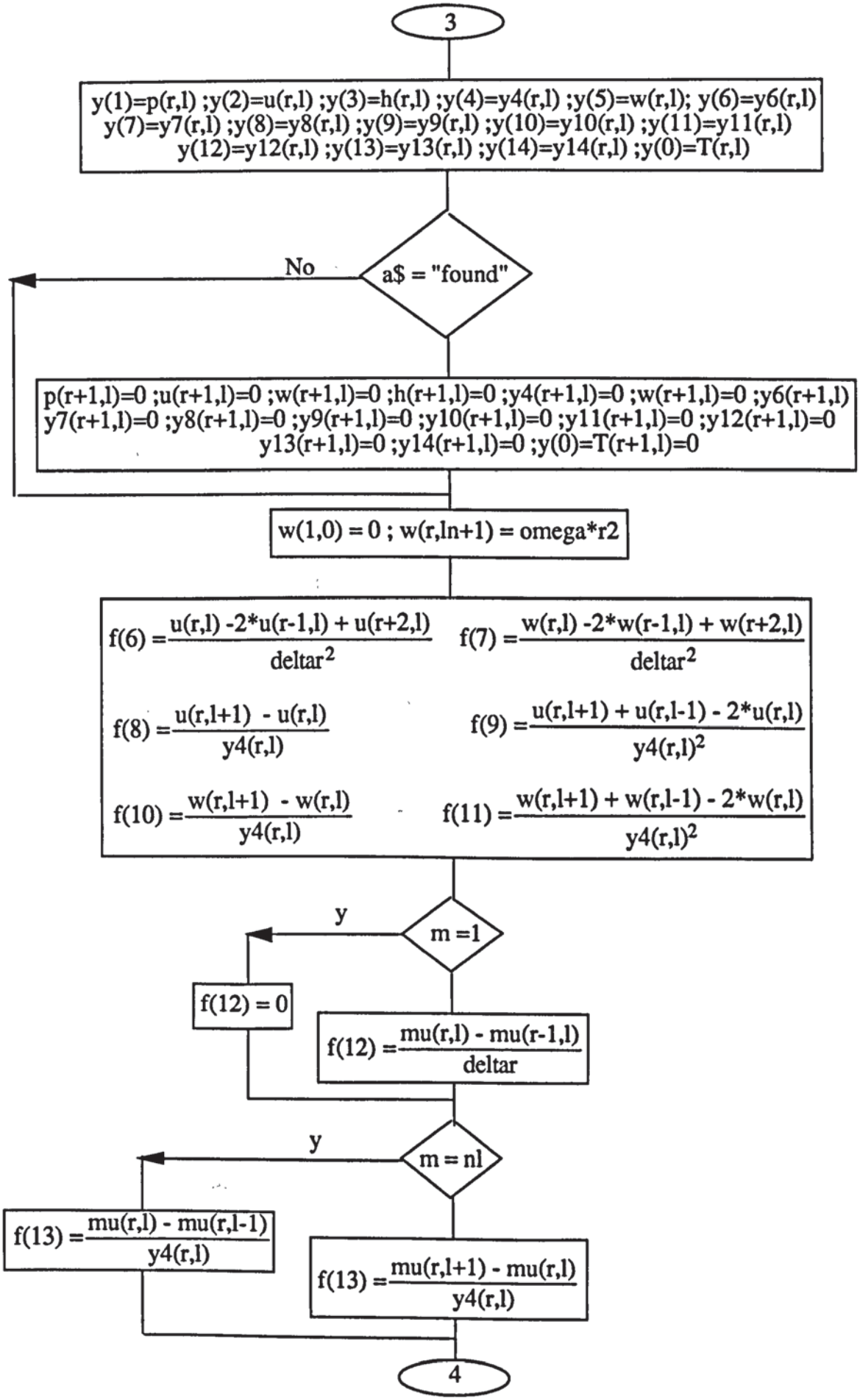
3
y(1)=p(r,l) ;y(2)=u(r,l) ;y(3)=h(r,l) ;y(4)=y4(r,l) ;y(5)=w(r,l); y(6)=y6(r,l)
y(7)=y7(r,l) ;y(8)=y8(r,l) ;y(9)=y9(r,l) ;y(10)=y10(r,l) ;y(11)=y11(r,l)
y(12)=y12(r,l) ;y(13)=y13(r,l) ;y(14)=y14(r,l) ;y(0)=T(r,l)
a$ = "found"
No
p(r+1,l)=0 ;u(r+1,l)=0 ;w(r+1,l)=0 ;h(r+1,l)=0 ;y4(r+1,l)=0 ;w(r+1,l)=0 ;y6(r+1,l)
y7(r+1,l)=0 ;y8(r+1,l)=0 ;y9(r+1,l)=0 ;y10(r+1,l)=0 ;y11(r+1,l)=0 ;y12(r+1,l)=0
y13(r+1,l)=0 ;y14(r+1,l)=0 ;y(0)=T(r+1,l)=0
w(1,0) = 0 ; w(r,ln+1) = omega*r2
f(6) = u(r,l) -2*u(r-1,l) + u(r+2,l) / deltar^2
f(7) = w(r,l) -2*w(r-1,l) + w(r+2,l) / deltar^2
f(8) = u(r,l+1) - u(r,l) / y4(r,l)
f(9) = u(r,l+1) + u(r,l-1) - 2*u(r,l) / y4(r,l)^2
f(10) = w(r,l+1) - w(r,l) / y4(r,l)
f(11) = w(r,l+1) + w(r,l-1) - 2*w(r,l) / y4(r,l)^2
m =1
y
f(12) = 0
f(12) = mu(r,l) - mu(r-1,l) / deltar
m = nl
y
f(13) = mu(r,l) - mu(r,l-1) / y4(r,l)
f(13) = mu(r,l+1) - mu(r,l) / y4(r,l)
4

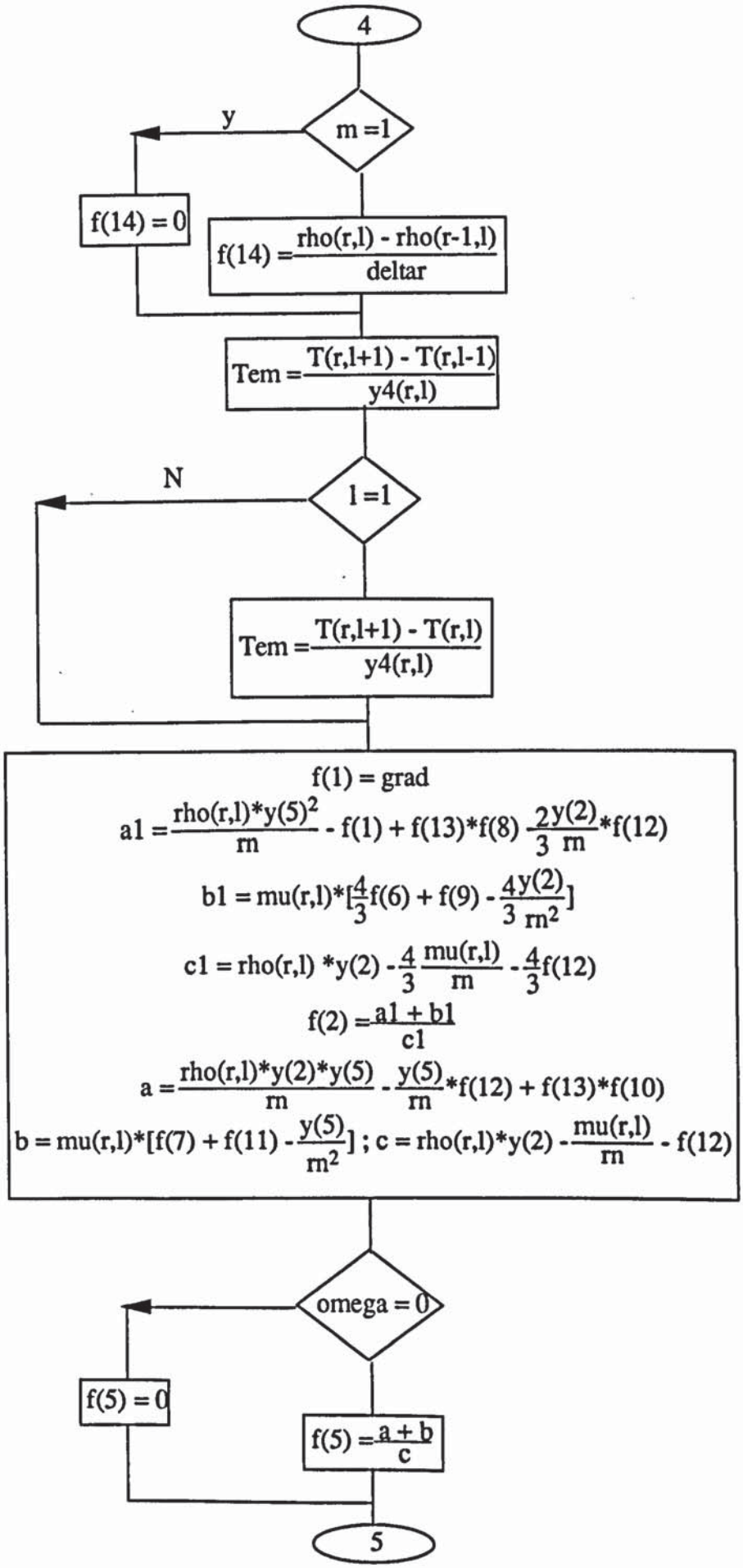
4
m =1
y
f(14) = 0
f(14) = rho(r,l) - rho(r-1,l) / deltar
Tem = T(r,l+1) - T(r,l-1) / y4(r,l)
l =1
N
Tem = T(r,l+1) - T(r,l) / y4(r,l)
f(1) = grad
a1 = rho(r,l)*y(5)^2 / rm - f(1) + f(13)*f(8) 2y(2) / 3 rm *f(12)
b1 = mu(r,l)*[4/3 f(6) + f(9) - 4y(2) / 3 rm^2]
c1 = rho(r,l) *y(2) - 4/3 mu(r,l) / rm - 4/3 f(12)
f(2) = a1 + b1 / c1
a = rho(r,l)*y(2)*y(5) / rm - y(5) / rm *f(12) + f(13)*f(10)
b = mu(r,l)*[f(7) + f(11) - y(5) / rm^2] ; c = rho(r,l)*y(2) - mu(r,l) / rm - f(12)
omega = 0
f(5) = 0
f(5) = a + b / c
5

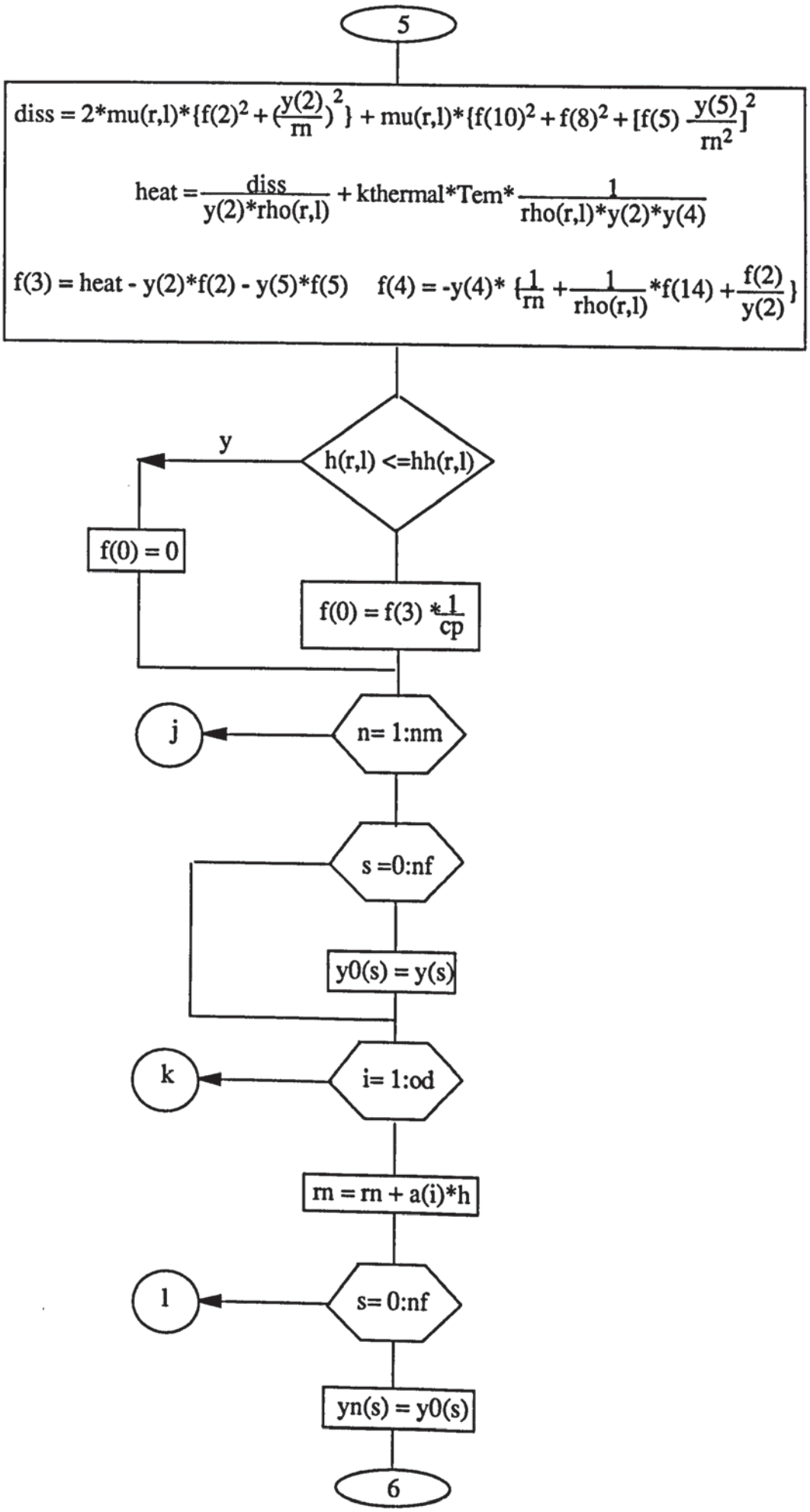
5
diss = 2*mu(r,l)*{f(2)^2 + (y(2)/rn)^2} + mu(r,l)*{f(10)^2 + f(8)^2 + [f(5) y(5)/rn^2]^2
heat = diss/(y(2)*rho(r,l)) + kthermal*Tem* 1/(rho(r,l)*y(2)*y(4))
f(3) = heat - y(2)*f(2) - y(5)*f(5)
f(4) = -y(4)* {1/rn + 1/rho(r,l) *f(14) + f(2)/y(2)}
h(r,l) <=hh(r,l)
y
f(0) = 0
f(0) = f(3) *1/cp
n= 1:nm
j
s =0:nf
y0(s) = y(s)
i= 1:od
k
rn = rn + a(i)*h
s= 0:nf
l
yn(s) = y0(s)
6

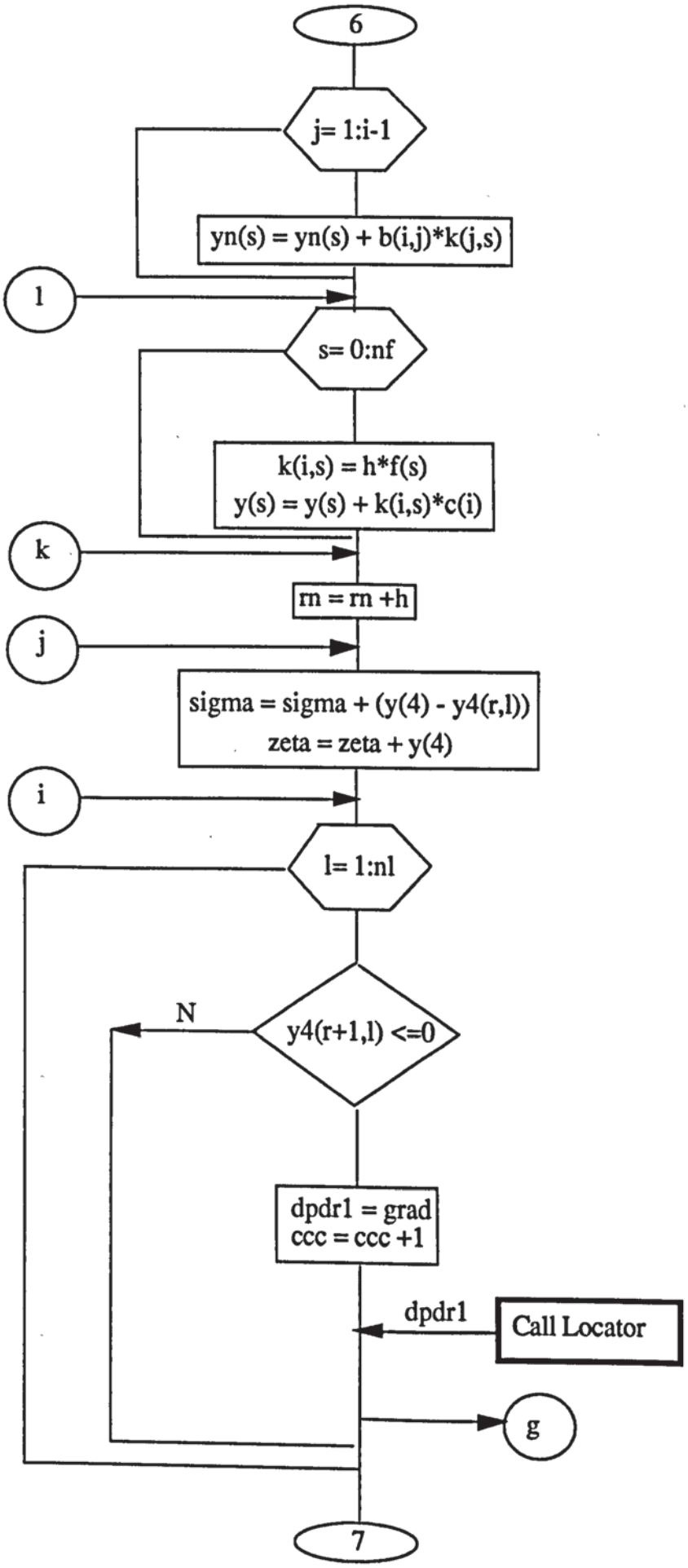
6
j= 1:i-1
yn(s) = yn(s) + b(i,j)*k(j,s)
l
s= 0:nf
k(i,s) = h*f(s)
y(s) = y(s) + k(i,s)*c(i)
k
rn = rn +h
j
sigma = sigma + (y(4) - y4(r,l))
zeta = zeta + y(4)
i
l= 1:nl
N
y4(r+1,l) <=0
dpdr1 = grad
ccc = ccc +1
dpdr1
Call Locator
g
7

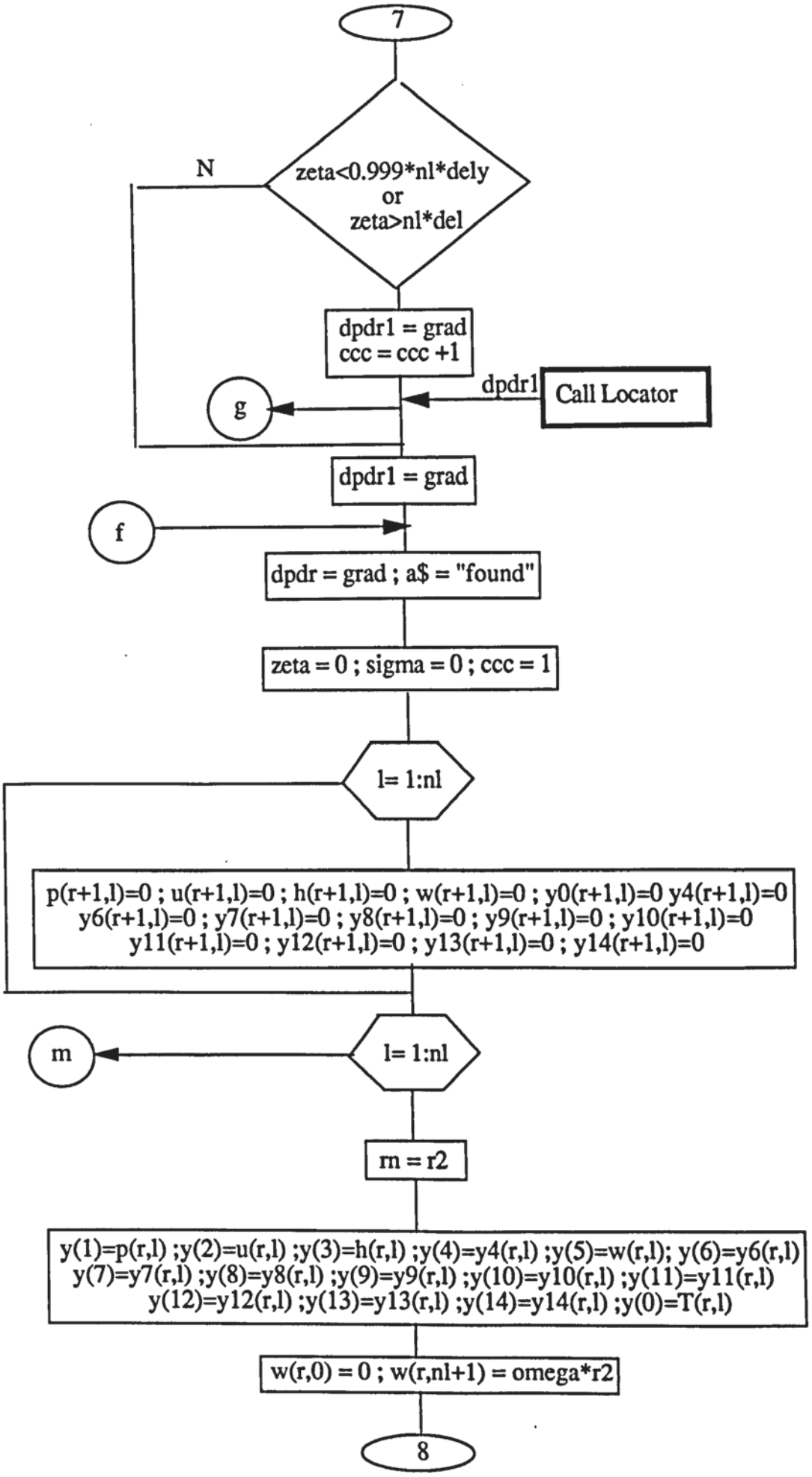
7
N
zeta<0.999*nl*dely
or
zeta>nl*del
dpdr1 = grad
ccc = ccc +1
dpdr1
Call Locator
g
dpdr1 = grad
f
dpdr = grad ; a$ = "found"
zeta = 0 ; sigma = 0 ; ccc = 1
l= 1:nl
p(r+1,l)=0 ; u(r+1,l)=0 ; h(r+1,l)=0 ; w(r+1,l)=0 ; y0(r+1,l)=0 y4(r+1,l)=0
y6(r+1,l)=0 ; y7(r+1,l)=0 ; y8(r+1,l)=0 ; y9(r+1,l)=0 ; y10(r+1,l)=0
y11(r+1,l)=0 ; y12(r+1,l)=0 ; y13(r+1,l)=0 ; y14(r+1,l)=0
m
l= 1:nl
rm = r2
y(1)=p(r,l) ;y(2)=u(r,l) ;y(3)=h(r,l) ;y(4)=y4(r,l) ;y(5)=w(r,l); y(6)=y6(r,l)
y(7)=y7(r,l) ;y(8)=y8(r,l) ;y(9)=y9(r,l) ;y(10)=y10(r,l) ;y(11)=y11(r,l)
y(12)=y12(r,l) ;y(13)=y13(r,l) ;y(14)=y14(r,l) ;y(0)=T(r,l)
w(r,0) = 0 ; w(r,nl+1) = omega*r2
8

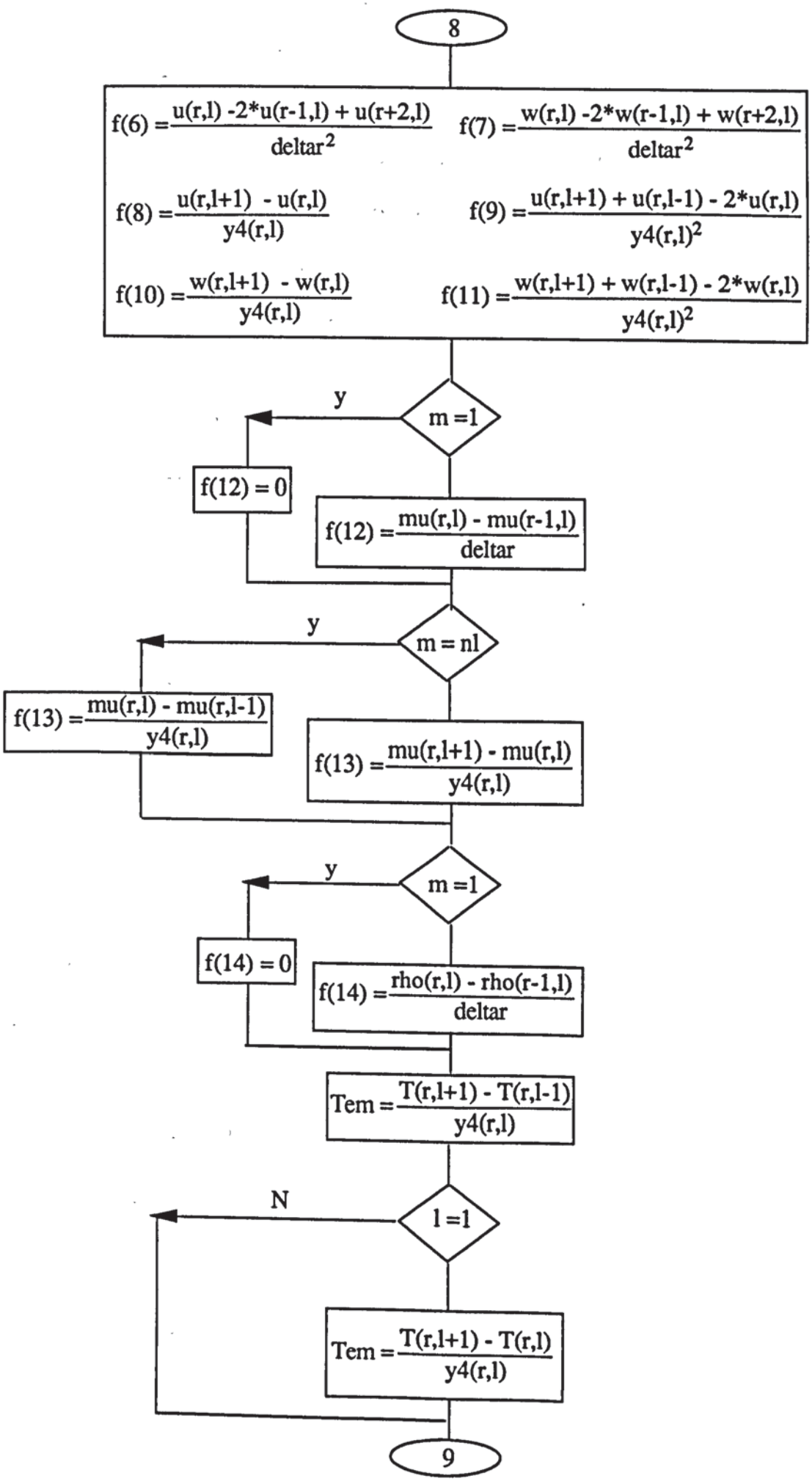
8
f(6) = u(r,l) -2*u(r-1,l) + u(r+2,l) / deltar^2
f(7) = w(r,l) -2*w(r-1,l) + w(r+2,l) / deltar^2
f(8) = u(r,l+1) - u(r,l) / y4(r,l)
f(9) = u(r,l+1) + u(r,l-1) - 2*u(r,l) / y4(r,l)^2
f(10) = w(r,l+1) - w(r,l) / y4(r,l)
f(11) = w(r,l+1) + w(r,l-1) - 2*w(r,l) / y4(r,l)^2
m =1
y
f(12) = 0
f(12) = mu(r,l) - mu(r-1,l) / deltar
m = nl
y
f(13) = mu(r,l) - mu(r,l-1) / y4(r,l)
f(13) = mu(r,l+1) - mu(r,l) / y4(r,l)
m =1
y
f(14) = 0
f(14) = rho(r,l) - rho(r-1,l) / deltar
Tem = T(r,l+1) - T(r,l-1) / y4(r,l)
l =1
N
Tem = T(r,l+1) - T(r,l) / y4(r,l)
9

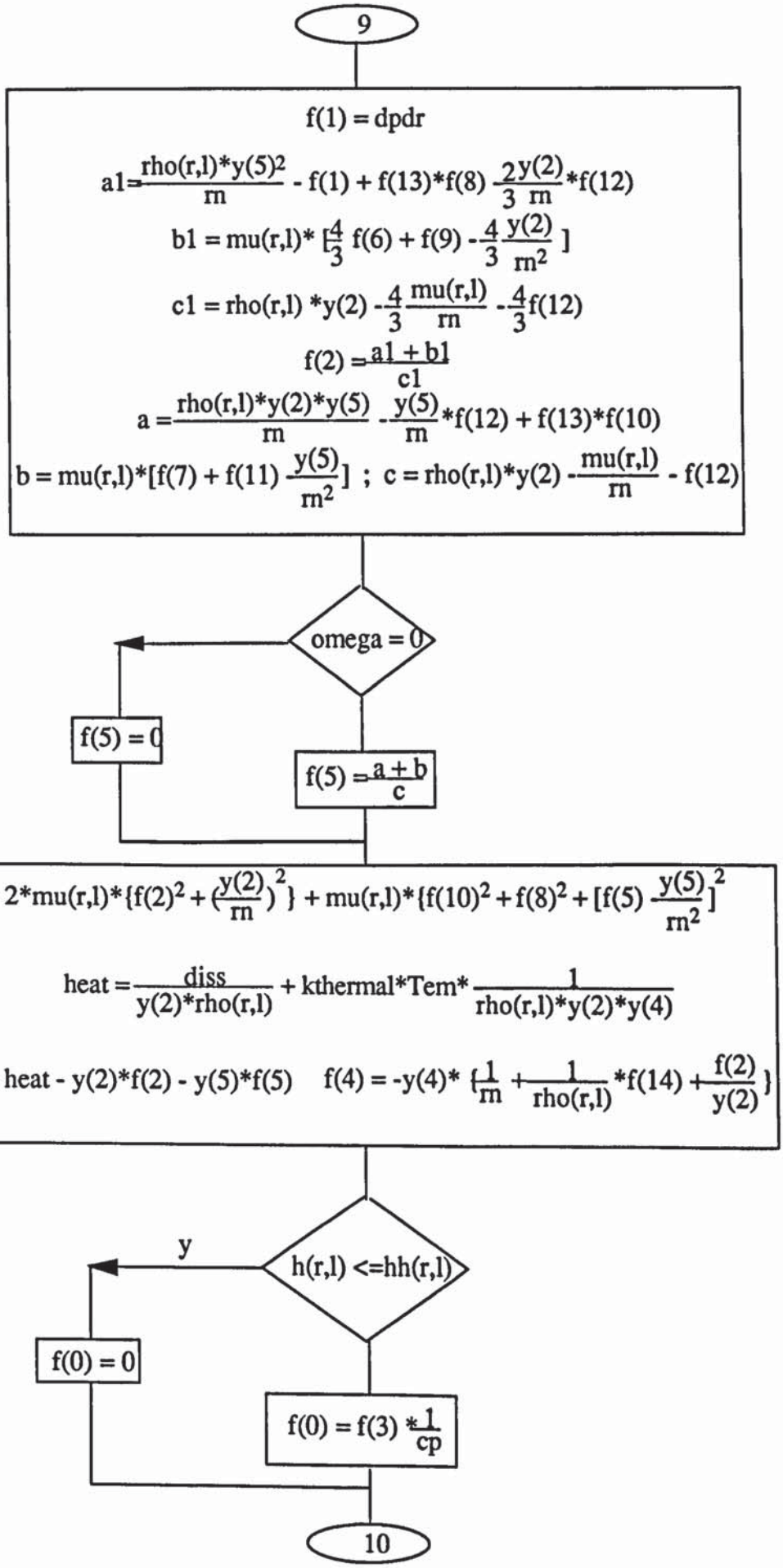
9
f(1) = dpdr
a1=rho(r,l)*y(5)2/rm - f(1) + f(13)*f(8) 2y(2)/3 rm*f(12)
b1 = mu(r,l)* [4/3 f(6) + f(9) -4/3 y(2)/rm2]
c1 = rho(r,l) *y(2) -4/3 mu(r,l)/rm -4/3f(12)
f(2) =a1 + b1/c1
a =rho(r,l)*y(2)*y(5)/rm - y(5)/rm*f(12) + f(13)*f(10)
b = mu(r,l)*[f(7) + f(11) y(5)/rm2] ; c = rho(r,l)*y(2) -mu(r,l)/rm - f(12)
omega = 0
f(5) = 0
f(5) =a + b/c
diss = 2*mu(r,l)*{f(2)2 + (y(2)/rm)2 } + mu(r,l)*{f(10)2 + f(8)2 + [f(5) y(5)/rm2]2
heat =diss/y(2)*rho(r,l) + kthermal*Tem* 1/rho(r,l)*y(2)*y(4)
f(3) = heat - y(2)*f(2) - y(5)*f(5) f(4) = -y(4)* {1/rm +1/rho(r,l) *f(14) +f(2)/y(2) }
y
h(r,l) <=hh(r,l)
f(0) = 0
f(0) = f(3) *1/cp
10

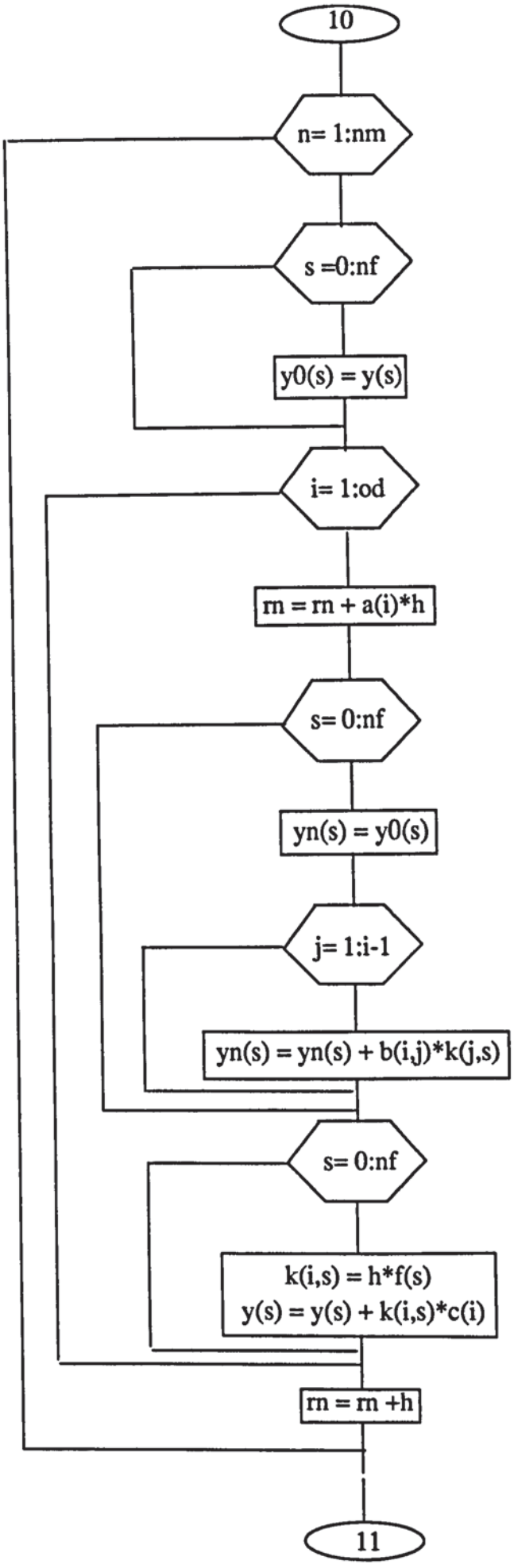
10
n= 1:nm
s =0:nf
y0(s) = y(s)
i= 1:od
rn = rn + a(i)*h
s= 0:nf
yn(s) = y0(s)
j= 1:i-1
yn(s) = yn(s) + b(i,j)*k(j,s)
s= 0:nf
k(i,s) = h*f(s)
y(s) = y(s) + k(i,s)*c(i)
rn = rn +h
11

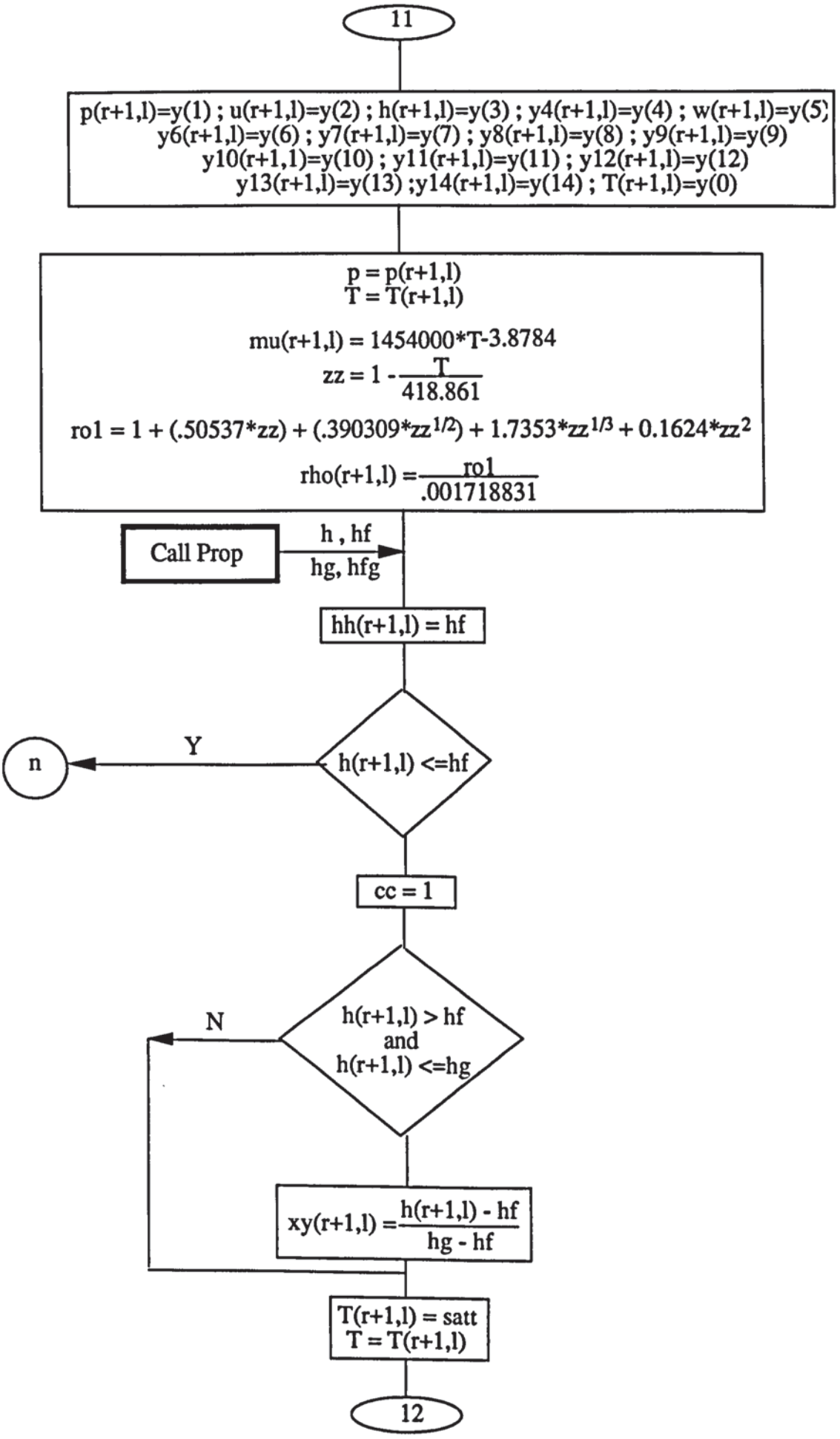
11
p(r+1,l)=y(1) ; u(r+1,l)=y(2) ; h(r+1,l)=y(3) ; y4(r+1,l)=y(4) ; w(r+1,l)=y(5)
y6(r+1,l)=y(6) ; y7(r+1,l)=y(7) ; y8(r+1,l)=y(8) ; y9(r+1,l)=y(9)
y10(r+1,1)=y(10) ; y11(r+1,l)=y(11) ; y12(r+1,l)=y(12)
y13(r+1,l)=y(13) ;y14(r+1,l)=y(14) ; T(r+1,l)=y(0)
p = p(r+1,l)
T = T(r+1,l)
mu(r+1,l) = 1454000*T-3.8784
zz = 1 - T/418.861
ro1 = 1 + (.50537*zz) + (.390309*zz^1/2) + 1.7353*zz^1/3 + 0.1624*zz^2
rho(r+1,l) = ro1/.001718831
Call Prop
h , hf
hg, hfg
hh(r+1,l) = hf
h(r+1,l) <=hf
Y
n
cc = 1
h(r+1,l) > hf
and
h(r+1,l) <=hg
N
xy(r+1,l) = h(r+1,l) - hf / hg - hf
T(r+1,l) = satt
T = T(r+1,l)
12

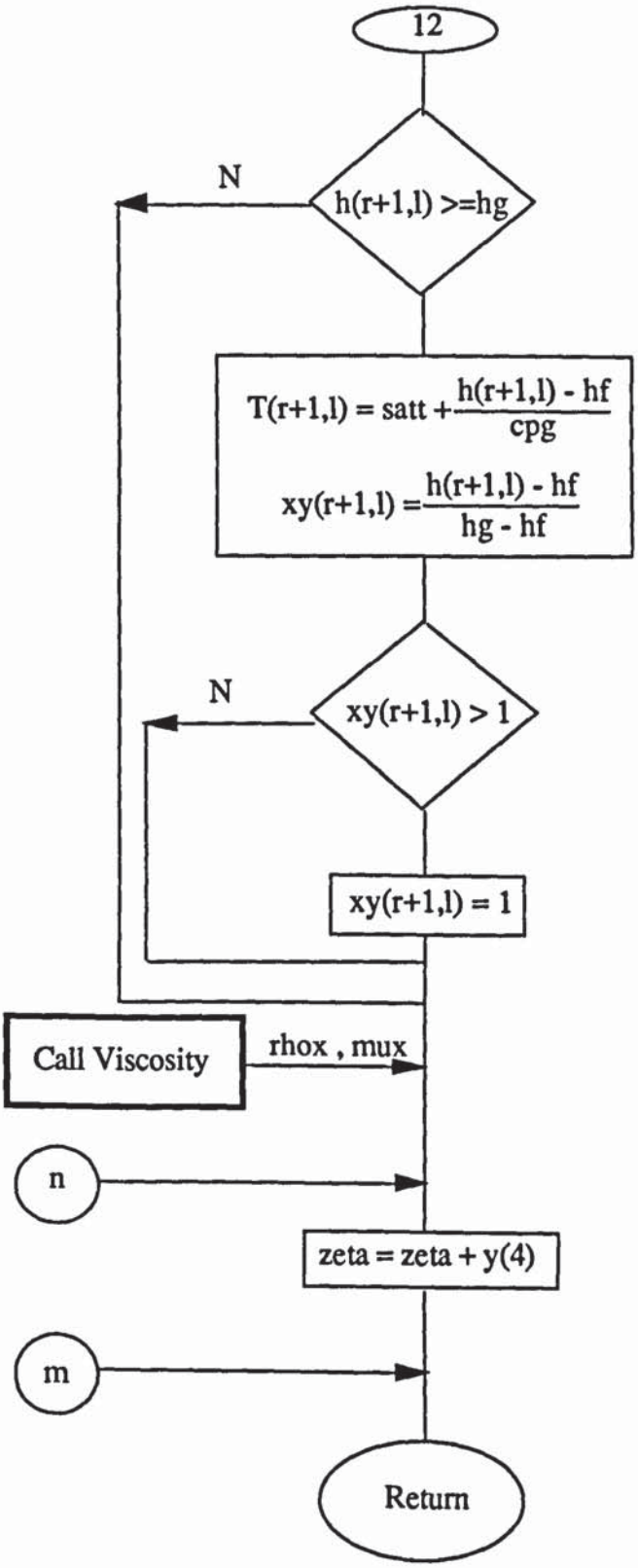
12
N
h(r+1,l) >=hg
T(r+1,l) = satt + h(r+1,l) - hf / cpg
xy(r+1,l) = h(r+1,l) - hf / hg - hf
N
xy(r+1,l) > 1
xy(r+1,l) = 1
Call Viscosity
rhox , mux
n
zeta = zeta + y(4)
m
Return

SUBROUTINE VISCOSITY

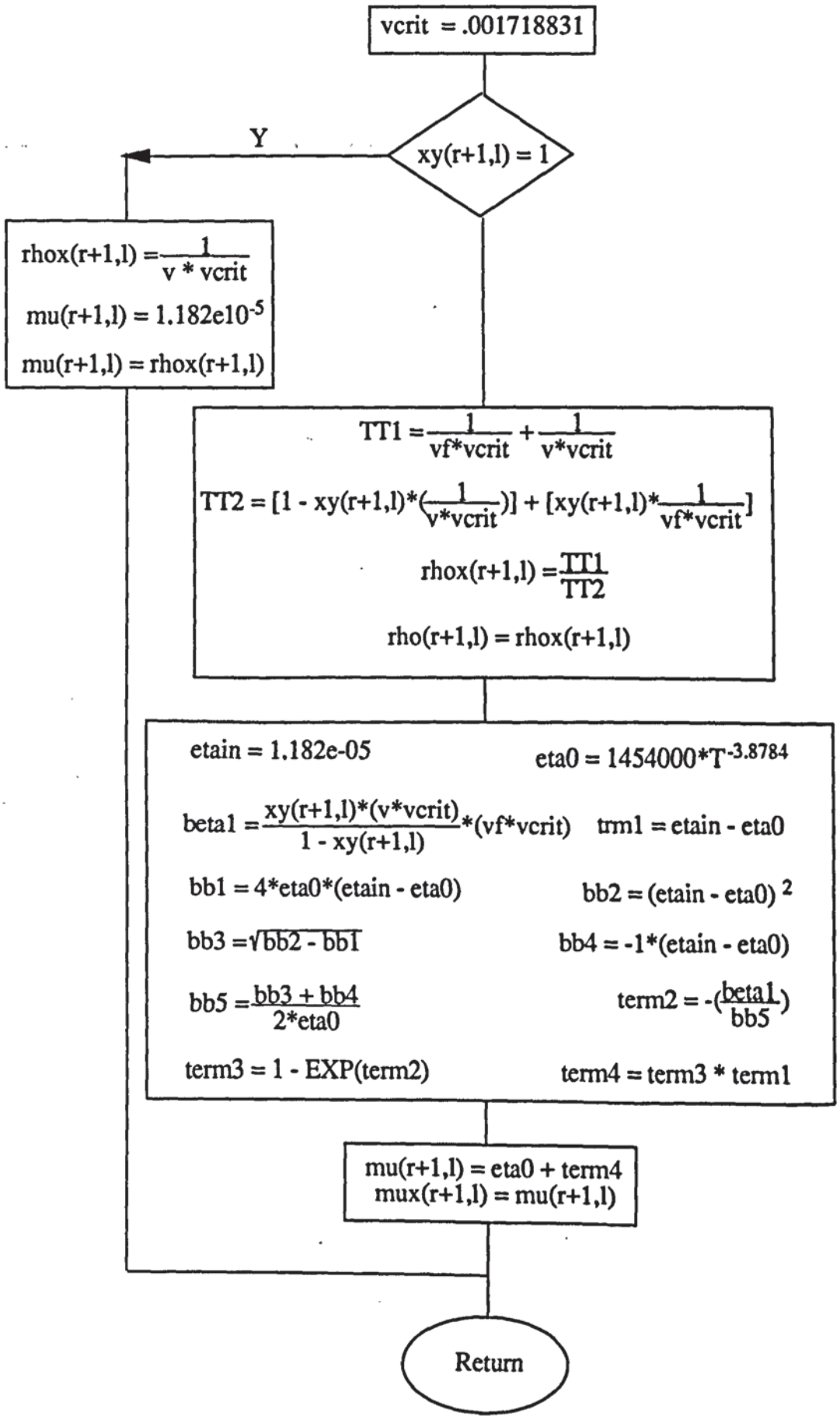

A4.2 Some Typical Programme Results

Table A4.2.1 shows a typical comparison between the calculated enthalpies and those available in the literature.

		Calculated Values			Available Data		
T (K)	P (bar)	hl (KJ/kg)	hlg (KJ/kg)	hg (KJ/kg)	hl (KJ/kg)	hlg (KJ/kg)	hg (KJ/kg)
210	0.0301	47.895	152.50	200.39	46.136	154.09	200.18
220	0.0594	56.723	149.36	206.09	55.135	150.77	205.91
230	0.1096	64.875	147.03	211.90	63.430	148.30	211.73
240	0.1908	72.849	144.98	217.83	71.530	146.13	217.66
250	0.3165	80.957	142.90	223.86	79.753	143.93	223.69
260	0.5028	89.384	140.58	229.97	88.288	141.52	229.80
265	0.6245	93.751	139.30	233.05	92.704	140.18	232.88
270	0.7690	98.236	137.91	236.15	97.230	138.75	235.98
275	0.9386	102.82	136.43	239.25	101.86	137.23	239.09
280	1.1365	107.53	134.83	242.37	106.62	135.59	242.21
285	1.3656	112.36	133.13	245.50	111.48	133.85	245.34
290	1.6289	117.29	131.33	248.62	116.45	132.01	248.47
205	1.9297	122.33	129.41	251.75	121.53	130.06	251.59
300	2.2711	127.47	127.39	254.87	126.71	128.01	254.72
305	2.6564	132.71	125.27	257.99	131.97	125.86	257.83
310	3.0888	138.03	123.06	261.09	137.32	123.61	260.94
315	3.5718	143.43	120.74	264.17	142.75	121.27	264.03
320	4.1085	148.91	118.33	267.24	148.25	118.84	267.09
325	4.7024	154.44	115.84	270.28	153.81	116.32	270.14
330	5.3569	160.04	113.27	273.29	159.43	113.72	273.15
335	6.0757	165.68	110.58	276.27	165.09	111.03	276.12
340	6.862	171.36	107.83	279.19	170.80	108.25	279.05
350	8.654	182.87	102.01	284.88	182.34	102.39	284.73
360	10.767	194.54	95.71	290.26	194.03	96.09	290.11
370	13.238	206.39	88.77	295.17	205.89	89.14	295.03
380	16.116	218.53	80.82	299.36	218.05	81.18	299.23
390	19.464	231.22	71.07	302.29	230.69	71.46	302.16
400	23.364	245.43	58.05	303.48	243.38	59.95	303.95
418.71	32.625	282.01	-0.83	283.70	283.71	0.0	283.71

Table A4.2.1
Comparison of enthalpy of liquid refrigerant R114 calculated by the computer model with those available from ICI

From Table A4.2.1 it can be observed that the calculated values of enthalpy for R114 within the large range of temperature are reasonably close to those published by ICI The calculation by this part of program are therefore reliable.

Table A.4.2.2 contains some predictions from the computer model and available data in literature for density and viscosity of liquid refrigerant.

	Calculated Values		Available Data	
T (K)	Density kg/m^3	Viscosity Ns/m^2 x 10^{-6}	Density kg/m^3	Viscosity Ns/m^2 x 10^{-6}
180	1788	2610	------	3183
190	1763	2111	1745	2385
200	1738	1731	1727	1819
210	1712	1432	1691	1434
220	1686	1195	1566	1153
230	1660	1000	1554	954
240	1633	841	1550	785
250	1605	720	1539	661
260	1577	620	1529	566
270	1548	540	1512	496
280	1519	469	1494	430
290	1488	409	1472	380.3
300	1457	359	1447	334.8
310	1427	316	1419	301.8
320	1390	279	1387	268.7
330	1355	248	1337	248
340	1317	221	1318	227
350	1277	198	1279	206.7
360	1234	178	1237	190.6
370	1188	159	1192	175.7
380	1136	143	1114	159.2
390	1076	129	1048	138.9
400	1002	117	1014	117.4
410	900	69.4	918	87.2
418.86	581	38.5	557	31

Table A.4.2.2
Comparison of density and viscosity of liquid refrigerant R114 calculated by the computer model with those available from ASHRAE

A4.3 Theoretical Results Corresponding to Measured Values in Chapter 7

Table A4.3.1 shows the predicted results corresponding to the inlet conditions which apply to the experimental results listed in Table 7.3.1.1, section 7.3.1, Chapter 7.

Radius(m)	Pressure (bar) (m = 0.26)	Pressure (bar) (m = 0.27)	Pressure (bar) (m = 0.29)	Pressure (bar) (m = 0.3)	Pressure (bar) (m = 0.32)	Pressure (bar) (m = 0.33)	Pressure (bar) (m = 0.35)
0.03	2.010	2.080	2.145	2.259	2.425	2.650	2.995
0.0338	2.0410	2.1159	2.1960	2.4876	2.4689	2.7199	3.0793
0.0386	2.0567	2.1355	2.2178	2.5285	2.4988	2.7671	3.1385
0.0433	2.0580	2.1393	2.2262	2.5454	2.5058	2.7882	3.1676
0.0481	2.0512	2.1340	2.2238	2.5485	2.501	2.7943	3.1791
0.0528	2.0399	2.1237	2.2151	2.5434	2.4901	2.7913	3.1799
0.0576	2.0259	2.1103	2.2026	2.5332	2.4758	2.7827	3.1740
0.0623	2.0104	2.0952	2.1879	2.5198	2.4598	2.7706	3.1639
0.0671	1.9942	2.0792	2.1720	2.5047	2.443	2.7563	3.1510
0.0718	1.9777	2.0627	2.1554	2.4884	2.4259	2.7408	3.1365
0.0765	1.912	2.0462	2.1386	2.4716	2.4089	2.7245	3.1210
0.0813	1.9449	2.0298	2.1217	2.4545	2.3922	2.7078	3.1049
0.086	1.9289	2.0136	2.1050	2.4374	2.3758	2.6911	3.0885
0.0908	1.9132	1.9978	2.0886	2.4204	2.3599	2.6744	3.0721
0.0955	1.8979	1.9823	2.0724	2.4037	2.3444	2.6579	3.0557
0.1003	1.8829	1.9671	2.0567	2.3873	2.3294	2.6416	3.0395
0.1098	1.8543	1.9381	2.0263	2.3554	2.322	2.6100	3.0078
0.1145	1.8406	1.9241	2.0116	2.3400	2.3172	2.5947	2.9924
0.1193	1.8273	1.9106	1.9974	2.3250	2.3154	2.5798	2.9773
0.124	1.8144	1.8974	1.9835	2.3103	2.3124	2.5652	2.9626

Table A4.3.1
Predicted values of the pressure distribution for a gap of 0.17 mm and a range of mass flow rates corresponding to the inlet conditions listed in Table 7.3.1 in Chapter 7.

Theoretical solutions corresponding to the experimental results shown in Table 7.4.1.1 in Chapter 7, section 7.4.1 are presented in tabular form in Table A4.2.2.

Radius (m)	Pressure (bar) (T= 306.4)	Pressure (bar) (T= 308.1)	Pressure (bar) (T= 309.4)	Pressure (bar) (T= 310.7)	Pressure (bar) (T= 312.1)	Pressure (bar) (T= 314.3)	Pressure (bar) (T= 315)
0.03	2.791	3.01	3.112	3.19	3.385	3.595	3.785
0.0338	2.8336	3.0712	3.1746	3.2536	3.4496	3.6612	3.8517
0.0386	2.8644	3.1133	3.2182	3.2982	3.4953	3.7086	3.8996
0.0433	2.8739	3.1332	3.2394	3.3202	3.5182	3.7328	3.9243
0.0481	2.8723	3.1402	3.2474	3.3290	3.5277	3.7435	3.9353
0.0528	2.8648	3.1393	3.2475	3.3296	3.5290	3.7459	3.9380
0.0576	2.854	3.1335	3.2426	3.3253	3.5253	3.7430	3.9354
0.0623	2.8415	3.1247	3.2345	3.3177	3.5182	3.7368	3.9295
0.0718	2.8241	3.1021	3.2131	3.2972	3.4987	3.7187	3.9118
0.0766	2.8142	3.0895	3.2011	3.2856	3.4875	3.7081	3.9014
0.0813	2.803	3.0765	3.1887	3.2735	3.4758	3.6970	3.8905
0.0861	2.7866	3.0634	3.1760	3.2612	3.4638	3.6856	3.8793
0.0908	2.7731	3.0502	3.1634	3.2489	3.4518	3.6741	3.8680
0.0956	2.7599	3.0372	3.1508	3.2366	3.4399	3.6626	3.8566
0.1003	2.747	3.0243	3.1383	3.2244	3.4280	3.6512	3.8454
0.1051	2.7345	3.0116	3.1261	3.2124	3.4163	3.6400	3.8342
0.1098	2.7284	2.9992	3.1140	3.2007	3.4048	3.6289	3.8233
0.1145	2.7243	2.9870	3.1022	3.1891	3.3935	3.6180	3.8125
0.1193	2.7223	2.9751	3.0907	3.1778	3.3824	3.6073	3.8091
0.1241	2.7211	2.9635	3.0794	3.1667	3.3716	3.5968	3.7916

Table A4.3.2
Predicted values of the pressure distribution for a gap of 0.17 mm, common mass flow rate of 0.30 kg/s, inlet conditions corresponding to measured values listed in table 7.3.1.1 in Chapter 7 and a range of inlet temperatures.

Theoretical predictions corresponding to the inlet conditions presented in section 7.5.1 ,Chapter 7 are shown in tabular form in Table A4.3.3.

Radius (m)	Pressure (bar) (T= 308.1)	Pressure (bar) (T= 302.7)	Pressure (bar) (T= 304.6)	Pressure (bar) (T= 307.9)	Pressure (bar) (T= 307.7)
0.03	3.103	2.579	2.703	3.000	2.876
0.0338	3.1211	2.5977	2.7227	3.0249	2.9039
0.0386	3.1298	2.6061	2.7321	3.0386	2.9197
0.0433	3.1297	2.6051	2.7319	3.0415	2.9236
0.0481	3.1248	2.5989	2.7265	3.0382	2.9207
0.0528	3.1172	2.5897	2.7180	3.0313	2.9138
0.0576	3.1080	2.5790	2.7078	3.0223	2.9046
0.0623	3.0979	2.5674	2.6968	3.0121	2.8940
0.0671	3.0875	2.5554	2.6853	3.0013	2.8828
0.0718	3.0769	2.5433	2.6736	2.9902	2.8711
0.0766	3.0663	2.5312	2.6620	2.9791	2.8594
0.0813	3.0558	2.5194	2.6506	2.9680	2.8477
0.0908	3.0336	2.4942	2.6261	2.9441	2.8225
0.0956	3.0258	2.4853	2.6176	2.9358	2.8136
0.1003	3.0163	2.4746	2.6071	2.9255	2.8028
0.1051	3.0071	2.4642	2.5969	2.9155	2.7922
0.1098	2.9981	2.4540	2.5870	2.9058	2.7819
0.1146	2.9894	2.4441	2.5774	2.8963	2.7719
0.1193	2.9810	2.4345	2.5680	2.8871	2.7621
0.1241	2.9728	2.4251	2.5599	2.8781	2.7526

Table A4.3.3
Predicted values of the pressure distribution for a gap of 0.17 mm, different mass flow rates, inlet conditions corresponding to measured values listed in Table 7.5.1 in Chapter 7 and a range of inlet temperatures.

Radius (m)	Pressure (bar) m=0.26 T= 296.1	Pressure (bar) m=0.26 T= 310.5	Pressure (bar) m=0.27 T= 296	Pressure (bar) m=0.27 T= 309.5	Pressure (bar) m=0.28 T= 298	Pressure (bar) m=0.28 T= 310.8	Pressure (bar) m=0.30 T= 298.1	Pressure (bar) m=0.30 T= 311
.03000	2.6633	3.1090	2.6120	3.151	2.791	3.113	2.791	3.122
0.0338	2.7007	3.1566	2.6496	3.1990	2.8347	3.1657	2.8446	3.1855
0.0386	2.7222	3.1885	2.6711	3.2313	2.8613	3.2018	2.8790	3.2302
0.0433	2.7276	3.2026	2.6764	3.2458	2.8700	3.2185	2.8924	3.2523
0.0481	2.7238	3.2063	2.6725	3.2499	2.8685	3.2239	2.8937	3.2611
0.0528	2.7147	3.2038	2.6633	3.2477	2.8610	3.2224	2.8879	3.2618
0.0575	2.7024	3.1975	2.6510	3.2416	2.8499	3.2168	2.8777	3.2575
0.0623	2.6883	3.1888	2.6369	3.2331	2.8368	3.2085	2.8649	3.2500
0.0671	2.6732	3.1786	2.6218	3.2232	2.8223	3.1986	2.8505	3.2404
0.0718	2.6577	3.1676	2.6062	3.2124	2.8073	3.1876	2.8352	3.2296
0.0765	2.6420	3.1296	2.5904	3.2011	2.7919	3.1761	2.8195	3.2180
0.0861	2.6108	3.1326	2.5592	3.1779	2.7613	3.1524	2.7877	3.1937
0.0910	2.5956	3.1220	2.5440	3.1685	2.7462	3.1404	2.7720	3.1814
0.0956	2.5807	3.1164	2.5291	3.1629	2.7314	3.1321	2.7566	3.1692
0.1003	2.5662	3.1111	2.5145	3.1576	2.7170	3.1265	2.7414	3.1570
0.1051	2.5520	3.1061	2.5003	3.1526	2.7028	3.1212	2.7265	3.1462
0.1098	2.5382	3.1014	2.4865	3.1479	2.6891	3.1163	2.7120	3.1406
0.1146	2.5248	3.0969	2.4731	3.1435	2.6756	3.1115	2.6978	3.1354
0.1193	2.5117	3.0926	2.4600	3.1392	2.6626	3.1071	2.6840	3.1304
0.1241	2.4990	3.0886	2.4473	3.1351	2.6498	3.1028	2.6706	3.1258
0.125	2.4965	3.0878	2.4448	3.1343	2.6473	3.1020	2.6679	3.1248

Table A4.3.4
Theoretical values of the pressure distribution corresponding to inlet conditions listed in Table 7.6.1.1 in Chapter 7